Order Number 9229131

Brownian motion in disordered media

Jacobs, Donald John, Ph.D.

Purdue University, 1992

U·M·I
300 N. Zeeb Rd.
Ann Arbor, MI 48106

Graduate School Form 9
(Revised 8/89)

PURDUE UNIVERSITY
GRADUATE SCHOOL
Thesis Acceptance

This is to certify that the thesis prepared

By Donald John Jacobs

Entitled

Browian Motion in Disordered Media.

Complies with University regulations and meets the standards of the Graduate School for originality and quality

For the degree of Doctor of Philosophy

Signed by the final examining committee:

Hosea McDaniel, chair

M Jordan

Paul T. Yi

Arnold Tubis

Approved by:

Arnold Tubis
Department Head

5/1/92
Date

This thesis ☐ is ☑ is not to be regarded as confidential

Hosea McDaniel
Major Professor

BROWNIAN MOTION IN DISORDERED MEDIA

A Thesis

Submitted to the Faculty

of

Purdue University

by

Donald John Jacobs

In Partial Fulfillment of the

Requirements of the Degree

of

Doctor of Philosophy

May 1992

To my family

and to my best friend

Neena

ACKNOWLEDGMENTS

I wish to thank Professor Hisao Nakanishi for his confidence in me and for giving me much freedom in my research. He always encouraged me to continue with my ideas while politely pointing out my mistakes. He has helped me in many ways that are very much appreciated. I thank Dr. R. Muralidhar for his collaboration with me on two projects and for the many enjoyable discussions between us. I thank Professor N. Fuchs and Dr. J. Moon many fruitful discussions. I am thankful to the many friends that I have made in Indiana, especially to Sung Choi, Bill Geisler, Louise Lin, Sonali Mukherjee, Steve Riggs and Rose Wang who helped me to grow in knowledge about life in general.

I thank my family for their love and concern. Although they do not understand what I do, they know I enjoy physics and have always supported me. During the time at Purdue I have meet someone very special to me. My wife to be, Neena. She has helped me tremendously over the years. Yet, I cannot leave out the most important *one* to thank. Thank you God for all your blessings, and for making my life meaningful. I can only hope to continue my life along a spiritual path. Inshallah.

TABLE OF CONTENTS

Page

LIST OF TABLES

Table Page

Table Page

LIST OF FIGURES

Figure Page

Figure Page

Figure Page

Figure Page

Figure Page

Figure Page

Figure Page

Figure Page

ABSTRACT

Jacobs, Donald John. Ph.D., Purdue University, May 1992. Brownian Motion in Disordered Media. Major Professor: Hisao Nakanishi

The Brownian motion in quenched disordered media is studied from a stochastic point of view using random walk models and to a lesser extent a Langevin approach. Focus is placed on highly ramified media that exhibits self-similarity over a wide range of length scales. Accurate estimates are obtained for the dynamical exponents for the blind and myopic ant random walks on percolation clusters in two and three dimensions at criticality and DLA (diffusion limited aggregation) clusters in two dimensions. The method employed exactly enumerates all Brownian paths from all starting points in a cluster. The scaling properties found in the probability density for the position of the random walker is exploited to develop an approximation scheme for the mean squared displacement. Moreover, a simple connection between the anisotropic properties of the diffusion process to the geometric structure of the clusters is established.

Regular oscillations are found to persist in the step correlation function for the myopic ant on bipartite clusters. In the regime of self-similarity, these oscillations decay as a power-law with an exponent given by half the spectral dimension. A

formal mapping from a discrete time random walk to a continuous time master equation applicable to quenched disordered media is developed. Moreover, the frequency dependent diffusion coefficient is expressed in terms of the step correlation function. A kinematic analysis reveals that a generalized Langevin equation with a power-law friction kernel adequately describes the anomalous diffusion.

A random walk model with persistence is introduced for the analysis of the electrical conductivity of disordered composite materials. Features of the model include; a phenomenological parameterization with a high frequency cut off determined by the coarse grain length scale, a Drude-like mobility in homogeneous media, and the relative carrier concentrations and mobilities of the constituents are treated independently. The interplay between the mean free paths of each constituent, the disorder length scale, and the correlation length of the disorder is investigated. Results are presented which indicate that scaling theories utilizing only conductivities are generally inadequate.

1. INTRODUCTION

1.1 Brownian Motion and its Relationship to Diffusion

In 1829 the botanist Robert Brown observered that pollen grains suspended in fluids moved about erratically.[1] This type of motion was unexpected since the system was hydro-statically in equilibrium, and the molecular nature of matter was not appreciated at that time. Although Brown was unable to give a physical explanation for this behavior, indeed this type of motion has come to be known as *Brownian motion* . In 1905, Einstein made an initial break through on the Brownian motion of a heavy particle in a fluid.[2] As first pointed out by Einstein, the entire essence of the problem is that the fluid itself is composed of many discrete particles. Therefore, although the large particle encounters many collisions with the fluid particles, it suffers an erratic trajectory because of the discrete nature of matter. The study of Brownian motion has been continuing on since the pioneering work of Einstein because of its fundamental and practical importance.[1, 3]

In this thesis, the term Brownian motion will refer to the *random* movement of a tracer particle within a given physical system in equilibrium. Brownian motion is modeled mathematically as a random process. There are multitudes of possible models that can be constructed in order to characterize the Brownian movement in various systems, therefore, the meaning of *random* is very much problem

dependent. A tracer particle is considered here to be labeled or tagged in some way as to distinguish it from all other particles in the system. The physical properties of the tracer particle is to be specified from the physical problem at hand. The main problem of interest is to determine how far the tracer particle will wander from its initial position after some time. As will be seen, the mean squared displacement is of fundamental importance in characterizing the movement of the tracer particle.

Now suppose that the position of the tracer particle is measured regularly at fixed time intervals T_o. Then the simplest model as discussed by S. Chandrasekhar[3] assumes that one can choose the time T_o such that the displacement of the tracer particle $\vec{\rho}(i)$ during the ith time interval is independent to its displacement during any other time interval. However, within a given time interval, the displacement of the tracer particle is a random variable characterized by a probability distribution such that the average displacement of the particle is zero and the mean squared displacement is finite. The net displacement of the tracer particle after n measurements is given by

$$\vec{R}(nT_o) = \sum_{i=1}^{n} \vec{\rho}(i) \tag{1.1}$$

and the mean squared displacement is given by

$$\langle R(nT_o)^2 \rangle = \sum_{i=1}^{n} \langle \rho(i)^2 \rangle + \sum_{i \neq j} \langle \vec{\rho}(i) \cdot \vec{\rho}(j) \rangle \ . \tag{1.2}$$

Since $\vec{\rho}(i)$ and $\vec{\rho}(j)$ are independent random variables for $(i \neq j)$ with $\langle \vec{\rho} \rangle = 0$, it is seen that the mean squared displacement after time $t = nT_o$ is given by

$$\langle R(t)^2 \rangle = \frac{\langle \rho^2 \rangle}{T_o} t \ . \tag{1.3}$$

The linear time dependence of the mean squared displacement is a very familiar result in the theory of Brownian motion. This result hinges on the *assumption*, that a separation in time scales exist. A separation in time scales means that the tracer particle will retain negligible memory of its initial condition after a certain time passes called the *correlation time*. Therefore, if the time scale T_o in the above model is chosen smaller than the correlation time, then the assumption that $\langle \vec{\rho}(i) \cdot \vec{\rho}(j) \rangle = 0$ for $i \neq j$ is invalid. Clearly, the correlations in the tracer particle's observered displacements is dependent on the time scale of interest. Since a separation of time scales usually exist, the long time behavior of Brownian motion is accurately described with the above model.

Instead of a single particle, suppose a large number of tracer particles are injected into a local region and followed simultaneously. The time development of the tracer particle concentration (C) defines a *diffusion process*. In systems where the number of tracer particles is conserved, the time development of the concentration is governed by a continuity equation without sources or sinks. As early as 1855 through the work of Fick[4] the particle current density ($\vec{J}_p$) was empirically found to be directly proportional to the gradient of the concentration. The diffusion constant D is defined through the relation

$$\vec{J}_p(\vec{r},t) = -D\vec{\nabla}C(\vec{r},t) \tag{1.4}$$

which is known as Fick's first law. Fick began to realize at that time the general nature of transport theory and had drawn upon analogies with Ohm's law and

Fourier's heat equation to arrive at the diffusion equation

$$\frac{\partial}{\partial t} C(\vec{r},t) = D \bigtriangledown^2 C(\vec{r},t) \tag{1.5}$$

which is also known as Fick's second law.

In elementary transport theory[5], the transport of energy or mass occurs in systems that are not in an equilibrium state. For systems not too far from equilibrium, a set of macroscopic variables can still be used to define the state of the system provided that these variables are functions of position and time. The inhomogeneities in those macroscopic variables is the self driving mechanism responsible for currents that try to re-establish equilibrium. Transport coefficients are defined through the relationship between the current density and the gradient of the corresponding macroscopic state variable such as Fick's first law. Of course all of the microscopic dynamics taking place ultimately must determine the transport properties of the system under study. In the case of diffusion, the motion of the tracer particles is the underlying microscopic process of interest. Under the assumption that each of the particles will respond identically in the same way as if solely present, it intuitively follows that diffusive transport can be understood from Brownian motion.

In most applications the transport of mass or energy is occurring in a steady state condition, however, the system is not in equilibrium. A system is said to be in a steady state if all physical properties of the system are not changing with time, and there are macroscopic currents present. Thus the environment surrounding the

system is changing in time (ie. mass and/or energy transport). To fully describe the transport properties of a given system all possible coupling between the many transport mechanisms must be included.[6, 7] By adjusting external biases it is possible to bring a system to a new inhomogeneous equilibrium state and relate different transport coefficients to one another. For example, if a uniform electric field is set up across an ionic solution, a concentration gradient will build up such that the diffusion and electrical drift currents cancel yielding no net particle flow. Using this simple idea, Einstein[2, 8] was able to relate the electrical conductivity σ to the diffusion constant of the charge carriers. The well known Einstein relation is commonly expressed as

$$\sigma = \frac{nq^2}{k_B T} D \tag{1.6}$$

where k_B is the Boltzmann constant, T is the absolute temperature and n is the concentration of charge carriers with charge q.

The statistical mechanical approach to transport theory is to relate the macroscopic response of a system to the microscopic fluctuations from the equilibrium state. In particular, the *fluctuation dissipation theorem* [5] forms the basis for the connection between the microscopic *after-effects* to the macroscopic response and dissipation. The microscopic after-effects[3] describe how an initial fluctuation (defined by a microscopic sub-ensemble) will relax back into equilibrium. This approach is useful in the linear response regime where the external perturbation to the system does not change the system's microscopic character (usually valid for

sufficiently weak perturbations). For example, the concentration of diffusing particles must be sufficiently low such that the assumption that each particle undergoes Brownian motion independently is valid. Thus, within the linear response regime, the dynamics of Brownian motion at the microscopic level determine the diffusive and electrical transport at the macroscopic level.

1.2 Mathematical Models for the Brownian Motion

The random walk model, the Langevin equation of motion and the Fokker-Planck equations are the three most common mathematical formalisms used in the theory of Brownian motion.[1, 3] The emphasis of this thesis is placed on random walk models, although a complimentary discussion on the Langevin approach will be given in Chapter 3. For completeness, brief discussions are included on the connection between the random walk model and a Fokker-Planck equation. A common goal among all of these formalisms is to describe with sufficient accuracy the time development of the tracer particle's movement. Before the problem of Brownian motion in disordered media is tackled, a short overview of these mathematical approaches is given here for homogeneous and isotropic media to illuminate their general features.

The random random walk model is very useful in describing the Brownian motion.[1, 9, 10] In a random walk model, the tracer particle's net displacement is broken up into a sum of individual *step* displacements in conjunction with a series of associated time intervals taken for each step. Both the time intervals and step

displacements are regarded as random events. The design of a particular model must address how the individual steps are correlated with one another, and how the step displacements are inter-related to the time intervals. For introductory purposes, consider a random walk model with uncorrelated step displacements. Then consequently, the model is defined by the specification of a joint probability density for a step displacement and corresponding time.[11] A *separable* model is one in which the joint probability density factors into a product of two functions; one for the step displacements and another for the time intervals. In this thesis, a random walk model will be called *simple* if it has the following properties. (1) The model is separable. (2) The step displacements are independent identically distributed random variables. (3) The first moment in the displacement is zero, and the second moment in the displacement of one step is finite. (4) The time intervals for each step are also independent identically distributed random variables. (5) Finally, the average time between steps is finite and moreover there is a probability of one that the particle will make a finite displacement after an indefinitely long time.

A random walk model defines a stochastic process from which the probability density for a particle's net displacement can be obtained. As an illustration of the basic concepts involved, consider a simple random walk with the probability density for a single step displacement $\vec{\rho}$ given by $w(\vec{r}_o + \vec{\rho}, \vec{r}_o)$ where $\vec{r}_o$ is the particle's current position. By virtue of property (2), w is translationally invariant. The probability density that the particle (random walker) will acquire a net

displacement of $\vec{R}$ after $n+1$ steps is given by the recursion relation

$$P_{n+1}(\vec{R}) = \int_{\text{vol}} w(\vec{\rho},0) P_n(\vec{R}-\vec{\rho})\, d^d\rho \quad , \tag{1.7}$$

in d dimensions. On taking the Fourier transform of the above recursion relation, and denoting the Fourier transform of $w(\vec{\rho},0)$ as

$$\tilde{w}(\vec{k}) = \int_{\text{vol}} e^{i\vec{k}\cdot\vec{\rho}}\, w(\vec{\rho},0)\, d^d\rho \tag{1.8}$$

the desired distribution is given by

$$P_n(\vec{R}) = \frac{1}{(2\pi)^d} \int_{\text{vol}} e^{-i\vec{k}\cdot\vec{R}}\, \tilde{P}_n(\vec{k})\, d^dk \quad , \tag{1.9}$$

where

$$\tilde{P}_n(\vec{k}) = [\tilde{w}(\vec{k})]^n \quad . \tag{1.10}$$

In the limit of a large number of random events, the inverse Fourier transform of $\tilde{P}_n$ will be dominated by the small k contributions.[5] Using property (3) and denoting the mean squared displacement of a single step as a^2, it follows from a Taylor expansion of $\tilde{w}(\vec{k})$ to second order in k that

$$\tilde{P}_n(\vec{k}) \rightarrow \exp\left(-\frac{n}{2}a^2k^2\right) \tag{1.11}$$

when n is sufficiently large. Proceeding with the inverse Fourier transform, the distribution for the particle's displacement tends to a Gaussian given by

$$P_n(\vec{R}) = \frac{1}{(2\pi n a^2)^{\frac{d}{2}}} \exp\left(-\frac{R^2}{2na^2}\right) \quad , \tag{1.12}$$

which is independent of the details of the single step distribution.

The above result is a particular example of the *central limit theorem* [5] which states that the probability distribution for a random variable Y_n defined as an average over the set of n independent identically distributed random variables $\{X_i\}_n$ will tend to a Gaussian for large n. Furthermore the standard deviation in Y_n will be a factor of $1/n^{\frac{1}{2}}$ less than the standard deviation in the X random variable. The details of the distribution function for X are not important except for the restriction that the first and second moments of X are finite. In applying the central limit theorem for the time needed by the random walker to take n steps, the fluctuations in the time needed can be neglected for n sufficiently large. Therefore, the mapping between the number of random events and the time the particle takes to make n steps is given by $t = n\langle\Delta t\rangle$ where $\langle\Delta t\rangle$ is the average time interval for each step.

The probability density for the displacement of a tracer particle in terms of time (not the number of steps) is asymptotically given by

$$P(\vec{R},t) = \frac{1}{(4\pi dDt)^{\frac{d}{2}}} \exp\left(-\frac{R^2}{4dDt}\right) \tag{1.13}$$

where $D = \frac{a^2}{2d\langle\Delta t\rangle}$. The variable D is called the diffusion constant since Eq. (1.13) is also the solution to the diffusion equation Eq. (1.5) with an initial concentration of particles at the origin.[1, 2, 5] The connection between the random walk model and diffusion equation is made possible by interpretating the probability density for *one* tracer particle as a concentration profile for a collection of many diffusing particles. In essence, the random walk model attempts to describe the time development of

a typical diffusing particle. Since $\langle R(t)^2 \rangle = 2dDt$ as calculated from Eq. (1.13), it follows that the diffusion constant D can be obtained from the slope of the mean squared displacement at long times. Notice further that the microscopic details have been conveniently buried in the distribution functions for the step displacement and time intervals.

Alternatively, the asymptotic properties of the random walk model can be obtained by a partial differential equation for the probability density known as a Fokker-Planck equation. The Fokker-Planck equation essentially contains the same physical content as the random walk model at times sufficiently large such that $t = n\langle \Delta t \rangle$ is valid. A Taylor expansion of $P_n(\vec{R} - \vec{\rho})$ from Eq. (1.7) can be made about $\vec{R}$ to obtain

$$P_{n+1}(\vec{R}) - P_n(\vec{R}) = \langle \rho_i \rangle \frac{\partial}{\partial r_i} P_n(\vec{R}) + \frac{1}{2} \langle \rho_i \rho_j \rangle \frac{\partial^2}{\partial r_i \partial r_j} P_n(\vec{R}) + \cdots \qquad (1.14)$$

where the summation on the repeated indices is implied. Usually $w(\vec{\rho})$ decays exponentially fast so that the expansion needs to be carried only to second order. Under the assumption of homogeneous and isotropic media, all odd moments in ρ_i will vanish. Dividing both sides of Eq. (1.14) by $\langle \Delta t \rangle$ it follows that in the long time limit, the discrete difference in n can be passed to a continuous time derivative. With the same identification of D as above the recursion relation reduces to the diffusion equation. This brief discussion on the Fokker-Planck approach should make clear that a general Fokker-Planck equation (possibly much more complex than the above example) can be considered to be an approximation scheme to

some random walk model.[1, 3, 12]

In contrast to the random walk model, the Langevin approach[1, 3, 12, 13] to Brownian motion is to consider equations of motion directly. Explicit use is made of the fundamental assumption in transport theory that *linear* macroscopic equations describing the relaxation of a perturbed system toward equilibrium is essentially the same as the relaxation of the microscopic fluctuations.[3, 14]. Whereas the macroscopic equations are deterministic dealing with average quantities, the microscopic equations are stochastic since they must contend with fluctuations induced by the discrete nature of matter. Therefore, an equation of motion is written down for a single tracer particle, and all other particle interactions in the system are incorporated via introducing an effective force. The effective force is broken down into a *systematic* and *random* part. To some extent this separation of the effective force appears artificial, however, as will be discussed in Chapter 3 there is a well defined procedure in determining this separation. Only the systematic part of the tracer particle's equation of motion will survive the averaging, and thus become a macroscopic relaxation equation. In short, the Langevin approach attempts to extend linear macroscopic laws by adding a random force term accounting for molecular collisions (or scattering).

The simplest dynamical equation to model Brownian motion known as the Langevin equation is given by

$$\frac{d}{dt}\vec{v} + \gamma\vec{v} = \frac{\vec{f}(t)}{M} \tag{1.15}$$

where $\vec{v}$ is the velocity, and M is the mass of the tracer particle. The random force is denoted as $\vec{f}(t)$ with the *defining* properties that $\langle \vec{f}(t) \rangle = 0$ and $\langle v_i(0) f_j(t) \rangle = 0$. The angular brackets $\langle \cdots \rangle$ denote an average over all possible realizations that can occur in a system at equilibrium. Furthermore, the random force at any time is uncorrelated to the random force at any other time. The assumption of uncorrelated random forces is *not* a defining property, but rather part of the above model. Finally, the parameter γ is the characteristic rate at which the velocity fluctuations decay or equivalently is a macroscopic relaxation rate.

The results from the Langevin and random walk models for the mean squared displacement of a tracer particle can be compared using the general relation

$$\frac{d^2}{dt^2}\langle r_i(t) r_j(t) \rangle = \langle v_i(t) v_j(0) \rangle + \langle v_j(t) v_i(0) \rangle \tag{1.16}$$

for stationary systems. Because the random force and initial velocity are uncorrelated, it follows from the Langevin equation that

$$\frac{d}{dt}\langle v_i(t) v_j(0) \rangle = -\gamma \langle v_i(t) v_j(0) \rangle \tag{1.17}$$

where $\langle v_i(0) v_j(0) \rangle = 0$ for $i \neq j$. Thus

$$\langle \vec{v}(t) \cdot \vec{v}(0) \rangle = \langle v(0)^2 \rangle e^{-\gamma t} \quad , \tag{1.18}$$

is the solution for the velocity auto-correlation function. After two integrations of the velocity auto-correlation function (VACF) the mean squared displacement is found to be given by

$$\langle R(t)^2 \rangle = \frac{2\langle v(0)^2 \rangle}{\gamma^2}(\gamma t - 1 + e^{-\gamma t}) \tag{1.19}$$

for which the linear time dependence agrees with the simple random walk model at times $\gamma t \gg 1$ provided that $D = \frac{\langle v(0)^2 \rangle}{d\gamma}$. The time $\tau = 1/\gamma$ is the correlation time which defines the separation in time scales insuring the simple random walk model to be valid asymptotically. The correlation time will be much longer than the time between collisions because the tracer particle must encounter many collisions for the memory of its initial momentum to be lost. Although explicit reference to the statistical properties of the random force was not made to obtain the VACF, they would need to be specified in order to obtain the distribution functions for the velocity and displacement of the tracer particle.

1.3 Brownian Motion in Solids

The connection between the diffusion process and Brownian motion is well established regardless of if the tracer particle is placed in a gas, liquid or solid. To be more specific, the problems of interest include the frequency dependent electrical conductivity of composite materials,[15, 16] diffusion controlled reactions in a solid matrix of catalyst[17] and the transport of a one component fluid through porous or fractured rocks.[18] Clearly the detailed physics of these problems are very different from one another, however, the stochastic description of Brownian motion (within the context of phenomenological models) is common to all. The basic set of approximations and assumptions used in modeling Brownian motion via random walks in either homogeneous or inhomogeneous solids is reviewed here.

The Brownian motion will be modeled on a lattice so that the trajectory of

the tracer particle will be discretized. The random walker will be allowed to hop between nearest neighbor sites only. In the case of atomic diffusion via a vacancy mechanism, the physical process dictates that the random trajectories be confined on a lattice. Thus the lattice structure may play an important role in atomic diffusion. In the case of electrons in metals, the details of the lattice structure will be neglected. Therefore, the constraining of the electron trajectory to a lattice structure must be regarded as a coarse graining scheme, and any properties that are lattice dependent will not be physically meaningful. Typically the coarse grained lattice constant is chosen to be equal to (or greater than) the mean free path of the tracer particle. The mean free path (denoted as l) is defined as the minimum length that the tracer particle must travel on average such that the next displacement of length l is independent to the previous one.

The main justification for coarse graining onto a lattice network and using nearest neighbor hopping rules is that the properties of a simple random walk is insensitive to the details of the single step probability density in the long time limit. Consequently, simple random walk models of this sort are limited to describing d.c. properties only. If however, a.c. properties are desired, then the details of a model can be expected to become important and the simple random walk model must be extended. Although it is not clear that a unique model should exist in describing experimentally observed phenomena, a model should incorporate the essential microscopic physics.

For example, in the case of atomic diffusion via a vacancy mechanism, the

atom can only hop into a nearest neighbor vacancy. If a hop occurs, the atom and vacancy will exchange locations and therefore there is a high probability that the atom will hop back where it started. Thus the random displacements of the tracer particle will be correlated to one another.[19] Since the diffusion constant D can be obtained from the slope of the mean squared displacement at long times in the simple random walk model, it is convenient to define a local slope after n random *events* given by

$$D_e(n) = \langle R(n+1)^2 \rangle - \langle R(n)^2 \rangle \ . \tag{1.20}$$

From Eq. (1.2) and using the property of stationarity (time translation invariance), the expression for the local slope in terms of the correlation in step displacements is given by

$$D_e(n) = \langle \rho^2 \rangle + 2 \sum_{m=1}^{n} \langle \vec{\rho}(m) \cdot \vec{\rho}(0) \rangle \ , \tag{1.21}$$

where the diffusion constant can be obtained from $D = \frac{D_e(n \to \infty)}{2d\langle \Delta t \rangle}$.

For example, we restrict the random walk to a hypercubic lattice in d-dimensions with nearest neighbor hopping. The *step displacement* auto-correlation function can be written as

$$\langle \vec{\rho}(m) \cdot \vec{\rho}(0) \rangle = a^2 \langle \cos(\theta_m) \rangle \ , \tag{1.22}$$

where a is the lattice constant and θ_m is the angle between the initial and mth hop of the tracer particle. In this correlated walk, the tracer particle has a higher probability to jump backward than forward, but by symmetry, the average displacement in any orthogonal direction will be zero. Thus by decomposing the mth

step displacement into components, one parallel to the $(m-1)$th step displacement and another perpendicular, it follows upon averaging that

$$\langle \vec{\rho}(m) \cdot \vec{\rho}(0) \rangle = \langle \cos(\theta) \rangle \times \langle \vec{\rho}(m-1) \cdot \vec{\rho}(0) \rangle \tag{1.23}$$

where $\langle \cos(\theta) \rangle$ is the average projection between any two successive steps. Therefore after m steps $\langle \cos(\theta_m) \rangle = \langle \cos\theta \rangle^m$ indicating that the correlation in the step displacements decay exponentially.[20] It is noted here that basically the same derivation can be applied to the continuum as well.

Specifically for a hypercubic lattice, there will be a probability (p_f, p_s, p_b) for the tracer particle to continue moving in a (forward, sideward, backward) direction respectively with $p_f + 2(d-1)p_s + p_b = 1$ as the normalization constraint. Since a (forward, sideward, backward) step has a projection of $(1, 0, -1)$ relative to the previous step, the average projection for a single step is given by $\langle \cos\theta \rangle = p_f - p_b$. From Eq. (1.21) in the limit that n goes to infinity, the diffusion constant is found to be

$$D = \frac{a^2}{2d\langle \Delta t \rangle} \frac{p_f + (d-1)p_s}{p_b + (d-1)p_s} \quad . \tag{1.24}$$

Clearly a correlated random walk can modify the simple random walk prediction for the diffusion constant. As expected, the anti-persistent correlations in the step displacements lowers the diffusion constant. Note that a simple random walk model can be used to obtain the correct diffusion constant provided that an effective lattice constant and/or effective average waiting time is implemented. However, unlike the simple random walk, the local slope $D_e(n)$ is not constant for all n and

therefore a frequency dependent diffusion coefficient will result from a correlated walk. A mapping from discrete time n (number of random events) to the frequency domain will be discussed in Chapter 3.

In Chapter 4, a persistent random walk model is introduced which is similar to the correlated random walk described above in that the correlation in the step displacements decay exponentially. However, the persistent random walk model is applied to a coarse grained lattice, and the persistence is introduced to obtain a Drude-like frequency dependent mobility in homogeneous metals. This novel persistent random walk model is analogous to the Langevin result where the velocity auto-correlation function decays exponentially and a finite correlation time exist. The persistent random walk also has a Fokker-Planck equivalent and is known as the telegrapher's equation.[1, 9, 21] The key point to this approach is that at short times the particle's motion is ballistic, and at long times it becomes diffusive.

The basic concepts of Brownian motion that have been introduced thus far are now going to be applied to inhomogeneous solids. The degree of inhomogeneity of a solid is actually *dependent* on both the length and time scales of interest. A solid can appear to be inhomogeneous to a tracer particle only if the time scale of the Brownian motion is much shorter than the time scale of the change in structural configuration. For the remainder of this work it will be assumed that a sufficiently large separation in time scales exist such that the structure of the solid matrix can be taken as static. The static inhomogeneity of a solid could range over microscopic, mesoscopic, or macroscopic length scales. Some applications

include: at microscopic length scales the transport properties of phonon assisted electron hopping in nearly compensated semi-conductors,[22] at mesoscopic length scales the electrical properties of composite materials[15] or of thin films with compositions near the metallic-insulator transition,[23, 24] and at mesoscopic up to macroscopic scales a one component fluid flow through fractured rock.[18]

Here the inhomogeneity of interest is when a host medium is disordered in a non-deterministic way. The term non-deterministic indicates that the local details of the configuration in some region cannot be concluded given the local configurational details of some other region. However, the *static* disorder will be characterized by its statistical properties. Furthermore, the underling distribution function in defining the disorder will be taken to be homogeneous. For a given disordered configuration all possible Brownian paths with their appropriate weights must be summed over in the calculation of the mean squared displacement or any other correlation function associated with the diffusion process. In contrast to homogeneous media, the location of the starting point of each random walk in the disordered solid matrix is important since the tracer particle will experience *different* environments.

Although reasonably large samples (to be qualified in Chapter 2) share similar properties with one another, there will nevertheless be fluctuations between sample to sample. Therefore it is convenient to discuss the typical properties of interest by introducing a quenched average. To obtain the desired quenched averages, a fixed coordinate system is chosen, and a configuration can be constructed *randomly* in

accordance to the statistical properties of the disordered system. Thus a given disordered system is viewed as a single realization and for this reason is sometimes referred to as a random medium. The average properties of the random motion of the tracer particle that characterize the diffusion process are actually conditional averages for a given realization. The quenched average is finally obtained from the *second* averaging over all possible realizations in the disorder and will be referred to as a configurational average.

The study of diffusion in inhomogeneous solids is much more difficult than homogeneous solids because the single step distribution function $w(\vec{\rho} + \vec{r}_o, \vec{r}_o)$ will not be translationally invarient. Unlike the homogeneous case, the tracer particle's step displacements will be *spatially* correlated. In this case, the central limit theorem will not be applicable because the successive displacements are *not* independent. Of course, if the correlation in the step displacements decay rapidly it can be expected that the Gaussian limit will still be reached resulting in the normal Fickian Brownian motion. The degree of the inhomogeneity and the quantity of interest will dictate the method of solution. Often times, a simple coarse graining over the disorder will be sufficient to define an effective homogeneous medium.[25] If this is the case, the correlations in the step displacements will be negligible over the length scales of the coarse graining and a simple random walk model will apply. However, if the a.c. properties of the diffusion process are of interest or if the correlations do not fall off sufficiently rapidly, a more sophisticated and/or correlated random walk model can prove to be a useful method of solution.

The main interest of this work is on disordered systems that are self-similar over a large range of length scales. The self-similar property of a disordered configuration is such that the statistical properties of the disorder remain unchanged as the magnification of the length scale is varied. In the self-similar regime, the d.c. and a.c. properties of the Brownian motion are expected to obey scaling. In the scaling regime, many of the microscopic details become irrelevant surrendering to the geometric properties of the disorder over many length scales. Although, the random walk approach as given in this thesis should be applicable outside the self-similar regime as well, the method itself will become less beneficial in favor of effective medium and perturbation methods.

1.4 Thesis Overview

In Chapter 2, we will begin with the simple question of what is the effective d.c. conductivity of a given randomly disordered system. To be more specific, the random media will consist of two component materials one being a perfect insulator the other a conductor. Although the question is simple it will be seen that the answer is generally difficult to obtain. The effective conductivity could in principle be calculated by determining the current density throughout the entire sample for a given applied electric field. However, the first problem that is encountered is in describing the disorder. Surely a complete microscopic knowledge of a given sample would be impossible to construct, but more importantly most of that information is useless. What is needed is to extract the essential properties of the medium.

The first and foremost property to consider is the connectivity of the conducting regions as a function of volume fraction.

For a volume fraction of conducting material (below, above) a critical volume fraction, the effective conductivity will be characteristic of an (insulator, conductor). Near the critical point, both the connectivity and conductivity obey scaling laws and respond in similar manner to other physical systems near a critical point where the correlation length measuring cooperative phenomena [26, 27, 28] diverge. Although, the connectivity is important, it is not sufficient to determine the conductivity because the details of the width and topology (ie series or parallel) of the connections play important roles. Many researchers[29] have modeled media as a random resistor network which effectively solves for the current density approximately by solving Kirchhoff's laws. However, as first pointed out by de Gennes[30] the resistor network problem can be transformed into a random walk problem. The random walk on the disordered medium is computationally much easier to perform (particularly for the frequency dependent properties) than solving Kirchhoff's laws. The key quantity of interest is the mean squared displacement of the random walker.

After introducing site percolation and DLA aggregates for modeling disordered media, the mean squared displacement for two random walk models (as to be defined; the blind and myopic ant) is obtained using an extended version of the exact enumeration method of Majid *et al.*[31]. From these results the walk exponents are extracted for various lattices. Moreover, the mean squared displacement char-

acterizes the diffusion of particles. Near the insulator-conductor critical threshold an approximation scheme is developed to determine the mean squared displacement as well as other quantities. The approximation scheme is mean field like in the sense that certain fluctuations and correlations are neglected, but it places heavy emphasis on the scaling properties of the average behavior. Also within this approximation scheme the anisotropy of the diffusion process is considered.

In Chapter 3, the focus of attention shifts from the mean squared displacement of a random walker to its velocity correlations, although in principle the same information is contained in either quantity. From the long time properties of the velocity auto-correlation function (VACF) the diffusion process is categorized as normal or anomalous. Different ranges in exponents for the algebraic decay in the long time tail of the VACF will lead to fast anomalous, normal or slow anomalous diffusion. The anomalous diffusion is probably best described in the frequency domain in terms of a frequency dependent diffusion coefficient.

In static disordered media, the spatial correlations in the structure will generally cause long time correlations in the VACF. As a consequence of these correlations a Langevin description of the Brownian motion will need to incorporate a non-local friction kernel. The relationship between the friction kernel, VACF and random noise term in a Langevin approach are discussed. Furthermore, it is shown that a simple power law friction kernel can be used in modeling anomalous diffusion. All of the above results on the Langevin approach have been obtained from the theory on the generalized Langevin equation[32] and self consistency.

A direct connection between the spatial disorder to the long time tails in the VACF is made by modeling the diffusion process in terms of a master equation.[9, 33, 34] The master equation is transformed into a discrete time random walk with a Poisson waiting time distribution. The frequency dependent diffusion coefficient is then related to the *step* displacement *auto-correlation function* (SACF) which plays an analogous role in discrete time (number of random events) as the VACF in continuous time (real time). The blind and myopic ant models are considered again in more detail in terms of their SACF. The frequency dependent diffusion coefficient as determined from either SACF clearly demonstrates that the diffusion is anomalous at high frequencies even when the volume fraction is not too far from the threshold value. Of course at low frequencies the diffusion is normal since the corresponding time scales are so long that the media will appear to be homogeneous.

In Chapter 4, a novel random walk model is introduced which incorporates persistence in the random walker's step displacement. The idea of a persistent random walk is not new[9, 21] and in fact is just the correlated random walk as discussed earlier. However, the details of the model considered here are somewhat different and from the resulting SACF a Drude-like mobility is shown to result. The model parameters (probabilities to hop and the characteristic rate of hopping) are determined from the physical parameters of a material exhibiting a Drude-like conductivity.

This persistent random walk model is introduced because it first of all exhibits

the correct frequency response within homogeneous media. Secondly, this model takes into account that the mean free path length of the tracer particle in different materials could be much different from one another. Furthermore, the mean free path in many cases will be of the same order or larger than typical cluster widths. In this work, the exact enumeration method is used in obtaining the SACF and/or mean squared displacement. However, a small discussion on the simulation of the persistent random walk is given.

In Chapter 5, the persistent random walk is studied in non-homogenous media. A simple couple of two materials in series is considered. Demonstration of coarse grain invariance and how the effective frequency dependent conductivity depends on more details than just the d.c. conductivity of each phase is given. In particular, the concentration of charge carriers, d.c. diffusion coeficient and transport time for each phase play in important role when the linear dimension of the issolated regions of constant phase are of the same order or smaller than the mean free path for that phase in homogeneous media.

We further consider the persistent random walk in random media over a broad range in the degree of disorder. The main focus is to constrast the results for the effective conductivity as the length of the mean free path of the tracer particle is varied. In the case that the mean free path is much smaller than the length scale of the ramification, the results reduce to the simpler blind or myopic random walk results. Chapter 5 basically presents a limited test of the persistent random walk model. Further work on the model and some variants are suggested.

2. BROWNIAN MOTION IN DISORDERED MEDIA AS A CRITICAL PHENOMENON

2.1 Introduction

As discussed in Chapter 1, an important application for studying diffusion, or more specifically the Brownian motion of charge carriers, in inhomogeneous media is that via the Einstein relation the electrical conductivity can be determined. Two excellent reviews on diffusion in regular and disordered lattices is given by Haus and Kehr[9] and on diffusion in disordered media is given by Havlin and Ben-Avraham.[35] To begin with, consider a disordered medium that is self-similar on all length scales L, with $a \ll L \ll \xi$ where a is some microscopic length and ξ (presumed very large) yields the minimum length scale for which the medium is homogeneous. The self-similarity property implies that the structural characteristics are the same at different levels of magnification. Self-similar objects are commonly called fractals[36] which may be deterministic or statistical. In Fig. 2.1 a section of a large statistical fractal shows many ramifications. A larger section of four times more area is shown in Fig. 2.2. Note that both pictures have remarkably similar ramification. In contrast, the degree of ramification will decrease as the length scale is increased for non-fractal objects.

The physical properties of an ensemble of statistical fractals will obey scaling

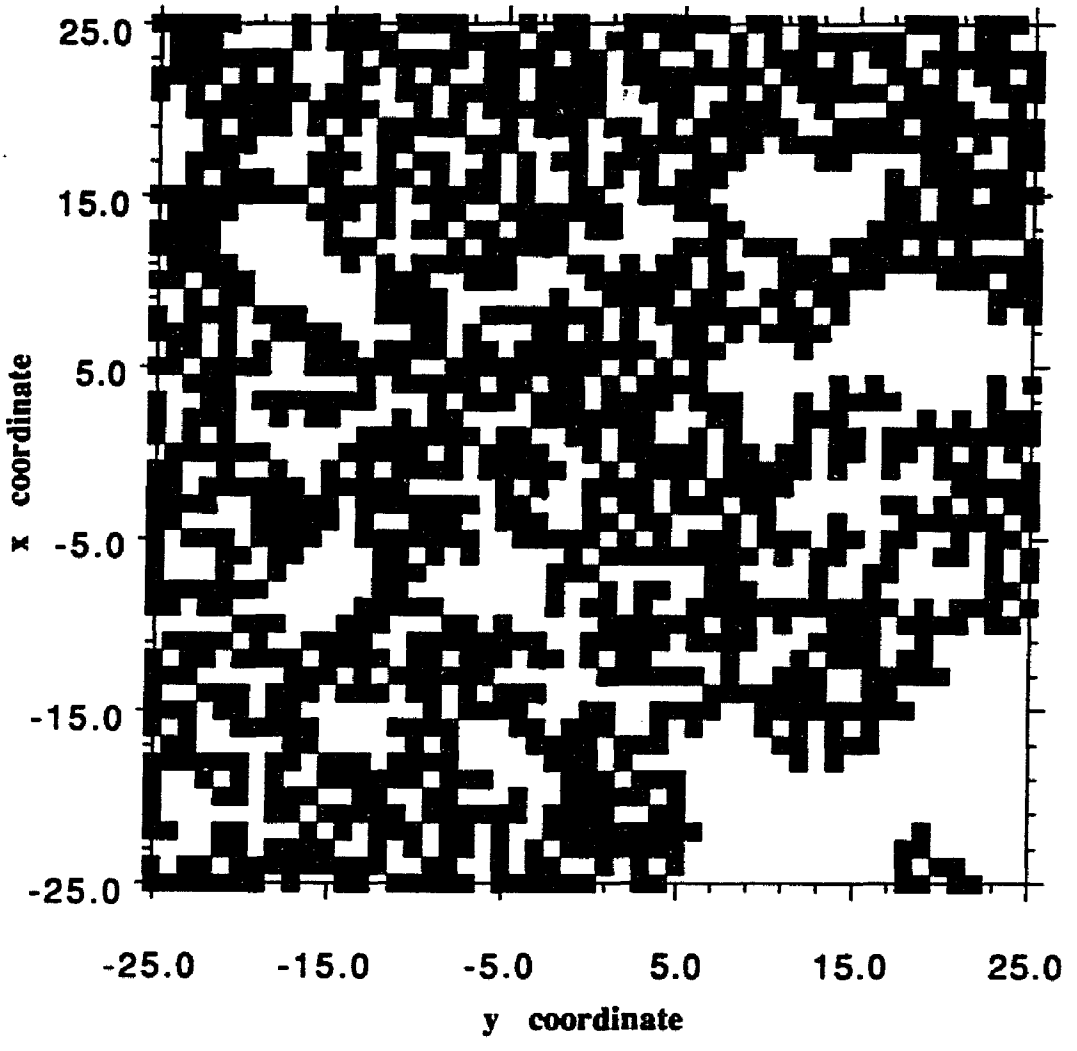

Figure 2.1

Here is a typical section of a "statistical" fractal that was randomly generated on a square lattice using a site percolation model at the critical threshold. The cluster was generated from a seed site and contained 100000 sites. This section contains 1376 sites, and much ramification is present. The next Figure shows a larger section with a change in length scale by a factor of two.

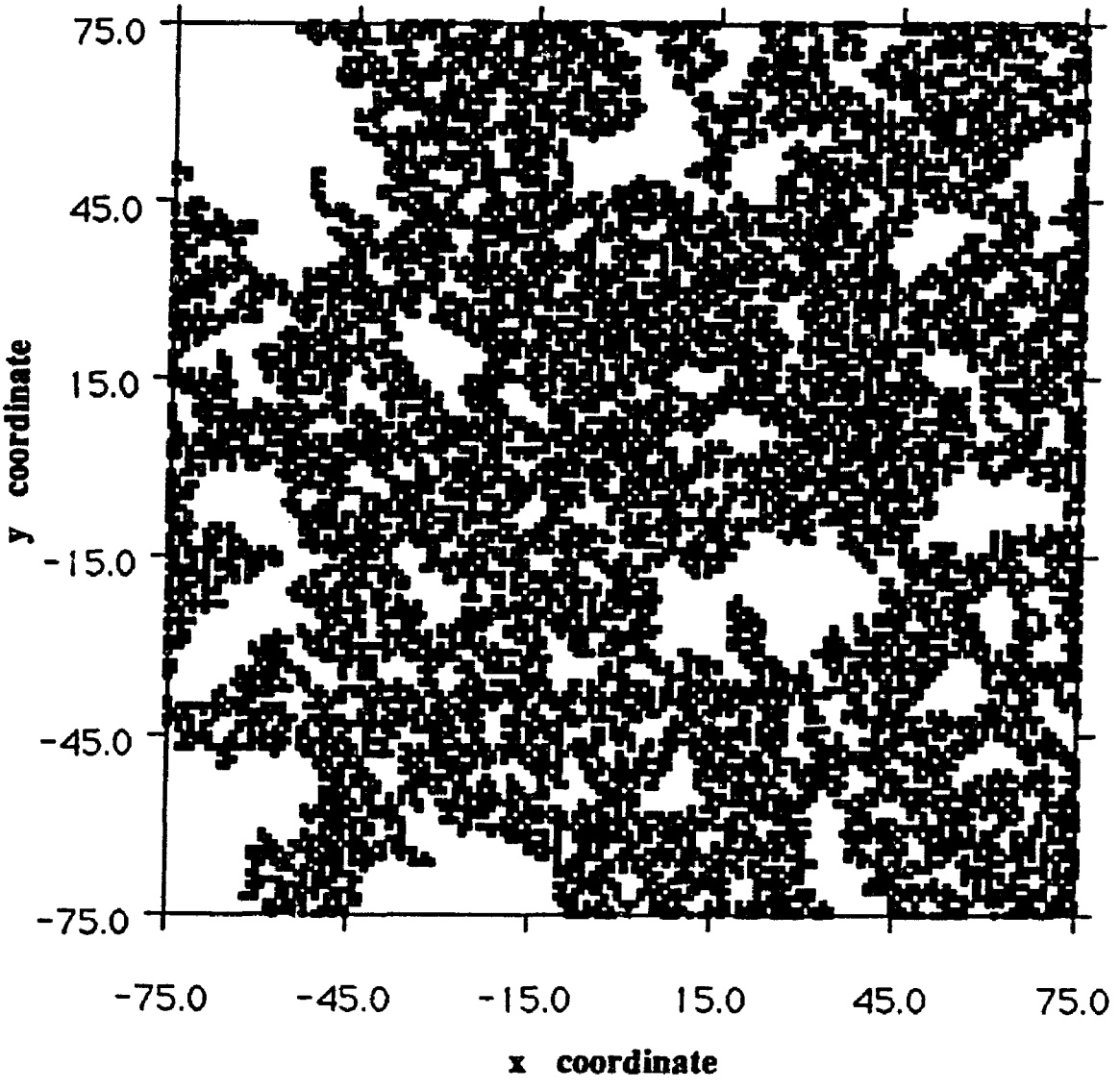

Figure 2.2

This region covers four times the area of the previous figure and contains 10587 sites. Note that the degree of ramification is very similar which is a characteristic of a fractal.

laws[26] such as the mass M of a cluster of linear size L which obeys

$$\overline{M(L)} \sim AL^{d_f} \tag{2.1}$$

where the bar denotes a configurational average. The exponent d_f is called the fractal dimension[26]. In this thesis, the fractal dimension of the clusters of interest will be less than the dimension d of the embedding space. In the case considered here the mass M refers to a metal cluster within an insulating matrix. As another example, the d.c. conductivity σ of a material that spans over a region of linear dimension L (a wire for one dimension, thin film in two dimensions, or small block for three dimensions) scales as

$$\overline{\sigma(L)} \sim BL^{-\tilde{\mu}} \tag{2.2}$$

where $\tilde{\mu}$ is a conductivity exponent[35, 37]. Although there may be many clusters of various sizes in the system, only the percolating cluster is responsible for d.c. conduction. As the system size becomes larger, according to Eq. (2.2) the d.c. conductivity decreases because there are less paths accessible to the carriers to get across the sample.

From numerical simulation[38, 39, 40] and exact enumeration[31, 41] the mean squared displacement of a random walker confined to a single metal cluster of fractal geometry is given by

$$\overline{\langle R(t)^2 \rangle} \sim Ct^{2/d_w} \tag{2.3}$$

for times such that $a \ll \sqrt{\langle R(t)^2 \rangle} \ll \xi$, where $d_w > 2$ is the walk exponent. Since for homogeneous media $d_w = 2$, this result implies that the particles diffuse

anomalously slowly on fractal media. An effective diffusion coefficient is defined by $D_{eff} = \overline{\langle R(t)^2 \rangle}/t$ and thus $R = \sqrt{D_{eff}t}$. The root mean squared displacement R of the random walker determines the length scale that is being probed so that $R \sim L$.

The walk exponent and the conductivity exponent can be related as follows. As the random walker explores more territory, its effective diffusion coefficient decreases because of the ever present ramifications at larger and larger length scales. Replacing the time t in favor of R, the effective diffusion coefficient is given by $D_{eff} = BR^{2-d_w}$. The carriers that participate in the d.c. conductivity are those confined to the percolating network. Therefore, the carrier density is proportional to M/L^d. From the Einstein relation, the effective d.c. conductivity is given by $\overline{\sigma} \propto R^{d_f - d + 2 - d_w}$. By matching this result with the scaling law from Eq. (2.2), the conductivity exponent $\tilde{\mu}$ can be determined by the scaling relation

$$\tilde{\mu} = d - d_f + d_w - 2 \quad . \tag{2.4}$$

A direct approach in calculating the exponent $\tilde{\mu}$ is to solve Kirchhoff's laws for an ensemble of random resistor networks[29]. However, it is much easier to obtain the fractal dimension and walk exponent computationally, and obtain $\tilde{\mu}$ indirectly.

Another conductivity exponent simply denoted as μ characterizes disordered systems in terms of their metallic volume fraction. Let p define the volume fraction of metal in a disordered metal-insulator mixture and p_c a specified critical threshold. For $p > p_c$ the material has a finite d.c. conductivity, otherwise the

conductivity is zero in the case that the insulating phase is perfect. Then it is found that the d.c. conductivity goes to zero as

$$\overline{\sigma} \sim (p - p_c)^{\mu} \quad \text{for } p \geq p_c \quad . \tag{2.5}$$

The two conductivity exponents $\tilde{\mu}$ and μ are related to one another using finite size scaling in the next Section.

Another way to characterize how fast a random walker explores a cluster is by its probability to return to its initial starting point taken as the origin. In homogeneous media, $P(0,t) \sim t^{-d/2}$ as obtained from Eq. (1.13) with $R = 0$. A simple argument for the leading time dependence in the return probability is that the probability should scale as the inverse of cluster mass currently explored. Thus $M \sim R^{d_f}$ and $R^2 \sim t^{2/d_w}$ so that

$$P(0,t) \sim t^{-d_f/d_w} = t^{-d_s/2} \tag{2.6}$$

where the exponent $d_s = 2d_f/d_w$ is called the spectral dimension. Note that this result is in agreement with the homogeneous case when $d_w = 2$ and $d_f = d$.

The spectral dimension was first introduced by Alexander and Orbach[42] in connection with the density of states for the lattice vibrations in fractal structures. They further observed that for percolation fractals $d_s \approx 4/3$ for $2 \leq d \leq 6$. If $d_s = 4/3$ exactly, then the fractal dimension and the walk exponent would not be independent! Unfortunately, there is currently no known super-universal scaling relation between the dynamical exponent d_w and *only the static exponents* of the fractals such as d_f. If a scaling relation is to exist, however, then it will surely

need to include other types of exponents that measure additional properties of the clusters. One possible exponent could be d_{BB} which is the fractal dimension of just the backbone of the cluster. Notice, however, that even if some relation did exist using d_{BB}, this exponent is really dynamical because the backbone of the cluster is defined by only the current carrying part. The non-existence of a super-universal relationship indicates that connectivity alone is not sufficient to determine the conductivity properties.

As in the general theory of critical phenomena[44], scale-invariance plays a crucial role in understanding physical properties of a system near criticality. Scaling arguments are given by Gefen *et al*[45] and Havlin *et al.*[46] In Section 2, a discussion on site percolation and diffusion limited aggregates (DLA) is given. Both models produce scale-invariant fractals. In this work d_w is the main exponent of interest, and in Section 3, it is determined from the mean squared displacement which is numerically obtained by exact enumeration. In addition to various scaling relations, the scale-invariance associated with fractal media will allow certain two-variable distribution functions such as $P(R,t)$ to be represented by a scaling function of a single similarity variable. Again data collapsing with properly scaled axes is a very common trait in the subject of critical phenomena. In Section 4, certain scaling functions are found and then used to construct a useful mean-field approximation for time dependent quantities.

2.2 Models of Structural Disorder

Most of the disordered structures that have been studied in this thesis have been generated from a site percolation model.[26] A few reasons for using a site percolation model is that (1) in many cases it accurately represents the disordered system under study. For example, composite materials and disordered thin films such as gold or lead deposits on an insulating substrate have been compared successfully with site percolation. (2) Without having a specific physical system in mind, it is best to choose a simple model with nontrivial and useful properties. (3) Many properties of percolation clusters are well known because they have been studied extensively.[26, 47, 48]

For a given lattice, the site percolation model assigns to every site an independent random variable having a value of 1 with probability p or 0 otherwise. The states 1 and 0 are said to define an *occupied* or *vacant* site respectively. The occupied sites represent a small localized region of metal and the vacant sites represent an insulator. Thus p is the volume fraction of metal in the system. All nearest neighbor occupied sites are then connected. A single realization of a static disordered system remains after this process is finished. There will be many metallic clusters (a set of occupied sites all connected to one another by nearest neighbor connections) of various sizes and shapes within the system. Below p_c an infinite cluster will not exist. Above p_c an infinite cluster will be present and the system is said to be in a percolating state.

Near the critical threshold, some connectivity properties of the disordered sys-

tem behave as

$$P_\infty(p) \propto (p - p_c)^\beta \quad p > p_c \tag{2.7}$$

$$\xi(p) \propto |\, p - p_c \,|^{-\nu} \tag{2.8}$$

$$\overline{S(p)} \propto |\, p - p_c \,|^{-\gamma} \tag{2.9}$$

where p_c is dependent on lattice type as well as other variants in the connectivity rules. However, the exponents β, ν and γ are universal in that they only depend on the dimension d of the embedding space.

The percolation probability $P_\infty(p)$ gives the probability that an occupied site is a member of the infinite cluster. Below the critical threshold $P_\infty(p) = 0$, but just above p_c, P_∞ increases as a power law governed by the exponent β. Note that the d.c. conductivity undergoes a similar change but the conductivity exponent μ is not simply related to β.

The correlation length $\xi(p)$ is the typical spanning length for which a pair of points are connected via some path. However, this length is calculated from finite clusters only. Therefore, above p_c, ξ will decrease as p increases because the presence of large isolated clusters is very improbable. Below p_c the probability of finding a large cluster is also very improbable. However, near p_c, the finite clusters are very large and consequently ξ diverges. If one only considers the set of clusters that have fractal characteristics (scaling properties), then the correlation length can be viewed as the typical spanning length of those *finite* clusters.

Moreover, if a disordered system is coarse grained into cells of volume L^d then on

length scales $L \geq \xi$ the system will behave as a homogeneous medium. On these length scales each cell can be treated as independent and fluctuations between cells can be neglected. Each cell can be replaced by an effective cell having the same properties as the average properties of the ensemble of cells. For length scales $a \ll L \ll \xi$ the medium is self-similar having those consequences previously discussed. Clearly, as the critical threshold is approached ξ diverges and the self-similar nature becomes increasingly more prominent.

The average cluster size $\overline{S(p)}$ for concentrations below the critical threshold also have a power law divergence as $p \rightarrow p_c$. Now with γ, ν and β being defined exponents, it follows from the scaling theory of percolation[26] that these static exponents are related to one another by the universal hyper scaling relation

$$2\beta + \gamma = \nu d \quad d \leq 6 \quad . \tag{2.10}$$

Noting that $P_\infty \sim \xi^{d_f}/\xi^d$ slightly above the threshold, it follows that

$$d_f = d - \frac{\beta}{\nu} \quad . \tag{2.11}$$

From finite size scaling[35] the two conductivity exponents from Section 1 are related by $\mu = \nu\tilde{\mu}$, and combining this with Eqs. (2.11 and 2.4) it follows that

$$d_w = 2 + \frac{\mu - \beta}{\nu} \quad . \tag{2.12}$$

The walk exponent d_w characterizes the Brownian motion on a restricted ensemble of *large* clusters that are self-similar on all length scales considered.

On the other hand, the mean squared displacement of the random walk is characterized by a different walk exponent called d'_w when the ensemble is over all clusters in the system. It has been shown[35, 37] that the relationship between the two walk exponents is given by

$$d'_w = \frac{d_w}{1 - \beta/2\nu} \quad . \tag{2.13}$$

Since the walk exponent d_w is much easier to calculate numerically than d'_w by using only a restricted ensemble, the remainder of this Chapter will deal exclusively with the restricted ensemble of large self-similar clusters. Besides percolation clusters, estimates for d_w can also be made for different types of fractal clusters with different fractal dimension d_f such as *diffusion limited aggregates*[49] (DLA.)

There are many different ways to generate a restricted ensemble of site percolation clusters. The simple and efficient method that was predominately used for generating clusters was a *breadth-first search* as introduced by Leath[27]. The algorithm used here is from an improved version by Alexandrowicz[28] and Fig. 2.3 shows a typical snap shot of the growing process.

Here the cluster is grown starting from an occupied seed site in a series of shells. Each perimeter site of a current shell is checked if it is occupied with probability p (otherwise vacant). After *all* the perimeter sites have been checked, then all possible nearest neighbor links are formed between occupied sites. The process continues because the collection of all unchecked nearest neighbor sites to the lastest set of occupied sites will form a new set of perimeter sites. It follows

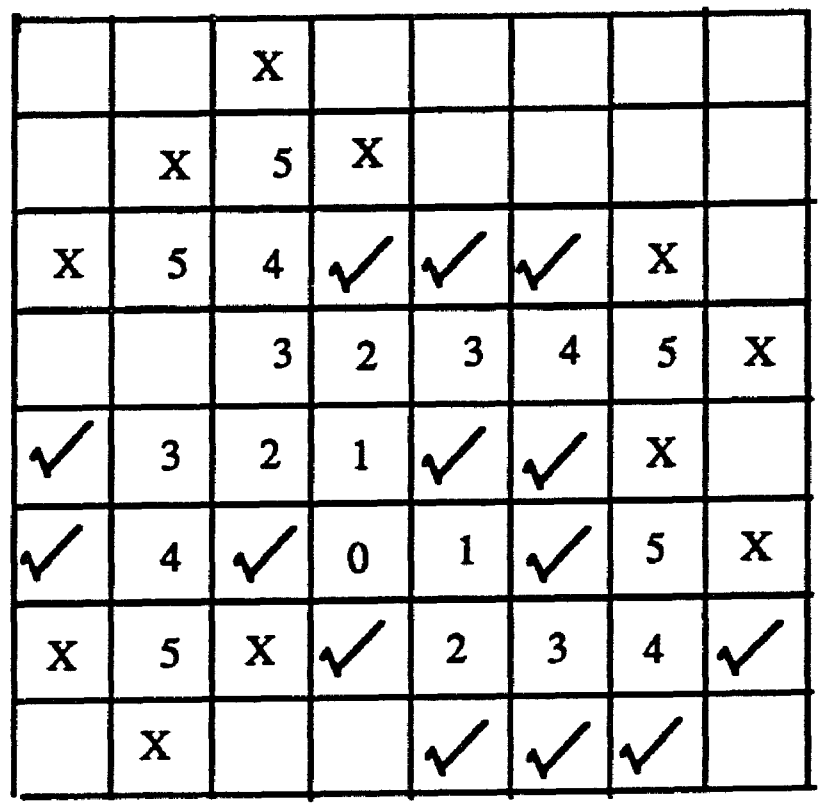

Figure 2.3

This cluster is being grown using the breadth-first search. Each site is numbered by generation corresponding to the chemical distance from the seed which itself is taken as the 0th generation. The $\surd$ sites are vacant and the $\times$ sites form the perimeter to be checked for the next generation.

that all sites within the cluster belong to a shell of certain generation defined by the *chemical distance* from the seed. The chemical distance (l) of a certain site is the shortest path between that site and the seed.

The clusters grown using the breadth-first search form *finite* clusters. The growth can either stop naturally, or is terminated after the cluster obtains a predetermined number of sites (S) or reaches a chemical distance l_o such that all sites contained within the cluster have a chemical distance $l \leq l_o$. These clusters will be referred to as being in the (p, S) or (p, l) ensembles. Unless explicitly stated no distinction between the clusters that naturally stopped growing (equilibrium clusters) and the ones terminated (growing clusters) will be made.

Another way to grow finite clusters uses a variant growth rule. These clusters will be referred to here as epidemic growth clusters. The epidemic growth clusters are grown by selecting a perimeter site (*growth* site) at random for the determination if the site is occupied or vacant. When the site is found to be occupied, it is connected to the cluster and then its unchecked nearest neighbors immediately become members of the set of growth sites. The epidemic growth clusters are *not* built up shell by shell but rather represent an epidemic growth process[50]. Both the equilibrium breath-first search and epidemic clusters form an identical ensemble. However, we have observed[51] that there are differencies between the still growing clusters depending on if grown from the breath-first search or epidemic growth rules. In this thesis, the differencies are of no concern because they enter only as correction terms to the leading scaling behavior. We give a detailed

comparison in ref.[51] where it is noted that the breath-first search and epidemic clusters were referred to as the Leath and Alexandrowicz clusters respectively.

On the square lattice, another method in generating large single site percolation clusters was used. Here a square mesh of side L which contains L^2 sites is first defined. Each site is independently determined to be occupied with probability p (otherwise vacant). Then all nearest neighbor occupied sites are linked together. If a connected path between the top and bottom sides as well as the left and right sides are found to exist then the system is percolating. Note that what is meant by a connected path between opposite edges is that *if* periodic boundary conditions were used, then the resulting medium *would* contain an infinite cluster extending in both the x *and* y directions. Figure 2.4 shows a configuration which is not percolating according to the above rules.

If a percolating cluster is not found then the realization is thrown away, otherwise only the percolating cluster is retained and the remaining isolated finite clusters are thrown away. With free boundary conditions, the procedure in determining the isolated finite clusters is straight forward. With periodic boundaries, additional links are *actually* formed between sites on opposite edges and therefore some *would be* finite clusters become part of the percolating cluster as Fig. 2.5 demonstrates. The clusters generated in this fashion will form a (p, L) ensemble.

In all of the above cases, $p = p_c$ was used in generating the clusters to create the self-similar fractal structure of interest. Although the correlation length ξ is infinite at p_c, the self-similarity property at large length scales obviously breaks

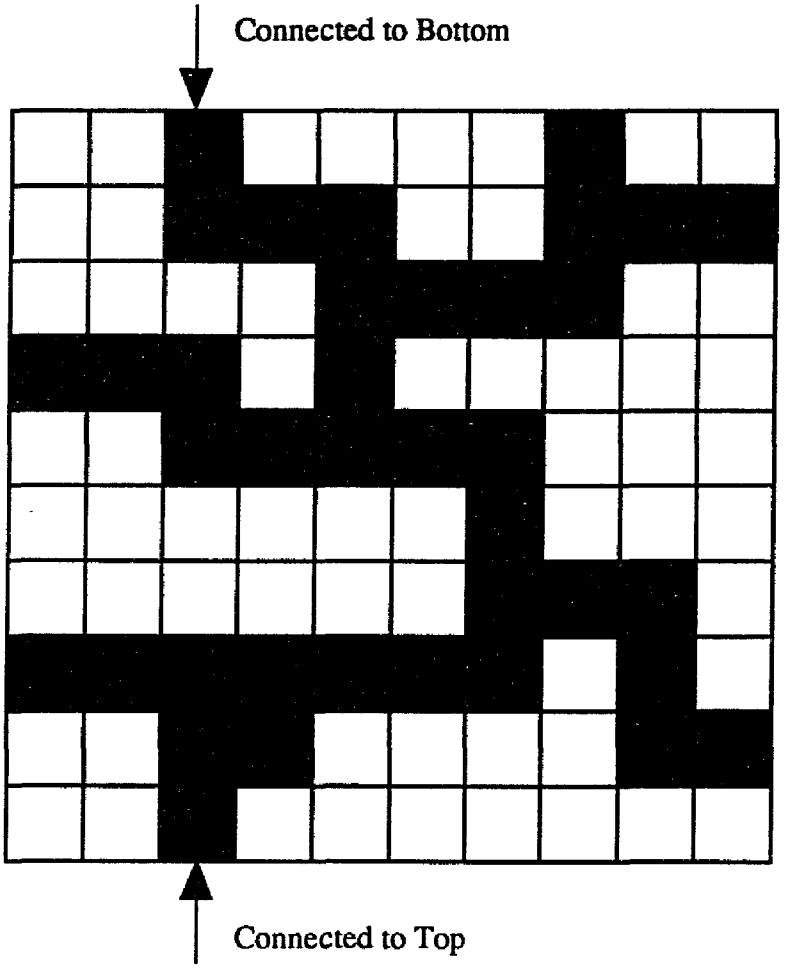

Figure 2.4

A square mesh of side $L = 10$ containing 100 sites. The colored sites are occupied. A connected path exist from top to bottom but not from right to left based on the strict definition that a periodic system must form a connection from $-\infty$ to $+\infty$. Thus this configuration is rejected.

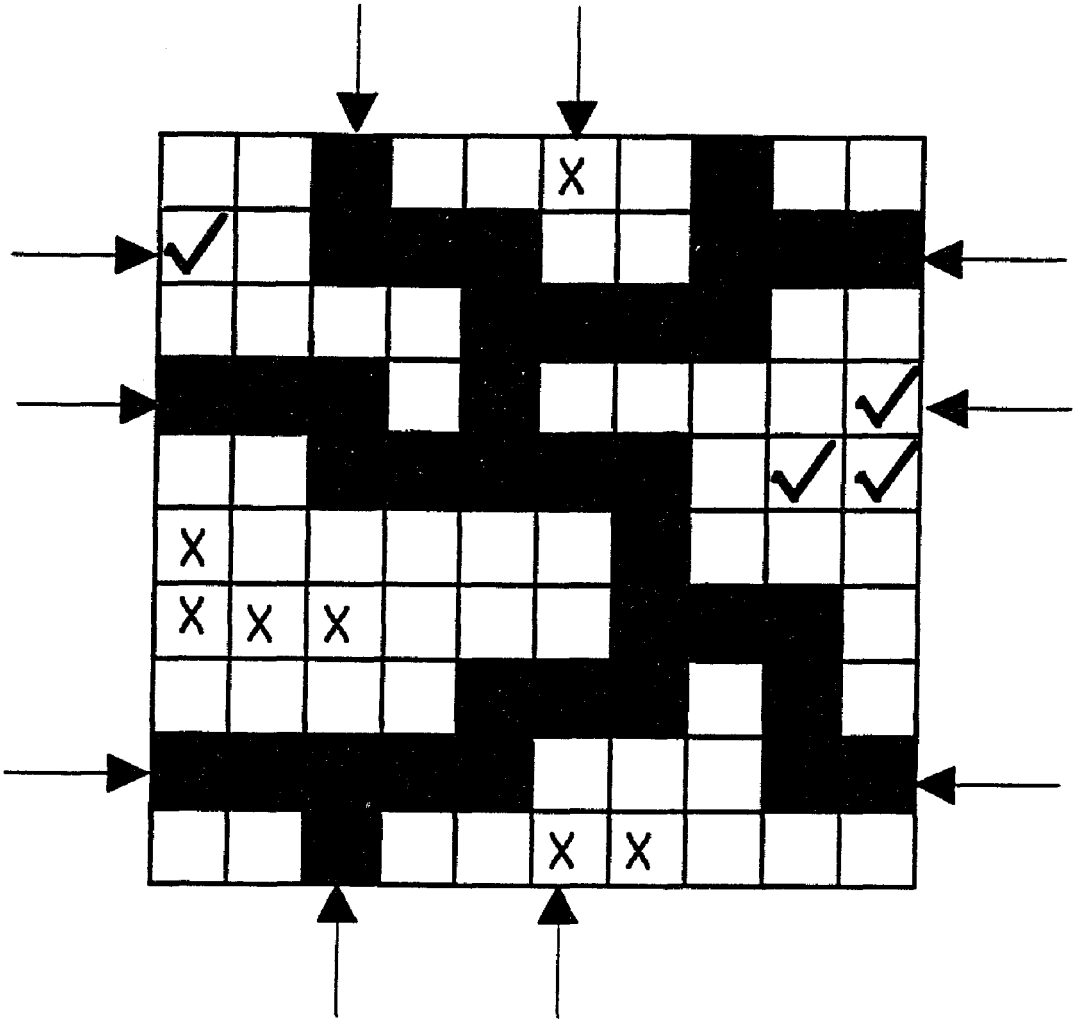

Figure 2.5

Sites with an $\times$, $\surd$ or are colored define occupied sites. As seen from the colored sites the system is percolating. The $\times$ sites (forming isolated clusters) are thrown away. The $\surd$ sites are (thrown away, connected) for (free, periodic) boundary conditions.

down for finite clusters. Also self-similarity breaks down in the so called "infinite" (p_c, L) clusters when periodic boundary conditions are implemented because of the enforced periodity of length L. Therefore, in the numerical analysis of the mean squared displacement corrections due to finite size effects (ie. the number of sites considered in a cluster is finite) and the type of boundary conditions must be taken into account to extract d_w.

Also on the square lattice, DLA clusters were generated to produce a different type of fractal structure.[49, 52] A typical DLA cluster is shown in Fig 2.6. In Appendix A, a short description of how the clusters were constructed is given. Basically, the DLA model

starts with a seed site at the origin and a random walker (diffusing particle) starting from infinity. Eventually the walker will sweep by the seed at a nearest neighbor distance. When the walker is at a nearest neighbor distance from any other particle of the aggregate there is a probability of p to stick. If the walker sticks it stays there forever and becomes part of the aggregate. Once the particle does stick, then another random walker is injected from infinity. As the cluster (or aggregate) grows in size, the easier it becomes to catch a random walker. The process is terminated when the cluster reaches a predetermined size S. The clusters form a (p, S) ensemble were p denotes the sticking probability. The DLA clusters generated here had a sticking probability of $p = 1$.

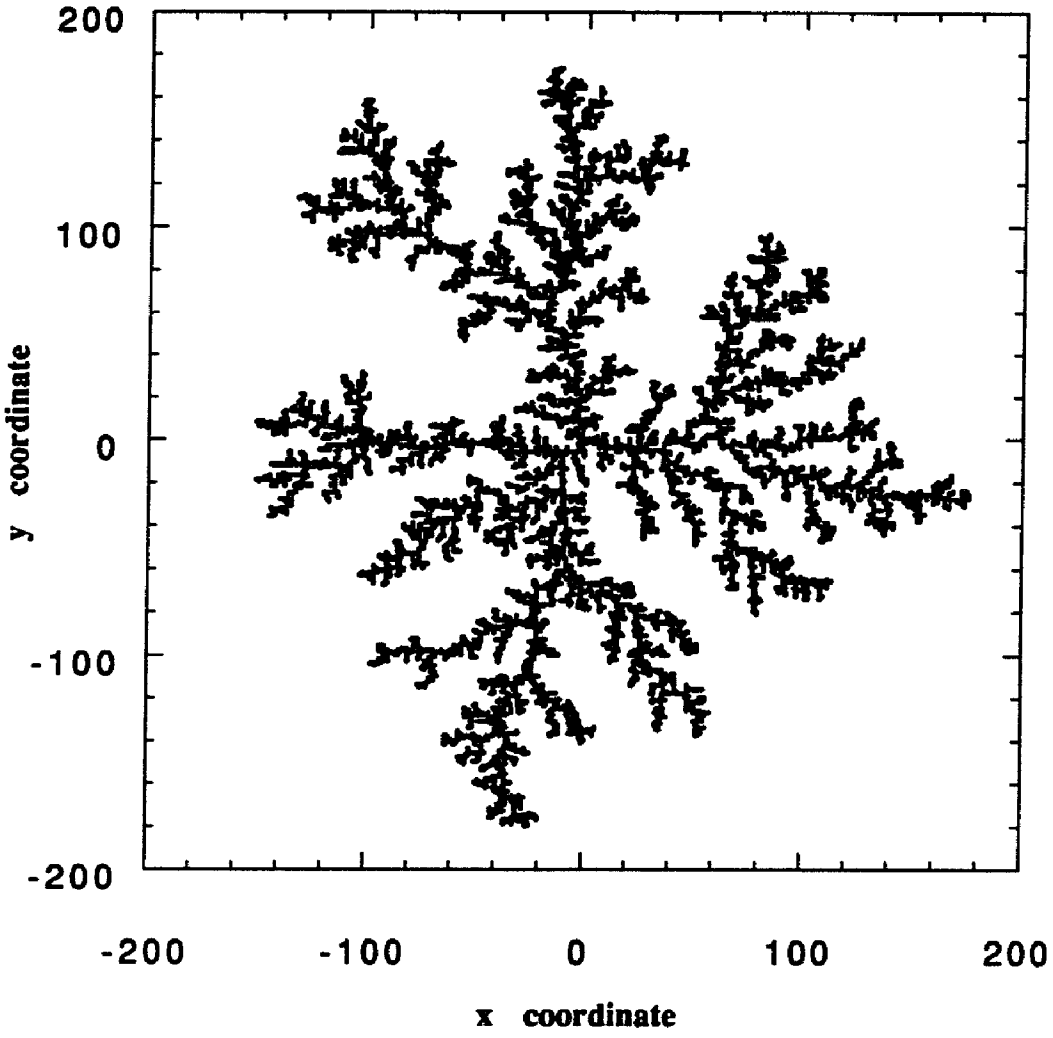

Figure 2.6

A typical picture of a diffusion limited aggregate. This aggregate was generated on a square lattice and contains 5000 sites.

2.3 Critical Exponents for Random Walks

The walk exponent d_w in Eq. (2.3) can be obtained from the mean squared displacement. A mathematical formalism suitable for studying discrete time random walks on a lattice is presented and then used to estimate d_w for the *myopic* and *blind* ant random walks. The choice of notation has been made for clarity and consistency throughout the thesis. Included in the discussion is the numerical methodology in the extraction of d_w from the numerical data. Furthermore, a comparison of the mean squared displacement on clusters generated with free and periodic boundary conditions is made for the square lattice.

For a given cluster, the mean squared displacement after n steps is expressed as

$$\langle R(n)^2 \rangle = \langle [\vec{r}(s_n) - \vec{r}(s_0)]^2 \rangle \quad , \tag{2.14}$$

where $\vec{r}(s_n)$ is the position vector of site s_n. More specifically $1 \leq s_n \leq S$ where S is the total number of sites in the cluster. The subscript n on s_n simply refers to the nth random event which defines discrete time. The sequence $\Omega_n = \{s_0, s_1, \ldots, s_n\}$ specifies one Brownian path (realization Ω_n) of a random walker. The entire set of *all* realizations $\{\Omega_n\}$ form the ensemble over which the average in Eq. (2.14) is taken. Only Markov processes are considered here so that the probability of a Brownian path is given by

$$P[\Omega_n] = \prod_{i=1}^{n} w(s_i, s_{i-1}) \tag{2.15}$$

where $w(s_f, s_o)$ gives the probability to hop from site s_o to site s_f. Note that

$w(s_f, s_o)$ is an element of a *transition probability matrix* $(\hat{W})$ in a S dimensional state space. Books on stochastic processes should be consulted for more details.[12, 53]

The step displacement auto-correlation function (SACF) is given by

$$\langle \vec{\rho}(n) \cdot \vec{\rho}(0) \rangle = \langle [\, \vec{r}(s_{n+1}) - \vec{r}(s_n) \,] \cdot [\, \vec{r}(s_1) - \vec{r}(s_0) \,] \rangle \quad , \tag{2.16}$$

and many other auto-correlation functions can be constructed such that their averages can similarly be expanded into terms of the form $\langle \vec{r}(s_i) \cdot \vec{r}(s_n) \rangle$. The latter function itself is a position auto-correlation function which will be written more simply as $\langle \vec{r}(i) \cdot \vec{r}(n) \rangle$.

In addition to knowing the probability for each Brownian path, the initial condition of the random process must be specified by $P_o[s_0]$ which gives the probability that the walker started at site s_0 at $n = 0$. Stationary processes will be the main focus here. Therefore let us begin by choosing the initial condition to be defined by the state vector $V_1(s_0)$ where V_1 is an eigenvector of $\hat{W}$ with eigenvalue 1. An eigenvalue of 1 must exist as it is a consequence of conservation of probability. Moreover, all the sites in a cluster are connected and only random walk models that allow for the walker to reach any point on the cluster from any starting point is considered. Therefore, it follows that the eigenvalue 1 is nondegenerate.[53]

A discrete time derivative of a function $F(n)$ will be defined as

$$\frac{d}{dn} F(n) \equiv F(n+1) - F(n) \quad . \tag{2.17}$$

With stationary initial conditions it follows that

$$\langle R(n)^2 \rangle_{eq} = 2\left[\langle r^2(0)\rangle_{eq} - \langle \vec{r}(n)\cdot\vec{r}(0)\rangle_{eq}\right] \tag{2.18}$$

$$\langle \vec{\rho}(n+1)\cdot\vec{\rho}(0)\rangle_{eq} = \frac{1}{2}\frac{d^2}{dn^2}\langle R(n)^2\rangle_{eq} \tag{2.19}$$

where the subscript eq denotes that the system is in equilibrium. The equilibrium state is assumed to be described by the stationary initial condition since no external biases are being considered. The mean squared displacement and SACF can be obtained by simply calculating the position auto-correlation function which is explicitly given as

$$\langle \vec{r}(n)\cdot\vec{r}(0)\rangle_{eq} = \sum_{j=1}^{d}\sum_{\{s_i\}_n} x_j(s_n)x_j(s_0)\prod_{i=1}^{n} w(s_i,s_{i-1})\,V_1(s_0) \tag{2.20}$$

where x_j is just the jth component of the position vector. Note that Eqs. (2.18 and 2.20) are valid only for finite clusters with free boundary conditions.

It follows from expanding Eq. (2.14) that the mean squared displacement can be calculated from the quantities $\langle r(0)^2\rangle$, $\langle r(n)^2\rangle$, and $\langle \vec{r}(n)\cdot\vec{r}(0)\rangle$ for non-stationary initial conditions. In particular, if the random walker starts at the origin ($\vec{r}(s_0=1)=\vec{0}$) with the initial probability given by $\delta_{s_0,1}$, then the mean squared displacement is equal to $\langle r(n)^2\rangle_o$ where the subscript o denotes starting at the origin. Furthermore, by expanding Eq. (2.16) it follows that the SACF can be calculated from $\langle \vec{r}(n)\cdot\vec{r}(0)\rangle$ and $\langle \vec{r}(n)\cdot\vec{r}(1)\rangle$. However, the simple relationship between the SACF and mean squared displacement as given in Eq. (2.19) will not be valid.

A configurational average must now be performed on Eq. (2.20). For simplicity only the jth component of the vector dot product will be considered. With a rearrangement of terms, it follows that

$$\overline{\langle x_j(n)x_j(0)\rangle_{eq}} = \sum_C P(C) \sum_{\{s_i\}_n} x_j(s_n) \prod_{i=1}^{n} w(s_i, s_{i-1} \mid C)\, x_j(s_0) V_1(s_0) \qquad (2.21)$$

where C is a random variable corresponding to a given cluster. The probability $P(C)$ is determined by the model of disorder and choice of ensemble. Explicit reference to the cluster C is made in the transition matrix to stress that this matrix is itself a random "variable". Note that the dimension of the state space and the stationary eigenvector are dependent upon the cluster C. The configurational average is done by averaging the results over many randomly generated clusters. Therefore, explicit reference to the configurational average will be dropped since numerically one cluster is dealt with at a time.

The formalism developed above is useful for finite clusters with free boundary conditions. However, if a cluster was generated from the (p, L) ensemble with periodic boundary conditions, then the position auto-correlation function is undefined because $\vec{r}(s)$ is not unique. However, the SACF is well defined since it only involves step displacements of the random walker. An expression for the SACF will be developed here in matrix notation. Let the matrix $\hat{P}$ have all zero off-diagonal elements and the diagonal elements are just given by the initial probability P_o. Also define a matrix $\hat{O}_{\rho_j}$ such that its elements are given as

$$o_{\rho_j}(s_f, s_o) \equiv w(s_f, s_o)[x_j(s_f) - x_j(s_o)] \quad . \qquad (2.22)$$

Then the SACF is given by

$$\langle \vec{\rho}(n)\vec{\rho}(0)\rangle = \sum_{j=1}^{d} TR[\hat{O}_{\rho_j}\hat{W}^{n-1}\hat{O}_{\rho_j}\hat{P}] \quad \text{for } n \geq 1 \tag{2.23}$$

and

$$\langle \rho(0)^2\rangle = \sum_{j=1}^{d}\sum_{s_1}\sum_{s_0}[x_j(s_1) - x_j(s_0)]^2\, w(s_1, s_0)P_o(s_0) \tag{2.24}$$

where the $n = 0$ term is treated as a special case.

Since the ensemble of realizations $\{\Omega_n\}$ in principle includes S^{n+1} elements, to assist in the calculation of the mean squared displacement, SACF or other average values, Monte Carlo *simulation* can be performed[38, 39, 40]. However, in most applications $w(s_f, s_o)$ is short ranged reducing the size of the ensemble greatly. Therefore it becomes not only possible but practical to perform an *exact enumeration* which sums over all Brownian paths[41] using recursion relations involving matrix multiplication. Specific details on the algorithms used can be found in Appendix B. These algorithms are extensions to that of Majid *et al*[31] because they can be applied to the calculation of correlation functions, and all starting points can be enumerated simultaneously. In particular, we consider the myopic and blind ant random walk models where the term "ant" refers to the random walker as introduced by de Genes.

A myopic ant will move to any of its *occupied* nearest neighbors with equal probability per step. Thus the myopic ant can see what options are available one step ahead. The myopic ant always makes a jump at each time step. Defining $\zeta(s)$ as the number of nearest neighbor occupied sites to site s the elements of the

myopic ant transition matrix are given by

$$w(s_f, s_o) = \begin{cases} \frac{1}{\zeta(s_o)} & \text{for nearest neighbors} \\ 0 & \text{otherwise} \end{cases} \tag{2.25}$$

Furthermore, from detailed balance, the normalized stationary eigenvector is given by

$$V_1(s) = \zeta(s) / \sum_{s'=1}^{S} \zeta(s') \tag{2.26}$$

A blind ant tries to move to any nearest neighbor site of an underling lattice with equal probability per time step. If the ant encounters a *vacant* site, then it cannot move and must stay at its current position. Thus the blind ant cannot see ahead. Defining z as the coordination number of the underlying lattice, the elements of the blind ant transition matrix are given by

$$w(s_f, s_o) = \begin{cases} \frac{1}{z} & \text{for nearest neighbors} \\ \frac{z-\zeta(s_o)}{z} & \text{for } s_f = s_o \\ 0 & \text{otherwise} \end{cases} \tag{2.27}$$

Furthermore, from detailed balance, the normalized stationary eigenvector is given by

$$V_1(s) = 1/S \tag{2.28}$$

The mean squared displacement for the myopic and blind ant on a typical site percolation cluster on the square lattice from a ($p_c \approx 0.593$, $S = 5000$) ensemble is shown in Fig. 2.7. The lattice constant is taken to be the unit of length ($a = 1$). This data was obtained using stationary initial conditions. Because all

the Brownian paths are enumerated at every starting point within the cluster, the mean squared displacement is a very smooth function. It is found that at early times the myopic ant explores more of the cluster than the blind ant. However, at extremely long times, both ants will explore the entire cluster. Obviously, because the cluster is finite the mean squared displacement will saturate to a maximum value characteristic of the cluster size. The curvature seen in the mean squared displacement in Fig. 2.7 is caused mainly by the fractal nature of the cluster as opposed to a simple consequence of saturation. The saturation values of the mean squared displacement for the myopic and blind ant for this cluster are 4249 and 4255 respectively. At time $n = 10000$ the myopic (blind) ant has explored approximately $\langle R(n)^2 \rangle / R_M^2 = 18\%$ (14%) of the cluster. Of course finite size effects do play a role in the curvature, therefore, they either need to be minimized so that they can be safely neglected or appropriate corrections must be taken into account.

There are two simple approaches to overcome the finite size effects. The first approach[31, 38, 54] is to use large clusters and start the random walker near the seed site. Then the probability for the random walker to reach the outer limit is sufficiently small so that the cluster appears infinite as long as the number of time steps is not too great. A problem of this approach is that thousands of large clusters and long times (without saturation effects) are required to accurately obtain d_w. The other approach is to use stationary initial conditions which decreases the number of random clusters needed for a configuration average. However, it becomes

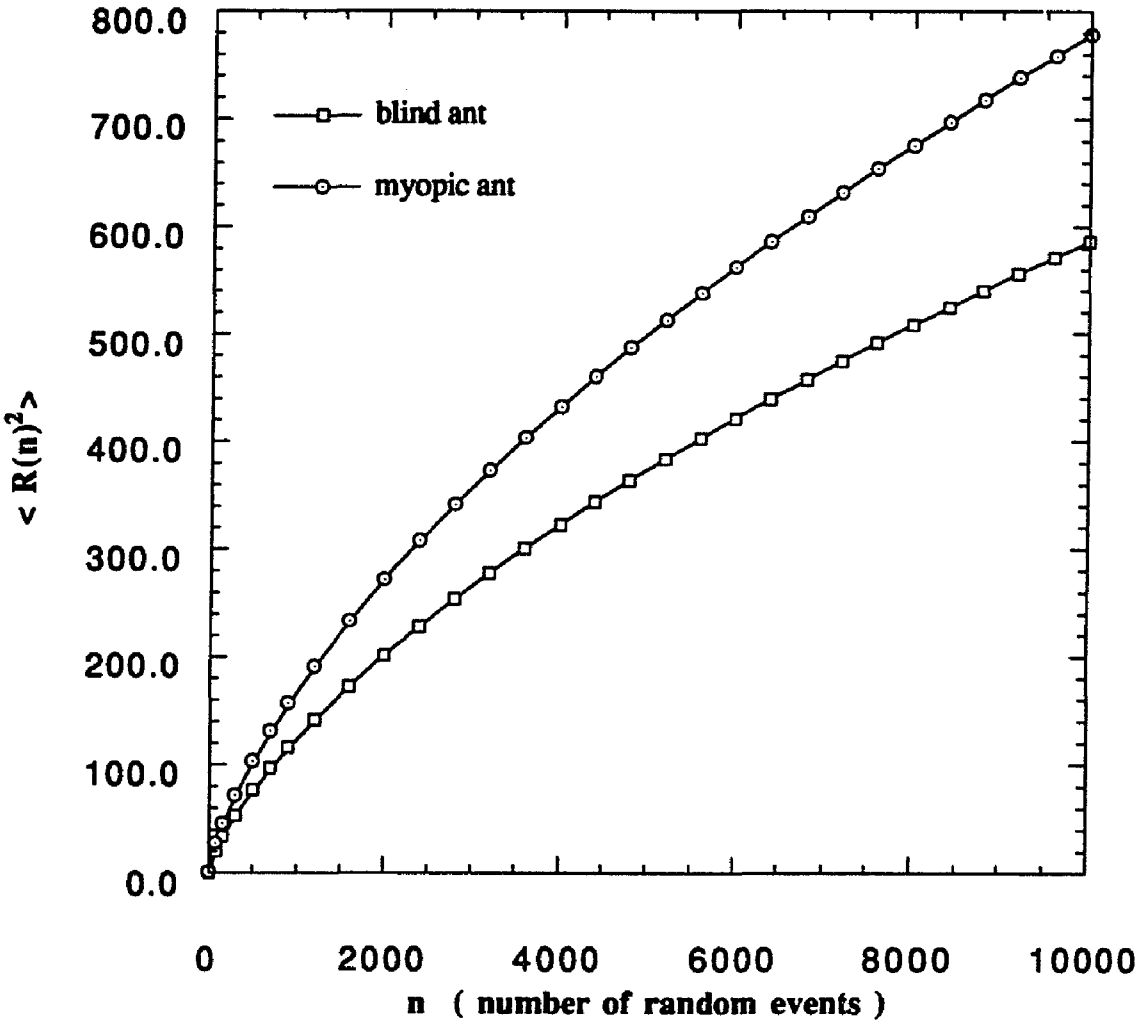

Figure 2.7

The mean square displacement for the myopic ant (○) and blind ant (□) on a typical percolation cluster of size $S = 5000$ at the percolation threshold. All starting points are enumerated with stationary initial conditions.

necessary to incorporate the saturation of the mean squared displacement by fitting the numerical data to a suitable function. The fitting function is in some sense phenomenological. Although, both methods are reasonable solutions in overcoming finite size effects, the latter approach is much less sensitive to the fit range as we pointed out[41].

The data will be fitted to a function given by

$$\langle R(n)^2 \rangle \approx R_M^2 \left[1 - A \exp(-(\frac{n}{B})^C) \right] \tag{2.29}$$

where A, B, and C are fitting parameters. Note that this fitting function works well for a single cluster. The leading term in the Taylor expansion of Eq. (2.29) should be independent of the size of the clusters for configurational averaged data. Therefore we can identify $C = 2/d_w$, and it follows that $B \propto (R_M^2)^{d_w/2}$. Note that B defines a crossover time for which saturation becomes dominant. For all the data that Eq. (2.29) was fitted, the ratio $n/B < 1$ so that saturation effects were not dominate. The saturation level of the mean squared displacement can be calculated exactly from

$$R_M^2 = 2 \sum_{s=1}^{S} r(s)^2 \, V_1(s) - 2 [\sum_{s=1}^{S} \vec{r}(s) V_1(s)]^2 \quad . \tag{2.30}$$

Note that R_M^2 is just the radius of gyration of the cluster if $V_1(s)$ is interpreted as the "mass" of site s. It has been shown[38] that $R_M^2 \propto S^{2/d_f}$ which implies $B \propto S^{d_w/d_f}$.

Some particular details of the fitting procedure to extract d_w are discussed here for the case of a square lattice. The numerical data for the mean squared

displacement was usually calculated in the range ($1 \leq n \leq 10000$). The results for the myopic mean squared displacement from a configurational average over 100 clusters from a ($p_c = 0.593$, $S = 60000$) ensemble is plotted on a log-log scale in Fig. 2.8. This data set corresponds to the largest size clusters generated. The maximum ratio of n/B occurring at $n = 10000$ was only ≈ 0.008 and therefore the finite size corrections are indeed small. After throwing away the first 100 time steps of the data (to assure that we meet the condition $a \ll L$), a least squares fit over the two remaining decades results in $d_w = 2.80$. This approach is very simple and quick, but it is too simple minded. Before this value is accepted, one should check for systematic tendencies in the fitting procedure.

Although Fig. 2.8 shows a nearly straight line, the slope is obtained over different time step domains. From a least squares fit the slope (hence d_w) is found for time steps between ($100 < n \leq N$), where N may vary between 200 to 10000. The walk exponent is now a function of N as Fig. 2.9 shows. Clearly there is a remarkable curvature to the line in Fig. 2.8. Thus, this simple estimation for d_w is very sensitive to the range of fitting. This curvature is not attributed to the asymptotic power-law corrections but rather to the finite size of the clusters. With stationary initial conditions, finite size corrections appear immediately because many walks start at or near the perimeter of the cluster. Therefore, the fitting function of Eq. (2.29) will be used to account for the curvature.

The fitting of Eq. (2.29) to the data can be obtained by multivariable non-linear regression. However, it was found that the best way to estimate A, B, and

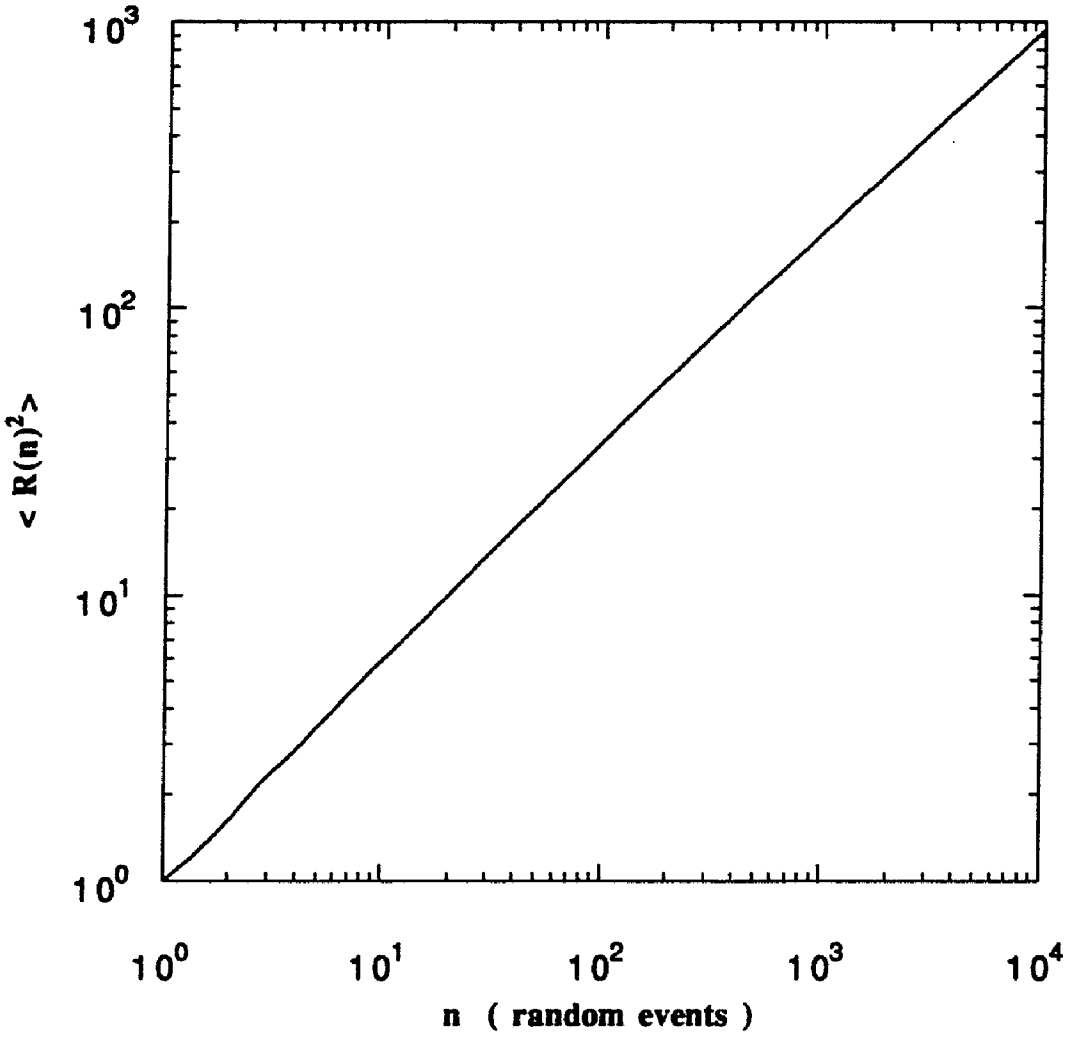

Figure 2.8

Typical plot of the mean square displacement for the myopic ant. This data has been averaged over 100 clusters of size 60000 sites at the critical threshold on the square lattice. The slope of this line yields $2/d_w$.

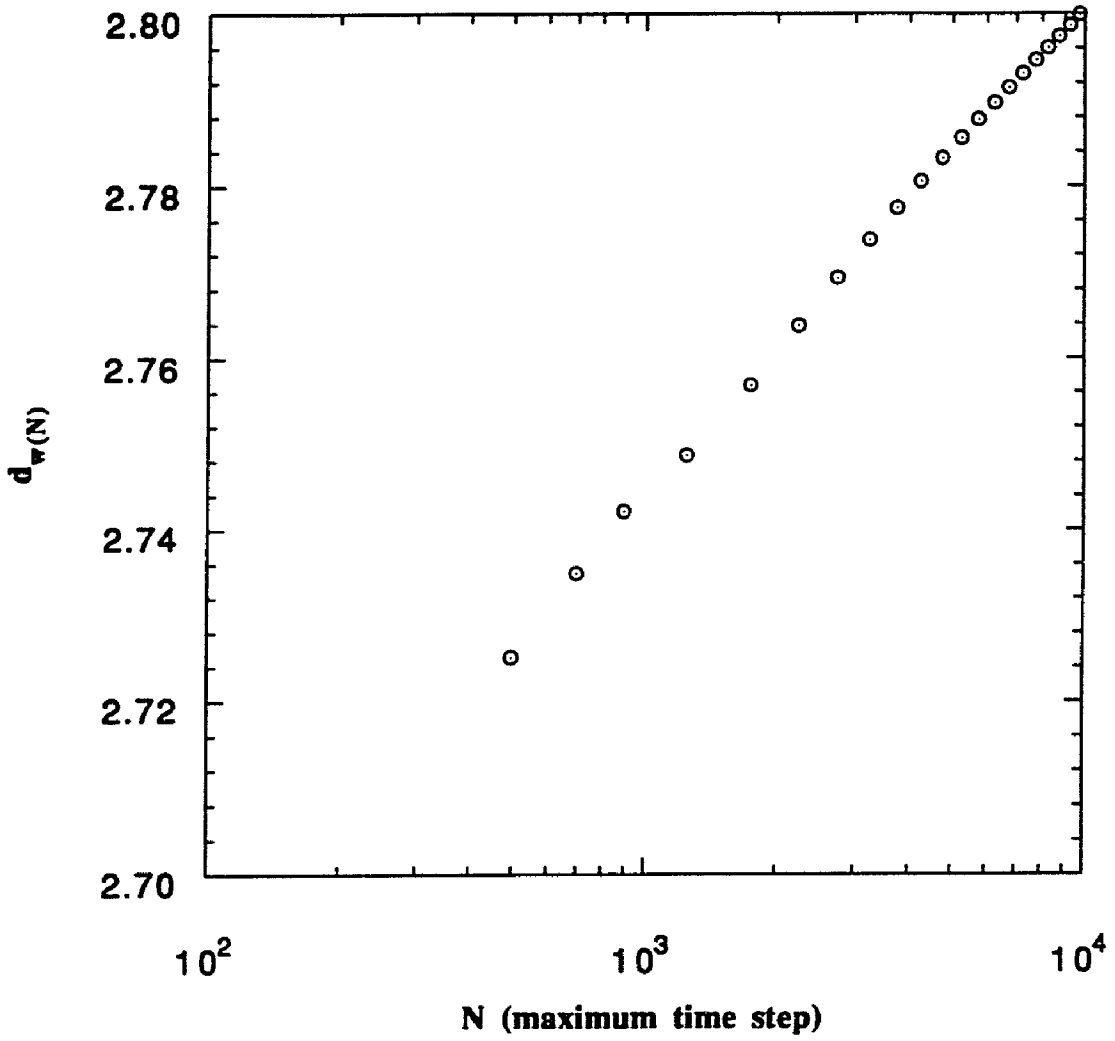

Figure 2.9

The walk exponent as obtained from a log-log plot of the mean squared displacement as a function of N where the fitting range over step number (n) was performed between ($100 \leq n \leq N$). These fits were taken on the same data as in Fig. 2.8.

C was to guess A and apply a standard linear least squares fit to the data set $\{X(n), Y(n)\}$ where $X(n) \equiv \ln(n)$ and

$$Y(n) \equiv \ln \mid \ln \mid \frac{R_M^2 - (R(n)^2)}{AR_M^2} \mid\mid \quad . \tag{2.31}$$

If Eq. (2.29) is approximately correct, then for the best value of A it should produce a linear Y verses X plot. Indeed this is found to be true, and by guessing many values of A a global minimum in the error can be found in order to obtain the desired three parameter fit. The slope of the Y verses X plot is equal to C and the $\ln B$ is just the Y intercept.

Again the estimated value for d_w should not be accepted until the dependence on the step range is checked. The procedure of obtaining a global minimum is repeated for various step ranges. The parameter A is varied slightly around its global minimum as a way to estimate uncertainties and to observe internal consistency in the procedure. Therefore the walk exponent is viewed as a function of N and A as shown in Fig. 2.10. A two parameter fit was performed for each specified value of A. The collection of fits show a large spread in the estimates for d_w, however, the extreme limits that are plotted are not nearly as good fits as in the center regions. Therefore, by knowing the optimal fit as well as seeing the maximum spread that define reasonable fits, an estimated error bar can be assigned to the extracted d_w.

The optimal fit shown in Fig. 2.10 is not as sensitive to the fit range as the direct two parameter power-law fit. But more importantly, the direct power-law

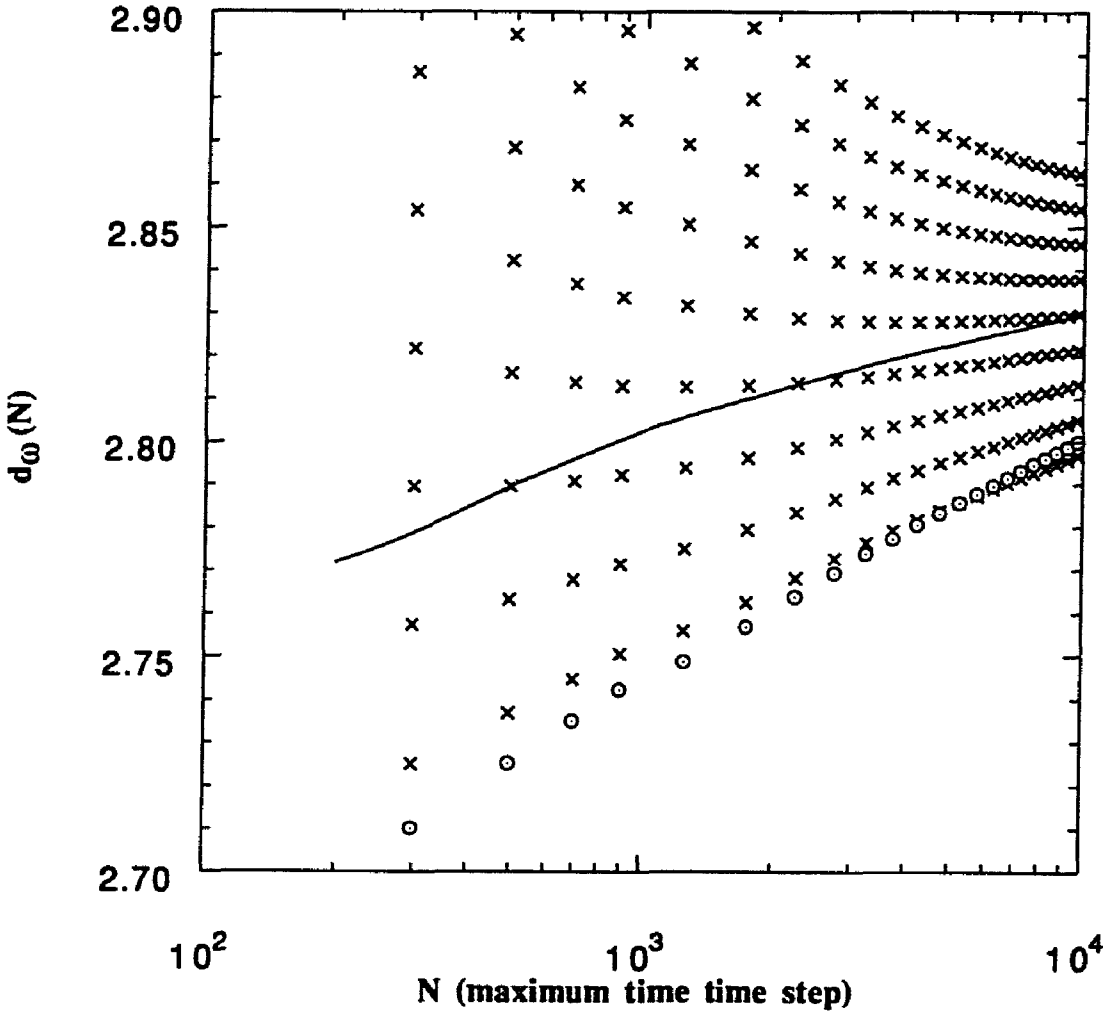

Figure 2.10

The walk exponent as determined from Eq. (2.28) is viewed as a function of (N, A) and is plotted verses N for various values of A. $R_M^2 = 61123.5$ as calculated from the same data as in Fig. 2.8. The value of A ranges from 0.5×10^{-5} to 8.5×10^{-5} in increments of $\Delta A = 1 \times 10^{-5}$. Note that the lines $(\times)$ of constant A do not intersect, and the (lowest, greatest) A corresponds to the (bottom, top) curve. The optimal fit (A not constant) is shown by the solid line. Also Fig. 2.9 is repeated $(\bigcirc)$ for comparison.

fit is an unreliable procedure because inevitably it indicates that $d_w(N) \to \infty$ as $N \to \infty$. In contrast, the optimal fit for Eq. (2.29) will level out as the finite size corrections become stronger. Note that after 10000 time steps the myopic ant only explored approximately 1.5% of a cluster and yet Fig. 2.10 already indicates a convergence of $d_w \approx 2.83$. As long as Eq. (2.29) is a good representative fitting form (as verified from residual plots) a better fit can be obtained when the walker is allowed to explore more of the cluster. Interestingly, the initial problem was to avoid the finite size of the clusters, but now the finite size actually helps to estimate d_w. Note that the fitting form is valid in the range $1 \ll n \ll B$ allowing an ant to explore as much as 50% of a cluster. Additional details can be found in ref.[41] on clusters of average size ≈ 12000.

A summary of the estimated values for d_w on various lattices for the myopic (blind) ant is given in Table 2.1 (2.2) and the best fit parameters obtained for Eq. 2.29 are given in Table 2.3 (2.4). A summary of the crucial points in the fitting to Eq. (2.29) are as follows: (1) The method is self consistent in the sense that d_w is insensitive to the fitting range. (2) The overall spread in the estimated value of d_w decreases as N increases. (3) As N increases the fitting error per data point remains nearly a constant. (4) The method is also insensitive to the size of the clusters. For example, the estimated d_w for clusters of size $S = 15000$ are in good agreement with those of $S = 60000$.

Our final estimate for d_w for the (blind, myopic) ant is given as (2.84 ± 0.03, 2.83 ± 0.03) on $2-d$ percolation clusters, (3.59 ± 0.04, 3.57 ± 0.04) on $3-d$ percolation

Table 2.1

The large scale results for the estimates of the walk exponent for the myopic ant are summarized here.
[a b c] Average size of the clusters at $L = \{300, 200, 100\}$ respectively using a (p_c, L) ensemble.

trial	lattice	p	S	cluster #	d_w
M1	bcc	0.245	30000	100	3.62 ± 0.03
M2	sc	0.312	60000	100	3.65 ± 0.03
M3	sq	0.593	60000	100	2.83 ± 0.04
M4	sq	0.593	15000	200	2.84 ± 0.03
M5	sq	0.593	5000	60	2.84 ± 0.02
M6	sq	0.593	32944[a]	20	2.83 ± 0.03
M7	sq	0.593	14465[b]	20	2.84 ± 0.04
M8	sq	0.593	3740[c]	20	2.80 ± 0.04
M13	fcc	0.200	10000	20	3.51 ± 0.02
M14	fcc	0.200	5000	20	3.54 ± 0.03
M15	tr	0.500	15000	20	2.82 ± 0.03
M12	sq	DLA	15000	100	2.63 ± 0.04

Table 2.2

The large scale results for the estimates of the walk exponent for the blind ant are summarized here.

trial	lattice	p	S	cluster #	d_w
B1	bcc	0.245	15000	20	3.63 ± 0.04
B2	sc	0.312	15000	20	3.61 ± 0.03
B3	fcc	0.20	15000	20	3.61 ± 0.04
B4	fcc	0.20	10000	20	3.57 ± 0.03
B5	fcc	0.20	5000	20	3.54 ± 0.03
B6	sq	0.593	5000	60	2.85 ± 0.02
B7	sq	0.593	15000	20	2.82 ± 0.03
B8	tr	0.50	15000	20	2.84 ± 0.03

Table 2.3

A summary for the myopic ant on the parameters $\{R_M^2, A, B, C\}$ where R_M^2 was calculated exactly with Eq. (2.29) and the remaining parameters were obtained from fitting to Eq. (2.28) over a time step range $100 \leq n \leq 10000$.

trial	R_M^2	A	B	C
M1	10471.5	1.00061	1.196×10^6	0.55261
M2	6057.34	1.00042	3.360×10^6	0.54796
M3	61123.5	1.000045	3.640×10^6	0.70670
M4	14400.7	1.00021	4.805×10^5	0.70440
M5	4361.4	1.00070	8.821×10^4	0.70440
M6	25990.0	1.00009	1.091×10^6	0.70750
M7	11406.0	1.00022	3.500×10^5	0.70470
M8	2869.0	1.00059	4.740×10^4	0.71120
M13	2965.43	1.00104	2.029×10^5	0.56900
M14	1792.74	1.00126	3.349×10^5	0.56421
M15	17928	1.00010	8.535×10^5	0.70320
M12	35731.0	1.00005	8.524×10^5	0.76030

Table 2.4

A summary for the blind ant on the parameters $\{R_M^2, A, B, C\}$ where R_M^2 was calculated exactly with Eq. (2.29) and the remaining parameters were obtained from fitting to Eq. (2.28) over a time step range $100 \leq n \leq 10000$.

trial	R_M^2	A	B	C
B1	6017.33	1.00076	1.402×10^6	0.55052
B2	1986.23	1.00074	1.024×10^6	0.55344
B3	4004.55	1.00071	1.581×10^6	0.55413
B4	2972.9	1.00079	8.693×10^5	0.56054
B5	1792.74	1.00126	3.349×10^5	0.56421
B6	4378.7	1.00043	1.394×10^5	0.70250
B7	14437.9	1.00009	7.132×10^5	0.70950
B8	17928	1.00010	8.535×10^5	0.70320

clusters and $d_w = 2.63 \pm 0.04$) for the myopic ant on $2-d$ DLA clusters.

Since the particular boundary conditions become less important as the surface to volume ratio decreases, it is also interesting to compare the mean squared displacement results of finite clusters with free boundary conditions to those generated with periodic boundary conditions. As a first step, a simple comparison is made here without incorporating corrections for either type of boundary condition. This comparison will demonstrate the difficulties in estimating the walk exponent.

A comparison of the myopic mean squared displacement for clusters (on the square lattice) in the $(p_c \approx 0.593\,, L)$ ensemble with free and periodic boundary conditions is made from a total of six sets of data where each set represents a configurational average over 20 clusters. Three different mesh lengths of ($L_1 = 100$, $L_2 = 200$, $L_3 = 300$) have been considered. Every cluster that was used in the ensemble was percolating as discussed in Section 2. For each configuration generated, either free boundary conditions or periodic boundary conditions were imposed. The average size of the clusters were ($S_1 = 3740$, $S_2 = 14465$, $S_3 = 32944$), and ($S_1' = 4680$, $S_2' = 17914$, $S_3' = 37882$) for free and periodic boundaries respectively. The number of sites increases with periodic boundaries because connections between occupied sites are made between opposite edges.

As shown in Fig. 2.11, the mean squared displacement for each data set are compared. It is seen that as the cluster size increases, the influence of the boundary condition decreases as expected. Apparently, the mean squared displacement from (free, periodic) boundary conditions is an (under, over) estimate. This is not

a surprising result either, since there is saturation in the finite clusters and an apparent homogeneity in the "infinite" clusters. However, note that almost no change occurred in the mean squared displacement for the clusters with a periodic boundary condition when increasing from $L_2 = 200$ to $L_3 = 300$. This result implies that up to time step $n = 10000$, the effects of periodicity does not enter the mean squared displacement. Therefore, a third approach in estimating d_w could be with using a (p, L) ensemble with periodic boundary conditions.

Continuing in the same way as before, the walk exponent is obtained from a simple power-law fit over a variable fitting range and $d_w(N)$ is plotted in Fig. 2.12 for all six data sets. Clearly there is an amazing difference in $d_w(N)$ for the clusters with free verses periodic boundary conditions. The characteristics of $d_w(N)$ for the clusters with free boundaries in the (p_c, L) ensemble are the same as the clusters generated from a seed site.

From a simple power-law fit applied to the clusters with periodic boundaries, an estimation as low as $d_w \approx 2.75$ could be made. This result unfortunately puts a big question mark as to the true value of d_w and the validity of using the finite size clusters. However, from studying random walks that start only from a seed site[31, 38, 54] (also done in the next section) it appears that $d_w > 2.80$ which suggest that more analysis with periodic boundary conditions is needed. It is noted that when we applied Eq. (2.29) to a fully occupied cluster but finite in size, we found $d_w = 2.04$. We suspect that the margin of error should be less in the disordered case because of the overall slower diffusion.

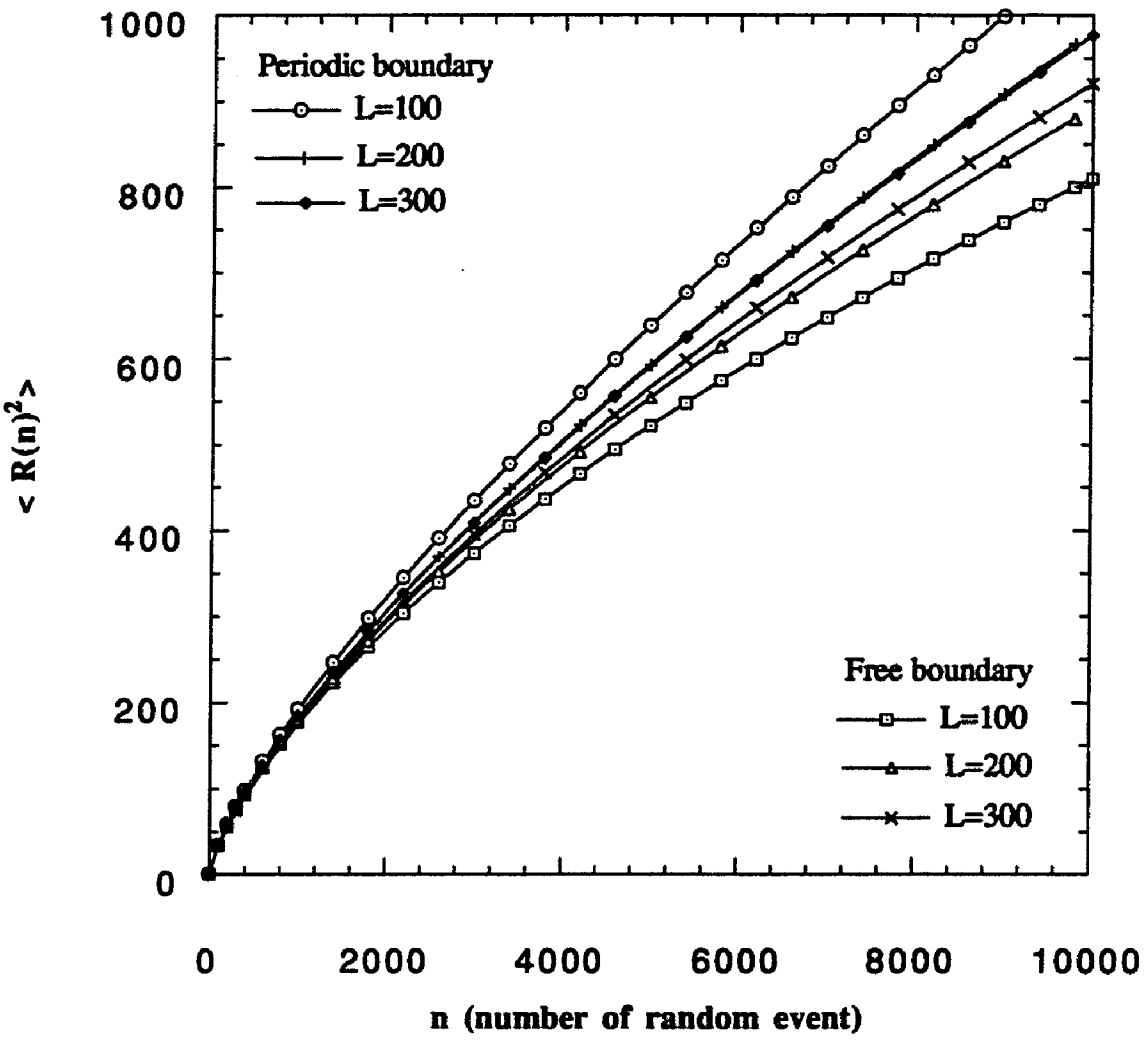

Figure 2.11

The mean squared displacement is plotted for six different data sets each representing an average over 20 clusters on the square lattice from a $(p = 0.593, L)$ ensemble. Three different mesh lengths of $L_1 = 100$, $L_2 = 200$ and $L_3 = 300$ were considered. The above curves ($\Box$, $\triangle$, $\times$) correspond to the (L_1, L_2, L_3) ensemble with free boundary conditions applied. The above curves ($\bigcirc$, $+$, $\diamond$) correspond to the (L_1, L_2, L_3) ensemble with periodic boundary conditions applied.

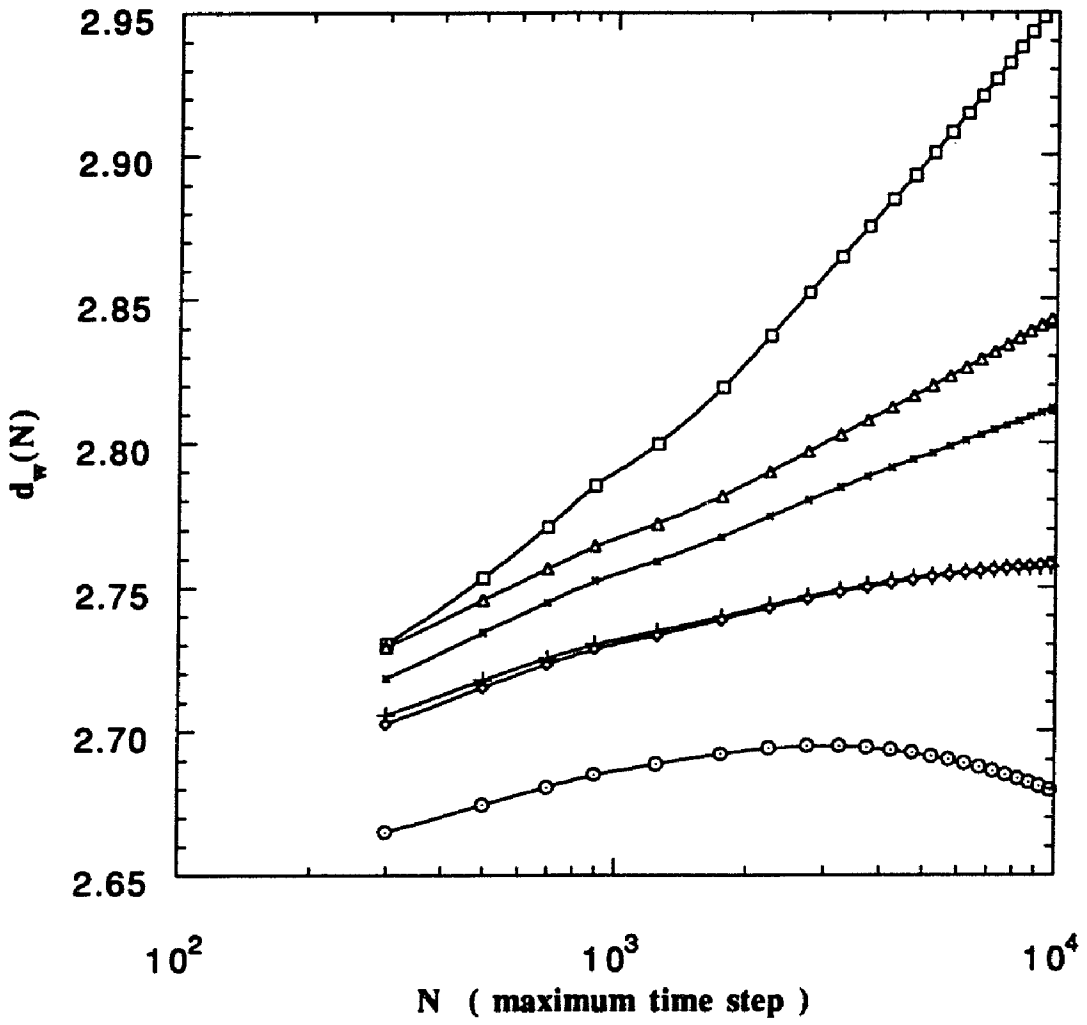

Figure 2.12

The walk exponent as obtained from a log-log plot of the mean squared displacement as a function of N where the fitting range over step number (n) was performed between ($100 \leq n \leq N$). These fits were taken on the same data as in Fig. 2.11 where the above curves (○, +, ◇) correspond to the (L_1, L_2, L_3) ensemble with periodic boundary conditions applied.

If anything, the periodic boundary condition would tend to decrease the global ramification, and since the ensemble considered consisted of only percolating clusters in a strict sense, the results here may be biased. For example, if the percolating state is defined as having a connected path between top and bottom edges (without rapping around) then there would be a mixture of finite and "infinite" clusters in the ensemble. When the finite clusters are included in the ensemble, the estimated value for d_w would increase. Further analysis on clusters in the (p_c, L) ensemble has not been made, but the resolution of the above discrepancy should be pursued.

2.4 Random Walk Scaling and Mean Field Approximations

By Fick's second law, the probability density for the displacement is given by Eq. (1.13) and the mean squared displacement is linear in time ($d_w = 2$). However, the mean squared displacement on fractal percolation and DLA clusters is anomalously slow as Tables (2.1 and 2.2) indicate since $d_w > 2$. Apparently, Fick's second law does not hold on fractal objects. The reason is that in the anomalous regime, long-range correlations in the step displacements exist and furthermore, the central limit theorem breaks down. Therefore the probability density for the displacement will deviate from a Gaussian[55, 56, 57]. A modified diffusion equation is required[58] to obtain the appropriate probability density. These and many other interesting features of diffusion on fractals have been reviewed by Havlin and Ben Avraham[35].

A mean field approximation is developed for $p(s, n \mid s_0, 0)$ which gives the

probability that a random walker (confined to a given cluster) is at site s after n time steps given that it started at site s_0 at time $n = 0$. No reference is made to any particular model in the following derivations, however, all explicit calculations have been done with the blind ant for site percolation clusters at $p = 0.593$ on the square lattice. A similar derivation can be done in the continuum[51] to arrive at the probability density for the displacement given by $P(\vec{R}, t \mid 0, 0)$.

Intuitively, particles are expected to diffuse faster along directions with the least number of restrictions corresponding to regions of high connectivity between sites. Clearly the local bond or site density will be a major factor in the diffusion profile. The approximation separates $p(s, n \mid s_0, 0)$ into a geometrical and dynamical part. The nature of the approximation assumes that any typical cluster will have a similar dynamical characteristic provided they share the same global fractal properties. The local geometrical differences are assumed to be responsible for the dominant fluctuations in the mean squared displacement.

Without loss of generality, the initial site will be chosen as the origin of coordinates. For simplicity $p(s, n \mid s_0, 0)$ will be written as $p(s, n)$. Let $p(s, l, n)$ define a joint probability that the walker is on site s *and* in chemical distance shell l at the nth time step. This allows the structure of the cluster to be coarse grained into separate bins defined by chemical distance shells. A summation over all chemical distance shells recovers the usual site probability $p(s, n)$. A mean field

approximation is now made to the function $p(s,l,n)$ given by

$$p(s,l,n) \approx g(s,l)\,\tilde{p}(l,n) \tag{2.32}$$

where $g(s,l)$ is defined as

$$g(s,l) = \begin{cases} 1 & \text{if site } s \text{ is in shell } l \\ 0 & \text{otherwise} \end{cases} \tag{2.33}$$

The function $g(s,l)$ is purely geometrical, and it follows that the number of sites contained in the lth shell is given by

$$G(l) = \sum_{s=1}^{\infty} g(s,l) \tag{2.34}$$

and the total number of sites in the cluster up to chemical distance l_o is given by

$$S(l_o) = \sum_{l=0}^{l_o} G(l) \quad . \tag{2.35}$$

The entire time dependence of Eq. (2.32) is contained in $\tilde{p}(l,n)$ which gives the *mean* probability per site that the walker is located at chemical distance l at time n. In other words, if $p(l,n)$ is the probability for the random walker to be located in chemical distance shell l at time n then

$$\tilde{p}(l,n) = \frac{p(l,n)}{G(l)} \quad . \tag{2.36}$$

Physically, the approximation ignores the fluctuation in probability among sites at the same chemical distance from the origin. This approximation should be valid if the fluctuations in $p(s,n)$ are small compared to the mean value $\tilde{p}(l,n)$. As an explicit check, Fig. 2.13 shows a normalized distribution of the ratio $p(s,n)/\tilde{p}(l,n)$

obtained from 600 random epidemic growing clusters generated from a seed site. Before normalization, a histogram was created by counting the occurrence of all ratios $p(s,n)/\tilde{p}(l,n)$ within a given chemical distance shell from all the clusters generated. These distributions (one per shell) were found to be the same for different chemical distances provided $y = l/n^{1/d_w^l}$ is constant, where the exponent d_w^l is defined through the relation $\overline{\langle l(n)^2 \rangle} \sim n^{2/d_w^l}$. Furthermore, the distribution broadens as the scaling variable y increases. This sort of behavior suggests multifractal characteristics in the diffusion process[57]. As Fig. 2.13 suggest, the approximation is good for $y \approx 3$ or less, but becomes poor as y increases. Fortunately, the region where the approximation becomes extremely poor is in the tail of the $p(l,n)$ distribution where the discrepancy is less important because of the rapid decay in $p(l,n)$ as $l/n \rightarrow 1$.

Using the approximation of Eq. (2.32) the mean squared displacement can be calculated by

$$\langle R(n)^2 \rangle \approx \sum_l \frac{1}{2} TR[\,\vec{\vec{I}}\,(l)\,]\,\tilde{p}(l,n) \tag{2.37}$$

where $\vec{\vec{I}}\,(l)$ is the moment of inertia tensor of the lth shell about the origin. A further mean field approximation is now made by replacing $\tilde{p}(l,n)$ by its configurational average denoted by $\overline{\tilde{p}(l,n)}$. Our motivation for this approximation is that it is plausible for any typical cluster of the ensemble to share similar dynamics in the mean probability per site because local spatial fluctuations should not influence the overall scaling property which is believed to be the essential feature. It is

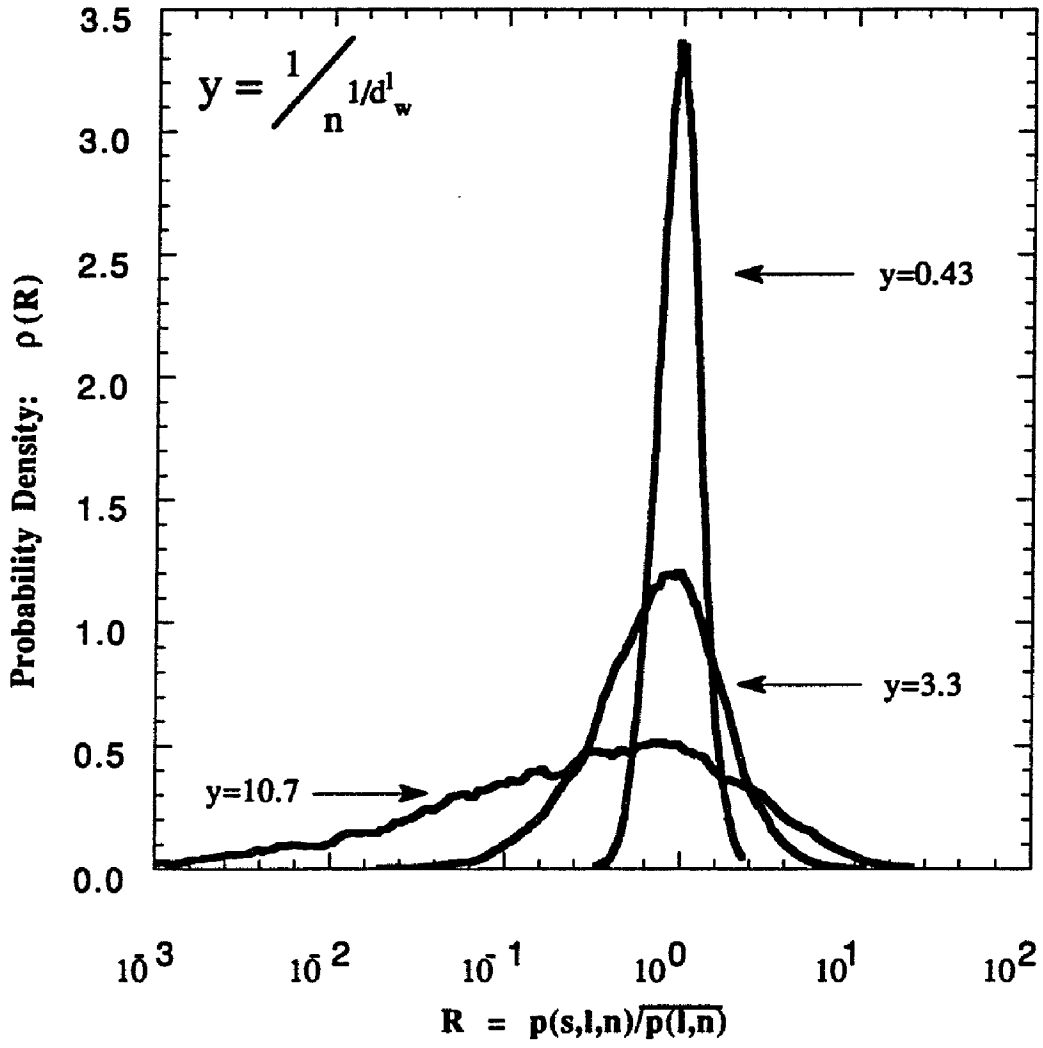

Figure 2.13

The probability density of the ratio of the site probability divided by the average probability per site over the set of sites contained within the same chemical distance shell. All the distributions collapse as functions of l and n into one curve such that $l/n^{1/d_w^l} = y$. A different distribution results for each value of y.

possible that the dominate fluctuations in the mean squared displacement derive from local spatial fluctuations. If this is the case, then a configurational average effectively smoothes over the non-essential properties.

A subtle point to this approximation is that the simple substitution of the configurational average, $\overline{\tilde{p}(l,n)}$, in place of $\tilde{p}(l,n)$ will not allow for proper normalization. This is because the normalization of $\tilde{p}$ is dependent on the cluster configuration:

$$\sum_{l=0}^{\infty} G(l)\,\tilde{p}(l,n) = \sum_{l=0}^{\infty} p(l,n) = 1\ . \tag{2.38}$$

Thus, in order to preserve this form of normalization, we must replace $\tilde{p}(l,n)$ by $\overline{\tilde{p}(l,n)}/C(n)$ where $C(n)$ is a normalization coefficient defined by

$$C(n) = \sum_{l=0}^{\infty} G(l)\,\overline{\tilde{p}(l,n)} \tag{2.39}$$

which depends on the structure of the cluster through $G(l)$. Therefore, this second mean field approximation retains some of the cluster to cluster fluctuations within the normalization coefficient.

More generally, a position correlation matrix can be defined as

$$\vec{\vec{\mathcal{P}}}(n) = \langle \vec{R}(n)\vec{R}^{T}(n)\rangle \tag{2.40}$$

which in two dimensions is explicitly given as

$$\vec{\vec{\mathcal{P}}}(n) = \begin{bmatrix} \langle x(n)x(n)\rangle & \langle x(n)y(n)\rangle \\ \langle y(n)x(n)\rangle & \langle x(n)y(n)\rangle \end{bmatrix}\ . \tag{2.41}$$

Analogously, a geometric matrix $\overleftrightarrow{T}(l)$ is defined as (remaining in two dimensions)

$$\overleftrightarrow{T}(l) = \sum_{s=1}^{\infty} \begin{bmatrix} x(s)x(s) & x(s)y(s) \\ y(s)x(s) & x(s)y(s) \end{bmatrix} g(s,l) \quad , \tag{2.42}$$

which can be extended to three dimensions as well. The position correlation matrix allows the study of anisotropic diffusion. With these definitions it follows that the mean field expression for the position correlation matrix is given as

$$\overleftrightarrow{\mathcal{P}}(n) \approx \frac{\sum_{l=0}^{\infty} \overleftrightarrow{T}(l)\, \overline{\tilde{p}(l,n)}}{\sum_{l=0}^{\infty} G(l)\, \overline{\tilde{p}(l,n)}} \, . \tag{2.43}$$

The result of Eq. (2.43) leads to a nice physical picture of the diffusion process. If $\overline{\tilde{p}(l,n)}$ were independent of l, then the position correlation matrix would just equal the radius of gyration tensor. However, $\overline{\tilde{p}(l,n)}$ is a time dependent weighting function that determines the relative importance of the sites within chemical distance shell l. The usefulness of Eq. (2.43) becomes clear when we consider the scaling properties of $\overline{\tilde{p}(l,n)}$. The function $\overline{\tilde{p}(l,n)}$ is expected to have the same scaling behavior as $\overline{p(l,n)}/\overline{G(l)}$. Havlin *et al.*[55] showed from exact enumeration of random walks that $\overline{p(l,n)}$ has a scaling form given by

$$l\,\overline{p(l,n)} = y^{d_l} \exp(-by^{\beta_s}) \quad , \quad \beta_s = 1.9 \pm 0.1 \tag{2.44}$$

when using the similarity variable $y = l/n^{1/d_w^l}$ as before. The relationship $S(l) \sim l^{d_l}$ defines the exponent d_l. Noting that $\overline{G(l)} \sim a l^{d_l - 1}$ we make the scaling anzatz that

$$\overline{\tilde{p}(l,n)} = \Phi(y)\, n^{-d_s/2} \quad , \tag{2.45}$$

where $d_s = 2d_l/d_w^l$ is the same spectral dimension as defined earlier.

From 400 breath-first generated clusters of chemical distance $l = 200$ and another 400 clusters of chemical distance of $l = 400$ and using four different time frames at time steps 500, 1000, 2500 and 5000 the scaling properties of $\overline{\tilde{p}(l,n)}$ has been checked. With the values of $d_s \approx 1.30$ and $d_w^l \approx 2.54$ as determined by Havlin *et al.*[35] we indeed observed scaling. The smoothed plot for the scaling function $\Phi(y)$ is shown in Fig. 2.14. In addition to $\overline{\tilde{p}(l,n)}$, we have observed scaling in the following fluctuations given by

$$\overline{\sigma(p(s,l,n) - \tilde{p}(l,n))} = \Delta\phi(y)\, n^{-d_s/2} \tag{2.46}$$

$$(\overline{\tilde{p}(l,n)^2} - \overline{\tilde{p}(l,n)}^2)^{1/2} = \Delta\Phi(y)\, n^{-d_s/2} \ , \tag{2.47}$$

where σ in Eq. (2.46) refers to the root mean square of an ensemble of sites s contained in shell l of one cluster. The scaling functions $\Delta\phi(y)$ and $\Delta\Phi(y)$ are also presented in Fig. 2.14. We find that the fluctuations defined above are of the same order as the mean probability density per site and furthermore, from Fig. 2.13 we can expect these deviations from the mean to be a few orders of magnitude for large y. However, the essential physics can still be captured in Eq. (2.43) since $\tilde{p}(l,n)$ decays rapidly over many decades for large y.

The $\mid \ln[\Phi(y)] \mid$ is plotted against y on a Log-Log plot in Fig. 2.15. The scaling function $\Phi(y)$ is found to be approximately a stretched exponential for large values of y with the power $\beta_s = 1.65 \pm 0.05$. We note here that this value of β_s is consistent with the theoretical prediction of Havlin *et al*[55] that $\beta_s = d_w^l/(d_w^l - 1)$, although they were considering the scaling of $\overline{lp(l,n)}$ (not $\tilde{p}(l,n)$). The direct

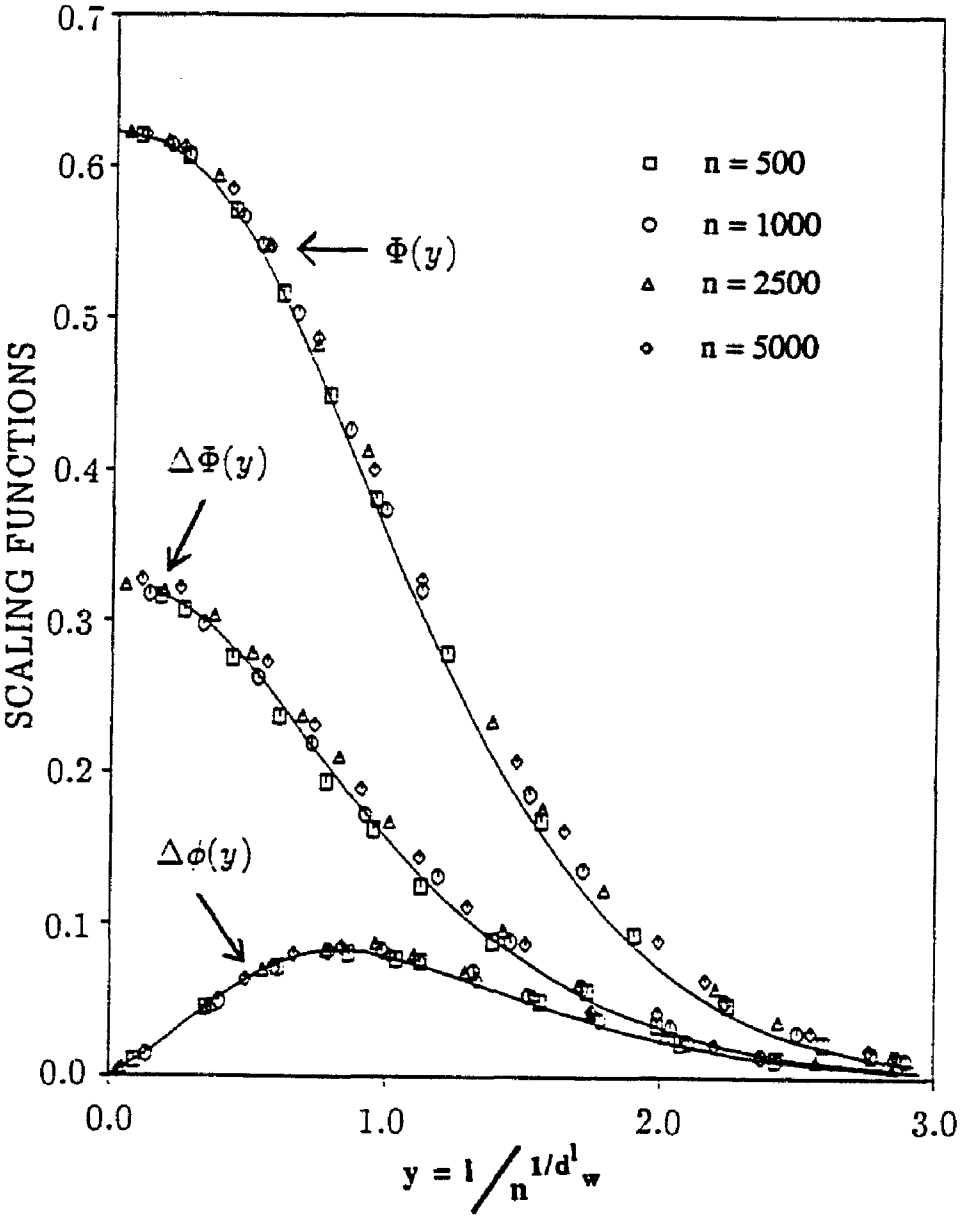

Figure 2.14

The scaling functions $\Phi(y)$, $\Delta\phi(y)$ and $\Delta\Phi(y)$ are plotted against the similarity variable $y = l/n^{1/d^l_w}$ with l having a range from 0 to 400. The symbols specify different times: □, n=500; ○, n=1000; △, n=2500; ◇, n=5000 and the solid lines are obtained from smoothing the collapsed data. In this plot $d_s = 1.30$ and $d^l_w = 2.50$.

scaling of $\overline{p(l,n)}$ was also checked, and was approximately equivalent to the product $\overline{\tilde{p}(l,n)} \times \overline{G(l)}$. For large values of y there is no difference between the average of the product to that of the product of the averages. Moreover, the exponent β_s remained the same.

Although the data in (fig. 2.14 and 2.15) pertain to breath-first generated clusters, the same results were found for the epidemic growth generated clusters. With 600 epidemic growing clusters and 800 breath-first search generated clusters totaling to 1400 clusters, it is found that the best data collapse was obtained when $d_s = 1.30 \pm 0.02$ and $d_w^l = 2.47 \pm 0.05$ yielding the power $\beta_s = 1.65 \pm 0.05$ as above. The uncertainties in these numbers were determined from the extreme limits on successful data collapse.

As a consistency check, the configurational average of the position correlation matrix as given in Eq. (2.43) should reproduce the correct time dependence for the mean squared displacement. In this case, it follows that

$$\langle R(n)^2 \rangle \approx \frac{\sum_{l=0}^{\infty} TR[\overleftrightarrow{T}(l)]\,\overline{\tilde{p}(l,t)}}{\sum_{l=0}^{\infty} G(l)\,\tilde{p}(l,t)} \,. \tag{2.48}$$

Performing a configurational average over an ensemble of clusters of a given chemical distance, the asymptotic scaling behavior of the time dependence can be obtained from Eq. (2.48) by simply replacing $TR[\overleftrightarrow{T}(l)]$ (simply denoted as $\mathcal{T}_o(l)$) and $G(l)$ by their configurational averages. Since $\overline{G(l)} \sim l^{d_l - 1}$ and as we have previously shown[51] $\overline{\mathcal{T}}_o(l) \sim l^{d_l}$ where $d_l = (2 + d_f)d_l/d_f$, it follows that the leading

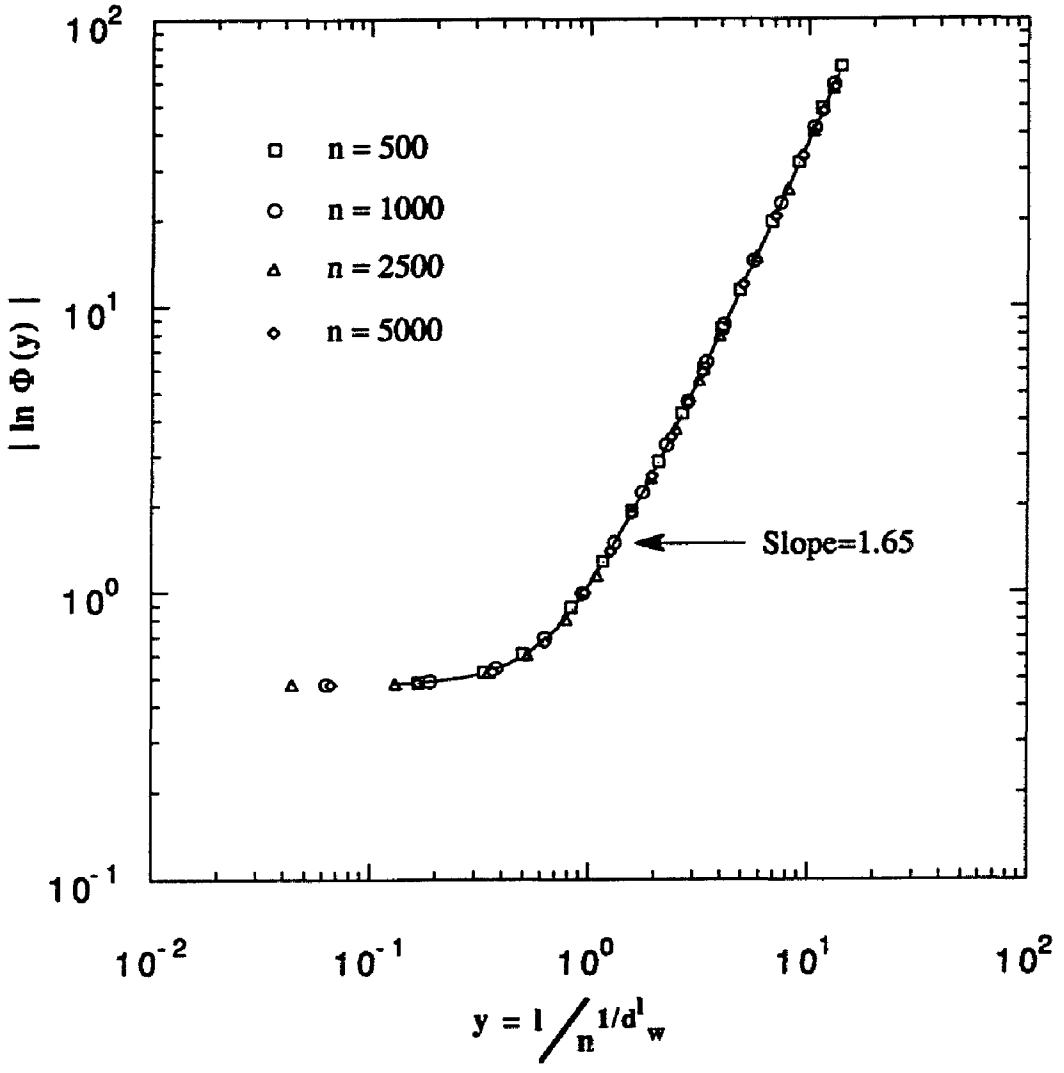

Figure 2.15

The $|\ln \Phi(y)|$ is plotted against the similarity variable y on a logarithmic scale. The symbols specify different times: □, n=500; ○, n=1000; △, n=2500; ◇, n=5000 and the solid line is obtained from smoothing the collapsed data. The scaling function $\Phi(y)$ is asymptoticly a stretch exponential with the power $\beta_s = 1.65 \pm 0.05$ when chosing $d_s = 1.30$ and $d_w^l = 2.50$.

time dependence at long times of the mean squared displacement is given by

$$\overline{\langle R^2(n)\rangle} \sim \frac{n^{(d_f-1)/d_w^l}\int_0^\infty y^{d_f-1}\,\Phi(y)\,dy}{n^{(d_l-1)/d_w^l}\int_0^\infty y^{d_l-1}\,\Phi(y)\,dy}\,, \tag{2.49}$$

where summations have been replaced by integrations. Noting further that d_l/d_w^l is equal to d_f/d_w, we finally obtain

$$\overline{\langle R^2(n)\rangle} \sim n^{2/d_w}\ . \tag{2.50}$$

Thus the correct power-law dependence of the mean-square displacement is recovered.

The initial motivation for constructing a position correlation matrix was to study the anisotropic properties of diffusion on ramified clusters. At each time step the position correlation matrix for a given cluster can be diagonalized. In two dimensions, a measure of the anisotropy is taken as the difference of the minimum from the maximum eigenvalue of the position correlation matrix. In particular, let

$$\langle \Delta Q(n)\rangle \equiv \langle q(n)^2\rangle_{max} - \langle q(n)^2\rangle_{min} \tag{2.51}$$

where $\langle q(n)^2\rangle_{max,min}$ denote the eigenvalues of the position correlation matrix at the nth time step. It has been found that

$$\frac{\overline{\langle \Delta Q(n)\rangle}}{\overline{\langle R^2(n)\rangle}} \approx 0.36 \tag{2.52}$$

independent of n for $n > 100$. Therefore, the degree of anisotropy remains roughly a constant. This result is similar to the geometric anisotropy[48]. These results imply that an ensemble of walkers starting from a common origin will diffuse anisotropicly.

The approximations made in Eq. (2.43) are assessed by studying the evolution of the position correlation matrix first by numerically calculating the righthand side of this equation for a set of randomly generated clusters and then comparing these results with the actual ones obtained from the exact enumeration method. Within the anomalous diffusion regime ($a \ll n^{1/d_w} \ll \xi$) we have incorporated the scaling form for $\overline{\tilde{p}(l,n)}$ explicitly. This reduces Eq. (2.43) to

$$\overleftrightarrow{\mathcal{P}}(n) \approx \frac{\int_0^\infty \overleftrightarrow{T}(l)\,\Phi(l/n^{1/d_w^l})\,dl}{\int_0^\infty G(l)\,\Phi(l/n^{1/d_w^l})\,dl} \tag{2.53}$$

where again the summations have been replaced by integrals.

The evaluation of the righthand side of Eq. (2.53) consisted of generating a cluster, calculating the number of sites and the moment of inertia tensor for each chemical distance shell, and then numerically summing the integrals using the smoothed numerical fit for the scaling function Φ. To facilitate this, the scaling function is stored in a table consisting of y and $\Phi(y)$. The scaling variable is calculated for each chemical distance at each time of interest. The method of linear interpolation was used to find $\Phi(y)$ for values of y not contained in the table. Furthermore, reasonable comparison is expected for $n^{1/d_w} \gg a$ where the scaling form for $\overline{\tilde{p}(l,n)}$ is valid.

A plot of $\overline{\langle R(n)^2 \rangle}$ and $\overline{\langle \Delta Q(n) \rangle}$ verses n on a logarithmic scale is given in Fig. 2.16 for both the mean field approximation and the actual data from a configurational average over 23 clusters. Also in Fig. 2.17 the typical accuracy of the approximation for the mean-square displacement is presented for two different

clusters out of the set of 23 clusters. Clearly, the approximations are excellent over the whole range of n studied.

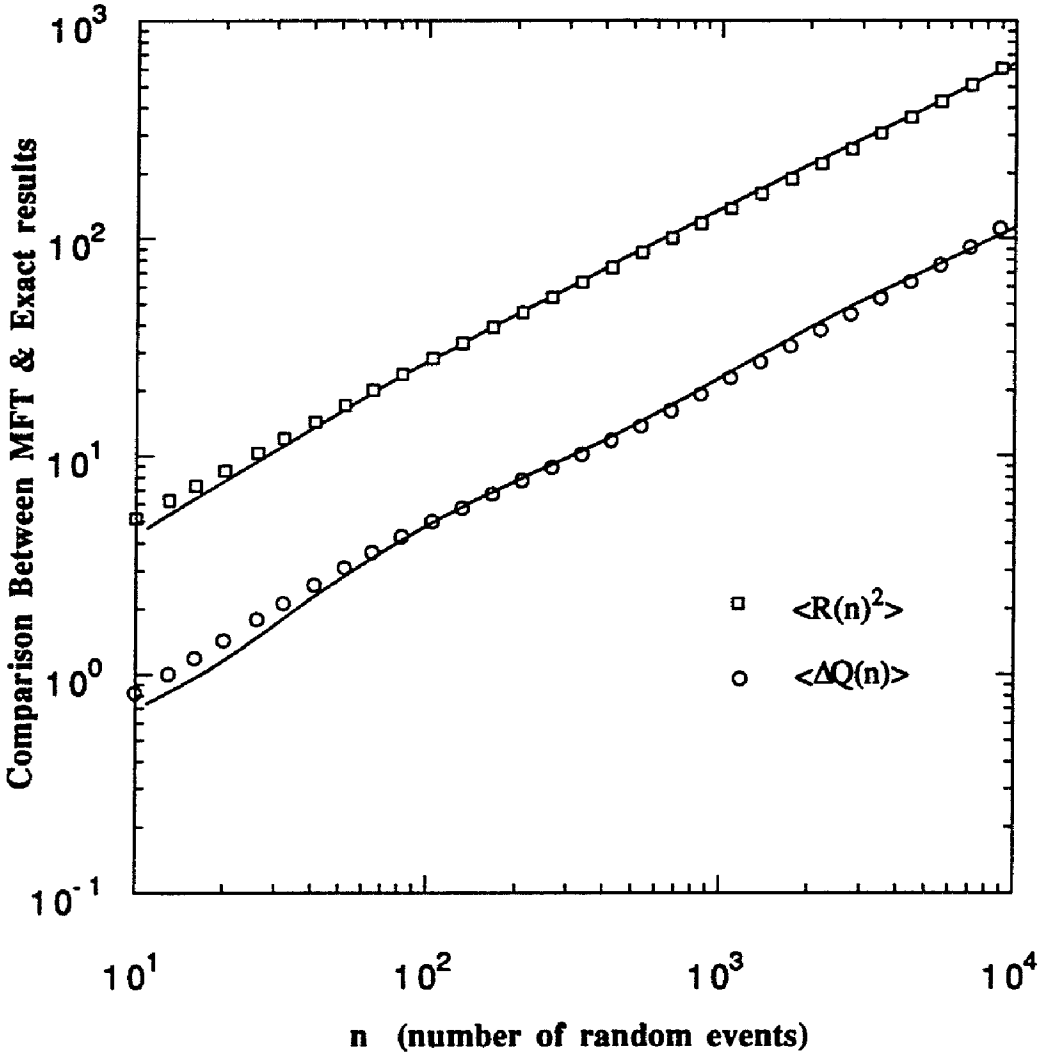

Figure 2.16

Comparison of the mean field results to the exact results of a configurational average over 23 clusters for $\langle R(n)^2 \rangle$ and $\langle \Delta Q(n) \rangle$ verses n on a logarithmic scale. The mean field result for $\overline{\langle R(n)^2 \rangle}$ is denoted by a □ and $\overline{\langle \Delta Q(n) \rangle}$ is denoted by a ○. The solid lines going through the symbols are the exact results.

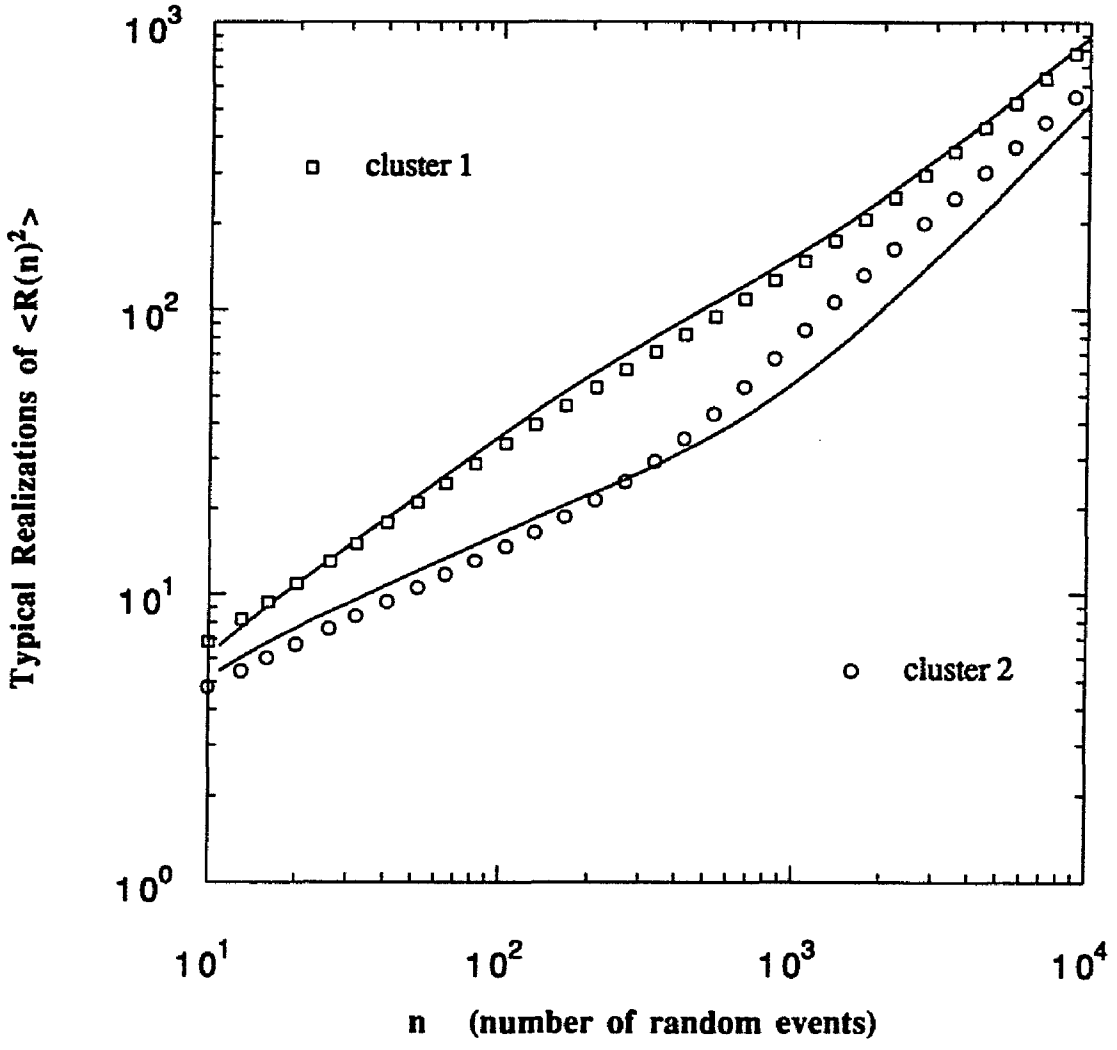

Figure 2.17

A typical plot of $\langle R(n)^2 \rangle$ verses n on a logarithmic scale for two different cluster realizations. The symbols (□ and ○) correspond to the mean field calculation for each cluster and the solid lines give the exact results.

3. BROWNIAN MOTION WITH LONG TIME CORRELATIONS

3.1 Anomalous Diffusion

An anomalous diffusion process may either be a very surprising result or an obvious one depending on ones perspective. As discussed in Chapter 1 at great length, the normal diffusion process can be summarized very simply by the mean squared displacement of the random motion of particles being proportional to time at long times. By definition, a diffusion process is determined to be *normal* or *anomalous* by its asymptotic properties of the mean squared displacement being or not being linear in time. Faster than normal diffusion has been noted in turbulence by Richardson[59] where $\langle R(t)^2 \rangle \sim t^{3/2}$ had been observed as early as 1926. From the defining relation that $\langle R(t)^2 \rangle \sim t^{2/d_w}$, it follows that in this case $d_w = 4/3$. More recently, slower than normal diffusion has been found to occur in fractal media ($d_w > 2$) as discussed at length in Chapter 2. It would seem that normal diffusion is a "special case" in that $d_w = 2$ exactly, however, it is perhaps the most common case and understandably so because of the powerful central limit theorem and law of large numbers.

As discussed in Chapter 2, a disordered structure may have fractal characteristics over a limited length scale ($a < L < \xi$). It is often said that up to time t_ξ for which the tracer particle is beginning to explore regions of length scale greater

than ξ, the diffusion is anomalous, but this usage of anomalous diffusion does not follow the strict distinguishing factor originally defined at asymptotic times. If one is willing to use this weaker sense of the term anomalous diffusion, then the concept of normal diffusion becomes more restrictive in that the mean squared displacement should be linear in time at all times. If this is the case, anomalous diffusion (in this weaker sense) is not surprising at all, and "normal" diffusion will not be so common because usually the short time behavior in the mean squared displacement is more complex than a linear time dependence.

The mean squared displacement is related to the velocity-velocity correlation function or more simply velocity auto-correlation function (VACF) by the observation that

$$\langle R(t)^2 \rangle_{eq} = \int_0^t dt_1 \int_0^t dt_2 \, \langle \vec{v}(t_1) \cdot \vec{v}(t_2) \rangle_{eq} \ . \tag{3.1}$$

The correlation function is time translationally invariant, therefore, by suitable change of variables and reordering of the integrations it can be shown that

$$\langle R(t)^2 \rangle = 2t \int_0^t \langle \vec{v}(t') \cdot \vec{v}(0) \rangle \, dt' - 2 \int_0^t t' \langle \vec{v}(t') \cdot \vec{v}(0) \rangle \, dt' \tag{3.2}$$

where the subscript eq has been dropped. Often times the VACF is a rapidly decaying function of time, such as an exponential decay, as modeled by the simple Langevin equation from Chapter 1. The full time dependence for the mean squared displacement from an exponentially decaying VACF has been given in Eq. (1.19). Clearly at long times, the mean squared displacement is linear in time, and thus the diffusion process is normal.

Generally, an exponential decay in the VACF is an over simplification. It has been shown from molecular dynamic studies by Alder and Wainright[60] that in three dimensions the VACF for self diffusion in hard-sphere fluids at long times deviate from an exponential decay. At long times there is a positively correlated VACF decaying as a power-law $\sim C(t/t_o)^{-d/2}$ with $C > 0$ for two and three dimensions where t_o is the mean collision time. This positive long time tail is a non-Markovian effect[62, 60, 61] caused by hydrodynamic vortex modes that couple to the diffusing particle.[62, 63] As another example, negative correlated long time tails were found by computer simulation of the Lorentz gas model. Basically, the Lorentz gas model consist of a tracer particle in the presence of a low concentration of fixed scatterers. The mechanism responsible for these negative correlations can be attributed to the particle's higher probability to be scattered backward than diffusion without fixed scatterers. From microscopic calculations[64, 65, 66], the VACF should decay as $\sim -t^{-(d+2)/2}$, however, there had not been satisfactory agreement with simulations[66, 67] until very recently[64]

A simple look at Eq. (3.2) can help categorize what type of VACF will lead to anomalous diffusion (in the strict sense) or to normal diffusion. Since asymptotic power-law decays have been found in the VACF for various systems as the above examples demonstrate, we choose to consider a VACF of the form

$$C_v(t) = \langle \vec{v}(t) \cdot \vec{v}(0) \rangle \sim c_o t^{-\alpha} \quad \text{asymptotically.} \tag{3.3}$$

The VACF will be considered to be equal to the leading contribution as given

above for times $t \geq T$, and for times $t < T$ the function is left unspecified. Then by direct substitution into Eq. (3.2) the mean squared displacement for times $t \geq T$ is found to be

$$\langle R(t)^2 \rangle = \begin{cases} B_o(T)t + \frac{c_o}{\alpha^2-3\alpha+2}t^{2-\alpha} - B_1(T) & \alpha \neq 1\ ,\ \alpha \neq 2 \\ A_o(T)t + c_o t \ln \frac{t}{T} - c_o(t-T) - A_1(T) & \alpha = 1 \\ B_o(T)t - c_o \ln \frac{t}{T} - c_o - A_1(T) & \alpha = 2 \end{cases} \tag{3.4}$$

with the following definitions:

$$A_o(T) = \int_0^T C_v(t)\,dt \tag{3.5}$$

$$A_1(T) = \int_0^T tC_v(t)\,dt \tag{3.6}$$

$$B_o(T) = A_o(T) - \frac{c_o}{1-\alpha}T^{1-\alpha} \tag{3.7}$$

$$B_1(T) = A_1(T) - \frac{c_o}{2-\alpha}T^{2-\alpha}\ . \tag{3.8}$$

From these results, Table 3.1 is constructed to list the different cases for which anomalous or normal diffusion occurs. This list is complete for simple power-law decays, although other situations are possible. For example, the leading time dependence in a VACF that has an oscillatory component may not correspond to the leading time dependence in the mean squared displacement. For a system in equilibrium, the VACF is related to the mean squared displacement as

$$C_v(t) = \langle \vec{v}(t) \cdot \vec{v}(0) \rangle = \frac{-1}{2}\frac{d^2}{dt^2}\langle R(t)^2 \rangle\ . \tag{3.9}$$

Thus it may be the case that if $\langle R(t)^2 \rangle \sim At^{2/d_w}$ then $c_o = A\,2/d_w\,(2/d_w - 1)$ and $\alpha = 2/d_w - 2$, however, if there is an oscillatory component in the mean

squared displacement such as $t^{2/d_w - x}\cos(\omega t)$ where $0 \leq x < 2$, then the leading characteristic of the VACF will be oscillatory given by $-\omega^2 t^{2/d_w - x}\cos(\omega t)$. More details are given by Muralidhar *et al*[32] about the asymptotic properties of the VACF and mean squared displacement. The important term that determines the type of diffusion process is the leading asymptotic non-oscillating term in the VACF.

Both fast and slow anomalous diffusion necessarily arises from long time tails in the VACF for which a characteristic time scale is not present. For slow anomalous diffusion the first moment of the VACF will diverge (ie. $A_1(T \rightarrow \infty)$, but this is not a sufficient condition because the zeroth moment is required to equal zero (ie. $A_o(T \rightarrow \infty) = 0$). The absence of a characteristic time scale alone implies that the stochastic process is non-Markovian in character because the tracer particle retains memory of its past velocity. The stochastic process for slow anomalous diffusion was modeled by a Markovian random walk in Chapter 2 at the expense of specifying the entire configuration. If one restricts the random variables to velocity space, then the past history of the velocity can be used in a Langevin formalism to be discussed in the next section. No unit of time can be chosen for which the past history of the tracer particle can be neglected and thus the central limit theorem does not apply.

Another way to characterize the diffusion process is to study the various correlations in the frequency domain. Making use of the Fluctuation-Dissipation Theorem[5], the frequency dependent self diffusion coefficient is defined as the

complex Laplace transform of the mean squared displacement of the tracer particle. In particular, the frequency dependent diffusion coefficient is given by

$$D(\omega) = \frac{-\omega^2}{2d} \int_0^\infty \langle R(t)^2 \rangle_{eq} e^{-ut}\, dt \tag{3.10}$$

where the Laplace variable u is taken to be

$$u = \eta - i\omega \qquad \text{in the limit } \eta \to 0^+ \ . \tag{3.11}$$

The derivation of Eq. (3.10) was given by Scher and Lax[68] applied to hopping models. However, in this thesis the complex conjugate of their expression is used. The choice of using the complex conjugate of their expression comes from hindsight, so that in Chapter 4 the expressions for Drude-like mobilities will agree with convention.

A more conventional definition for the frequency dependent diffusion coefficient is given by

$$D(\omega) = \frac{1}{2d} \int_0^\infty \langle \vec{v}(t) \cdot \vec{v}(0) \rangle_{eq} e^{-ut}\, dt \tag{3.12}$$

which is equivalent to Eq. (3.10) provided that at small times the time dependent diffusion coefficient goes to zero. In other words, $\frac{d}{dt}\langle R(t)^2 \rangle_{eq}\big]_{t=0} = 0$ which is a physically reasonable condition to satisfy. However, in hopping models the time of flight between hops is taken to be instantaneous (surely an unphysical assumption) in comparison to the mean waiting time at a site. Therefore, in these cases the two expressions from Eq. (3.10) and Eq. (3.12) can be made equivalent by introducing a Dirac delta function for the VACF in Eq. (3.12) at $t = 0$.

Additional motivation to calculate the frequency dependent diffusion coefficient and focus on the self-diffusion properties of charge carriers is to find the electrical conductivity. The electrical conductivity for a system of charge particles is given by the Kubo formula[6],

$$\sigma(\omega) = \frac{1}{Vdk_BT}\int_0^\infty \langle \vec{j}(t)\cdot\vec{j}(0)\rangle_{eq} e^{-i\omega t}\,dt \tag{3.13}$$

where V is the volume of the system and $\vec{j}$ is the current density. Since $\vec{j} = q\delta(\vec{r})\vec{v}$, it follows that Eq. (3.13) and Eq. (3.12) can be matched to obtain the Einstein relation generalized to all frequencies so that

$$\sigma(\omega) = \frac{nq^2}{k_BT}D(\omega) \tag{3.14}$$

where n is the charge carrier density and q is the charge of one carrier.

The *generalized Einstein relation* [69] of Eq. (3.14) is a very simple result but not valid in general. Some restrictions include, one type of charge carrier, non-interacting particles and no spatial dependence in the transport coefficients (ie $\sigma(\vec{x},\omega)$). The first restriction is for convenience, and could be relaxed if necessary. The second restriction derives from a fundamental assumption which works surprisingly well. Finally, the third restriction of spatial homogeneity for the transport coefficients for homogeneous disordered systems is usually not a practical problem because the wave length of the probing signal is large enough to self-average the disorder. The pertinent information about the structure of the disorder is contained in the time response of the mean squared displacement or VACF.

If the mean squared displacement is linear in time at all times, then $D(\omega) = D$ at all frequencies characteristic of normal diffusion. If the diffusion is anomalous with a long time tail in the VACF of the form $\sim t^{-\alpha}$, it follows from the complex Laplace transform that $D(\omega \to 0) \to \omega^{\alpha-1}$ for $\alpha \neq 1$. More generally, deviation from a constant diffusion coefficient is considered to be anomalous diffusion in the weaker sense where it is expected that the same power-law dependence in $D(\omega)$ will be present at high frequencies but over a limited frequency range.

3.2 The Generalized Langevin Equation

The Langevin equation from Chapter 1 attempts to model the dynamical nature of the forces acting on a tracer particle. The forces acting on the tracer particle were broken into a systematic part and a random part. Once the separation is made, the systematic part defines a linear equation in terms of velocity (only linear systems should be used in the Langevin approach[12]). The random part is considered to be an external driving force acting on the linear system, therefore, the Langevin equation becomes a stochastic linear differential equation.

A linear differential equation may describe the response of a certain linear device in many engineering applications. The output of some system is determined once the input (or forcing function) is known. Noise in the input signal will affect the response of the system, but there is no special relationship between the kind of noise present to any characteristic of the system. In contrast, the Langevin equation must be designed so that the response of the system is self-consistent

with the driving force in order to maintain equilibrium.[70] Thus the random part of the force and systematic part are not independent at all.

A generalized Langevin equation[32] is required to describe the dynamics of Brownian motion with long-time memory of the tag particle's velocity. For isotropic media we can write,

$$\frac{d}{dt}v(t) = -\int_{-\infty}^{t} \kappa(t-\tau)v(\tau)\,d\tau + \frac{f(t)}{M} \quad , \tag{3.15}$$

where M is the mass of the tracer particle, and the systematic frictional force is represented by the memory kernel $\kappa(t)$. The random force $f(t)$ represents the rapid thermal fluctuations and is required that $\langle f(t)\rangle = 0$ and $\langle v(0)f(t)\rangle = 0$ for $t \geq 0$. The systematic forces are those that are correlated to the velocity and ultimately describe the macroscopic response of a system that has been perturbed slightly from equilibrium. The *random* force is projected out from the total force such that it is uncorrelated to the velocity. This defining constraint provides a self-consistent dynamical equation, and when combined with the assumption of stationarity leads to the second fluctuation dissipation theorem

$$\frac{\langle f(t_o+\tau)f(t_o)\rangle}{M^2\langle v^2\rangle} = \kappa(\tau) \quad . \tag{3.16}$$

The generalized Langevin equation considered above applies to isotropic media. However, as demonstrated using two dimensional percolation clusters in Chapter 2, the diffusion process is typically anisotropic about any starting point. Fortunately, we have observed numerically that when stationary initial conditions are used the diagonal terms of a velocity correlation matrix (defined by the elements

$\langle v_i(t)v_j(0)\rangle$) are nearly equal to one another, but typically two orders of magnitude larger than the off-diagonal elements. The result of using a stationary initial condition is to average over all the locally preferred directions, thereby regaining essentially isotropic diffusion. Therefore it is justifiable to consider an isotropic memory kernel as done above.

With the use of Eq. (3.15) and the stated properties of the random force, the Laplace transform of the VACF is related to the friction kernel by

$$\tilde{C}_v(z) = \frac{1}{z + \tilde{\kappa}(z)} \quad . \tag{3.17}$$

Noting the asymptotic properties of the VACF in the time domain from the previous section, it follows that $\lim_{|z|\to 0} \tilde{\kappa}(z) = 0$ implies anomalous fast diffusion. Furthermore, $\lim_{|z|\to 0} \tilde{\kappa}(z) \to \infty$ is a necessary condition for slow anomalous diffusion. The memory kernel, in the Langevin formalism, accounts for the effects of the media in a mean field way with all structural details of the disordered media lost. As demonstrated by R. Muralidhar, et al[51] a memory kernel of the form

$$\kappa(\tau) = \frac{c}{\Gamma(1-\alpha)}\tau^{-\alpha} \tag{3.18}$$

where $\Gamma(x)$ is the gamma function is sufficient to produce slow anomalous diffusion.

It is noted here that the generalized Langevin equation can be used to simulate diffusion in fractal media once the statistical properties of the random force are determined. The random force has been determined not to be distributed as a Gaussian[56] in the case of diffusion on two dimension percolation fractals. Rather the probability density in the magnitude of the tracer particle's displacement was

found to be a stretched exponential. It appears that the random force must be chosen to be a non-Gaussian fractional noise. The generalized Langevin equation has the potential to serve as a starting point to derive partial differential equations of diffusion (the analog of the Fokker-Planck equation) which would serve as an equivalent mean field characterization of the fractal media. This approach, however, has not been pursed in favor of using a master equation.

3.3 The Continuous Time Master Equation: The Mapping to a Discrete Time Random Walk

The central quantity of interest in the study of Brownian motion is the probability density $P(\vec{r}, t \mid \vec{r}_o, 0)$ which also gives the diffusion profile. In applications of thermally activated hopping transport[71, 72], including atomic diffusion in solids[73, 74, 75], the allowed particle locations are discrete. On the other hand, if the movement of the particle is in the continuum as in the case of an electron in a metal, the trajectory of the particle will be coarse grained. Therefore, the Brownian motion will be characterized in this thesis with the function $P(m, t \mid m_o, 0)$ where m defines an "allowed state". Then $P(m, t \mid m_o, 0)$ is the probability that the random walker is in state m at time t given that it was in state m_o initially. Note that the state m may simply refer to a given site in a cluster as before, but it may be more complex than that.

The Brownian motion will be modeled by a continuous time master equation[33, 34] written as

$$\frac{\partial}{\partial t} P(m, t \mid m_o, 0) = -\gamma(m)\, P(m, t \mid m_o, 0) + \sum_{m'} \Gamma(m, m')\, P(m', t \mid m_o, 0) \quad (3.19)$$

where $\gamma(m) = \sum_{m'} \Gamma(m', m)$. This equation defines a stochastic Markov process where $\Gamma(m, m_o) > 0$ is the rate at which a particle attempts to change its state from m_o to m. The first term on the right side of Eq. (3.19) is the total rate at which the particle will leave state m. The net change in the occupation probability of state m is equal to the flow of probability into minus the flow out of state m. The rates are assumed time independent because we restrict our attention to static disordered configurations and to a system of independent particles. The probability flow into or out of a state at time t is determined at a *single instant of time,* therefore, no memory of the particle's trajectory is required.

The continuous time master equation can be mapped into a discrete time random walk with exponential waiting time distributions[9, 33]. Multiple waiting time distributions arise in static disordered systems because the diagonal terms $\{\gamma(m)\}$ are not identical. Note that waiting time distributions other than exponential can be considered[9, 68, 69, 76], but these models do not map to a simple master equation. The most straight forward way to accomplish the mapping is to consider two random processes at once. For example, if a random walker just entered state m_o at time $t = 0$, then for each infinitesimal time dt the probability for escape is $\gamma(m_o)\, dt$ and the probability to remain in state m_o will decay exponentially as $\exp(-\gamma(m_o)t)$. Once the particle does exit state m_o, it will enter state m_1 with probability given by the ratio $\Gamma(m_1, m_o)/\gamma(m_o)$. The instant the particle enters state m_1 the process continues as described above. Clearly one random process corresponds to a sequence of waiting times and the other to a discrete time ran-

dom walk. Usually it is assumed that $\Gamma(m,m) = 0$ for all m because a nonzero diagonal term contributes nothing to the right side of the Eq. (3.19). By removing this assumption, however, we are able to reduce the entire set of exponential distributions to one distribution function.

For convenience, Eq. (3.19) will be rewritten in matrix notation as

$$\frac{\partial}{\partial t}\hat{P}(t) = [\hat{\Gamma} - \hat{\gamma}]\,\hat{P}(t) \tag{3.20}$$

with the initial condition that $\hat{P}(t=0) = \hat{1}$. When the master equation is scaled to a time scale that is at least as fast as the fastest process occurring in the system, then it will be shown that only one waiting time distribution is necessary. To accomplish this let $\gamma_{max} \geq \max\{\gamma(m)\}$. A new matrix will be defined as

$$\hat{W} = \hat{1} + \frac{\hat{\Gamma} - \hat{\gamma}}{\gamma_{max}} \tag{3.21}$$

and it has the properties that $0 \leq w(m,m_o) \leq 1$ for all $\{m,m_o\}$ and that

$$\sum_m w(m,m_o) = 1 \quad \text{for all } m_o \ . \tag{3.22}$$

Therefore, the matrix $\hat{W}$ is interpreted as a transition probability matrix. The matrix $\hat{W}$ retains all the appropriate variations in jump rates defined by the original equation as well as all the spatial information throughout the system. The master equation can now be expressed as

$$\frac{\partial}{\partial t}\hat{P}(t) = \gamma_{max}\,[\hat{W} - \hat{1}]\,\hat{P}(t) \tag{3.23}$$

and has a formal solution given as

$$\hat{P}(t) = \sum_{n=0}^{\infty} \frac{(\gamma_{max}t)^n e^{-\gamma_{max}t}}{n!}\,\hat{W}^n \ . \tag{3.24}$$

The formal solution for the continuous time master equation involves a single Poisson distribution which will be denoted as

$$h(\gamma_{max}t, n) = \frac{(\gamma_{max}t)^n e^{-\gamma_{max}t}}{n!} \quad . \tag{3.25}$$

The function $h(x,n)$ gives the probability that n random events occur within the unitless interval $x = \gamma_{max}t$. The entire random time process has been successfully decoupled from the random walker's trajectory. The different waiting times that exist for various states are now accounted for by the *diagonal* terms of the transition probability matrix. A diagonal transition described by $\hat{W}$ is a random event, although a change of state does not occur. Note that the blind ant model from Chapter 2 Section 3 is an example where diagonal transitions are random events. The diagonal transitions correspond physically to "wasting time" and thus accounting for the true waiting time.

Given that the position vector of the particle in state m is given by $\vec{r}(m)$, the mean squared displacement is given by

$$\langle R(t)^2 \rangle = \sum_{m,m_o} \mid \vec{r}(m) - \vec{r}(m_o) \mid^2 \; P(m,t \mid m_o, 0)\, P_o(m_o) \quad , \tag{3.26}$$

where P_o is the initial probability distribution. Using the above expression for the mean squared displacement in Eq. (3.10), it follows that the frequency dependent diffusion coefficient can be expressed as

$$D(\omega) = \frac{-\omega^2}{2d\gamma_{max}} \sum_{n=0} \langle R(n)^2 \rangle \frac{1}{(1 - i\frac{\omega}{\gamma_{max}})^{n+1}} \quad . \tag{3.27}$$

The above expression for $D(\omega)$ is not too useful because as the summation is carried out its convergence properties are quite bad. Usually $\langle R(n)^2 \rangle \rightarrow \infty$ as

$n \to \infty$ unless the particle is trapped in a finite region. An integration by parts can be performed in order to arrive at an expression which has better convergence properties. Effectively, the derivation can easily be done within the framework of discrete time. The mean squared displacement can be written as

$$\langle R(n)^2 \rangle = \langle R(n+1)^2 \rangle - D_e(n) \tag{3.28}$$

where $D_e(n)$ was defined in Eq. (1.20) as a local slope. The subscript e indicates that D is a function in terms of random events. Substituting the above expression into Eq. (3.27), it follows after one resummation that

$$D(\omega) = \frac{-i\omega}{2d} \sum_{n=0} D_e(n) \frac{1}{(1 - i\omega\tau)^{n+1}} \tag{3.29}$$

where $\tau = 1/\gamma_{max}$. This new expression for $D(\omega)$ contains the same information as Eq. (3.27) except that it has better convergence properties. For example, for normal diffusion at long times the mean squared displacement diverges linearly, yet $D_e(n)$ goes to a constant.

Since integration by parts worked so well, it is tempting to do another one. However, in order to arrive at a simple and useful expression, the restriction of using stationary initial conditions is required. Although stationary initial conditions should be used when calculating equilibrium fluctuations in Eq. (3.27) or Eq. (3.29), these formulae do not a priori assume this to be the case. In contrast, it is now explicitly assumed that stationary initial conditions are used so that

$$D_e(n) = D_e(n+1) - 2\langle \vec{\rho}(n+1) \cdot \vec{\rho}(0) \rangle_{eq} \quad \text{for } n \geq 0 \tag{3.30}$$

and $\langle \rho(0)^2 \rangle_{eq} = D_e(0)$ where $\vec{\rho}$ is a nearest neighbor displacement vector. Once these relations are taken advantage of, Eq. (3.29) can be partially resummed agained with the final result given as

$$D(\omega, N) = \frac{1}{2d\tau} \left[\langle \rho(0)^2 \rangle_{eq} + 2 \sum_{n=1}^{N} \langle \vec{\rho}(n) \cdot \vec{\rho}(0) \rangle_{eq} \frac{1}{(1 - i\omega\tau)^n} \right] \tag{3.31}$$

where an explicit cut off N in the number of terms summed over has been introduced. The true diffusion coefficient is obtained in the limit that $N \rightarrow \infty$, although often times Eq. (3.31) will converge at $\omega = 0$ very quickly.

It is interesting to note that using $D(\omega)$ from Eq. (3.31) and combining it with the general expression of Eq. (3.12), the continuous time velocity auto-correlation function (VACF) can be related to the step displacement auto-correlation function (SACF) as

$$\begin{aligned} \langle \vec{v}(t) \cdot \vec{v}(0) \rangle_{eq} &= \frac{\gamma_{max}^2}{d} e^{-\gamma_{max} t} \sum_{n=1}^{\infty} \langle \vec{\rho}(n) \cdot \vec{\rho}(0) \rangle_{eq} \, h(\gamma_{max} t, n) \\ &+ \langle \rho(0)^2 \rangle_{eq} \frac{\gamma_{max}}{2d} \delta(t) \end{aligned} \tag{3.32}$$

The singular part will always be present as a consequence of using the frame work of hopping transport because the particle waits for a random interval of time in a state and will then make a transition to another state in a time much shorter than the average waiting time. The time of flight is so small that there is no short time structure to be characterized. The singular part is a consequence of modeling the time of flight between states as instantaneous but is an unphysical artifact in the case of a coarse grained model. Therefore, a coarse grain length scale sets

a limit to the high frequency response. In other words, although the details of the short time behavior cannot be determined, the long time behavior is correctly represented using a delta function impulse.

Again considering a simple random walk, the SACF is zero for all time steps $n \geq 1$ and at $n = 0$ $\langle \rho(0)^2 \rangle_{eq} = a^2$. Therefore only one term is present in Eq. (3.31) to find that $D(\omega) = a^2/2d\tau$ at all frequencies. The other expressions for $D(\omega)$ of Eq. (3.27) and Eq. (3.29) would have required an infinite number of terms. As this example demonstrates, the rate of convergence is much faster by considering the SACF rather than the mean squared displacement of the random walker. Therefore, in the next section the myopic and blind ant models will be considered again, but in terms of the SACF.

3.4 Example: Blind and Myopic Random Walks

The blind and myopic ant random walks have been discussed in Chapter 2 Section 3 and explicitly defined in Eq. (2.27) and Eq. (2.25) respectively. The focus of that section was on the mean squared displacement and the calculation of the walk exponent d_w. In this section, the focus will shift to the step displacement auto-correlation function (SACF). First some numerical results for the blind and myopic ants will be presented. The behavior of the SACF for the myopic ant is found to be more complex than that of the blind ant. The SACF will be analyzed by decomposing an expression involving the transition probability matrix into an eigenvector expansion. Some exact properties, and general scaling arguments are

given; including the conjecture that the envelope for the oscillations in the myopic SACF on bipartite lattices decay as a power-law with exponent given by half the spectral dimension. Furthermore, the spectral dimension has been numerically determined for the square, simple and body centered cubic lattices. Finally, the SACF from the blind and myopic walks are used to determine the frequency dependent diffusion coefficient.

3.4.1 Complexities in Autocorrelation Functions

The SACF will be denoted as $C_\rho(n)$ to simplify the notation. A typical SACF is shown in Fig. 3.1 for the blind ant on a square lattice. Unless otherwise stated, the function $C_\rho(n)$ is calculated using stationary initial conditions as calculated from the transition matrix. From the same data set that was used for the mean squared displacement, as shown in Fig. 2.7, the SACF as plotted in Fig. 3.1 is from a blind ant on one percolation cluster in a $(p_c \approx 0.593, S = 5000)$ ensemble. The decay in the SACF appears to to be very rapid, but in fact the decay is algebraic. The first several time steps have been omitted for clearity. It is observed that $C_\rho(n) < 0$ for $n > 0$ with $C_\rho(0)$ being the only positive correlation. In particular, $C_\rho(0) = a^2\overline{\zeta}/z$ for the blind ant on lattices having all equal nearest neighbor bond lengths. For example, the average number of bonds per site was found to be $\overline{\zeta} = 2.5100$ for the cluster used in Fig. 3.1 and with $a = 1$ it follows that $C_\rho(0) = 0.6275$.

Assuming that $\langle R(n)^2 \rangle_{eq} \sim An^{2/d_w}$, then the SACF is expected to decay as a

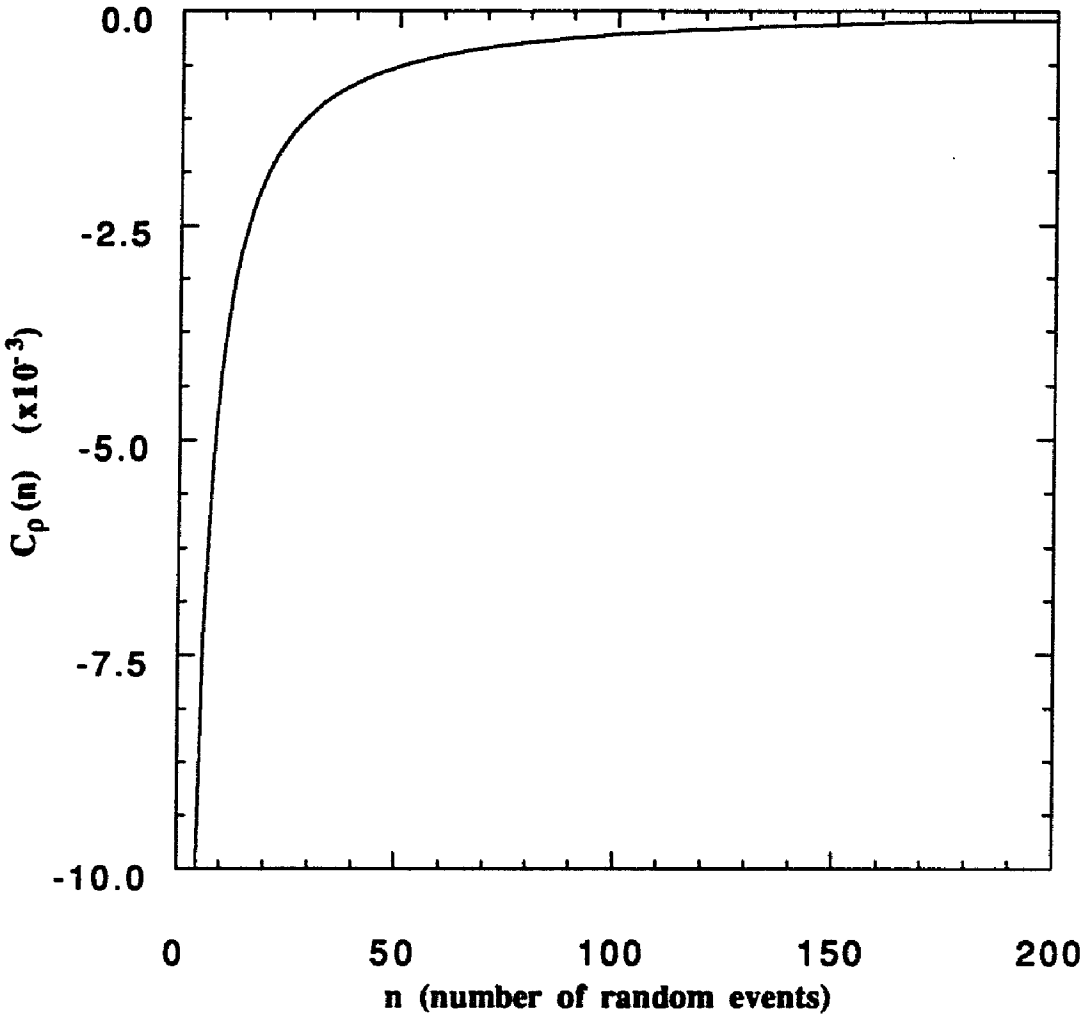

Figure 3.1

The step displacement auto-correlation function (SACF) for the blind ant on a given percolation cluster generated on the square lattice in the ($p_c \approx 0.593, S = 5000$) ensemble is plotted above. The resulting mean squared displacement from two summations has been plotted in Fig. 2.7.

power-law such that

$$\langle \vec{\rho}(n) \cdot \vec{\rho}(0) \rangle_{eq} \equiv C_\rho(n) \sim \frac{1}{2}\frac{2}{d_w}\left(\frac{2}{d_w} - 1\right) A n^{-d_v} \tag{3.33}$$

where $d_v = 2 - 2/d_w$ analogous to two differentiations in continuous time. As calculated using Eq. (2.19), the SACF is plotted in Fig. 3.2 on a log-log scale verifying the above expectations. For example, from the mean squared displacement it has been found that $A \approx 1.00 \pm 0.13$ and $2/d_w \approx 0.706$, thus predicting that the amplitude of the SACF should be $A' \approx 0.105$ and $d_v \approx 1.29$. As determined from Fig. 3.2 with $A' \approx 0.076 \pm 0.004$ and $d_v \approx 1.25$ it is seen that rough agreement is obtained. Moreover, the simple power-law behavior that is found for the blind SACF from differentiating the leading term in the mean squared displacement twice is observed for all lattices considered.

Of course we expect deviations in $C_\rho(n)$ from a pure power-law decay since the mean squared displacement itself has various corrections associated with the free boundary conditions. This is why only rough agreement is obtained when simple log-log plots are compared. Furthermore, it would be possible to see a crossover from a power-law to an exponential decay if the random walk is calculated to extremely long times. This crossover is caused by the fact that the transition probability matrix is of finite size so that the largest eigenvalue less than one will become the dominant contribution[77] in the limit $n \to \infty$. However, this crossover is not of interest here, and as discussed before, this time regime is easily avoided. Because the mean squared displacement saturates to a maximum value, the local

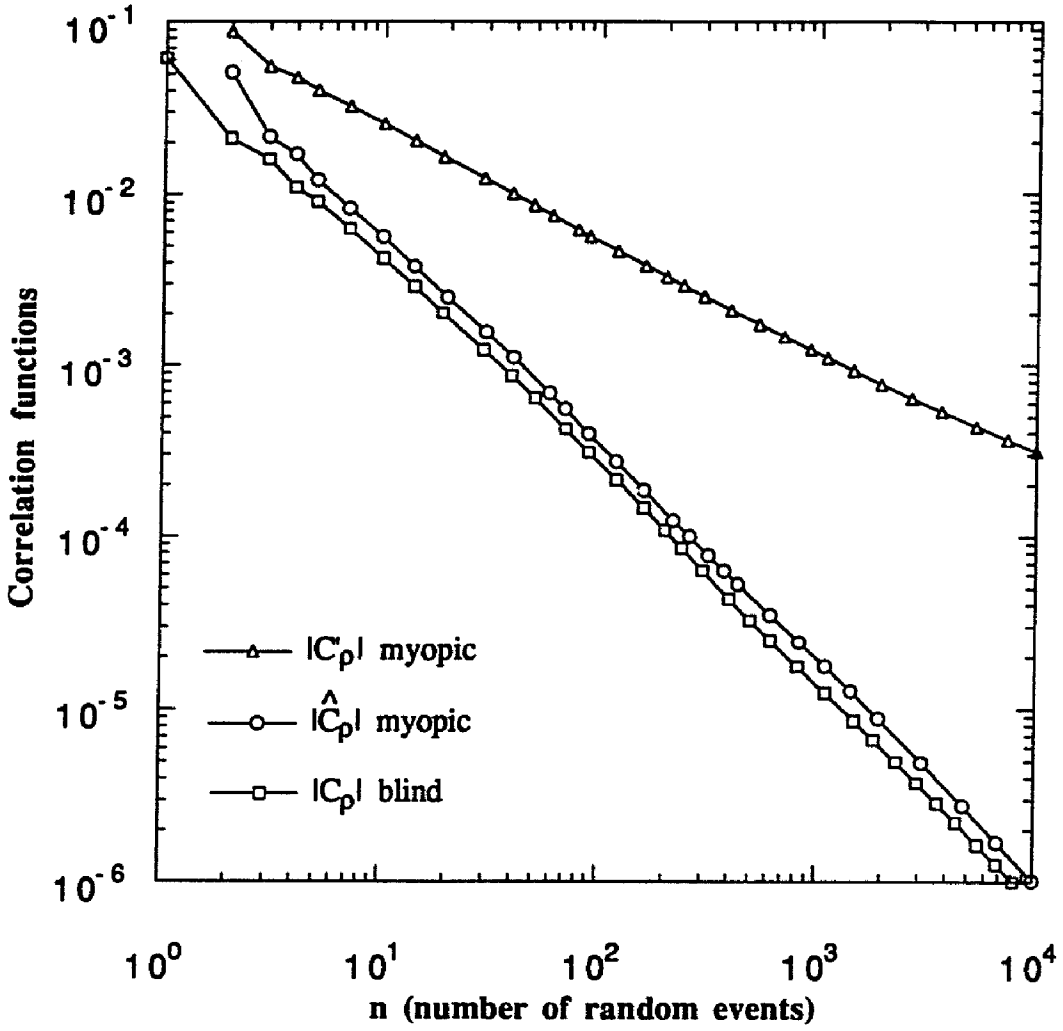

Figure 3.2

From Fig. 3.1 the magnitude of the SACF, denoted as $\mid C_\rho(n) \mid$ and represented by a □ symbol, clearly decays as a power-law as demonstrated on the above Log-Log scale. Also plotted in this same figure is the magnitude of the two parts of the myopic SACF denoted as $\mid \hat{C}_\rho(n) \mid$ and $\mid C'_\rho(n) \mid$ and represented by the ○ and △ symbols respectively. Both the myopic and blind ant data are from the same cluster generated in a $(p_c \approx 0.593, S = 5000)$ ensemble. It is noted that $C_\rho(n)$ of the blind ant is essentially the same as $\hat{C}_\rho(n)$ of the myopic ant.

slope $D_e(n \rightarrow \infty) \rightarrow 0$ implying that

$$C_\rho(0) + 2\sum_{n=1}^{\infty} C_\rho(n) = 0 \quad . \tag{3.34}$$

The crucial point of this sum rule is that the negative correlations are collectively important over long times.

The SACF for the myopic ant on the square lattice is plotted in Fig. 3.3 for the same cluster used for the blind ant above. The first several points are not plotted for clarity. We note that $C_\rho(0) = a^2$ for the myopic ant on lattices with equal bond length where $a = 1$ for the square lattice. There is a remarkable difference between the myopic SACF to that of the blind SACF. As clearly seen, the myopic SACF undergoes a change in sign at each time step where a positive (negative) correlation in the step displacement relative to the initial step displacement is found at all even (odd) time steps. The two curves that form an envelope (one for the even time steps and one for the odd time steps) are not symmetrical about the time axis, but rather are skewed downward. These regular oscillations are found to persist for all time and will generally not decay to zero. A residual oscillation amplitude of $\mid C_\rho(n \rightarrow \infty) \mid = 6.595 \times 10^{-5}$ was found for the myopic SACF that was plotted in Fig. 3.3.

The myopic SACF is split into two parts defined by $C_\rho(n) = \hat{C}_\rho(n) + C'_\rho(n)$ where

$$\hat{C}_\rho(n) = \frac{1}{2}\{ C_\rho(n) + \frac{1}{2}[C_\rho(n-1) + C_\rho(n+1)]\} \tag{3.35}$$

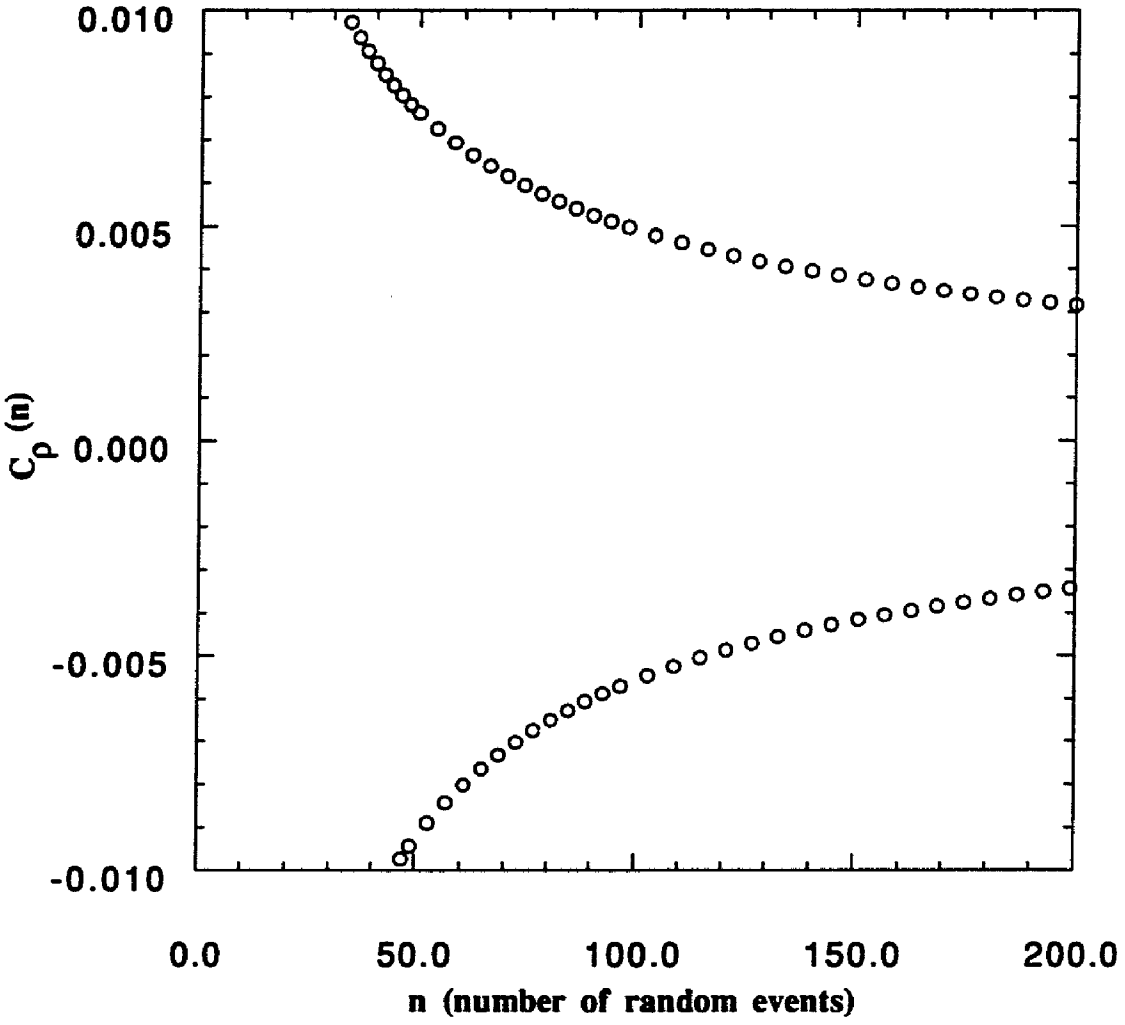

Figure 3.3

The myopic SACF for the same generated percolation cluster as used for the blind ant in Fig. 3.1 is plotted above. For clarity, all even and odd time steps are plotted up to $n = 50$, then every other odd-even pair $\{(53,54),(57,58),...\}$ is plotted up to $n = 100$ and finally a skip of two odd counts $\{(103,104),(109,110),(115,116),...\}$ is plotted. Note that the resulting mean squared displacement obtained after two summations has been plotted in Fig. 2.7.

is the *center* part of the SACF and

$$C'_\rho(n) = \frac{1}{2}\{\, C_\rho(n) - \frac{1}{2}[\, C_\rho(n-1) + C_\rho(n+1)\,]\,\} \tag{3.36}$$

defines the *oscillating* part of the SACF. The function $C'_\rho(n)$ is also positive (negative) for even (odd) time steps, however, the two envelopes that are formed are nearly symmetrical about the time axis. Therefore, the envelope of the oscillating component to the SACF is taken to be the absolute value of $C'_\rho(n)$. Although the terminology has not been used in this thesis, the SACF has been called[41] a *discrete time velocity auto-correlation function* for obvious reasons. In this context, it is noted here that $C'_\rho(n+1) = \frac{-1}{4}\frac{d^2}{dn^2}C_\rho(n)$ and is equal to 1/4 times the *discrete time acceleration auto-correlation function.*

Similarly the function $C'_\rho(n)$ could be split into two parts such that $C'_\rho = \hat{C}'_\rho + C''_\rho$, and then C''_ρ can be split into two parts, etc. If any oscillations are present at all, then they will show more strongly in higher order correlation functions. This continued process, however, does not lead to any advantage in the analysis of the SACF. In fact, splitting $C_\rho(n)$ into two parts $(\hat{C}_\rho, C'_\rho)$ has been found advantageous only in cases where there is a strong oscillating component in $C_\rho(n)$ as usually obtained by the myopic ant. Because the mean squared displacement is obtained from two summations over the SACF, (analogously two integrations over the VACF) the rapid oscillations that are present in the myopic SACF sum up into a negligible contribution for the mean squared displacement. Thus the ever present negative contribution from $\hat{C}_\rho(n)$ for $n \geq 1$ is responsible

for the anomalous characteristics of the mean squared displacement.

The SACF for the blind ant can also be split into the two parts $\hat{C}_\rho$ and C'_ρ. However, because $C_\rho(n)$ has a relatively smooth power-law decay, it follows that $\hat{C}_\rho(n) \approx C_\rho(n)$ with no essential difference between these functions. Moreover, with the exception of the first ten to twenty time steps, the function $C'_\rho(n)$ can be completely neglected since it decays as a power-law with exponent $-2 - d_v$. Therefore the function $C_\rho(n)$ for the blind ant is compared with $\hat{C}_\rho(n)$ for the myopic ant in Fig. 3.2 on a Log-Log scale. These two functions exhibit the same power-law behavior. The leading power-law characteristics in the mean squared displacement of the myopic ant is determined by $\hat{C}_\rho(n)$. Also shown in Fig 3.2 is the envelope of the strong oscillating component contained in $C_\rho(n)$ as described by $\mid C'_\rho(n) \mid$. The envelope for the oscillations decay as a power-law but much slower with an exponent of ≈ -0.70.

A strong oscillation envelope for the myopic ant is present when the cluster is bipartite. A bipartite cluster can be separated into two subsets of sites with a definite "parity" defined by an even or odd chemical distance. That is, for nearest neighbor connection rules, a site can only connect to another site with one higher or lower chemical distance. Obviously, no connections can be between sites with the same chemical distance. In general, a large randomly generated cluster will not be bipartite unless the underlying lattice is bipartite such as the sq, sc or bcc lattices.

Three distinct types of characteristics have been found for the SACF for the

Brownian motion on statistical fractals depending in part on the type of ant and whether the clusters are bipartite or not. A smooth power-law decay is obtained for the blind ant on any type of lattice. The myopic SACF will oscillate strongly with an envelope decaying as a power-law for bipartite clusters. Furthermore, the oscillation envelope will generally decay to a finite value. For non-bipartite lattices the myopic SACF will have a oscillation envelope that decays exponentially to zero.

A comparison of the function $\mid C'_\rho(n) \mid$ for the blind and myopic ants is given in Fig. 3.4 for the fcc lattice. These results are from a configurational average over 20 clusters within the $(p_c = 0.200, S = 1000, 5000, 10000)$ ensembles for the myopic ant and the $(p_c = 0.200, S = 5000)$ ensemble for the blind ant. Also included in the figure is the results for the myopic ant for the bcc lattice from an average over 100 clusters in the $(p_c \approx 0.245, S = 30000)$ ensemble. The results up to a time step of 10000 for the blind ant on the fcc lattice and myopic ant on the bcc lattice are independent of the size of the clusters provided $S > 1000$. The three curves for the myopic ant on the fcc lattice demonstrate that $\mid C'_\rho(n) \mid$ has a specific characteristic time dependence. Unfortunately, large variations in crossover times (as indicated in Fig. 3.4 as η_1 and η_2) prevented us to parameterize the curves as a function of cluster size.

The oscillation envelope for the myopic ant on the bcc lattice decays as a power-law with an exponent of ≈ -0.66 and is the same for the sc lattice at criticality indicating universality. For the myopic ant on the fcc lattice, there appears to be

three distinct regions as indicated by Fig. 3.4. For time steps less then n_1 the oscillation envelope decays roughly as a power-law. This power-law regime is very short lived and the exponent does not tend to follow the bcc or sc results. Between time steps n_1 and n_2 the oscillation envelope, $\mid C'_\rho(n) \mid$, decays exponentially fast. Consequently, after time step n_2, the myopic C'_ρ is essentially the same as that of the blind ant. The blind C'_ρ does not describe an oscillation envelope but rather a smooth positive power-law decay.

We expect that the even-odd oscillations in the SACF for the myopic ant is an indication of a more general result that oscillations with longer period can occur from multiple scattering events (or equivalently from consecutive scattering of a random walker from different vacancies.) At sufficiently high dilution the occupied sites on a lattice will form a precarious network with many singly connected bonds, and thereby reduce the distinctions among different lattice structures. For example, the myopic SACF did contain oscillations in the close packed fcc lattice. Even in the continuum, ill-connected networks are expected to give rise to multiple scattering events and consequently develop oscillations in at least some auto-correlation functions. However, the other important ingredient is to have a myopic like dynamics for the random walker.

Multiple scattering events also occur on regularly shaped clusters that are completely filled containing no vacancies, but are bounded by the last chemical distance shell. In these regular geometric structures, the myopic and blind ants have oscillations with an exponential decay in their SACF for bipartite lattices and no

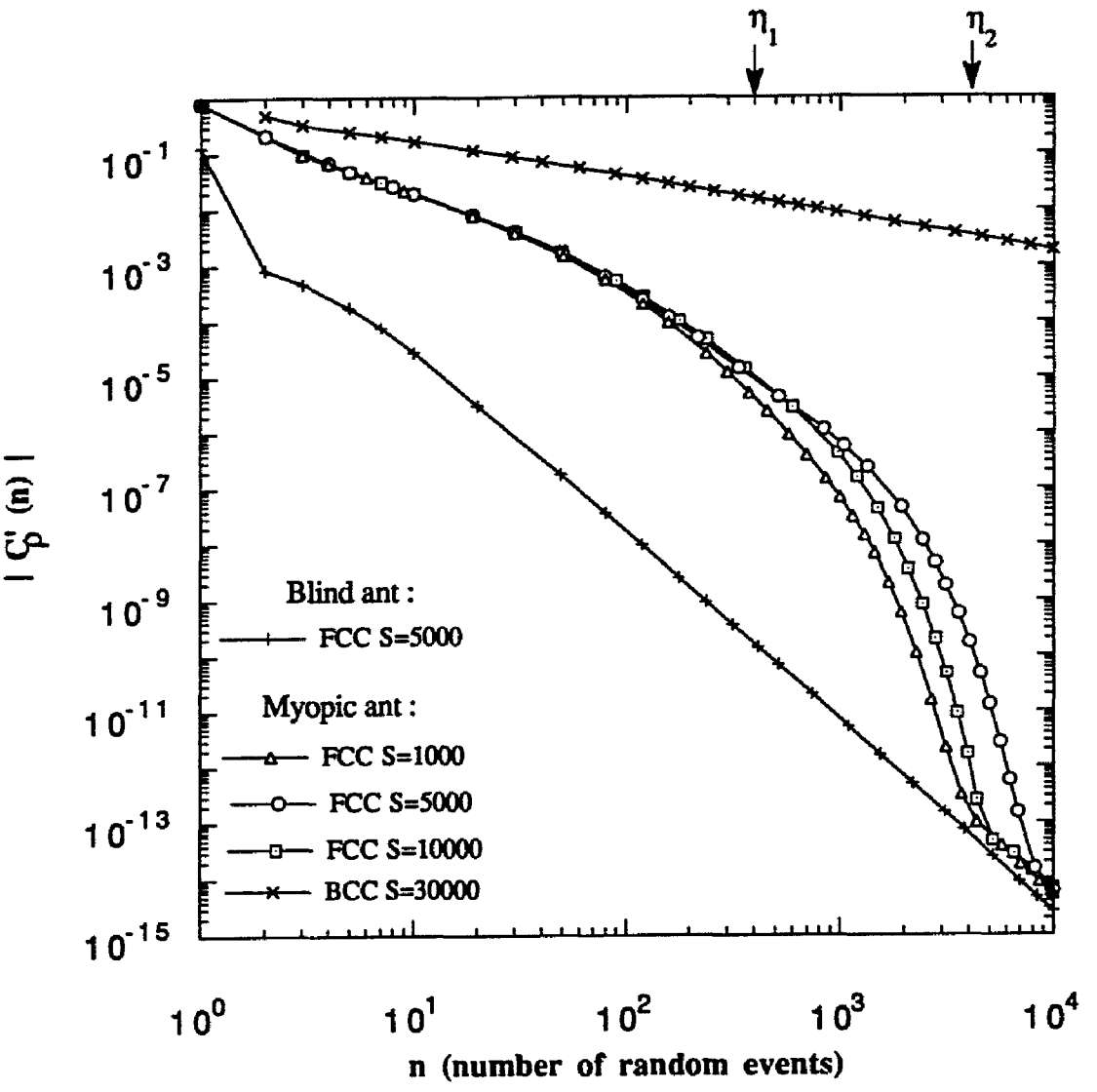

Figure 3.4

The function $\mid C'_\rho(n) \mid$ is plotted for 5 different cases. The line with the + symbol is for the blind ant over an average of 20 clusters of size $S = 5000$ on the fcc lattice. The three curves with symbols $\triangle, \bigcirc, \square$ correspond to the myopic ant over an average of 20 clusters on the fcc lattice of size $S = 1000, 5000, 10000$ respectively. Finally, the line with the $\times$ symbols is for a myopic ant over an average of 100 clusters of size $S = 30000$ on the bcc lattice. The oscillations in the myopic SACF on the fcc lattice decay exponentially between $n_1 \leq n \leq n_2$. In this figure, $\{n_1, n_2\}$ refer to the curve defined by the $\square$ symbol.

oscillations for non-bipartite lattices. This gives an indication that oscillations may be present for mesoscopic and macroscopic disordered media. On the other hand, these results also suggest that a coarse grained model may artificially affect the oscillations in the correlation functions depending on the choice of a bipartite or non-bipartite lattice grid. Of course, the oscillations (if they exist) only play a role in the fine structure in the description of the random walk. Herein lies the reason that these oscillations had not been reported earlier by a large body of literature now available on diffusion on fractals[35, 45] or on various Lorentz gas models[66]. Obviously, there are a large number of complexities involved which depend on the details of the medium and dynamical model.

3.4.2 Analysis of the Transition Probability Matrix

To understand the general features of the SACF, Eq. (2.20) will be expanded in terms of the eigenvalues and eigenvectors of $\hat{W}$. In the case of the blind ant $\hat{W}$ is a Hermitian matrix (real and symmetric,) thus the eigenvectors form a complete set and the eigenvalue spectrum is real. Although it is not always possible to diagonalize a transition probability matrix, a sufficient condition for diagonalizability is that a detailed balance relation exits with respect to a positive definite stationary state vector[12]. For the myopic ant, the detailed balance relation

$$w(s',s)V_1(s) = w(s,s')V_1(s') \tag{3.37}$$

can be used to transform $\hat{W}$ into a symmetric matrix $\hat{W}_s = \hat{M}^{-1}\hat{W}\hat{M}$, where $\hat{M}$ is a diagonal matrix with its elements given by $\sqrt{V_1}$. It follows that both the left

eigenvectors $\{U_\Lambda\}$ and right eigenvectors $\{V_\Lambda\}$ are complete with a real eigenvalue spectrum, being identical to the spectrum of the Hermitian matrix $\hat{W}_s$. As N. Fuchs became interested in calculating the myopic eigenvalue spectrum[78] he notice the above transformation, and then it was pointed out by R. Muralidhar that this is a general result.

In general it is possible to construct stochastic models for which $\hat{W}$ cannot be transformed into a Hermitian matrix. It can happen that $\hat{W}$ is not diagonalizable[12] so that the eigenvalue spectrum is degenerate and the set of eigenvectors are not complete.[12] If $\hat{W}$ is diagonalizable without detailed balance, then a complete set of eigenvectors exist but the eigenvalue spectrum will include complex numbers where $\mid \Lambda \mid \leq 1$. However, these additional complications are not present for either the blind or myopic ant models.

The position auto-correlation function for the blind and myopic ants as described by Eq. (2.20) reduce to

$$\langle \vec{r}(n) \cdot \vec{r}(0) \rangle = \sum_{\Lambda} a_\Lambda \, \Lambda^n \tag{3.38}$$

where the eigenvalues are real with range $-1 \leq \Lambda \leq 1$. The coefficients a_Λ are given by

$$a_\Lambda = [\sum_{s_f} V_\Lambda(s_f)\vec{r}(s_f)] \cdot [\sum_{s_o} U_\Lambda(s_o)\vec{r}(s_o)V_1(s_o)] \tag{3.39}$$

in terms of the left (U_Λ) and right (V_Λ) eigenvectors. The eigenvectors are chosen such that

$$\sum_{s=1}^{S} U_\Lambda(s)V_{\Lambda'}(s) = \delta_{\Lambda,\Lambda'} \quad . \tag{3.40}$$

Assuming no permanent traps the eigenvalue $\Lambda = 1$ is non-degenerate, and noting $U_1(s) = 1$, the sum rules

$$\sum_{s=1}^{S} V_\Lambda(s) = \delta_{\Lambda,1} \quad \text{and} \quad \sum_{s=1}^{S} U_\Lambda(s) V_1(s) = \delta_{\Lambda,1} \tag{3.41}$$

immediately follow from the above orthonormality condition. These sum rules can be used to show that with the exception of $\Lambda = 1$ the coefficients a_Λ are independent of the origin of coordinates. All the coefficients are non-negative as can be verified easily by working in terms of $\hat{W}_s$.

Noting that the mth order discrete time differentiation of the position auto-correlation function is given by

$$\frac{d^m}{dn^m}\langle \vec{r}(n) \cdot \vec{r}(0) \rangle = \sum_\Lambda a_\Lambda \, \Lambda^n \, (\Lambda - 1)^m \quad , \tag{3.42}$$

and using Eq. (2.18) it follows that

$$C_\rho(n) = -\sum_\Lambda \Lambda^n (\Lambda - 1)^2 \quad . \tag{3.43}$$

The higher order correlation functions, which correspond to higher order derivatives, have expansion coefficients proportional to $a_\Lambda(\Lambda - 1)^m$ where $m = 2$ for $C_\rho(n)$, $m = 4$ for $C'_\rho(n)$, etc. Thus, $(\Lambda - 1)^m$ is just a kinematic factor that weights the negative eigenvalues increasingly more strongly as m increases.

We now prove that the eigenvalue spectrum of the myopic ant on a bipartite cluster is even. We label the sites of a cluster as $s_{l,j}$ where l denotes the chemical distance shell relative to an arbitrarily chosen seed site, and j, $1 \leq j \leq G(l)$,

labels the sites within that chemical distance shell. From the myopic ant rules (Eq. (2.25)), it follows that

$$w(s_{l',j'}, s_{l,j}) \propto \delta_{l'\pm 1,l} \quad . \tag{3.44}$$

If V_Λ is an eigenvector of $\hat{W}$ with eigenvalue Λ then consider the vector $V'(s_{l,j}) = (-1)^l V(s_{l,j})$. Then the operation $\hat{W}V'$ is explicitly given as

$$\sum_{l',j'} w(s_{l,j}, s_{l',j'})(-1)^{l'} V_\Lambda(s_{l',j'}) = \sum_{l',j'} (-1)^{l\pm 1} w(s_{l,j}, s_{l',j'}) V_\Lambda(s_{l',j'}) \tag{3.45}$$

$$= (-1)^{l\pm 1}\Lambda V_\Lambda(s_{l,j}) = -\Lambda V'(s_{l,j}) \quad . \tag{3.46}$$

As proved by construction V' is an eigenvector, indicating that the eigenvectors themselves separate out into pairs as determined by the parity, $(-1)^l$, of each component.

Clearly, the -1 eigenvalue is responsible for the residual oscillation amplitude that is present for the myopic ant on bipartite clusters. From Eq. (3.43) the residual value for the SACF (defined as $C_\rho(\infty) =\mid C_\rho(n \to \infty) \mid$) is given as $4a_{-1}$ and similarly $C'_\rho(\infty) = 4a_{-1}$. An undamped oscillation in a correlation function physically implies a deterministic process is present. The residual oscillation in the myopic SACF indicates that if the ant started on an even parity site, then at all odd (even) time steps it must be on an odd (even) parity site. It is possible that $a_{-1} = 0$ even though this deterministic mechanism is present, as in the case of a diamond shaped configuration on the square lattice. Note that the mean squared displacement for a myopic ant on a finite bipartite cluster for $n \to \infty$ will oscillate

indefinitely such that $\langle R(n)^2 \rangle = R_M^2 + a_{-1}(-1)^n$ which Eq. (2.29) neglects the oscillating part.

For finite clusters with free boundary conditions, the coefficient a_{-1} can be calculated from

$$a_{-1} = [\sum_{s=1}^{S} \vec{r}(s)\,\zeta(s)\,(-1)^{l(s)}]^2 / [\sum_{s=1}^{S} \zeta(s)]^2 \tag{3.47}$$

where $l(s)$ is the chemical distance of site s. If periodic boundary conditions are used, there may be no saturation in the mean squared displacement, however, a finite residual value for the SACF will generally occur. An alternative expression for $C'_\rho(\infty)$ which can be used for free or periodic boundary conditions as derived from Eq. (2.24) is explicitly given by

$$C'_\rho(\infty) = \sum_{j=1}^{d} [\sum_{s_f, s_o} o_{\rho_j}(s_f, s_o)(-1)^{l(s_o)}\zeta(s_o)]^2 / [\sum_{s} \zeta(s)]^2 \quad . \tag{3.48}$$

The configurational average of $C'_\rho(\infty)$ is expected to be a function of the size of the clusters.

3.4.3 Scaling of the Myopic Oscillation Envelope

The dependence of $\overline{C'_\rho(\infty, S)}$ on S has been argued by Jacobs and Nakanishi[41] to be proportional to $1/S$ independent of the fractal nature of the clusters. The basic argument begins by observing that the residual oscillation amplitude can be written as a sum over all nearest neighbor step vectors within the cluster. It then follows that $\overline{C'_\rho(\infty)} = \overline{\vec{u} \cdot \vec{u}}$ where

$$\vec{u} = \frac{1}{N_b} \sum_{j=1}^{N_b} \vec{\rho}_j \tag{3.49}$$

and N_b is the number of bonds contained in the cluster. The vectors $\vec{\rho}_j$ are chosen to be directed from the positive to the negative parity sites. For homogeneous disorder, correlations between the set of vectors $\{\vec{\rho}_j\}$ are neglected for any large cluster and/or after a configurational average. The nearest neighbor vectors are treated as independent random variables where the probability distribution for $\vec{\rho}$ is isotropic. Note that the clusters themselves may be anisotropic because each cluster is a single realization. Therefore, $\overline{\vec{u}} = 0$ and from the central limit theorm it follows that $\overline{C'_\rho(\infty)} \propto 1/N_b$. Noting further that

$$\overline{N_b(S)} = \frac{\overline{\zeta}}{2} S\,[1 - AS^{-x} + ...] \quad , \tag{3.50}$$

we expect $\overline{C'_\rho(\infty, S)} \propto 1/S$ to hold for large clusters where the neglect of correlations is more justified and the number of nearest neighbor vectors is proportional to the number of sites. The results from numerical simulation as summarized in Table3.2 show fair agreement with the above argument.

The data, in the case of free boundary conditions, were acquired by generating clusters from a seed site until they naturally stop or reach a maximum allowed size S_{max}. Usually the maximum size was chosen to be 40000. The residual amplitude $C'_\rho(\infty)$ (as well as R^2_M) is calculated for a certain set of sizes $\{S_i\}$. A generated cluster of size $S \leq S_{max}$ is used to represent all clusters of sizes $S_i \leq S$. Thus, a given generated cluster is broken down into as many subclusters as possible. Also periodic boundary conditions were used for site percolation clusters on the square lattice at the critical threshold. The mesh length L was gradually increased

from 12 to 340 where L is always even to ensure a bipartite structure. The exact sizes cannot be predetermined, but a good spread of sizes ranging from $S = 50$ to $S = 70000$ was obtained. Our data consisting of a total of 15492 clusters was binned (for example 10 bins per decade on a logarithmic scale) to arrive at the size dependence of $C'_\rho(\infty)$.

For site percolation, the sample data will generally have a different number of realizations for different size clusters (or bins) for either type of boundary condition. In Table 3.2, the range in the number of clusters refers to the minimum and maximum number of clusters averaged over for a given size. Whenever there were different number of clusters contained in different bins, a weighted least squares fit was performed where the weight factor of a given bin is the ratio of the number of clusters contained in that bin to the average number of clusters per bin. The results of the weighted fits were very near those of a standard least squares fit. In the case of DLA clusters, they were all grown (with free boundary conditions) until they reached the size S_{max}, therefore a weighted fit was not necessary.

As Table 3.2 indicates, the residual oscillation amplitude scales in terms of the size of the clusters as $\overline{C'_\rho(\infty, S)} \approx AS^{-x}$ where the exponent x was found to be nearly one. Unfortunately, an exact value of one is found to lie outside the uncertainties. It appears that either $x = 1 + \epsilon$, where for example $\epsilon \approx 0.06$ for the square lattice, or corrections to scaling throw off the estimate for x when fitted to a simple power-law. For example, corrections to the simple proportionality between N_b and S will cause curvature in the scaling of the residual oscillation as

a function of size. Indeed, the direct scaling of $\overline{C'_\rho(\infty)}$ with respect to N_b showed less curvature ($\epsilon \approx 0.02$), however, this could not completely account for all the curvature.

To test whether the true asymptotic size dependence scales as $1/S$, Fig 3.5 shows a plot of $SC'_\rho(\infty, S)$ verses S for the $p = 0.6$ square lattice data. This data set is the largest and was chosen so because the residual oscillation amplitude of the SACF for percolation clusters on the square lattice near p_c appear to deviate from the expected $1/S$ behavior the most. The choice of $p = 0.6$ was to ensure that large clusters up to $S_{max} = 100000$ could easily be generated. From Fig 3.5 it appears that corrections are present but become negligible for sizes $S \geq 10000$. In view of this supporting evidence, the leading asymptotic scaling of the oscillation amplitude is taken to be proportional to the inverse of the size of the clusters.

The time dependence of the decay in the oscillation envelope for the myopic ant on a bipartite lattice is conjectured using the result that $\overline{C'_\rho(\infty)} \propto 1/S$. After some time, the random walker will only explore a part of the cluster. Therefore, it is expected that $C'_\rho(n) \propto 1/S(n)$ where $S(n)$ is the typical number of sites that the random walker will experience after n time steps. Since $S(n)$ can be estimated as $S(n) \propto [\langle R(n)^2 \rangle]^{d_f/2}$, it follows that $C'_\rho(n) \propto n^{-d_s/2}$ which is the same result (and basically the same scaling argument) as the return to the origin probability.

The crossover between the power-law decay to the residual oscillation amplitude

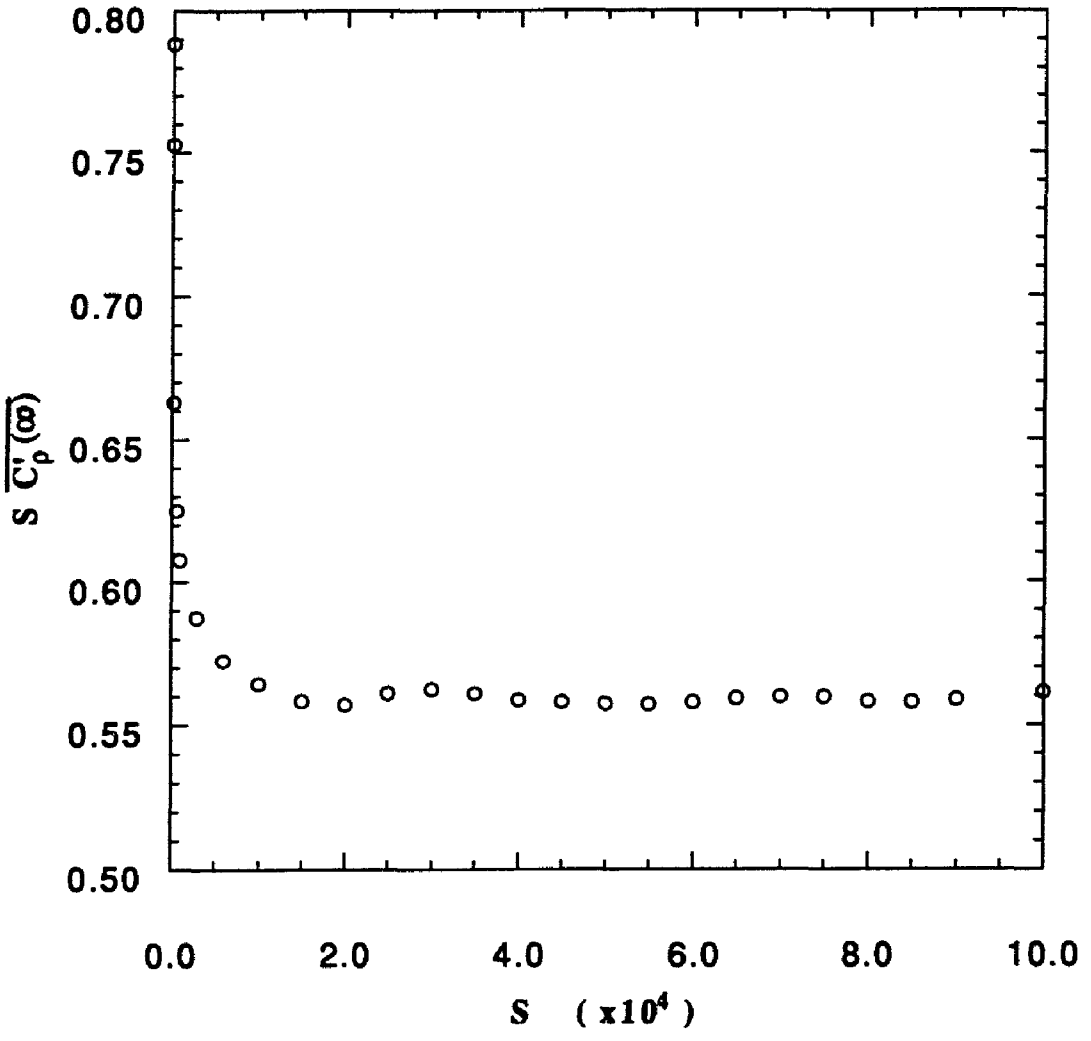

Figure 3.5

The residual oscillation amplitude of the SACF is multiplied by the size of the clusters and plotted against the cluster size. If the oscillation amplitude scales asymptotically as $1/S$, then the graph will be a flat line. Indeed it appears that this is the case for $S \geq 10000$.

can be accounted for very accurately using the fitting form

$$\mid C'_\rho(n) \mid \approx \frac{C'_\rho(\infty)}{1 - A\exp[-(\frac{n}{B})^C]} \tag{3.51}$$

which assumes a single stretched exponential similar to what was done for the mean squared displacement in Eq. (2.29). Since $C'_\rho(\infty)$ can be calculated exactly, there remains three parameters (A, B, C) that need to be fitted. After making an initial guess for A, the inverse of both sides of Eq. (3.51) is taken and then linearized in the same way as described in Chapter 2 for Eq. (2.29). For a given value of A, a standard linear least squares fit yields B and C. This procedure is repeated many times to find the best value of A that obtains a global minimum in error for the final three parameter fit. Observing that $\overline{C'_\rho(\infty)} \propto 1/S$ and for times $n/B < 1$ the function $C'_\rho(n)$ should be independent of the size of the cluster, it follows from a Taylor expansion of Eq. (3.51) that $B \sim S^{d_w/d_f}$ and $C \to d_f/d_w = d_s/2$ as suggested by the simple scaling argument. Note that the parameters (A, B, C) used in Eq. (2.29) for the mean squared displacement and Eq. (3.51) for the oscillation decay are unrelated.

The parameter C is obtained from a given fit over the step range of $100 \leq n \leq N$ for a particular value of A. The spectral dimension $d_S = 2C$ is viewed as a function of (A, N) like the exponent d_w as discussed in detail in Chapter 2. A typical plot of $d_s(A, N)$ verses N for a range of values of A is given in Fig 3.6 for the square lattice data from an average over 200 clusters of size $S = 15000$. The uncertainties for the estimate of d_s are obtained from this kind of plot. In this example, from

Fig 3.6 the spectral dimension was found to be $d_s = 1.36 \pm 0.03$. Conservative error bars have been placed on the exponent estimates because the width in the spread of $d_s(A \pm \delta A, N)$ is of course dependent on the choice of δA. Typically $\delta A = 1.6 \times 10^{-4}$ for clusters of size less than or equal to $S = 15000$, and half that much for larger clusters. The range is set so that, in the extreme limits, the error per data point from these fits are between one to two orders of magnitude greater than the best fit.

The percent error between the best fit and the actual data over the step range of $100 \leq n \leq 10000$ is shown in Fig 3.7. The "percent error residual plots" for the estimation of d_s from Eq. (3.51) (as well as for d_w from Eq. (2.29)) typically look like Fig 3.7. In this example, the data used is the same as that used in Fig 3.6. As in this case, the range of error for the best fit is always less than 3% and often times less than 1%. Note that direct power-law fits yield percent error residual plots having a range in error typically two to three times as much. Although the stretched exponential fitting form used here does not produce residual plots that have a random scatter characteristic, the fitting function of Eq. (3.51) for d_s (Eq. (2.29) for d_w) has been used because it does possess the correct generic saturation features. Moreover, this fitting form performed the best in comparison to other three parameter fitting functions.

Estimates for the spectral dimension from myopic ant random walks on fractal bipartite clusters are given in Table 3.3, and the corresponding values $\{C'_\rho(\infty), A, B, C\}$ from the best fits over the step interval $100 \leq n \leq 10000$

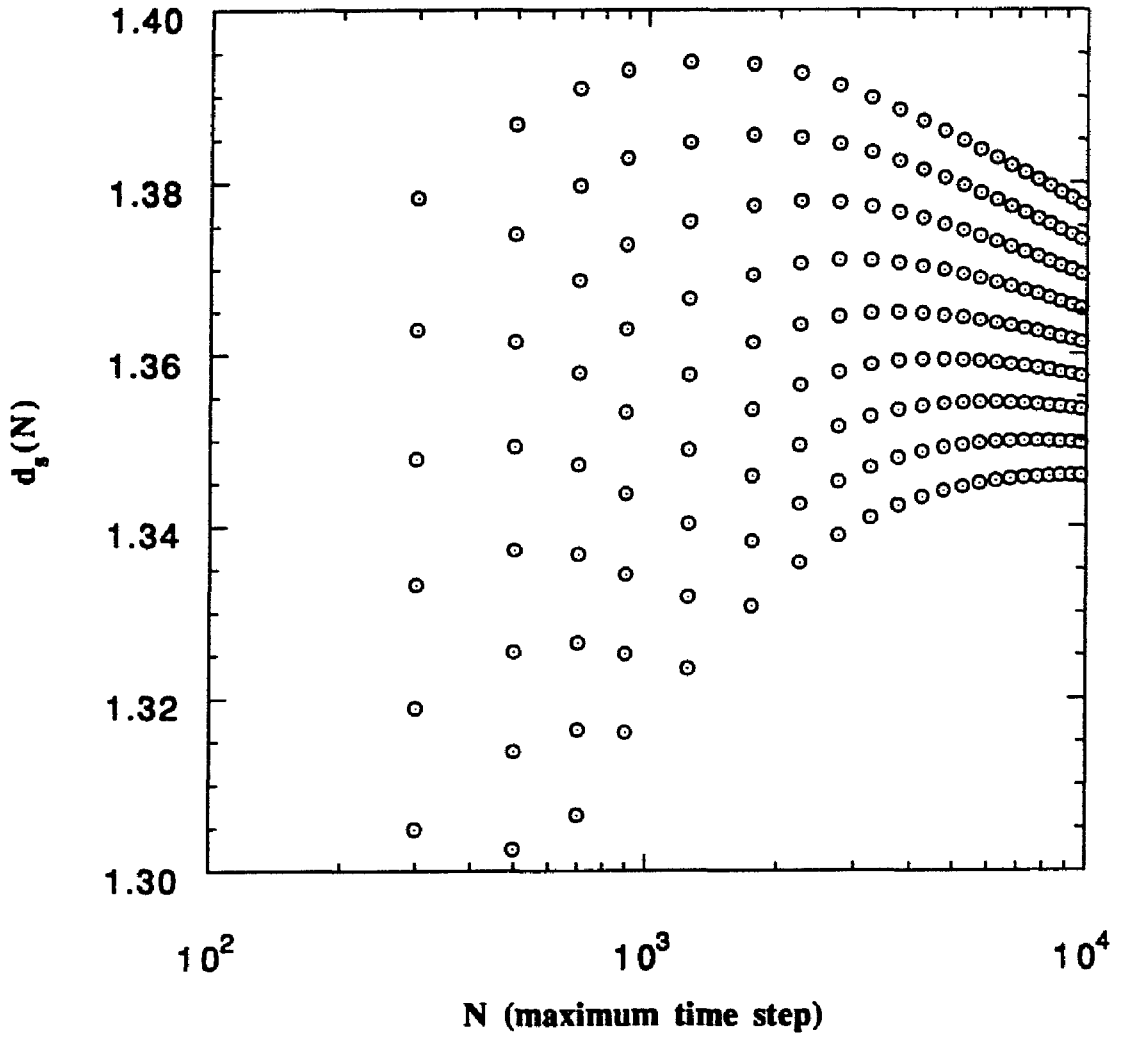

Figure 3.6

The spectral dimension as determined from Eq. (3.51) is viewed as a function of (A, N) and is plotted verses N for various values of A. The data presented here is from an average of 200 clusters of size $S = 15000$ for the myopic ant on the square lattice at the critical threshold. These results correspond to trial M4 as summarized in Tables (3.3 and 3.4). The values of A range from 1.00017 to 1.00049 in increments of 2×10^{-5} where the (lowest, greatest) A corresponds to the (top, bottom) curve.

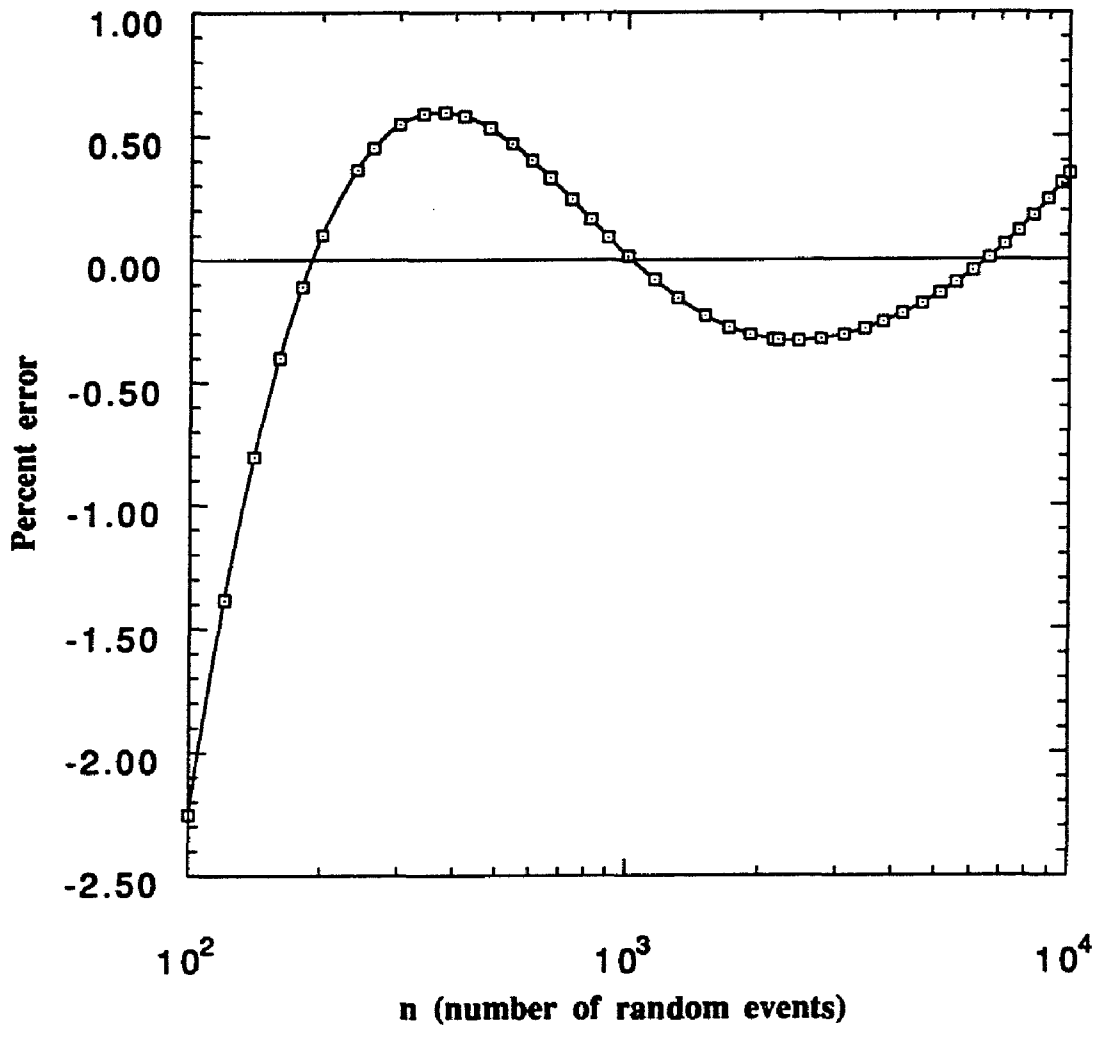

Figure 3.7

The percent error between the fitting function of Eq. (3.51) (denoted as $F(n)$) and the actual data (denoted as $f(n)$) is defined as $E = 100 \times [\, F(n) - f(n) \,]/F(n)$. The percent error residual and is plotted over the range $100 \leq n \leq 10000$ for which the function was fitted. The data and fitting parameters used here are from trial M4 as summarized in tables (3.3 and 3.4) respectively.

are given in Table 3.4. The final spectral dimension estimate for percolation is $d_s = 1.35 \pm 0.03$ in two dimensions, $d_s = 1.34 \pm 0.03$ in three dimensions and for DLA clusters $d_s = 1.19 \pm 0.03$ in two dimensions. Recall that the spectral dimension obtained from the best data collapse in the mean site probability was found to be $d_s = 1.30 \pm 0.02$ on two dimensional percolation clusters. It is unclear why better agreement has not been obtained from these two independent approaches. However, the estimated value for d_s for the DLA clusters is in good agreement with the final estimate of $d_s = 1.19 \pm 0.02$ by Sahimi *et al*[54].

3.4.4 The Frequency Dependent Diffusion Coefficient

The frequency dependent diffusion coefficient, $D(\omega)$, is calculated using Eq. (3.31) with the numerical data for the step displacement auto-correlation function (SACF or $C_\rho(n)$) taken from the myopic ant results on the simple cubic and square lattice. The numerical data is from an average over 10 clusters from the $(p_c, S = 60000)$ ensemble for both cases and ranged to 10000 time steps. Single precision accuracy was used throughout the summation over the numerical data and complex variables were directly used. However, after realizing that more time steps were needed for convergence, in Chapter 5 the summation was performed with double precision for both the real and imaginary parts separately using cosine and sine functions. Although the SACF for the blind and myopic ant models can differ considerably, the function $D(\omega)$ as calculated from the blind ant random walks are practically identical to the myopic walks on corresponding lattices.

Since the models have not yet been devised to correspond to a particular physical system, the choice of the characteristic waiting time τ is completely arbitrary. Although it is probably best to display the function $D(\omega)$ on a frequency scale in units of $1/\tau$, for definiteness the time scale has been chosen in these examples to be $\tau = 1 \times 10^{-12}$ seconds. This time scale is a physically reasonable choice because many a.c. conduction experiments on disordered solids having carrier hopping transport (such as amorphous semiconductors,[22, 79] ionic conductive glasses,[73, 80] and superionic conductors[81]) exhibit an increasing conductivity at high frequencies up to a cut-off frequency of the order 10^{12}Hz. At higher frequencies still, experiments show that the conductivity levels off and/or decreases. However, the high frequency response greater than 10^{12}Hz will begin to be influenced more by resonance effects and less so by the free carrier hopping. These observations suggest that the maximum rate in these systems are in fact typically of the order 10^{12}Hz.

The real part of the function $D(\omega, N = 10000)$ is plotted in Fig. 3.8. The true frequency response $D(\omega)$ can be inferred for sufficiently large frequencies where convergence is obtained in the summation of Eq. (3.31). From the general form of Eq. (3.31), it is clear that at sufficiently high frequencies ($\omega\tau \geq 0.1$) the summation will converge even if $C_\rho(n \rightarrow \infty) =$ constant. Moreover, at extremely high frequencies ($\omega\tau > 10$) the only contributing term in the sum for $D(\omega)$ will be $C_\rho(0)/2d\tau$. Therefore, at very high frequencies $D(\omega)$ levels out to a constant denoted as D_∞, and this result is a general feature of hopping models. In a coarse

grain model, this saturation is an unphysical artifact in chosing a finite minimum length scale.

When the SACF is such that $\hat{C}_\rho(n) < 0$ for $n \geq 1$ the function $D(\omega)$ will be an increasing monotonic function of frequency until saturation at D_∞ is reached. The d.c. diffusion coefficient $D(\omega = 0, N \rightarrow \infty)$, denoted as D_o, will be the lowest value of diffusivity. Unfortunately, unless the sum over the SACF converges sufficiently rapidly, the d.c. properties will not be able to be determined using this numerical approach. In Fig. 3.9 the rate of convergence in the sum of Eq. (3.31) is monitored at different frequencies. This plot is used to determine the range of frequencies for which the function $D(\omega, N)$ accurately converges to $D(\omega)$. For a slowly converging SACF, the general rule of thumb that $N = 1/\omega\tau$ will usually be sufficient for a minimal acceptable level of convergence. As Fig. (3.9) shows, a summation over 10000 time steps is just enough to see Eq. (3.31) begin to converge at $\omega\tau = 10^{-4}$. The wiggles seen in Fig. 3.8 in this frequency range are erroneous. If the SACF does not decay rapidly, the best one could hope for using this method is to obtain $D(\omega)$ for frequencies $\omega\tau \geq 10^{-6}$ corresponding to a million time steps.

We found in Chapter 3 Section 1 that the d.c. diffusion coefficient for fractal media is zero, and moreover $D_o = 0$ for finite clusters with free boundaries. However, a finite d.c. diffusivity is obtained when the frequency range plotted in Fig. 3.8 is extended to lower frequencies because the summation of Eq. (3.31) is truncated. Thus, slow convergence in the SACF makes the estimation of D_o very costly in CPU time if not impossible. As a side remark, note that a random walker

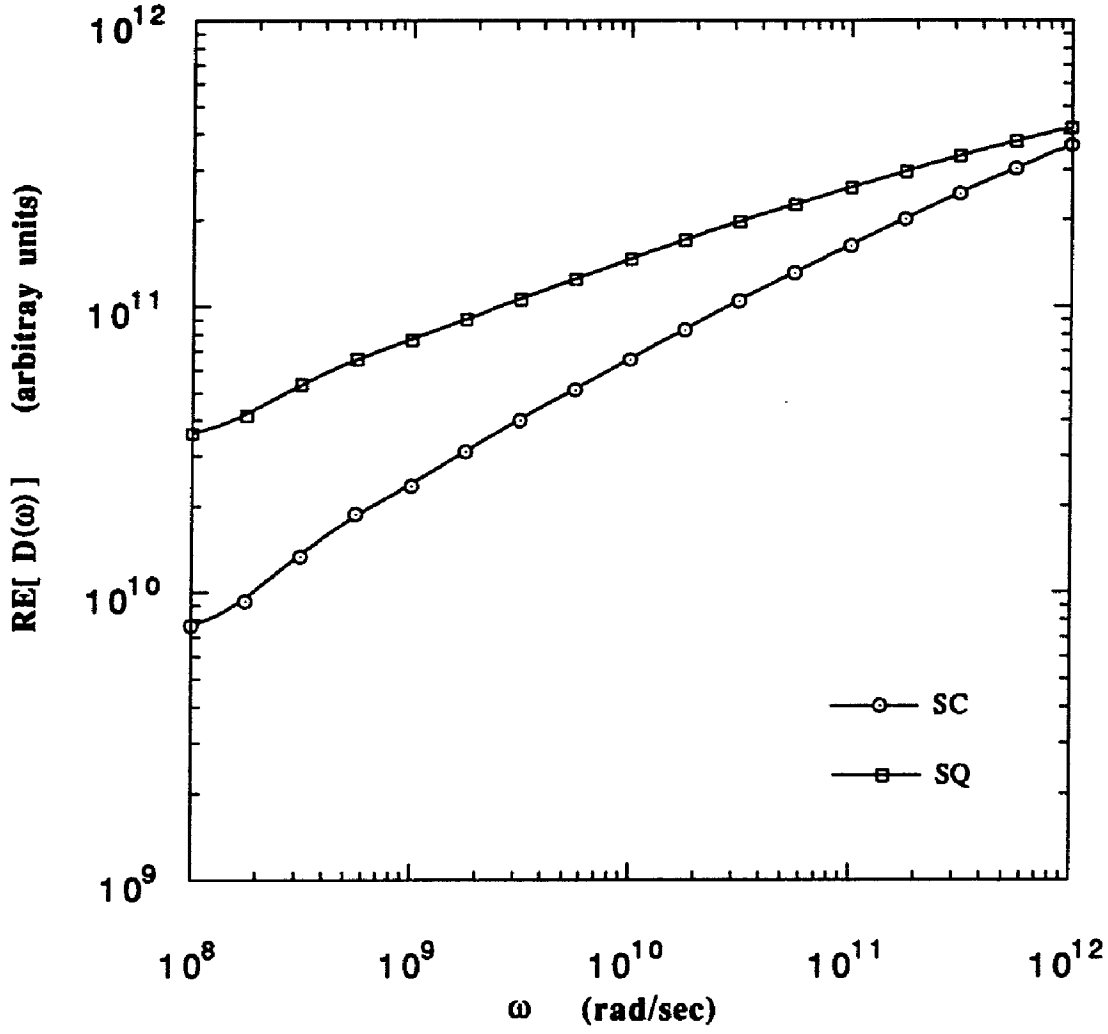

Figure 3.8

The real part of the frequency dependent diffusion coefficient $D(\omega)$ verses frequency ω is plotted. The function $D(\omega)$ was calculated from the myopic SACF for the square □ and simple cubic ○ lattices using a characteristic time of $\tau = 10^{-12}$sec. Only for $\omega \geq 10^{9}$ rad/sec has the summation over the SACF converged.

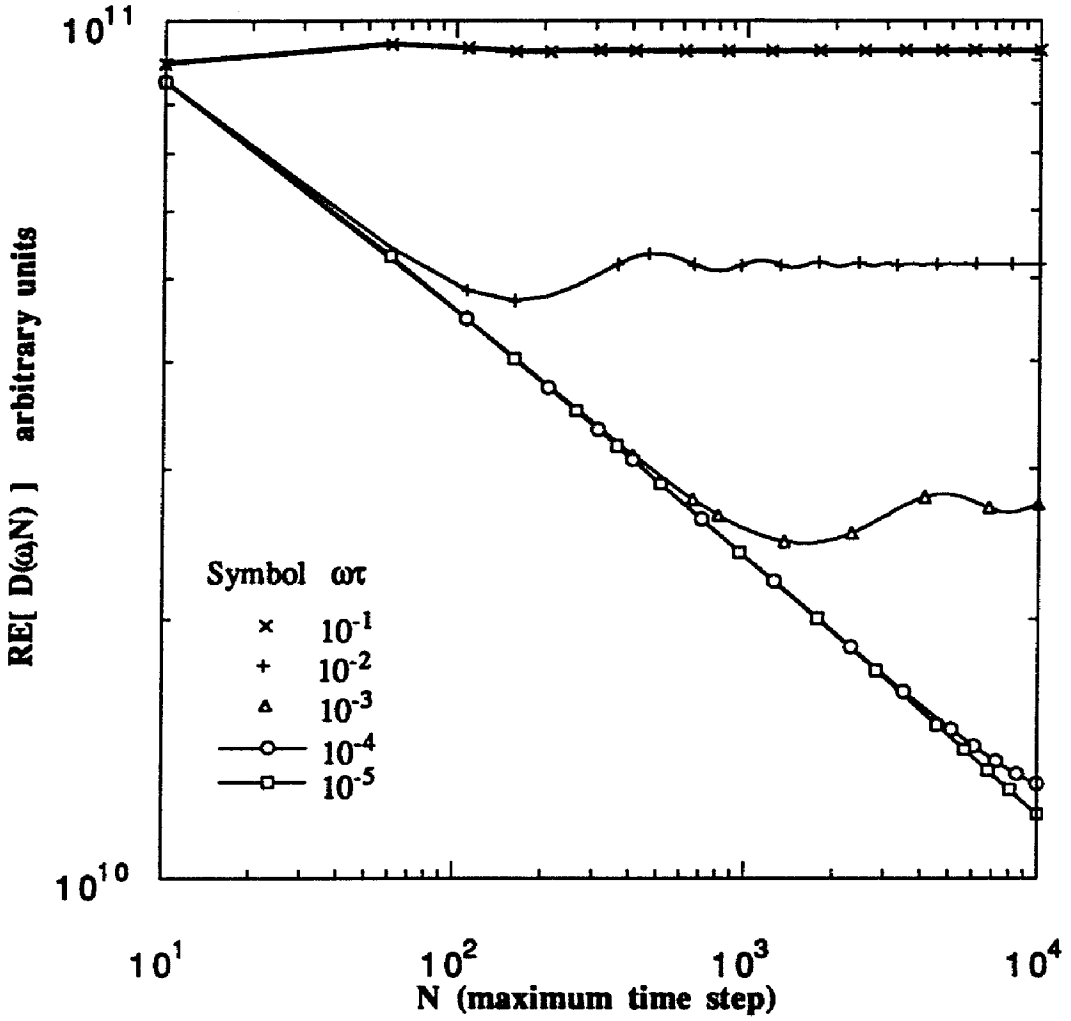

Figure 3.9

The real part of the function $D(\omega, N)$ is plotted verses N for various values of frequency. The function was constructed by summing over N terms on the SACF using a characteristic time of $\tau = 10^{-12}$ sec . The curves with the symbol (x, +, △, ○, □) correspond respectively to $\omega\tau$ equal to $(10^{-1}, 10^{-2}, 10^{-3}, 10^{-4}, 10^{-5})$. Acceptable convergence has set in at $\omega\tau = 10^{-3}$, although $\omega\tau = 10^{-4}$ is just begining to converge.

confined to a finite cluster will have the property that $RE[\,D(\omega \to 0)\,] \propto \omega^2$ as derived by Scher and Lax[22].

A general feature of a.c. conduction in disordered systems is that the real part of $D(\omega)$ often times increases as a power-law ($RE[D(\omega)] \propto \omega^s$) over a restricted range in frequency. For example, $s \approx 0.8$ is typically found in amorphous semiconductors[71, 73]. However, these power-laws are at best only approximate. As seen in Fig. 3.8 power-laws are present with exponents determined as $s = 0.28 \pm 0.01$ and $s = 0.45 \pm 0.01$ for the square and simple cubic lattice respectively. These estimates were made from a standard least squares fit over the frequency range 10^9rad/sec $\leq \omega \leq 10^{11}$rad/sec. It is expected that this power-law region will extend to many decades below. At much lower frequencies still, the exponent will crossover to $s = 2$ characteristic of the finite size of the clusters.

Of course the power-laws for the frequency dependent diffusion coefficient derive from the fact that the SACF decays as a power-law. In a simple minded way, if the SACF is viewed as an exact power-law in continuous time, then a Laplace transform from the time domain to the frequency domain shows that $s = 1 - 2/d_w$. Using typical estimates from Tables (2.1 and 2.2) the expected values are $s = 0.29 \pm 0.02$ and $s = 0.45 \pm 0.02$ for the square and simple cubic lattice respectively which are in gōod agreement with Fig. 3.8. Without much dispersion in the jump rates, it is seen how the long range spatial correlations in the geometric structure plays in important role in the frequency response of the diffusivity or conductivity. The imaginary part of $D(\omega)$ is plotted in Fig. 3.10. Since bound charge influences

the dielectric coefficient to a large degree, the response from just the free charge carriers is not complete, therefore the focus in this thesis is placed on the real part.

It should be noted that in both the blind and myopic ant models, there are only a few different characteristic rates built into the master equation. That is, the dispersion in the frequency dependent diffusion coefficient does not result from a broad distribution in waiting times. Although a broad distribution in jump rates may lead to dispersion in the diffusion coefficient, it was noted by Haus *et al*[82] that a necessary condition for a non-constant $D(\omega)$ was to break inversion symmetry in the rates. In other words, if for any given direction the rate for a particle to hop a certain distance is the same as in the opposite direction without exception, then normal diffusion will occur regardless if there is dispersion in the rates. This is easy to understand in terms of the SACF since by symmetry $C_\rho(n) = C_\rho(0)\delta_{0,n}$. Thus, the dispersion in $D(\omega)$ from either the blind or myopic models comes from the fact that the media is highly ramified.

Various effective medium approaches approaches[69, 71, 72, 83] typically attribute the dispersion of $D(\omega)$ to the dispersion in jump rates. Although the dispersion in jump rates are a physical reality and major player in determining the frequency dependent diffusion coefficient, it follows from the blind and myopic ant models on disordered media that the geometry is an important aspect as well. As a final remark, it is noted that the generalized Langevin equation could describe anomalous diffusion in terms of a non-Markovian process, where as the

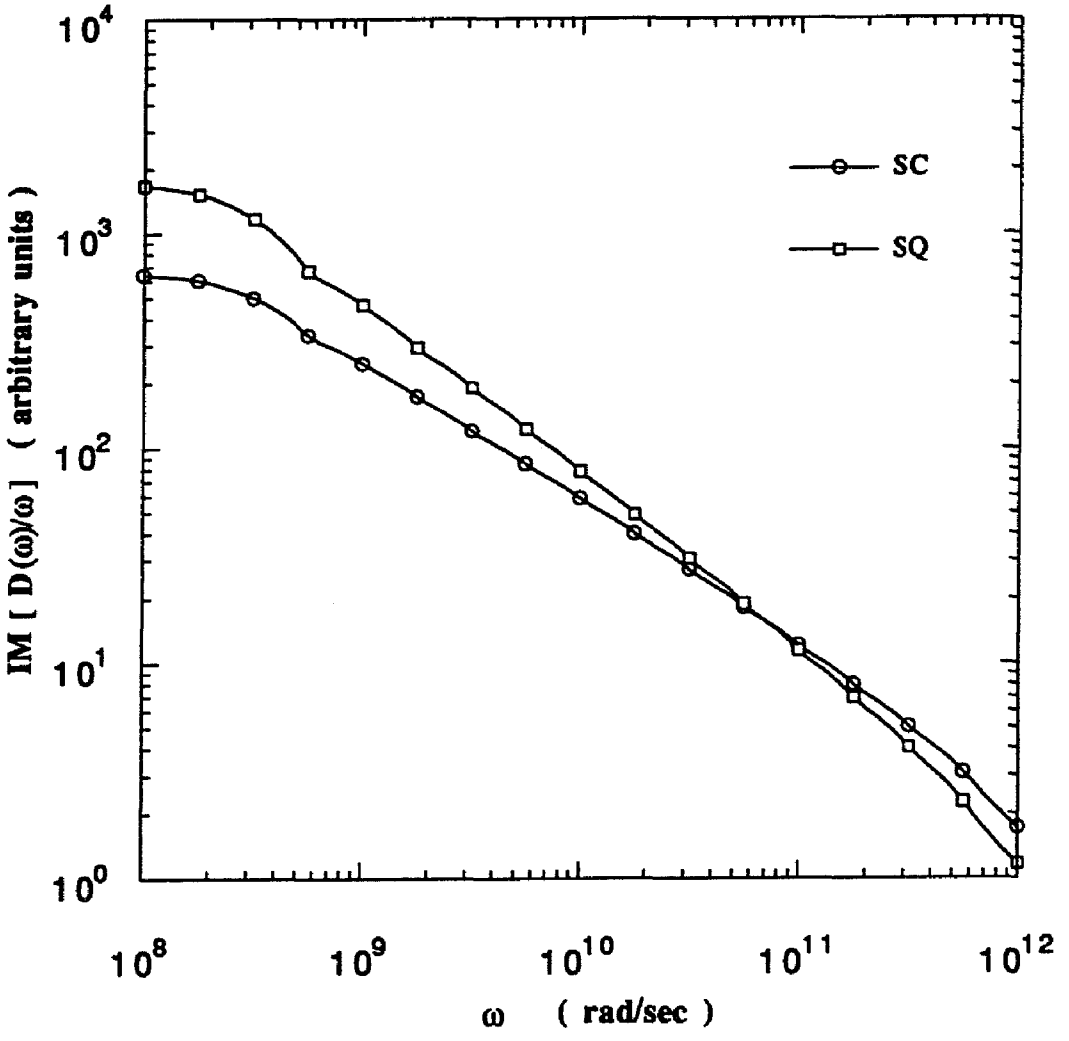

Figure 3.10

The imaginary part of the frequency dependent diffusion coefficient $D(\omega)$ verses frequency ω is plotted. The function $D(\omega)$ was calculated from the myopic SACF for the square □ and simple cubic ○ lattices using a characteristic time of $\tau = 10^{-12}$sec. Only for $\omega \geq 10^9$ rad/sec has the summation over the SACF converged.

same physical system is described later using Markov chains as derived from the continuous time master equation. Of course the reason that this is possible is that the Markov property is recovered at the expense of using a coordinate state space. Thus, the ramification in the geometry translates to a time process that depends on the entire history of the particle's trajectory.

Table 3.1

A summary of certain conditions that follow from equations 3.4 to 3.8 to obtain anomalous or normal diffusion. The presence of a bar in a column indicates that the sign of the coefficient is arbitrary. Also included is the possibility of the particle being trapped, implying a saturation in the mean squared displacement.

diffusion type	exponent	$B_o(T \to \infty)$	c_o
fast	$\alpha \leq 1$	—	> 0
normal	$1 < \alpha$	> 0	—
slow	$1 < \alpha \leq 2$	$= 0$	< 0
trapped	$\alpha > 2$	$= 0$	> 0

Table 3.2

The residual oscillation amplitude in the SACF for the myopic ant on bipartite lattices is expected to scale as a function of cluster size. The numerical results for site percolation clusters with free boundary conditions on the sq, sc and bcc lattices as well as for DLA clusters on the sq lattice were fitted to a simple power-law form given by $\overline{C'_\rho(\infty, S)} \approx AS^{-x}$.
[a] Periodic boundary conditions were used and the cluster sizes were binned.

trial		range in			
Lat.	p	cluster #	S_{max}	A	x
sq	0.593	780 - 1160	40000	0.22 ± 0.005	1.073 ± 0.007
sq	0.6	27040 - 24180	100000	0.21 ± 0.015	1.039 ± 0.004
sq	0.8	400 - 420	40000	0.23 ± 0.025	1.064 ± 0.01
sq	0.9	1060	40000	0.26 ± 0.07	1.07 ± 0.02
[a]sq	0.593	60 - 763	50118	0.12 ± 0.01	0.98 ± 0.004
sc	0.312	440 - 1780	40000	0.53 ± 0.04	1.015 ± 0.005
sc	0.4	460	40000	0.48 ± 0.05	1.03 ± 0.01
sc	0.5	480	40000	0.28 ± 0.06	0.95 ± 0.02
bcc	0.245	140 - 1040	40000	1.83 ± 0.13	1.02 ± 0.006
sq	DLA	123	40000	0.078 ± 0.007	1.024 ± 0.006

Table 3.3

The spectral dimension d_s is obtained from the oscillation envelope and the Alexander and Orbach relation. Here d_w is obtained from the mean squared displacement as summarized in Table 2.1. In calculating d_s, we used $d_f = 1.896$ for 2-d percolation clusters, $d_f = 2.51$ for 3-d percolation clusters and $d_f = 1.666$ for 2-d DLA clusters.

[a] As obtained from fitting to Eq. (3.51)

[b] As calculated from the Alexander and Orbach relation.

[c], [d], [e] Average size of the clusters at $L = \{300, 200, 100\}$ respectively.

trial	lattice	B.C.	p	S	cluster #	d_s [a]	$\frac{2d_f}{d_w}$ [b]
M1	bcc	free	0.245	30000	100	1.34 ± 0.03	1.39 ± 0.06
M2	sc	free	0.312	60000	100	1.36 ± 0.03	1.38 ± 0.06
M3	sq	free	0.593	60000	100	1.35 ± 0.04	1.34 ± 0.05
M4	sq	free	0.593	15000	200	1.36 ± 0.03	1.34 ± 0.04
M5	sq	free	0.593	5000	60	1.35 ± 0.02	1.34 ± 0.03
M6	sq	free	0.593	32944[c]	20	1.39 ± 0.04	1.34 ± 0.04
M7	sq	free	0.593	14465[d]	20	1.35 ± 0.04	1.34 ± 0.05
M8	sq	free	0.593	3740[e]	20	1.35 ± 0.03	1.35 ± 0.05
M9	sq	pbc	0.593	37882[c]	20	1.44 ± 0.05	1.37 ± 0.06
M10	sq	pbc	0.593	14465[d]	20	1.43 ± 0.03	1.37 ± 0.05
M11	sq	pbc	0.593	4680[e]	20	1.55 ± 0.03	1.41 ± 0.05
M12	sq	free	DLA	15000	100	1.19 ± 0.03	1.27 ± 0.05

Table 3.4

A summary on the parameters $\{C'_\rho(\infty), A, B, C\}$ where $C'_\rho(\infty)$ was calculated exactly with Eq. (3.48) and the remaining parameters were obtained from fitting to Eq. (3.51) over a time step range $100 \leq n \leq 10000$.

trial	$C'_\rho(\infty)$	A	B	C
M1	4.6981×10^{-5}	0.99995	2.332×10^{6}	0.6719
M2	1.8650×10^{-5}	0.99994	1.405×10^{6}	0.6789
M3	2.7000×10^{-5}	1.00009	4.928×10^{6}	0.6783
M4	1.0496×10^{-5}	1.00033	6.564×10^{5}	0.6804
M5	2.8445×10^{-5}	1.00084	1.649×10^{5}	0.6742
M6	3.0739×10^{-6}	1.00006	3.453×10^{6}	0.6927
M7	7.4018×10^{-6}	1.00021	1.140×10^{6}	0.6762
M8	4.7077×10^{-5}	1.00194	6.817×10^{4}	0.6789
M9	2.5022×10^{-6}	0.99999	3.429×10^{6}	0.7206
M10	5.8403×10^{-6}	1.00003	1.075×10^{6}	0.7141
M11	4.5189×10^{-5}	0.99915	4.252×10^{4}	0.7746
M12	1.6624×10^{-5}	1.00006	3.230×10^{6}	0.5948

4. PERSISTENT RANDOM WALK MODEL

4.1 Drude-Like Mobility in Homogeneous Media

The objective of this section is to construct a random walk model such that the resulting Brownian motion of a particle with charge q in homogeneous media is well characterized by a simple Drude-like mobility.[84, 85, 86, 87] A Drude-like mobility has the familiar form of

$$\mu(\omega) = \frac{\mu_o}{1 - i\omega\tau_{tr}} \tag{4.1}$$

were μ_o is the d.c. mobility and τ_{tr} is the transport time or the mean free time between scattering. The electrical conductivity is given by $\sigma = qn\mu$ where n is the concentration of the free charge carriers. The frequency dependent diffusion coefficient and mobility are related by the generalized Einstein relation as $D(\omega) = \frac{k_B T}{q}\mu(\omega)$. In terms of the Brownian motion of the free charge carriers, the Drude-like frequency response is the consequence of an exponential decay in the real time velocity auto-correlation function (VACF). As discussed in Chapter 1, the Langevin equation is a stochastic model which yields an exponential decay in the VACF. The simple random walk with a Poisson waiting time distribution is an inadequate model to produce Drude-like diffusion because there is no correlation in the particle's velocity (ie. step displacement.) Therefore, the scenario used here

is to incorporate correlated displacements[9, 21, 77] into a random walk model. To be more specific, a two dimensional persistent random walk for infinite media will be introduced using a square lattice. Although the one dimensional case is easier to present, the solution does not offer a form that can be visually extended to d-dimensions. Following the analysis for the homogeneous case, scattering rules at the interface between different media are defined. These results will carry directly over to Chapter 5 where persistent random walks are studied on a disordered square lattice.

From the relation given in Eq. (3.31) the complex frequency dependent diffusion coefficient is obtainable from the step auto-correlation function (SACF). The relation is valid for hopping transport where the mean waiting time spent at a local site is much longer than the time of flight between sites. In contrast, electrons (treated semi-classically) in the conduction band of a given material remain in the same velocity state until a scattering process occurs which is assumed to be virtuely instantaneous. However, by interpreting a site to correspond to a coarse grain cell of certain volume, a lattice network of these cells can be constructed such that almost surely the electron will be found in some cell and not between cells. Thus the coarse graining artificially divides the electron's time of flight into cells with the result that space has been discretized. The collection of these cells (or sites) define a discrete state space for which the hopping transport formalism can be applied.

The correlated random walk model in homogeneous media as discussed in the

introduction[12, 77] is revisited here but in a different context. An exponential decay in the VACF can be produced by a forward persistence in the random walker's step displacement. The persistence is incorporated by introducing z internal states within each cell where z is the coordination number of the lattice. A random walker is allowed to hop to a nearest neighbor cell (site) or to make a transition to an internal state while remaining within a cell as Fig. 4.1 schematically shows. The internal transitions are responsible for the random walker to lose its memory of its initial direction upon entering the cell. They should not be viewed as real physical scattering processes, although they are supposed to account for them in an effective way.

A continuous time master equation is used to define the hopping model. The time is then discretized, so that the master equation maps to a discrete time random walk with a random Poisson process in time. As discussed in Section 3 of Chapter 3, the transition probability matrix $\hat{W}$ is defined (recall Eq. (3.21)) by

$$\hat{W} = \frac{\hat{\Gamma} - \hat{\gamma}}{\gamma_{max}} + \hat{1} \tag{4.2}$$

where γ_{max} can be any rate greater than or equal to the maximum hopping rate of the system. Thus γ_{max}^{-1} sets the unit of time for the coarse grain time scale, or more simply the mean time between steps. Once the $\hat{W}$ matrix is defined the focus of attention turns to a discrete time random walk. In this application, the general state m of Eq. (3.19) goes to (s, j) where s denotes the site as before and j defines the internal state runing from 1 to z. Refer to Figure 4.2 for the general layout of

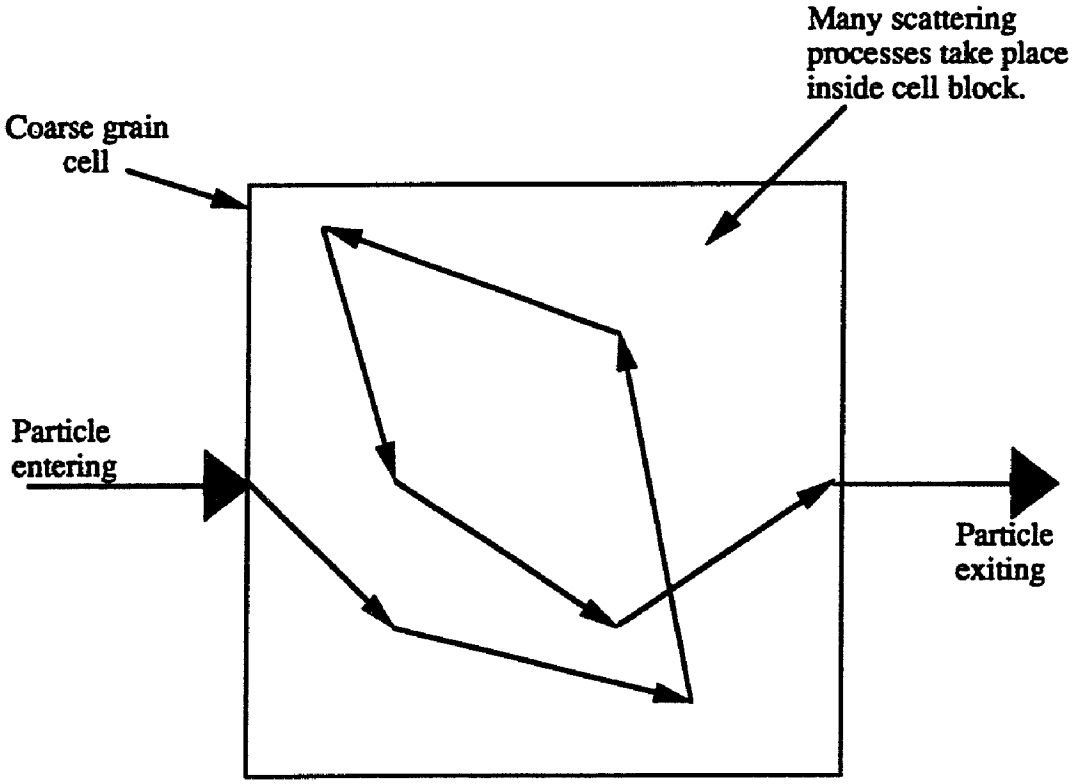

Figure 4.1

A schematic picture illustrating that many scattering processes could take place within a coarse grain cell before the walker exits.

the state space. The internal states are used to define a *preferred* direction. A random walker in the state (s_0, j) can either make an internal transition to state (s_0, j^*) where $j^* \neq j$ or it can hop out of the cell (refer to Figure 4.2) into state (s_j, j) where s_j denotes the nearest neighbor site which is in the j direction relative to site s_0. For example, if the particle is in the internal state $j = 1$ of a given site, the preferred direction is to the right. Thus the random walker can either *change* its preferred direction { upward, to the left, downward } by making an *internal transition* to $j = \{2, 3, 4\}$ respectively or hop to the nearest neighbor site to the right while maintaining the preferred direction.

A general element from the matrix $\hat{W}$ is denoted as $w(s_f, j_f \mid s_o, j_o)$ which gives the probability for the random walker to make a transition from the initial state (s_o, j_o) to the final state (s_f, j_f). In this model only internal transitions or nearest neighbor transitions are allowed. In the case of homogeneous media $\hat{\gamma} = \gamma \hat{1}$ so that with the choice of $\gamma_{max} = \gamma$ all the diagonal terms of the probability transition matrix are zero. Restricting attention to homogeneous media, an entire infinite medium can be represented by *one* cell using periodic boundary conditions. In this case the transition probability matrix is completely defined by the internal states and requires a 4×4 matrix for a square lattice. The form of the transition

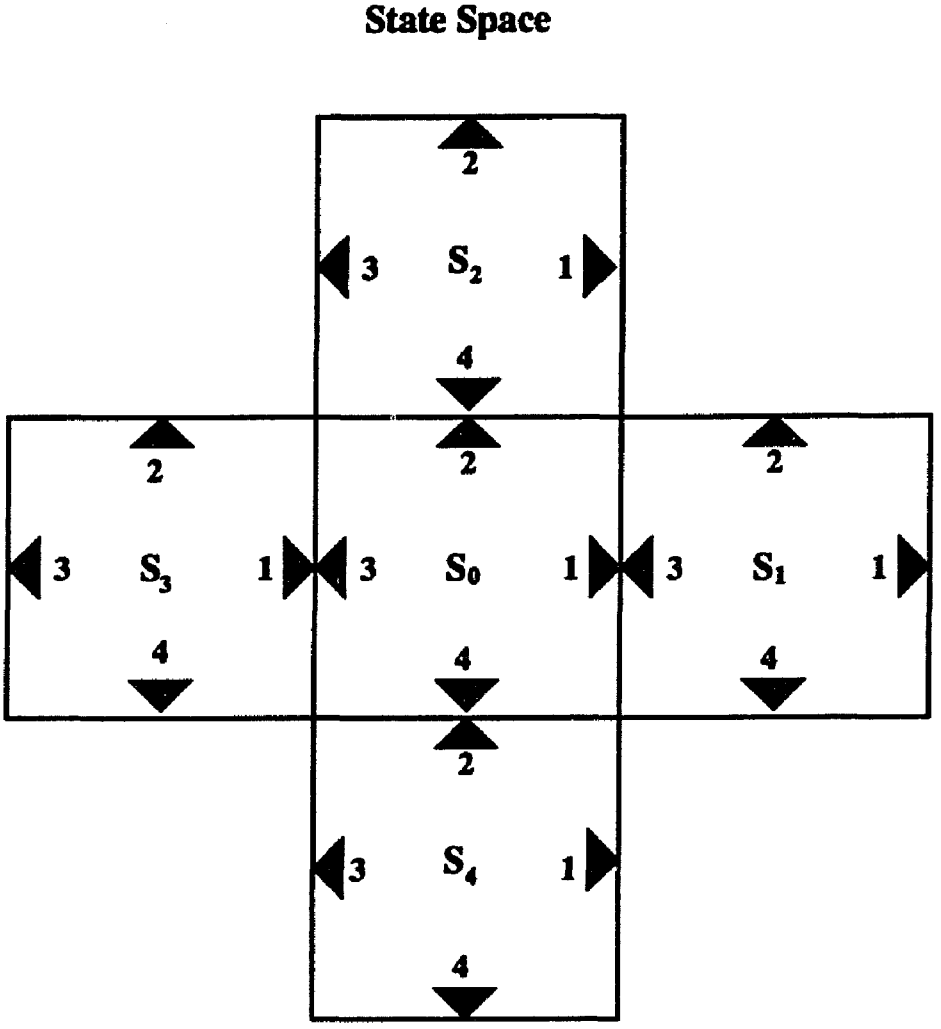

Figure 4.2

The general layout of the state space for the persistent random walk on the square lattice is shown. Each cell is identified by a site label $\{s_0, s_1, s_2, ...\}$ and contains four internal states $j = \{1, 2, 3, 4\}$ indicating a preferred direction (denoted by the arrows) to the { right, upward, left, downward } respectively.

elements *reduce* to $w(j_f, j_o)$ where

$$\hat{W} = \begin{pmatrix} p_h & p_s & p_b & p_s \\ p_s & p_h & p_s & p_b \\ p_b & p_s & p_h & p_s \\ p_s & p_b & p_s & p_h \end{pmatrix} \tag{4.3}$$

and (p_h, p_s, p_b) denote the probability for the walker to (*hop* in the preferred direction, change the preferred direction *side-ward*, change the preferred direction *backward*) respectively.

Using the same example as above, the probability for the random walker to hop from state $(s_0, 1)$ to state $(s_1, 1)$ is given by the *diagonal* term $w(1,1) = p_h$ in the reduced matrix. The non-zero diagonal terms are an artifact of choosing a single cell. If four cells plus periodic boundary conditions are used, then the size of the state space would increase by a factor of 4 (16 states) and provided that $\gamma_{max} = \gamma$ all the diagonal elements would be zero. The reduced matrix will be used for further analysis for homogeneous media, and the freedom of choosing γ_{max} greater than γ will be explicitly demonstrated.

Let the ratio $e = \gamma/\gamma_{max}$ where $0 < e \leq 1$ for a particular choice of γ_{max}. From Eq. (4.2) the probability transition matrix for one cell with periodic boundary

conditions now becomes

$$\hat{W} = \begin{pmatrix} p_h e + 1 - e & p_s e & p_b e & p_s e \\ p_s e & p_h e + 1 - e & p_s e & p_b e \\ p_b e & p_s e & p_h e + 1 - e & p_s e \\ p_s e & p_b e & p_s e & p_h e + 1 - e \end{pmatrix} \tag{4.4}$$

with the scaling factor e explicitly incorporated. The result of chosing a maximum rate greater than γ is seen to reduce the off-diagonal elements by a factor of e and introduce $(1 - e)$ as a constant diagonal term. It is easy to see that the stationary eigenstate is uniform and by inspection the remaining eigenvectors and eigenvalues can easily be obtained. The set of eigenvectors and eigenvalues are given as;

$$V_1 = \frac{1}{4} \begin{bmatrix} 1 \\ 1 \\ 1 \\ 1 \end{bmatrix} \qquad \Lambda_1 = 1 \tag{4.5}$$

$$V_2 = \begin{bmatrix} 1 \\ 0 \\ -1 \\ 0 \end{bmatrix} \qquad \Lambda_2 = (p_h - p_b)e + (1 - e) \tag{4.6}$$

$$V_3 = \begin{bmatrix} 0 \\ 1 \\ 0 \\ -1 \end{bmatrix} \qquad \Lambda_3 = (p_h - p_b)e + (1 - e) \tag{4.7}$$

$$V_4 = \begin{bmatrix} 1 \\ -1 \\ 1 \\ -1 \end{bmatrix} \qquad \Lambda_4 = (p_h + p_b - 2p_s)e + (1 - e) \tag{4.8}$$

where Λ_2 and Λ_3 are degenerate. The quantity of interest is the SACF from which the frequency dependent diffusion coefficient and/or mobility can be determined.

To calculate the SACF, the evaluation of $\langle \rho_x(n)\rho_x(0) \rangle$ is first addressed. It is convenient to define a step displacement matrix in the x-direction given by

$$\hat{\rho}_x = \begin{pmatrix} ap_he & 0 & 0 & 0 \\ 0 & 0 & 0 & 0 \\ 0 & 0 & -ap_he & 0 \\ 0 & 0 & 0 & 0 \end{pmatrix} \tag{4.9}$$

where a is the lattice constant. All of the off-diagonal terms are zero because in this case they represent internal transitions within a cell. The (positive, negative) non-zero diagonal term corresponds to a step to the (right, left) of step length a with the probability p_he to hop. Moreover, the two diagonal terms that are zero are such because they correspond to movement in the y-direction having no

x component. For discrete time $n \geq 1$, the expression

$$\langle \rho_x(n)\rho_x(0)\rangle = TR[\hat{\rho}_x \hat{W}^{(n-1)} \hat{\rho}_x V_1] \tag{4.10}$$

is valid since the first and last steps of the walker correspond to two different random events. Therefore, noting that

$$\hat{\rho}_x V_1 = \frac{1}{4} V_2 \quad , \tag{4.11}$$

the $n-1$ multiplications of the $\hat{W}$ matrix on the V_2 eigenvector becomes trivial and the final result is given by

$$\langle \rho_x(n)\rho_x(0)\rangle = \frac{a^2 p_h^2 e^2}{2} \Lambda_2^{(n-1)} \quad . \tag{4.12}$$

For the case $n = 0$, the walker only takes one step so that the first and last step are the same single random event. By explicitly considering all possible step displacements to neighboring cells with probability $p_h e$ it follows that

$$\langle \rho_x^2(0)\rangle = (a^2 + 0 + (-a)^2 + 0)\frac{p_h e}{4} \tag{4.13}$$

where the factor of $1/4$ enters from the stationary initial condition.

The same procedure can be repeated for all the other elements in the step correlation matrix, but by symmetry the cross correlations are zero and the step displacement correlation in the y-direction is the same as in the x-direction. Thus the SACF for the persistent random walk model in homogeneous and isotropic media is given by

$$\begin{aligned} \langle \rho^2(0)\rangle &= a^2 p_h e \\ \langle \vec{\rho}(n) \cdot \vec{\rho}(0)\rangle &= a^2 p_h^2 e^2 [(p_h - p_b)e + (1-e)]^{(n-1)} \quad n \geq 1 \end{aligned} \tag{4.14}$$

which is an exponential decay dependent on the scale factor e. As $e \to 0$ the SACF decays slower since the average *real time* between steps ($\gamma_{max}^{-1} = e/\gamma$) is also proportional to e. As Eq. (4.14) clearly shows, the correlations in the step displacements are dependent on the time scale of interest. It is noted that Eq. (4.14) has the same form for a hypercubic lattice of d dimension.

The frequency dependent diffusion coefficient can be calculated using Eq. (3.31) with the SACF of Eq. (4.14) yielding the result

$$D(\omega) = \frac{a^2 p_h e \gamma_{max}}{2d} + \frac{a^2 p_h^2 e^2 \gamma_{max}}{d} \frac{1}{1 - \Lambda_2 + i\frac{\omega}{\gamma_{max}}} \tag{4.15}$$

for one component in the diffusion tensor in d dimensions. Defining $\tau = 1/\gamma$ as the characteristic time for the walker to make transitions, then the maximum rate can be expressed as $\gamma_{max} = \frac{1}{e\tau}$. Furthermore, noting that

$$1 - \Lambda_2 = e[1 - (p_h - p_b)] \tag{4.16}$$

the expression for $D(\omega)$ can be writen as

$$D(\omega) = \frac{a^2 p_h}{2d\tau} + \frac{a^2 p_h^2}{d\tau(1-\Lambda)} \frac{1}{1 + \frac{i\omega\tau}{1-\Lambda}} \tag{4.17}$$

where $\Lambda = p_h - p_b$ which is the eigenvalue of the V_2 and V_3 eigenvectors for the case $e = 1$. An important feature of the above equation is that it is independent of the scale factor e as should be since $D(\omega)$ is a physical quantity. Although p_s does not appear in the solution for $D(\omega)$ it is not an independent parameter because of the normalization constraint that $p_h + 2(d-1)p_s + p_b = 1$. Moreover, p_s determines the coupling strength between the different directions. For example, if $p_s = 0$ on

the square lattice, then the random walker is confined to move in either the x or y direction set by the initial condition at all time.

The persistent random walk parallels the Boltzmann approach[86] in calculating mobilities in the sense that the transport time is dependent on the particle's persistence. As a particle undergoes a scattering event, the more forward the scattering angle the less detrimental is the event on the mobility. The transport rate of scattering is obtained from an angular weighted average on the total scattering rate γ where $\{p_f, p_s, p_b\}$ are a coarse set of weights.

The solution for $D(\omega)$ in Eq. (4.17) is in a form that identifies $\tau/(1-\Lambda)$ as the transport time. However, the solution is not consistent with a Drude-like mobility because the term $a^2 p_h/2d\tau$ shifts the diffusivity by a real constant. The presence of this additive constant can be traced back to the coarse graining scheme and the shift in $D(\omega)$ is not necessarily small. The deviation from a Drude-like mobility will increase as the coarse grain length scale (defined by the lattice constant) is increased, especially in the high frequency limit. Therefore, as a consequence of taking a coarse grain approach, a cut-off frequency ω_c will exist such that for $\omega \leq \omega_c$ the solution will be acceptable.

4.2 Model Parameters

The first task of this section is to determine the parameters required to match the model solution to the Drude form. The Drude form for the frequency diffusion coefficient is completely specified by the d.c. *diffusion constant* D and

the transport time τ_{tr}. More specifically, the model parameters $\{p_h, p_s, p_b, \tau\}$ are desired as functions of $\{D, \tau_{tr}, a\}$ where D and τ_{tr} are physical quantities and a is a non-physical coarse grain length scale that is free to be varied. The second task is to determine the cut-off frequency ω_c, also as a function of $\{D, \tau_{tr}, a\}$, for which the model can be applied with reasonable accuracy. Finally, some general remarks about the persistent random walk model for homogeneous and isotropic media and a comparison between the simple random walk results are given.

Unfortunately, the solution for $D(\omega)$ from this persistent random walk model can *not* be perfectly matched to a Drude form because of the additive real constant $a^2 p_h / 2d\tau$ which derives from the coarse graining. However, from physical intuition it is expected that the low frequency properties of the diffusion process should be relatively unaffected by any reasonable coarse grain length. Therefore, realizing from the start that the model solution will fail at high frequencies, a perfect match is demanded at $\omega = 0$ only. Furthermore, the match is made for the real and imaginary parts separately. The real part is directly matched since the real part of the complex diffusion coefficient corresponds to the physical diffusivity. However, the imaginary part of the complex diffusion coefficient is first divided by ω since this is equivilent to matching the dielectric loss.[84] Therefore, the physical and model parameters are matched through the real part by

$$D = \lim_{\omega \to 0} RE[D(\omega)] \rightarrow \frac{a^2 p_h}{2d\tau} + \frac{a^2 p_h^2}{d\tau(1-\Lambda)} \tag{4.18}$$

and the imaginary part by

$$D\tau_{tr} = \lim_{\omega \to 0} IM[\frac{D(\omega)}{\omega}] \to \frac{a^2 p_h^2}{4d(1-\Lambda)^2} \tag{4.19}$$

where D and τ_{tr} are the *physical parameters* which characterize a material with a Drude-like mobility.

As will be seen below, it is convenient to define a unitless parameter, $\eta = a/\sqrt{dD\tau_{tr}}$ that compares the coarse grain length scale a to the mean free path $l = \sqrt{2D\tau_{tr}}$ of the particle. In two dimensions $\eta = a/l$, but as defined η is more generally only proportional to a/l. Proceeding to work with Eq. (4.19) first, it follows that

$$1 - \Lambda = \eta p_h \quad . \tag{4.20}$$

Note that p_h will not be zero for any problem of interest, although it can be arbitrarily small. Therefore, without loss of generality, p_s and p_b can be set proportional to p_h. After constructing these proportionalities, from Eq. (4.20) and with the normalization constraint $p_h + 2(d-1)p_s + p_b = 1$ for a hypercubic lattice, it is found that

$$p_h = \frac{2 + 2(d-2)\delta}{\Delta_d} \; , \; p_s = \frac{\eta\delta}{\Delta_d} \; , \; p_b = \frac{\eta(1-\delta)}{\Delta_d} \tag{4.21}$$

$$\Delta_d = 2 + 2(d-2)\delta + \eta(1 + (2d-3)\delta) \tag{4.22}$$

with $0 \leq \delta \leq 1$ for $d > 1$ and $\delta = 0$ for $d = 1$. This means that, the random walker has a probability p_h to hop forward or has the probability of $1 - p_h$ to stay in the cell. If the walker remains in the cell it has a probability of δ to take

a step in an orthogonal direction. Although it would be interesting to consider anisotropic cases, and/or to explore the $\delta \to 0$ or $\delta \to 1$ limits, in this work only the case $\delta = 1/2$ where $p_s = p_b$ has been considered. The motivation for chosing $\delta = 1/2$ is that neither extreme limit is approached. The $\delta \to 0$ limit decouples the orthogonal directions from one another and therefore may be pathological which is to be avoided here. On the other hand, two internal transitions are required (instead of one) for the walker to back track in the worst case for $\delta = 1$.

Substituting Eq. (4.20) into Eq. (4.18) it is found that

$$\tau = \tau_{tr} \eta p_h \frac{2+\eta}{2} \quad . \tag{4.23}$$

With this expression for the characteristic transition time and using Eq. (4.20), the model solution for the frequency dependent diffusion coefficient can be written as

$$D(\omega \mid \eta) = \frac{\eta}{2+\eta} D + \frac{2}{2+\eta} \frac{D}{1 + i\omega\tau_{tr}\frac{2+\eta}{2}} \tag{4.24}$$

for any component in the diffusion tensor for homogeneous and isotropic media in d dimensions. Clearly as the coarse grain scale is made smaller the model solution indeed approaches the Drude result which is given by $D(\omega \mid \eta = 0)$. Since $D(\omega \mid \eta)$ is an expression for a physical quantity and yet dependent on the coarse grain scale through η, a cut-off frequency exists such that for $\omega \leq \omega_c(\eta)$ the error between $D(\omega \mid \eta)$ and $D(\omega \mid 0)$ will be within exceptable bounds. However, a careful analysis will not be done because only the general features of a Drude-like mobility can be expected from this crude model. Nevertheless, the general

dependence of the cut-off frequency on η will be explored presently.

The biggest deviation between Eq. (4.24) and the Drude result, is that the model solution gives $\tau_{tr}(1 + \frac{1}{2}\eta)$ as the prediction for the transport time. The transport time of the model denoted as $\tilde{\tau}_{tr}$ is greater than the physical transport time τ_{tr} and can produce large errors at high frequency in the dielectric loss. In particular, the percent error between the real parts of $D(\omega \mid \eta)$ and $D(\omega \mid 0)$ denoted as E_R, as well as between the imaginary parts of $D(\omega \mid \eta)/\omega$ and $D(\omega \mid 0)/\omega$ denoted as E_I are calculated seperately. Using the physical transport time as a reference time scale, the errors will be functions of $\{x, \eta\}$ where $x = \omega\tau_{tr}$. As it turns out, the error as a function of η is greater for the dielectric loss than the diffusivity. The percent error in the imaginary part works out to be

$$E_I = 100[\frac{1 + x^2}{1 + x^2(1 + 0.5\eta)^2} - 1] \tag{4.25}$$

and is negative at all frequencies. Using $E_I = -1\%$ as an exceptable bound, Figure 4.3 displays the dependence of the cut-off frequency on the degree of coarse graining. The essential features of a Drude-like mobility are captured, although the persistent random walk model considered here does not identically reproduce the Drude result. These features include the distinction between a transport time and characteristic transition time.

Once η is specified, all of the model parameters $\{p_h, p_s, p_b, \tau\}$ as well as the cut-off frequency ω_c are completely determined. By substituting the probability to hop p_h from Eq. (4.22) into Eq. (4.23) it is interesting to note that the charac-

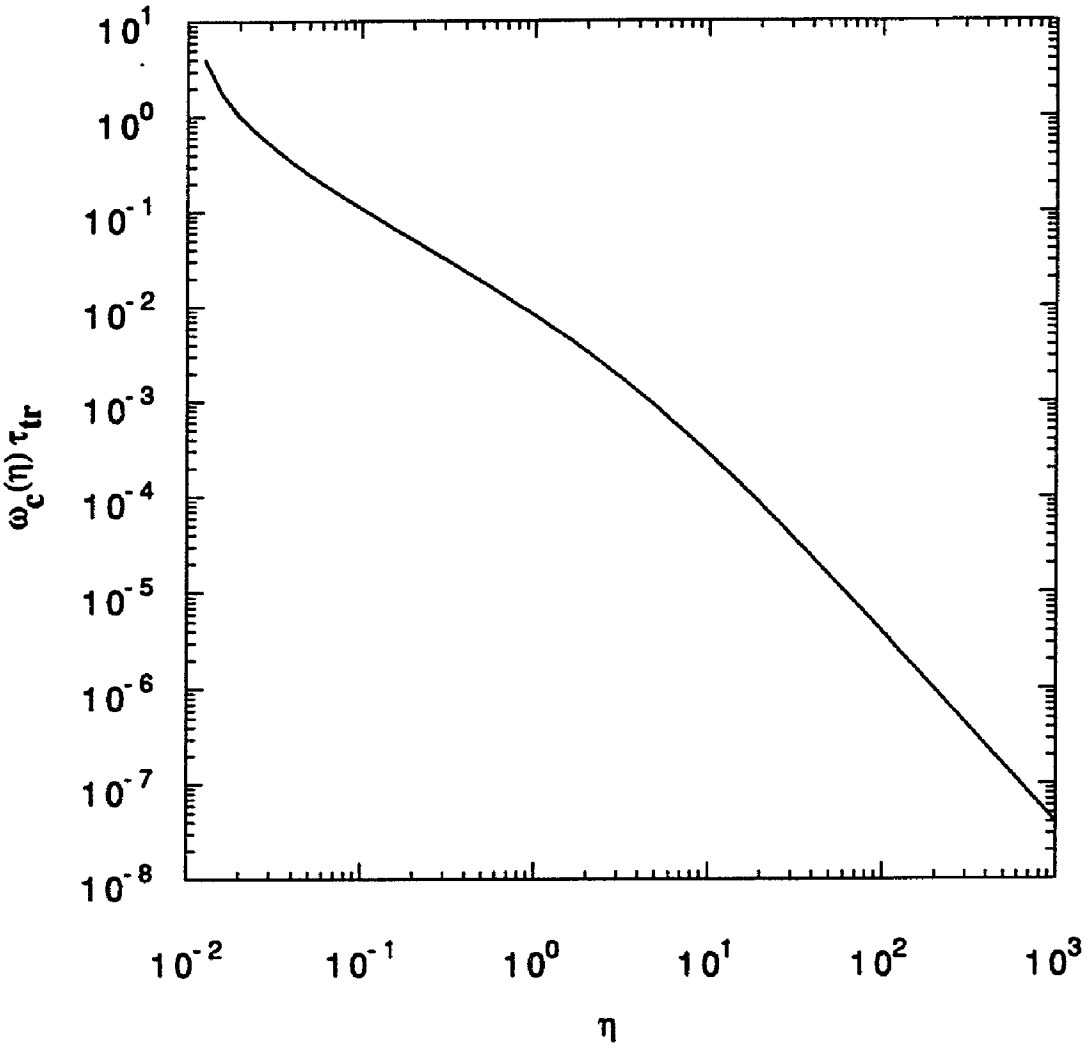

Figure 4.3

The ratio of the coarse grain length to the mean free path of a tracer particle, η, determines the maximum frequency ω_c from Eq. (4.25) for which the model results are within 1% error to the Drude result. This line is a plot of $x = \tau_{tr}\omega_c(\eta)$ verses η.

teristic transition time is nearly linear in η. As η is varied, both the characteristic transition time and the degree of persistency are regulated together to obtain a certain mean free path length. For $p_h \neq 1$, the long time limit for the mean squared displacement will be linear in time ensuring diffusive behavior. If $\eta \ll 1$ then at early times the mean squared displacement will be quadratic in time corresponding to ballistic motion. In the extreme case of no scattering events, the probability to hop can be set equal to *one* ensuring ballistic motion at all times. More Generally, the persistent walker will act in the ballistic (diffusive) limit at length scales less (greater) than the mean free path. Note that the simple random walk becomes applicable in the diffusive limit. The transition time is the only adjustable parameter for the simple random walk and is proportional to η^2 because the process requires four times the amount of time necessary to travel twice the distance.

The difference in character between these models become even more important when a multi-component composite system is considered. The maximum coarse grain length will be set by the geometry and degree of the disorder. In general the coarse grain length will not be equal to the mean free path of any of the composite materials. Moreover, it is expected that the accuracy in the estimation for an effective conductivity increases as the coarse grain length is decreased. However, the simple random walk model enforces the successive displacements to be uncorrelated. Therefore at some level of coarse graining the simple random walk will not be applicable. In contrast, the persistent random walk is more accurate as the coarse grain length is decreased and by design not sensitive to changes in

the coarse grain length at low frequencies. In short, the simple random walk can account only for the real part of $D(\omega = 0)$ and the persistent random walk has an extended range of validity in modeling both the real and imaginary parts of $D(\omega)$ for $0 \leq \omega \leq \omega_c$.

Although the central parameter η of the persistent model is unitless, it is useful to obtain some typical values of the diffusion constant and transport times for the charge carriers in metals. In applications to mesoscopic disordered systems, a convenient unit of length is the nanometer and the unit of time is chosen to be in seconds. Thus the diffusivity will be measured in units of nm^2/sec. Table 4.1 lists the concentration of charge carriers, conductivity, diffusion constant and transport times for a few metals at various temperatures. The mobilities for semiconductors and insulators can be more than 100 fold that of metals.[87] However, the large conductivity in metals derive from the large charge carrier concentrations whereas in the non-metals the carrier concentration is orders of magnitude lower. The temperature dependence on the effective d.c. conductivity is not considered here explicitly, but the scale factor η is an implicit function of temperature (and presure) through the diffusion constant and transport time. Taking copper as an example, $\tau_{tr} \approx 2 \times 10^{-14} sec$ at room temperature and $\tau_{tr} \approx 2 \times 10^{-9} sec$ at $4K$.[85] In the case of non-metals, the concentration of charge carriers will be a strong function of temperature as well. One additional restriction on the persistent (and simple) random walk model is that only one charge carrier type is followed at a time. Nevertheless, the persistent random walk model has the flexibility to control the

Table 4.1

The Einstein relation $D = k_B T\sigma/ne^2$ and the reference tables (1.1,2,3) from Ashcroft and Mermin were used to obtain typical diffusion constants for charge carriers in metals at various temperatures. The slight temperature dependence in the concentration of charge carriers (n) was neglected while using the room temperature value at all other temperatures considered.

metal	T (K)	n ($10^{22}/cm^3$)	$\sigma\ (\mu ohm - cm)^{-1}$	D (nm^2/sec)	τ_{tr} (sec)
Cu	77	8.47	5.00	2.5×10^{14}	2.1×10^{-13}
	273		6.41×10^{-1}	1.1×10^{14}	2.7×10^{-14}
	373		4.46×10^{-1}	1.1×10^{14}	1.9×10^{-14}
Au	77	5.90	2.00	1.4×10^{14}	1.2×10^{-13}
	273		4.90×10^{-1}	1.2×10^{14}	3.0×10^{-14}
	373		3.52×10^{-1}	1.2×10^{14}	2.1×10^{-14}
Al	77	18.1	3.33	7.7×10^{13}	6.5×10^{-14}
	273		4.08×10^{-1}	3.3×10^{12}	8.0×10^{-15}
	373		2.82×10^{-1}	3.1×10^{12}	5.5×10^{-15}
Pb	77	13.2	2.13×10^{-1}	6.7×10^{12}	5.7×10^{-15}
	273		5.26×10^{-2}	5.9×10^{12}	1.4×10^{-15}
	373		3.70×10^{-2}	5.7×10^{12}	9.9×10^{-16}

mean free path of any given tracer particle for different materials. The problem of Brownian motion in a multi-component composite medium can now be addressed with the assurance that the Brownian motion within each material forming the composite is described properly.

4.3 Scattering Rules at Interfaces

The persistent random walk model will be extended to disordered media in this section. The disorder will be modeled using site percolation on a hypercubic lattice where each site has a definite characteristic of either an A or B type material. Both materials A and B are assumed to have Drude-like mobilities characterized by $\{D^A, \tau_{tr}^A\}$ and $\{D^B, \tau_{tr}^B\}$ respectively. For short, it will be said that each site is of either A or B phase. The coarse grain scale is set equal to the lattice constant and the characteristic transition time for each phase $\{\tau^A, \tau^B\}$ are initially calculated from Eq. (4.23) using $\{\eta^A, \eta^B\}$, respectively. The maximum rate (γ_{max}) for the disordered system is determined by the largest reciprocal from τ^A or τ^B. The scale factors $e^A = \gamma^A/\gamma_{max}$ and $e^B = \gamma^B/\gamma_{max}$ are then calculated; one of which will equal unity. Once the scale factors have been found, the transition probabilities for each site s, as initially calculated from Eq. (4.22), are scaled by the factor $e(s)$ to arrive at the final set of probabilities $\{p_h(s), p_s(s), p_b(s)\}$ where the site dependence is through the phase only. Thus the characteristic transition time for each phase in the disordered system will be equal and given by $\tau = 1/\gamma_{max}$. The above procedure can be extended to any number of phases in the system, and is

tantamount to factoring out the maximum rate from the master equation allowing passage to a discrete time random walk.

We need to introduce a set of scattering rules for the persistent random walk model as we did for the simple random walk on disordered lattices. The blind and myopic ant models derive from two different scattering rules for the simple random walk. The scattering rule for the persistent walk between neighboring A and B cells is displayed in Fig. 4.4. The general form used in this thesis for the non-zero elements in the transition probability matrix $\hat{W}$, are given by

$$w(s_f, j_1 \mid s_o, j_1) = p_h(s_o)t + p_b(s_o)[1-\tilde{t}] \tag{4.26}$$

$$w(s_o, j_1 \mid s_o, j_1) = 1 - e(s_o) + p_h(s_o)[1-t]\Theta_f \tag{4.27}$$

$$w(s_o, j_2 \mid s_o, j_1) = p_s(s_o) + p_h(s_o)[1-t]\Theta_s \tag{4.28}$$

$$w(s_o, j_3 \mid s_o, j_1) = p_b(s_o)\tilde{t} + p_h(s_o)[1-t]\Theta_b \tag{4.29}$$

$$w(s_o, j_4 \mid s_o, j_1) = p_s(s_o) + p_h(s_o)[1-t]\Theta_s \quad . \tag{4.30}$$

The above matrix elements should be read with $j_1 = 1$, $j_2 = 2$, $j_3 = 3$, and $j_4 = 4$ or any cyclic permutation of these indices. Note that site s_f is a nearest neighbor in the j_1th direction relative to the s_o site. The parameters $\{t, \tilde{t}\}$ must be restricted to a range between $(0 \leq t, \tilde{t} \leq 1)$ and are treated as probabilities. The form of these matrix elements were designed so that the normalization $\sum_{j,s} w(s, j \mid s_o, j_o) = 1$ is preserved. Therefore, the characteristic time scale of a given phase is *not* changed by the scattering rule, but rather the local correlation is altered by the modification in the transition probabilities of site s_o. For instance, if a walker tries to hop to site

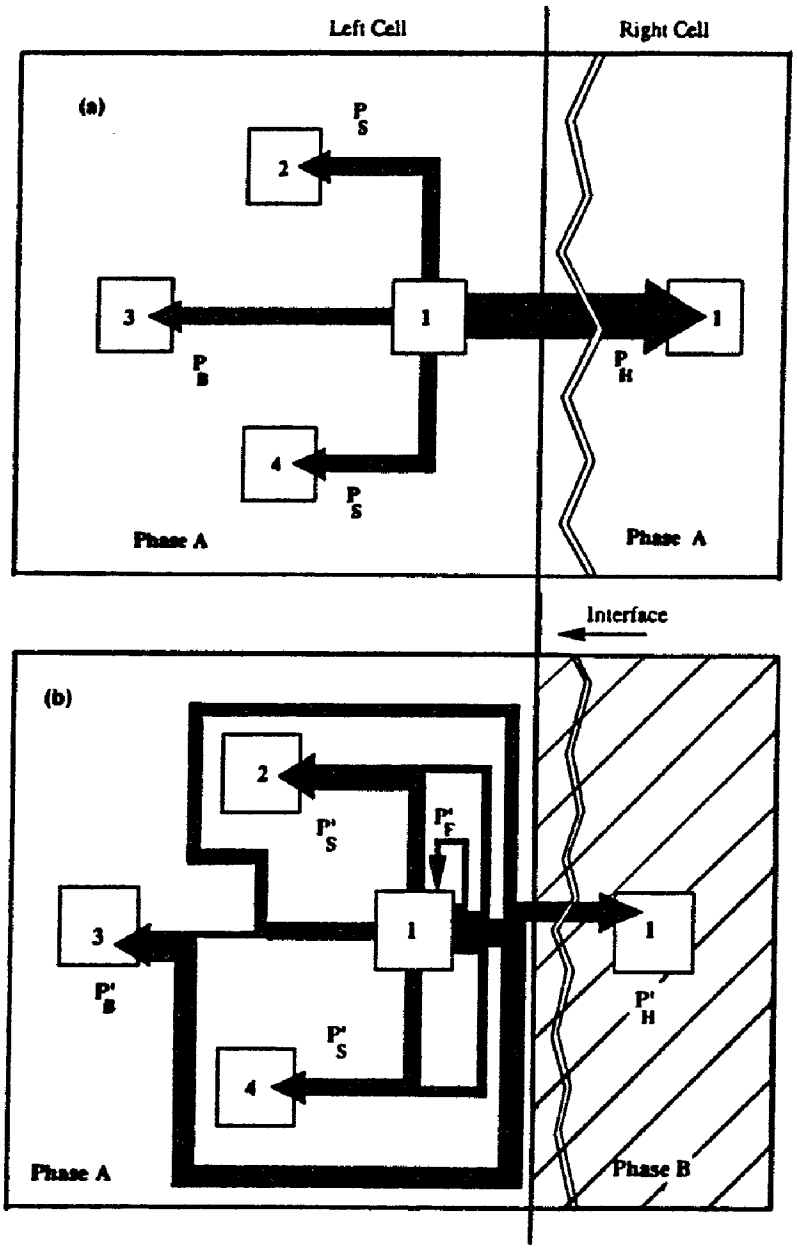

Figure 4.4

The probability flow in fig(a) leaving state 1 of the left cell is for no scattering at the interface. The probabilities $(p_b, p_s, p_f = 0, p_h)$ define the random process in the homogeneous case. In fig(b) we see a schematic of how the interface modifies the transmission probabilities to (p'_b, p'_s, p'_f, p'_h). The relationship between the unperturbed and perturbed probabilities is discussed in the text. The transmission probabilities $\{t, \tilde{t}\}$ and the additional probabilities $\{\Theta_f \Theta_s \Theta_b\}$ taken together define the scattering rule.

s_f from site s_o with probability $p_h(s_o)$, then across an interface boundary there will be a probability of t for the walker to pass through and a probability of $1-t$ that it will be reflected. Furthermore, if the walker is reflected back into site s_o, then it will have a probability of $\{\Theta_f, \Theta_s, \Theta_b\}$ to { keep its preferred direction, change its preferred direction orthogonally, or reverse its preferred direction } respectively. On the other hand, the probability $p_b(s_o)$ to reverse the walker's preferred direction (without the interface) is reduced by a factor of $\tilde{t}$ and the probability to hop is enhanced.

It is possible to construct other scattering rules which do not conform to the form of the $\hat{W}$ matrix as given above. However, even within this constraining framework there are an infinite number of possible scattering rules! The particular choice for the function Θ, for example, is one way to alter the scattering rule. For the square lattice the choice for Θ in this work is given by

$$\begin{aligned} \Theta_f &= \frac{\alpha}{1+4\alpha(1-\alpha)} \\ \Theta_s &= \frac{2\alpha(1-\alpha)}{1+4\alpha(1-\alpha)} \\ \Theta_b &= \frac{(1-\alpha)}{1+4\alpha(1-\alpha)} \end{aligned} \tag{4.31}$$

where α is a parameter dependent only on the phase of the initial site with range $0 \leq \alpha \leq 1$. This parameterization is arbitrary and is intended to satisfy the normalization condition $\Theta_f + 2\Theta_s + \Theta_b = 1$ and at the same time decrease the number of " free " parameters that will be varied. Other ways to change the scattering rule is by varying $\{t, \tilde{t}\}$; possibly in accordance to the details of the

local configuration at the interface.

The main concern in developing the scattering rule at an interface is, (1) to have the freedom to control the relative concentration of charge carriers between the two phases and (2) to find an exact expression for the stationary initial state vector for any disordered configuration. With suitable restrictions on the parameters that define the transition matrix as given above, the solution for the stationary state eigenvector is given by $V_1(s,j) = v(s)$ where all the internal states of each cell are weighted equally and $v(s) = v_X$ if site s is of phase X. Moreover, this solution generalizes to any number of phases present in the system. The required restrictions are $\alpha = 0$, and the probabilities $\{t, \tilde{t}\}$ need to be functions of the initial and final phases across the interface. With these restrictions, it can be shown by construction that v_A and v_B of the stationary eigenvector are related by

$$v_A[p_h^A t_{BA} + p_b^A(1 - \tilde{t}_{BA})] = [p_h^B t_{AB} + p_b^B(1 - \tilde{t}_{AB})]v_B \tag{4.32}$$

which is an extended detailed balance expression. For this reason, this special rule will be referred to as an *extended detailed balance* scattering rule.

The persistent random walk model does *not* obey a detailed balance relation because neighboring sites are coupled together in an alternating pattern of mismatched internal states. More specifically, if $w(s_2, j \mid s_1, j) \neq 0$ then it immediatedly follows that $w(s_1, j \mid s_2, j) = 0$ since the interchange of s_1 with s_2 reverses the direction of the hop making the preferred direction of the internal state j inconsistent. On the other hand, the probability for the tracer particle to hop from

site s_2 to site s_1 is given by $w(s_1, j_c \mid s_2, j_c) \neq 0$ where j_c is the complementary internal state to j having a reversed direction, and therefore it also follows that $w(s_2, j_c \mid s_1, j_c) = 0$. Thus it is impossible to have a detailed balance relation of the form $w(m_2, m_1)V(m_1) = w(m_1, m_2)V(m_2)$ even in homogeneous media. Without detailed balance, it is possible that the eigenvalue spectrum of $\hat{W}$ will contain complex eigenvalues although their presence is not guaranteed. With the extended detail balance rule, the internal states of each cell are degenerate giving the appearance of a generalized blind ant model applied to the sites. Moreover, the eigenvalue spectrum of $\hat{W}$ will consists of real eigenvalues only, and the step displacement correlation matrix will be symmetrical.

A model with an extended detailed balance scattering rule predicts (from the stationary state) that the concentration of charge carriers for any region in the disordered system of given phase maintain a uniform value. Therefore the ratio of the occupation probabilities v_A/v_B must equal the ratio of the concentration of charge carriers n^A/n^B, thereby producing a constraint for determining the transmission probabilities $\{t_{AB}, \tilde{t}_{AB}, t_{BA}, \tilde{t}_{BA}\}$. It is assumed that the charge carrier concentration within each phase is the same as if in homogeneous medium. Thus the extended detailed balance scattering rules do not allow for inhomogeneities in the carrier concentration within a cell or between different cells of the same phase. Although there may indeed be concentration inhomogeneities, the above constraint will be referred to as a physical constraint. Since there are four parameters to be determined with one physical constraint, the additional non-physical constraints

of $t_{AB} = \tilde{t}_{BA}$, $t_{BA} = \tilde{t}_{AB}$ and $\max(t_{AB}, t_{BA}) = 1$ are applied in order to proceed with a working model. The first two constraints are imposed so that the burden of maintaining the difference in carrier concentration will be shared somewhat " equally " between each phase. For example, if the probability to hop from phase A to phase B is decreased (because of the phase boundary) then concurrently the probability to hop from B to A is increased. The last constraint enforces the maximum possible coupling between the different phases consistent with the other constraints. Again the last three constraints are arbitrary and have been used mainly to obtain a particular scattering rule which will be referred to as extended detailed balance rule #1. Although many different rules were considered in the initial stages of developing the persistent random walk model in disordered media, the results of the extended detailed balance has been the focus of attention.

4.4 Simulation of Persistent Random Walks

The emphasis of this thesis is on the use of the exact enumeration method. Exact enumeration over all Brownian paths has been extremely useful in calculating the mean squared displacement (Section 3, Chapter 2), probability density profile (Section 4, Chapter 2) and the step displacement auto-correlation function (Chapter 3). However, it is advantageous to consider a Monte Carlo simulation of the random walks as well[88, 89]. For example, in cases where one may want a large sample of the disorder, (ie a large state space is needed) the exact enumeration becomes very time consuming. Moreover, it may be of interest to look at

much longer times than 10000 time steps after which the exact enumeration again consumes much CPU time. Also one may be interested in observing the typical fluctuations that the random walker encounters, rather than the exact averages.

The method that was used in simulating the random walks is sketched here. This method was applied to the persistent random walk in disordered media and is quite general. The random walk was simulated in terms of discrete time so that the results for the mean squared displacement can be directly compared to that obtained using the exact enumeration. When using Monte Carlo simulation, very little CPU time is needed for one random walk, however, to acquire good statistics many walks need to be generated. For the case of disordered media, it is best to use many different configurations with fewer walks per configuration in order to maximize the number of different environments encountered.

According to the persistent random walk model the walker may remain in the same state, hop to another internal state within the same cell or take a step into another cell. One matrix multiplication in the exact enumeration corresponds to one random event. For small hopping probability, many matrix multiplications are needed before there is a substantial chance that the particle will exit a cell. This is a deficiency in the exact enumeration method that can be overcome using Monte Carlo simulation. The basic idea behind simulating the random walk is to follow the tracer particle at each *step displacement* in contrast to each random event.

The Monte Carlo simulation performed here was done on the square lattice. The description of the method will be in the context of a square lattice, although

everything can be extended to other lattices and dimensions. The random walker will be followed from cell to cell in the simulation. At any instant of time only the local surroundings of the particle need to be known. The "local configuration" is defined by the specification of the phase of a given cell and its nearest neighbors. Disregarding orientation degeneracy, there are 2^{z+1} possible local configurations for a binary disordered Bravais lattice with coordination number z. The square lattice has 32 possible configurations.

In addition, there are four internal states available to the walker within a cell. The important information that is needed in the simulation is to know the internal state of the walker when it *first* enters a cell. Because of the Markov property, the random walker can be viewed as starting from that internal state as an initial condition. The details of the internal state transitions within a cell need not be tracked, but rather follow only the final outcome consisting of which nearest neighbor cell the particle hopped and the time required for hopping. Recall that when the particle hops, the final internal state of a nearest neighbor cell is uniquely defined by the step direction of the hop. As a result, the random walk is split into two distinct processes.[89] The first random process is the trajectory of the particle which disregards internal state transitions. The second random process accounts for the many internal state transitions (number of random events) that occurred before successfully escaping a cell.

The trajectory of a particle can be simulated with the specification of a set of probabilities $\{p_{ij}^{\infty}(k)\}$ for each possible type of local configuration as identified by

the label k, where $1 \leq k \leq 32$ for the square lattice. The j index of $\{1,2,3,4\}$ are initial state labels referring to the preferred direction {right, up, left and down} respectively. The i index of $\{5,6,7,8\}$ corresponds to the final internal state of $\{1,2,3,4\}$ for the nearest neighbor cell in the {right, up, left and down} direction respectively. For example, $p^{\infty}_{7,2}(k)$ is the probability that the random walker will hop to the left nearest neighbor ($i = 7$) given that the walker started in state $j = 2$ of a cell having a kth type of local configuration. In total there are $z^2 2^{z+1}$ probabilities to be specified. However, the set of probabilities $\{p^{\infty}_{ij}(k)\}$ are stored using only 2^{z+1} memory locations in the simulation program. This reduction in storage is possible by defining a preferred direction as a reference instead of using the fixed coordinate axes.

Eventually, a particle in a given cell must exit to a nearest neighbor as indicated by the sum rule

$$\sum_{i=5}^{8} p^{\infty}_{ij}(k) = 1 \quad . \tag{4.33}$$

For each initial state j, the interval between 0 and 1 is partitioned into four bins each proportional in size to the probability that the particle will escape in a given direction. The method of tracking a particle consists of the following items. 1) Determine the local configuration. 2) Set the initial condition by choosing the preferred direction j to be in the direction of the previous hop. 3) Generate a uniformly random number between 0 and 1, and take a step in a direction determined by the bin that the random number fell into. Then return to item one

to continue.

The probabilities $p_{ij}^{\infty}(k)$ are obtained by constructing a special transition probability matrix $\hat{W}_A$ where the subscript A stands for *absorbing* states. The elements $w_A(i,j)$ for $i,j = 1,2,3,4$ are identical with the probability transition matrix $\hat{W}$. Furthermore, the elements $\{w_A(5,j),\ w_A(6,j),\ w_A(7,j),\ w_A(8,j)\}$ give the probability to hop (also identical to $\hat{W}$) from state j to a nearest neighbor in the {right, up, left, down} direction respectively. The elements $\{w_A(5,5),\ w_A(6,6),\ w_A(7,7),\ w_A(8,8)\}$ are all equal to one and are therefore absorbing states. A different 8×8 absorbing transition probability matrix $\hat{W}_A(k)$ is constructed for each local configuration labeled by k. For the moment, let us drop explicit reference to the label k. An eight dimensional vector space is defined through $\hat{W}_A$.

By exact enumeration, the function

$$p_{ij}^{n} = \sum_{l} [\hat{W}_A{}^{n}]_{il} V_o(l) \quad \text{where } V_o(l) = \delta_{l,j} \tag{4.34}$$

can be calculated where V_o is the initial state vector. The function

$$f_{ij}^{n} = p_{ij}^{n} - p_{ij}^{n-1} \quad \text{for } n \geq 1 \tag{4.35}$$

gives the conditional probability that the tracer particle will hop to a particular nearest neighbor (ie $\{i = 5,6,7,8\}$) after precisely n random events given that it started from state j. In other words, the function f_{ij}^{n} is the first exit probability. Alternatively, p_{ij}^{n} gives the probability that the particle, initially in state j, had taken a step to the ith nearest neighbor after m random events such that $m \leq n$. In the limit that $n \to \infty$ the set of probabilities p_{ij}^{∞} are obtained.

The time required to make each hop needs to be included to completely describe the Brownian motion. After a step displacement is realized, the waiting time dt must be determined. The random time process is specified through cumulative distribution functions defined by $q_{ij}^n = p_{ij}^n/p_{ij}^\infty$. The difference between q_{ij}^n and p_{ij}^n is that q_{ij}^n is a *conditional probability* given that the particle does exit the cell from the j state to state i and therefore $q_{ij}^\infty = 1$. To realize a time dt, another independent uniformly random number r between 0 and 1 is generated. Then dt can be found by using the distribution function q_{ij}^n where i corresponds to the realized nearest neighbor. A comparison between r and the function q_{ij}^n such that

$$q_{ij}^m = \max\{q_{ij}^n\} \text{ of the set } \{q_{ij}^n\} \leq r \tag{4.36}$$

implies that $dt = m$. Although this is a straight forward way of generating dt, as will be shown later, the determination of dt is generally more involved than this.

In principle the functions $\{p_{ij}^n\}$, which give all the dynamic information needed for the simulation, could be calculated analytically from $\hat{W}_A$. However, at long times the limiting form for p_{ij}^n is expected to be

$$p_{ij}^n \approx p_{ij}^\infty - (p_{ij}^\infty - p_{ij}^m)\Lambda_{ij}^{n-m} \quad \text{for } n \geq m \tag{4.37}$$

for sufficiently large m. The function p_{ij}^n was numerically obtained using exact enumeration. For Eq. (4.37) to be valid it was found that m could be chosen as small as 8 in some cases or as large as 20000 in other cases. It was also observed for $n \geq m$ that $p_{ij}^n/p_{lj}^n \rightarrow$ *constant* independent of n. Therefore, it is possible to find (or at least estimate) p_{ij}^∞ from which q_{ij}^n can be obtained.

For small m, it is easy to store the function q_{ij}^n in memory for all n up to $n = m$, and then for $n > m$ Eq. (4.37) is used in place of memory storage. However, if m is large, the method of storing the function q_{ij}^n in memory is not practical. Therefore, it would appear that diagonalizing $\hat{W}_A$ for each distinct configuration is necessary to obtain the solution for p_{ij}^n. The manipulation of this general solution for determining dt is quite complicated, because the solution will involve a sum over four exponential decays plus a constant (four of the eight eigenvalues equal one.) An approximation can be made (which amounts to choosing a coarser time scale) that leads to a simple alternative method. Since m needs to be larger when the walker takes longer to exit a cell, m is dependent on the diagonal terms in $\hat{W}_A$. In particular the problem of large m arises when the non-absorbing diagonal elements are close to unity.

In the case of the extended detailed balance rule, all the non-absorbing diagonal matrix elements of a given phase are equal. Let us consider the matrix element $w_A(1,1)$, and defining $1 - w_A(1,1) = x$ for $0 < x < 1$ we denote the *smallest* m necessary for Eq. (4.37) to be valid as m_x. It is not implied that m_x is only a function of x since it also depends on the probability to hop out of a cell. However, we can reduce m_x by changing the time scale. Therefore we first fix the value of x, if $1 - w_A(1,1) \geq x$ no change in time scale is made so that the scale factor e is set to unity. Otherwise, the scale factor is chosen such that $e = [1 - w_A(1,1)]/x$. The approximation is made by using a rescaled absorbing probability transition matrix with elements given by $w'_A(i,j) = w_A(i,j)/e$ for $i \neq j$, $w'_A(i,i) = 1$ for

$i = \{5,6,7,8\}$ and $w'_A(j,j) = 1 - x$ for $j = \{1,2,3,4\}$. The absorbing diagonal probabilities of unity are *not* changed by the scale transformation because regardless of its arrival time, a particle cannot escape an absorbing state. The off-diagonal processes are speeded up so that the particle will exit the cell with less number of random events. One random event defined by the rescaled transition matrix on average corresponds to $1/e$ random events of the original transition matrix. The smaller x becomes the greater the approximation. For all cases considered, it was found that for $x = 0.1$ that $m_x \leq 50$ which is a reasonable number of terms to store in memory.

From exact enumeration $p_{ij}^{\infty}(k)$, $\Lambda_{ij}(k)$, $m_{ij}(k)$ and q_{ij}^{n} for all $n \leq m_{ij}(k)$ (where $m_{ij}(k)$ is chosen to be the smallest possible number for which Eq. (4.37) is valid) are determined for each distinct configuration. All of this information is acquired and stored in memory before the simulation part of the program is started. As an example, consider a local configuration consisting of a cell of phase A having all nearest neighbors of phase C where the physical properties of mobility and the model parameters are specified in Table (4.2 and 4.3) respectively. For this configuration, it was determined that $p_{51}^{\infty} = 0.34293$, $m_{51} = 20$, $q_{51}^{20} = 0.45200$ and $\log_{10}\Lambda_{51} = -6.583 \times 10^{-3}$. Also the results for $(i = 6,7,8\ j = 1)$ are identical where $p_{61}^{\infty} = 0.21902$, $m_{61} = 40$, $q_{61}^{40} = 0.39849$ and $\log_{10}\Lambda_{61} = -6.671 \times 10^{-3}$. The first passage probabilities f_{ij}^{n} are plotted in Fig. 4.5 for $(i = 5, j = 1)$ and $(i = 6, j = 1)$. After $n > 20$ for f_{51}^{n} and after $n > 40$ for f_{61}^{n} both functions converge to nearly the same curve. Each curve is characterized by a single exponential decay. In this

case $e = 0.001$ is the scale factor. An important feature of the model, as nicely displayed by f_{61}^n in Fig. 4.5, is that the effective waiting time distribution for a single nearest neighbor step displacement is *not* a simple exponential decay but is modified considerably by the internal transitions within a cell.

The time interval dt is considered to be continuous (real variable in FORTRAN) and the function q_{ij}^n is interpolated to the continuum. Once this is done, the waiting time is realized according to

$$dt = [n - \frac{q_{ij}^n - r}{q_{ij}^n - q_{ij}^{n-1}}]\frac{1}{e} + 0.5 \quad \text{for } q_{ij}^{n-1} < r \leq q_{ij}^n \tag{4.38}$$

when the random number r is less then q_{ij}^m. Note that the indices i and j are determined by the trajectory of the particle and m is determined by the local configuration. In the case $r < q_{ij}^1$, it may occur that $dt < 1$, however, if this occurs then the choice of $dt = 1$ is made instead because it takes at least one random event for the walker to hop out of the cell. Technically, the time interval dt should be taken as the greatest integer of the right hand side of Eq. (4.38) *without* the addition of one-half. Since dt is considered as continuous, the addition of 0.5 allows the net sum of time to be correct on average. On the other hand, if $r > q_{ij}^m$ then

$$dt = [\frac{\log[\frac{1-r}{1-q_{ij}^m}]}{\log \Lambda_{ij}} + m]\frac{1}{e} \quad \text{for } r > q_{ij}^m \tag{4.39}$$

having used Eq. (4.37). In the case that the random number r is greater than q_{ij}^m it is seen that $m/e \leq dt < \infty$ which covers all the remaining possible waiting times.

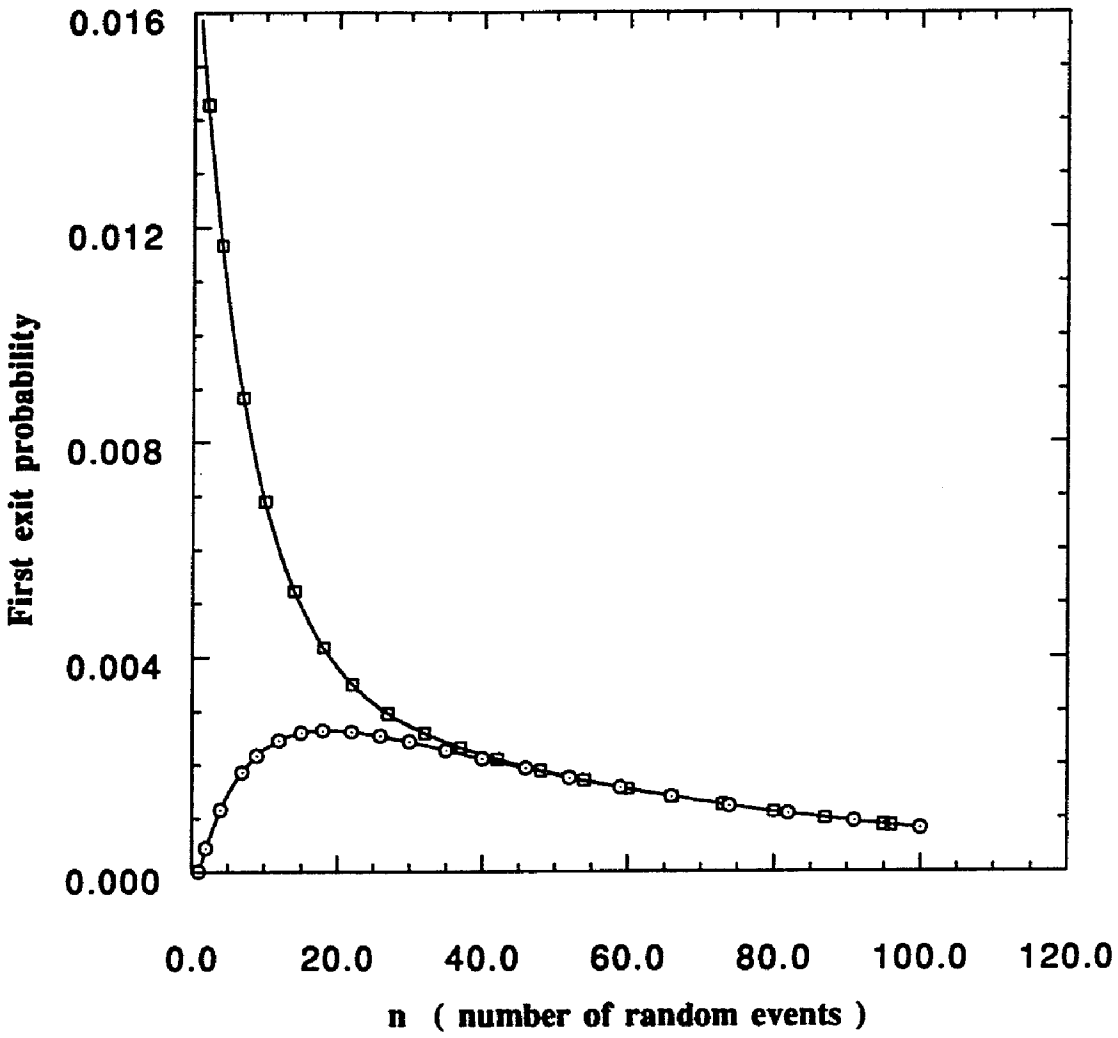

Figure 4.5

The first passage probabilities f_{ij}^{n} are plotted for the two cases f_{51} and f_{61} corresponding to the □ and ○ symbols respectively. A simple exponential decay occurs after $n = 20$ for f_{51} and after $n = 40$ for f_{61}. This plot is for the case when the scale factor was set at $e = 0.001$ which implies that between each random event on this graph there are actually 1000 random events with respect to the original time scale.

The random walk is finally constructed by combining the two separate random processes together. The simulations that were performed were on the same size configurations used in the exact enumeration, so that the entire configuration was stored in memory. Therefore, the stationary initial state vector was calculated and then used to determine which state the random walker starts. Once the random walker is released, the total time of the walk is calculated from the summation over all the individual waiting times between each step. Mathematically,

$$t(N) = \sum_{i=1}^{N} dt_i \quad \vec{R}(t) = \sum_{i=1}^{N} \vec{\rho}_i \tag{4.40}$$

where $t(N)$ is the total time that took place during the set of N random step displacements $\{\vec{\rho}_i\}_N$ that define the trajectory of the particle. The position information of the random walk data, is stored for a pre-selected set of times $\{t_i\}$ that are logarithmicly spaced. Since the random walker remains in the same cell for the waiting time dt, the position of the particle is precisely known at any time t.

The method of calculating dt turns out to be very crucial in obtaining the correct statistics. The method presented here should not be regarded as the best, cleanest or even fastest way, however, the simulation results are in good agreement with the exact enumeration. A word of caution should be made, however, that as the total simulation time is increased, small errors can accumulate very rapidly in the calculation of the total time $t(N)$. It is believed that the procedure described above, should reliably put the simulation results (with good statistics) to be within 10% error to the exact enumeration. That is, the d.c. diffusion constant

Table 4.2

For the square lattice ($a = 1nm$), the physical properties of mobility is summarize for three different phases. The transport times of phase A and B are equal, the diffusion constant of phase B and C are equal and the mean free path of phase C and A are equal. Refer to Table 4.3 for the model parameters.

parameter	phase A	phase B	phase C
D nm^2/sec	10^{10}	10^{14}	10^{14}
τ_{tr} sec	10^{-12}	10^{-12}	10^{-16}
η	7.07107	0.07071	7.07107

as measured by the simulation should be within 10% of the true value and this estimate is quite useful. The simulation technique can be much faster than the exact enumeration, especially if both phases are poor conductors where each phase have long waiting times for the walker to hop out of a cell. Unfortunately, if one phase is a poor conductor and the other a relatively good conductor, then a large fraction of the particle's trajectory may be spent in the good conducting phase and the simulation will not have any speed advantages over the exact enumeration.

A comparison of $(X(n)^2)$ from Monte Carlo simulation and exact enumeration is given here for a disordered configuration as specified in Fig. 4.6. The configuration is not a site percolation realization, although it models a percolating network. Periodic boundary conditions are applied, therefore, the diffusion process will be normal. Three different types of materials denoted as A, B and C are specified

in Table (4.2 and 4.3) and have been taken in pairs to represent the percolating and non-percolating phases. The d.c. conductivity of each phase (in homogeneous medium) was chosen to be identical (denoted as σ_o), however, each phase is uniquely distinguishable. Phase A and B have the same transport time, phase B and C have the same d.c. diffusivity and finally phase C and A have the same mean free path.

As Fig. 4.7 shows, the x-component of the mean squared displacement from simulation and exact enumeration agree with one another for each of the six different cases considered. Each case is labeled as $\overline{YX}$ where (Y, X) denotes the (percolating, non-percolating) phase of the configuration presented in Fig. 4.6. The exact enumeration used about 35 min of CPU time for each case to calculate the step correlation and mean squared displacement in the x-direction up to 10^5 time steps. Therefore, 1 hour and 45 min would have been required to calculate the entire position correlation matrix. On the other hand, the simulation CPU time is dependent on the parameters. In four simulations 40000 random walks were generated except for cases $\overline{AC}$ and $\overline{CA}$ where 10^6 walks were necessary for obtaining good statistics. The entire position correlation matrix up to 10^5 time steps is calculated in the simulation. For case $\overline{CB}$ the simulation took about 6 hours, case $\overline{BC}$ took about 3 hours and the remaining cases took between 12 to 8 minutes.

Clearly the simulation is not always faster than exact enumeration. However, the simulation CPU time is independent of configuration size and the total num-

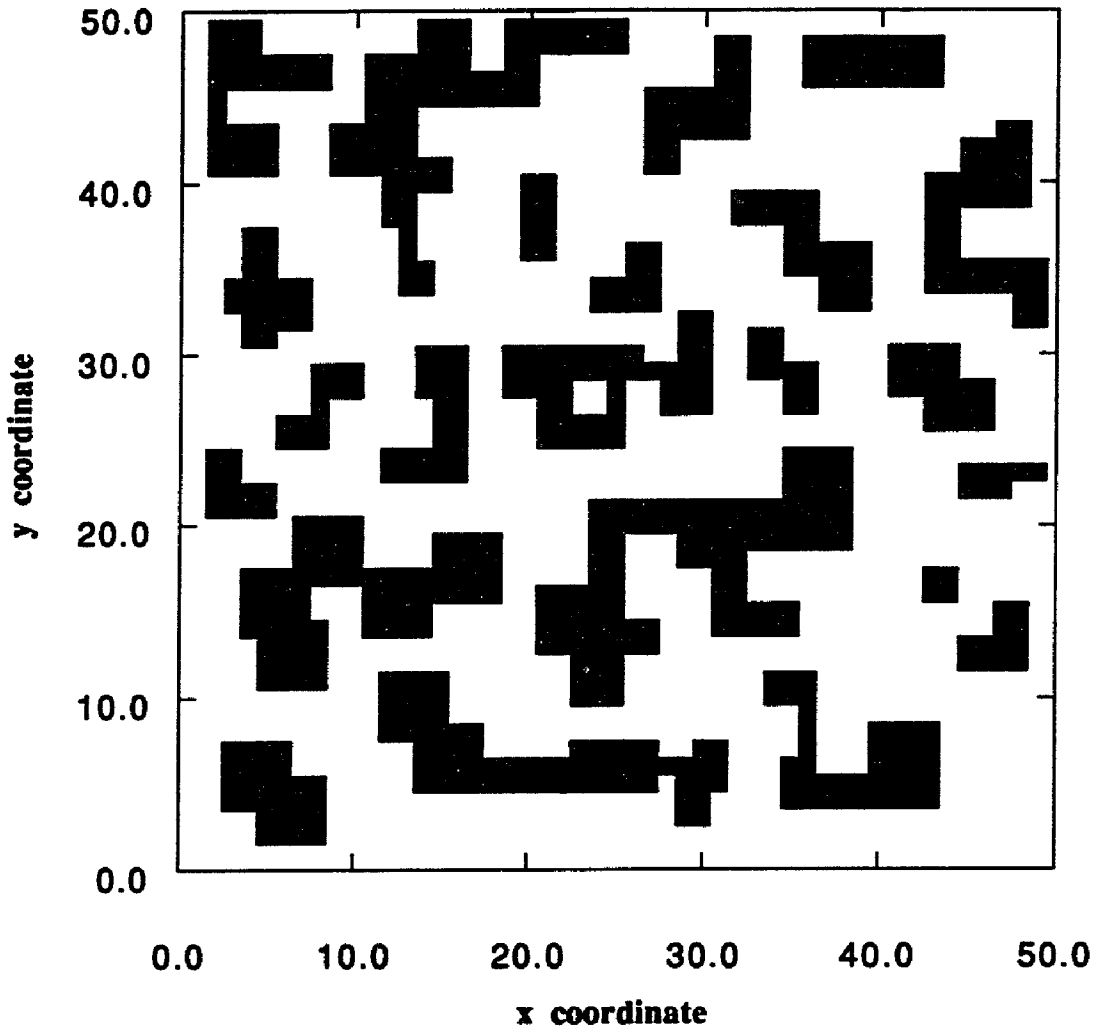

Figure 4.6

This is a single realization of a disordered configuration in a percolating state. The lattice constant is chosen to be $1nm$ in this example. The black region in the picture represents the non-percolating phase and the white represents the percolating phase. Periodic boundary conditions are applied to this configuration.

Table 4.3

The model parameters are summarized for the three different materials listed as A, B and C as defined in table 4.2. Each section refers to a two-phase mixture where the columns correspond to phase "X". The d.c. conductivity for each phase, the transport times of phase (A and B), the diffusion constant of phase (B and C), and the mean free path of phase (C and A) are respectively equal. ($a = 1nm$).

parameter	phase A	phase B	phase C
X-A phase mixture			
p_h	0.15865	0.94964	0.15865
p_s	0.28045	1.67874×10^{-2}	0.28045
n_X/n_A	1	10^{-4}	10^{-4}
t_{XA}	1	4.45464×10^{-2}	1
τ (sec)	5.08798×10^{-12}	6.95236×10^{-14}	5.08798×10^{-16}
X-B phase mixture			
p_h	2.16780×10^{-3}	0.94964	0.15865
p_s	3.83216×10^{-3}	1.67874×10^{-2}	0.28045
n_X/n_B	10^4	1	1
t_{XB}	1	1	1
τ (sec)	6.95236×10^{-14}	6.95236×10^{-14}	5.08798×10^{-16}
X-C phase mixture			
p_h	1.58647×10^{-5}	6.94977×10^{-3}	0.15865
p_s	2.80451×10^{-5}	1.22856×10^{-4}	0.28045
n_X/n_C	1	1	1
t_{XC}	1	4.45464×10^{-2}	1
τ (sec)	5.08798×10^{-16}	5.08798×10^{-16}	5.08798×10^{-16}

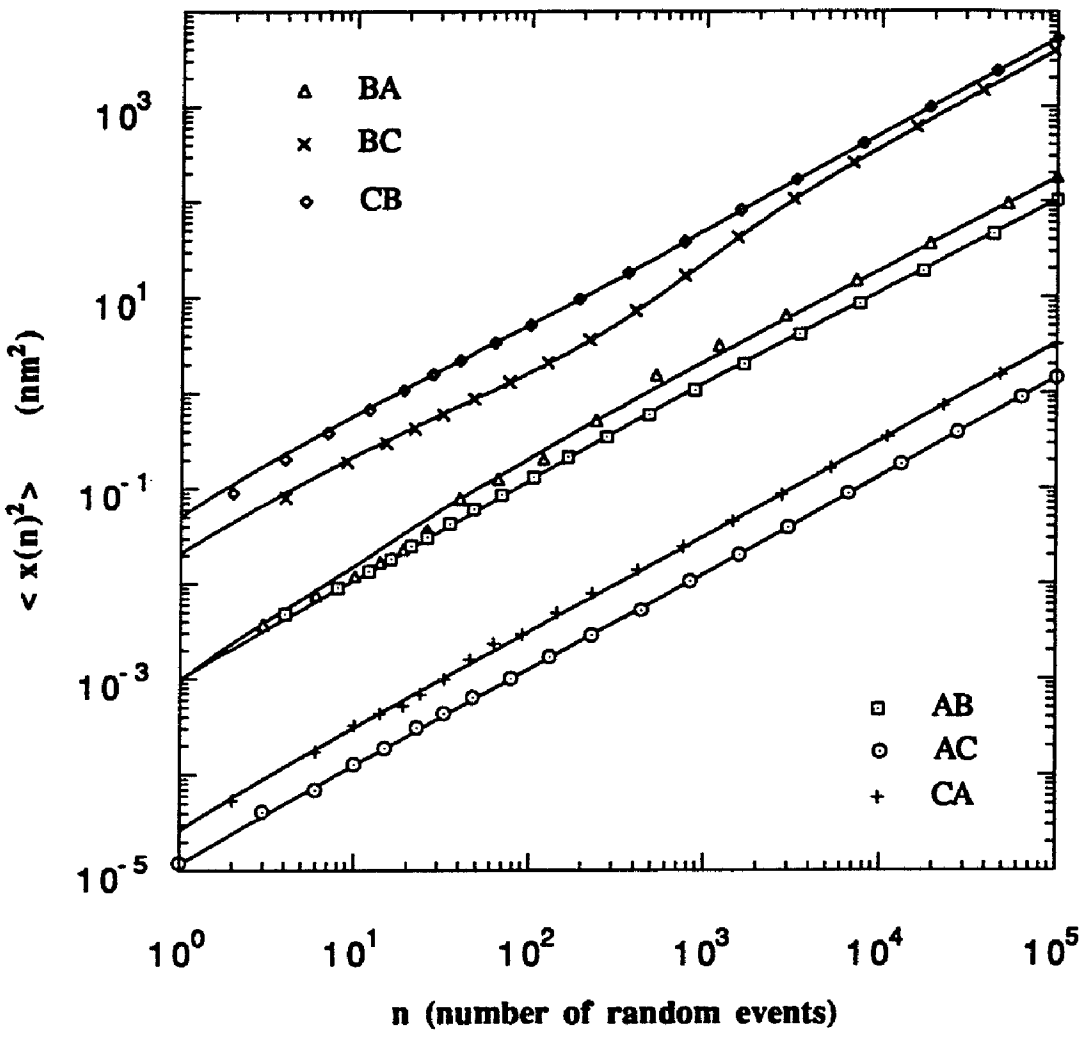

Figure 4.7

Here is a comparison of the results for $\langle X(n)^2 \rangle$ between the exact enumeration (solid line) and simulation (symbols) applied to the disordered configuration shown in Fig. 4.6 for six different cases. The $\{\diamond, \times, \triangle, \square, +, \bigcirc\}$ symbols correspond to the case $\{\overline{CB}, \overline{BC}, \overline{BA}, \overline{AB}, \overline{CA}, \overline{AC}\}$ respectively where the first letter identifies the percolating phase and the second letter identifies the phase of the clusters. The characteristics of phase A, B and C are listed in Tables (4.2 and 4.3). The simulation results agree within 3% error.

ber of walks can be divided among the configuration realizations, thereby making Monte Carlo simulation more feasible as the number and size of the configurations increase. For example, the CPU time for case $\overline{CB}$ from exact enumeration approaches the simulation CPU time for a disorder average over 10 configurations provided 4000 walkers are released per configuration. The general technique used in the simulation of persistent random walks in disordered media has been successfully demonstrated to agree with the exact enumeration. It is worth mentioning that the simulation can calculate the time (number of random events) the walker spends in each phase separately. The ratio of the time spent in a given phase to the total time will give the stationary probability that the walker is in that phase. This information is very useful if a non-extended detailed balance scattering rule is used where the initial stationary state eigenvector is not known apriori. Another feature of simulation is that the method can be extended to the continuum.

A full discussion about the effective d.c. conductivity of disordered composites will be deferred to Chapter 5. However, note that the effective conductivity (in the x-direction) for the configuration in Fig. 4.6 has been determined to equal σ_o for the cases $\overline{AC}$ and $\overline{CA}$, $0.51\sigma_o$ for the cases $\overline{AB}$ and $\overline{CB}$, and equal to $0.39\sigma_o$ for the cases $\overline{BA}$ and $\overline{BC}$. It is seen that the effective conductivity is *lower* than the conductivity σ_o of either phase separately for four cases out of six. Moreover, the same d.c. conductivity was obtained by substituting phase A for phase C or vice versa.

These results indicate that the mean free path of a particle must be the same in

both phases for the effective conductivity to be the same as the *degenerate* conductivity of the constituent phases. From Table 4.3 the only difference between phase A and C is a time scale. Therefore, if the substitution $A \rightleftharpoons C$ is made anywhere within a disordered system, no change in the trajectories will occur, although the time process does change. The effective d.c. conductivity is invariant under any substitutions between phase A and C because from Eq. (4.32) it is seen that the ratio in time scales are exactly compensated by the ratio in carrier concentration. However, because the time process is drastically different, the Brownian motion *is different* with the substitutional change.

To get an idea of how different the diffusion process can be among the six cases considered, a single realization of a walker's trajectory is shown in Fig. 4.8 for case $\overline{AC}$ or equivalently case $\overline{CA}$, Fig. 4.9 for case $\overline{BC}$ or equivalently $\overline{BA}$, and Fig. 4.10 for case $\overline{CB}$ or equivalently $\overline{CA}$. Note that the plotted trajectories do not give any information about the time passed. Also the start and finish points are not labeled because the important information to convey is the characteristic shape of a trajectory.

In cases $\overline{AC}$ and $\overline{CA}$ the non-percolating clusters are invisible to the random walker. The trajectory of Fig. 4.8 displays no noticeable persistence. The reason why the carrier concentration of phase A is 10^4 times as much as phase C is simply because the average waiting time for a particle to hop form an A phase cell is 10^4 times as long than from a C phase cell.

In contrast, the cases $\overline{BC}$ and $\overline{BA}$ represent a situation of a particle having a

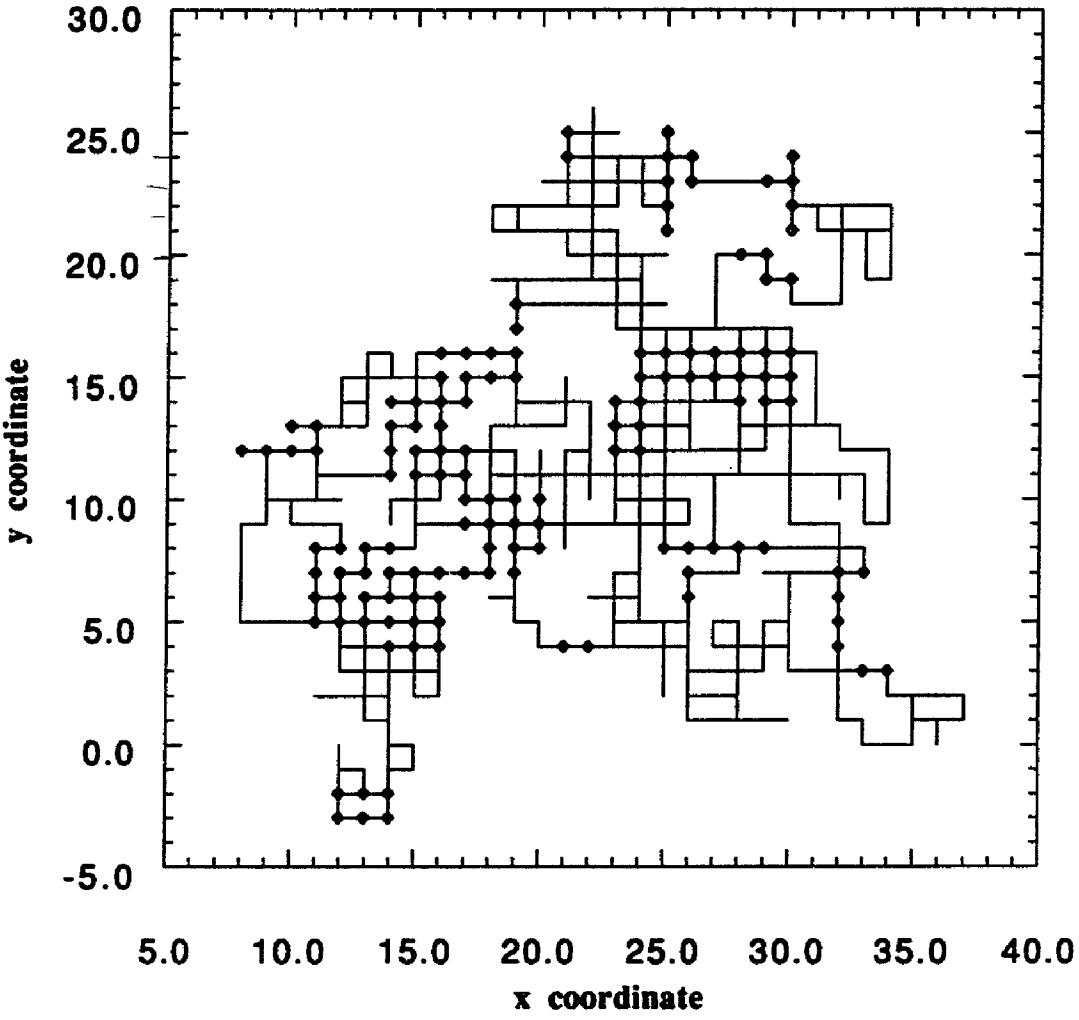

Figure 4.8

Here is a single realization of a trajectory of a random walker released on the disordered configuration of Fig. 4.6 at coordinates $(25, 25)$ for case $\overline{AC}$ which denotes that phase A is percolating and the clusters are of phase C. The random walker has taken 1000 random steps of which 324 of them are within clusters of phase C. The black diamonds denote the locations along the trajectory for which the particle travels through a cluster. The total time of the walk was 4.271×10^7 discrete random events corresponding to $22ns$ of real time.

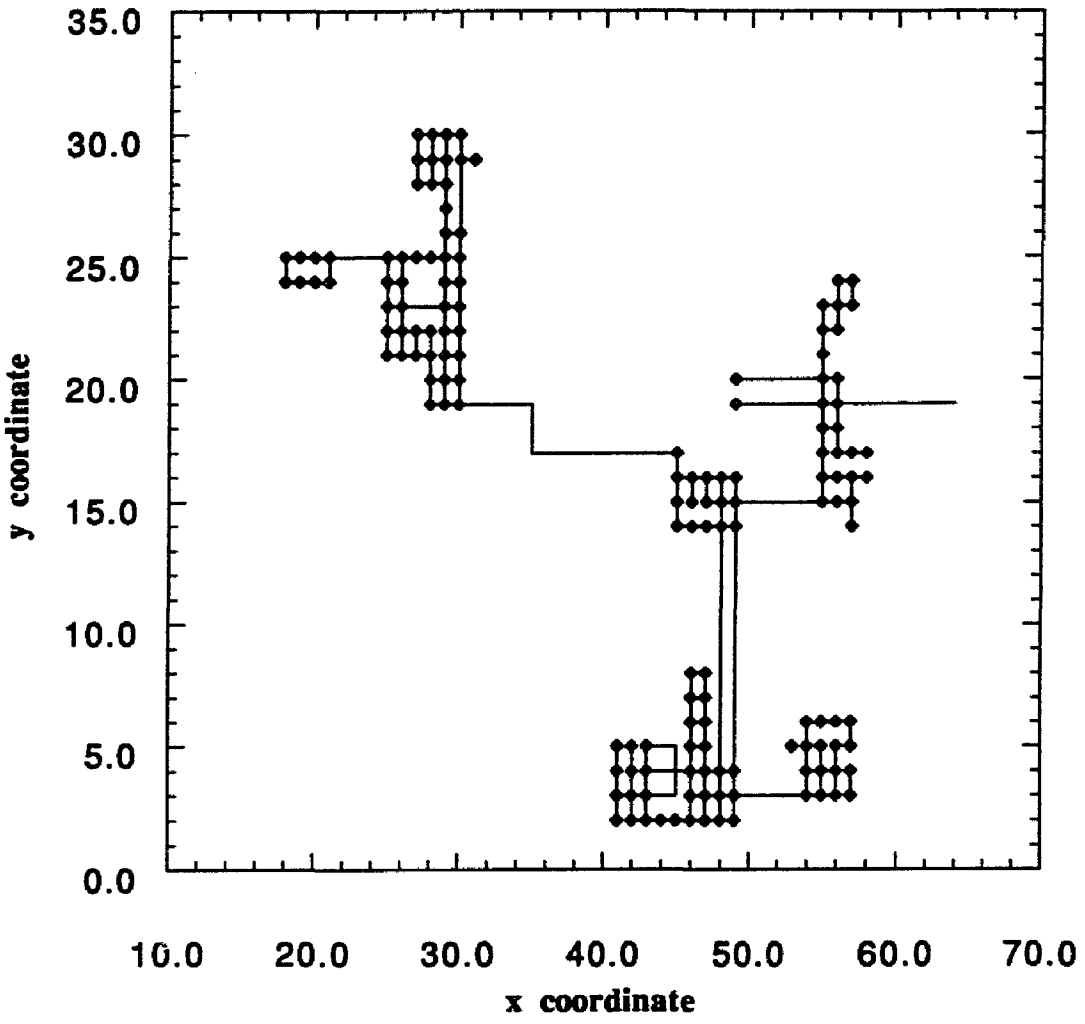

Figure 4.9

Here is a single realization of a trajectory of a random walker released on the disordered configuration of Fig. 4.6 at coordinates $(25, 25)$ for case $\overline{BC}$ which denotes that phase B is percolating and the clusters are of phase C. The random walker has taken 1000 random steps of which 906 of them are within clusters of phase C. The black diamonds denote the locations along the trajectory for which the particle travels through a cluster. The total time of the walk was 21231 discrete random events corresponding to $0.012ns$ of real time.

much longer mean free path in the percolating phase than the typical distance that can be traveled before running into a cluster as Fig. 4.9 clearly displays. Here the particle prefers to take steps in phase C or A over phase B. Therefore, a typical trajectory looks like the particle leaps from cluster to cluster, while most of the time is spent within a cluster. The effective conductivity decreases because the clusters embedded in the B phase cause premature scattering to occur within the B phase, thereby reducing the effective mean free path of the particle.

Finally, fig. 4.10 shows a typical trajectory of the cases $\overline{CB}$ and $\overline{AB}$ where a particle in the percolating network has a mean free path shorter than the typical cluster to cluster separation. Again the particle will prefer to take steps in phase C or A over phase B. Therefore, more often than not the particle will take steps within the percolating phase and will have to diffuse around the clusters. The effective conductivity decreases because the tagged particle undergoes Brownian motion in a ramified environment.

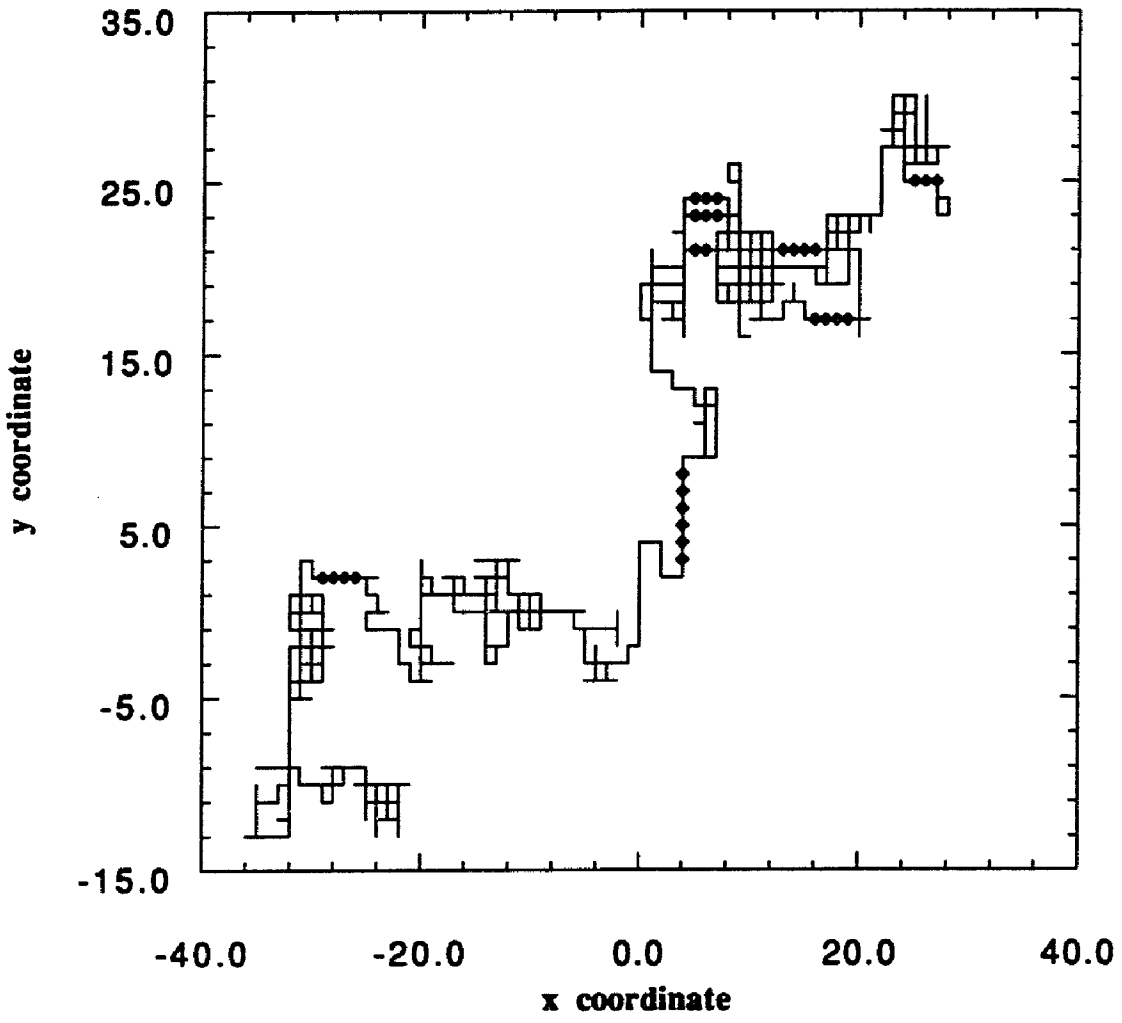

Figure 4.10

Here is a single realization of a trajectory of a random walker released on the disordered configuration of Fig. 4.6 at coordinates $(25, 25)$ for case $\overline{CB}$ which denotes that phase C is percolating and the clusters are of phase B. The random walker has taken 1000 random steps of which 32 of them are within clusters of phase B. The black diamonds denote the locations along the trajectory for which the particle travels through a cluster. The total time of the walk was 10938 discrete random events corresponding to $0.006ns$ of real time.

5. TRANSPORT IN TWO-COMPONENT DISORDERED SOLIDS

5.1 Introduction

In this Chapter, the main interest will be on the frequency dependent diffusion coefficient in application to obtaining the effective electrical conductivity of disordered media consisting of a two component phase mixture. The persistent random walk is used here in order to model a Drude-like mobility of the charge carriers within a given phase. The nature of the persistent random walk in disodered media is studied here in more detail than Chapter 4. Preliminary results are given to determine general features of the model and their physical implications. In addition, further avenues of possible research will be discussed.

We begin by considering the ratio of the d.c. conductivities of two different materials that can be expressed as

$$\frac{\sigma_A}{\sigma_B} = \frac{n^A}{n^B} \times \frac{D^A}{D^B} \tag{5.1}$$

which follows from the Einstein relation. If the effective d.c. conductivity of a disordered composite material only depends on σ_A, σ_B and the geometry, then any distinction as to *why* the conductivities of the different phases are different is totally irrelevant. Equation (5.1) can be further broken down as

$$\frac{\sigma_A}{\sigma_B} = \frac{n^A}{n^B} \times \frac{l_A^2}{l_B^2} \times \frac{\tau_{tr}^B}{\tau_{tr}^A} \tag{5.2}$$

where l_A and l_B are the mean free paths of a carrier in homogeneous A and B phase respectively and τ_{tr}^A and τ_{tr}^B give the time scales for phase A and B respectively. In a simple random walk, $\tau_{tr} \rightarrow \tau$ since there is no concept of a "transport time".

In the scaling argument given by Bunde *et al*[15] for the frequency dependent conductivity of random binary composite materials, they assume an initial anzatz of $\sigma_{eff} = \sigma_{eff}(\omega \mid \sigma_A, \sigma_B, p_A)$ where p_A is the volume fraction of phase A. The implications of this anzatz is that the microscopic details are not important, because the effective conductivity is determined by the geometry of the disorder at large length scales. They further assume that the ratio in time scales for the diffusion process of a carrier is given as $\tau^B/\tau^A = \sigma_A/\sigma_B$. They also *implicitly* assumed that the mean free path of a carrier in each phase is equal. With these two latter assumptions, we can conclude that the ratio $n^A/n^B = 1$ for consistency. They use the time scale ratio to derive general consequencies from their scaling anzatz by matching to known limits. If their anzatz is correct, it does not matter that they considered a special case. In a later paper Straley[16] also assumes *implicitly* that $n^A = n^B$, $l_A = l_B$ and $\tau^B/\tau^A = \sigma_A/\sigma_B$. However, he works with the scaling anzats $D_{eff} = D_{eff}(\omega \mid D^A, D^B, p_A)$.

A disagreement between the results of Bunde *et al*[15] and that of Straley[16] was noted by Straley. This disagreement concerned itself with the assumption of whether two time scales or one time scale exists in the problem. Because both arguments have the same inherent assumptions, there is no difference between forming the theory in terms of diffusivity or conductivity. Straley showed by

computer simulation that indeed there is only one time scale, and although Bunde *et al* also verified their results by computer simulation they could not run for long enough times to verify a second time scale. However, their models used for simulation were not equivalent. If microscopic details are in fact not important, then the difference *should* not matter.

We looked at the problem from yet another angle. First we removed the constraint that $n^A = n^B$, but assumed that each scaling anzatz is generally true. We can have $\sigma_A = \sigma_B$, for two distinct cases, $n^A = n^B$ and $n^A \gg n^B$. By the scaling arguments in terms of conductivities, $\sigma_{eff}(\omega) = \sigma_A$ at all frequencies for either case of relative carrier concentration. In terms of diffusivities we see that $D_{eff}(\omega) = D^A$ at all frequencies for the case $n^A = n^B$, however, $D_{eff}(\omega) \neq constant$ in the case $n^A \gg n^B$. Both results can agree in the d.c. limit without contradiction, but clearly the two predictions for the a.c. properties are inconsistent.

It was not clear from either Bunde *et al* or Straley that their simulations enforced $n^A = n^B$. In general, however, it is possible to construct a generalized blind or myopic ant model which can account for both a difference in concentration of charge carriers as well as a difference in diffusion constants. Even in this case, the relative diffusion constants are adjusted only through the time scales of each phase. Therefore, we incorporate the persistent random walk model which allows us to independently vary the carrier concentration, mean free path and transport time for each phase. Under the assumption that the typical size of the domains of both phases are much larger than the mean free path of the carriers, the effective d.c.

conductivity will be *independent* of how the conductivity of a phase is modeled. However, this is not necessarily true for the a.c. properties.

The persistent random walk is well suited for mesoscopopic disordered systems. Our focus is on the interplay between the mean free path of a particle with the disorder length scale set by the ramification of the medium. The persistent random walk is at a coarse grain level, however, it is hoped that disordered systems with typical cluster widths that are of the same order or smaller than the mean free path of a carrier (with respect to homogeneous phase) can be accurately modeled without resorting to a full microscopic theory.

This model is being pushed to the limit where a classical analysis can be expected to hold. The regions of phase clustering will in general have narrow necks of width that will span less than the mean free path of a particle as defined in the homogeneous phase. For example, in the thin gold film experiment by Laibowitz [24] the typical length scale of the narrow necks of gold clusters was about 10 nanometers, and the electron mean free path at room temperature is also about 10 nanometers. It is also possible to have situations where the mean free path of a good conductor can be 100 nanometers. However, it is assumed that the regions defined by these narrow necks and islands are large enough such that the transport properties of the particles are the same as in homogeneous material.

We approach the problem of calculating the frequency dependent conductivity using the persistent random walk model as follows. Each material (phase X) is characterized by the d.c. conductivity σ_X, diffusion constant D^X, transport time

τ_{tr}^{X} and the concentration of charge carriers n^{X}. From the generalized Einstein relation it follows that the effective conductivity can be expressed by $\sigma_{eff}(\omega) = n\frac{q^2}{k_B T} D_{eff}(\omega)$ where n is the total number of charge carriers in the system divided by the volume of the system. The charge carrier density n of a two component media of phase A and B is given by

$$n = n^{A} p_{A} + n^{B}(1 - p_{A}) \tag{5.3}$$

where p_A is the volume fraction of phase A. The conductivity is determined by both the concentration and mobility of the charge carriers.

The fractal characteristics of a disordered medium is expected to appear over time scales such that the random walkers will remain confined within the cluster boundaries [15] and the diffusion length scale is less than the disorder correlation length ξ. Moreover, we expect that the persistent random walk and blind ant results should be the same when the mean free path is much shorter than the coarse grain length scale.

The ratio of the effective conductivity of the system $\sigma(\omega)$ to the d.c. conductivity of phase B is given by

$$\frac{\sigma(\omega)}{\sigma_B} = \frac{nD(\omega)}{n^B D^B} \tag{5.4}$$

where $D(\omega)$ is numerically obtained from the SACF using Eq. (3.31) . The real and imaginary parts of the effective diffusion coefficient are calculated separately with the following

$$RE[\, D(\omega, N)\,] = \frac{1}{2d\tau}[\, C_\rho(0) + 2\sum_{n=1}^{N} C_\rho(n) A(\omega)^n \cos(n\phi)\,] \quad , \tag{5.5}$$

and

$$IM[D(\omega,N)] = \frac{1}{d\tau}\sum_{n=1}^{N} C_\rho(n)A(\omega)^n \sin(n\phi) \tag{5.6}$$

where $A(\omega) = (1+(\omega\tau)^2)^{-1/2}$ and $\tan(\phi) = \omega\tau$.

The dielectric response $\epsilon(\omega)$ is related to the imaginary part of the electrical conductivity[84] given by

$$RE[\frac{\epsilon(\omega)}{\epsilon_o}] = 1 - IM[\frac{\sigma(\omega)}{\epsilon_o\omega}] \tag{5.7}$$

where ϵ_o is the permittivity of free space. The relationship between $\epsilon(\omega)$ and $\sigma(\omega)$ takes into account *all* charge particles in the system. However, in most circumstances the bound charges tend to yield dielectric responses that are virtually frequency independent at low frequencies, and strongly frequency dependent near resonance frequencies. Moreover, these resonance frequencies are usually greater than the plasma frequency. Therefore, it will be assumed that the part of the dielectric response due to the bound charge is just a constant that can be added to the part due to the free charge carriers at all frequencies up to the cut-off frequency as determined by the persistent random walk model.

5.2 Inhomogeneous Medium: The Simple Couple

The simple couple as shown in Fig. 5.1 is the first application of the persistent random walk to non-homogeneous media to be considered. Periodic boundary conditions are applied to the opposing edges of the couple. This geometry is chosen because there are only parallel interfaces allowing us to compare the static results of the persistent random walk with predicted values obtained from analyzing

the configuration as resistors in parallel or series. The couple geometry is useful in testing the properties of the persistent random walk across an interface. The width of the couple is set equal to one lattice constant because the periodic boundary condition makes the x-direction infinitely long regardless of the specified width.

The effective d.c. conductivity is calculated by considering the two phases in parallel along the x-direction and in series along the y-direction. From the calculation of equivalent resistance for the couple geometry, the effective diffusion constant is found to be

$$D_{eff} = \begin{cases} \frac{P_A P_B D^A D^B (d_A+d_B)^2}{d_A^2 P_B D^B + d_B^2 P_A D^A} & \text{in series} \\ \\ P_A D^A + P_B D^B & \text{in parallel} \end{cases} \tag{5.8}$$

where $\{d_A, d_B\}$ give the dimensions of the geometry as specified in Fig. 5.1. These equations are expected to be valid when all the geometrical dimensions are much greater than the mean free path length of the particle for either phase. The probabilities P_A and P_B are just the ratio of the number of carriers in phase A and B to the total number of carriers in the system respectively. It follows that $P_A + P_B = 1$ and in particular,

$$P_A = \frac{n^A d_A}{n^A d_A + n^B d_B} \quad . \tag{5.9}$$

The theoretical prediction of Eq. (5.8) is restricted to the d.c. limit as well as to the requirement that ($l_A/d_A \ll 1$, $l_B/d_B \ll 1$). When the latter requirement is satisfied, then the predicted results of Eq. (5.8) should be valid up to a certain frequency where the two phases begin to "decouple." The decoupling occurs if

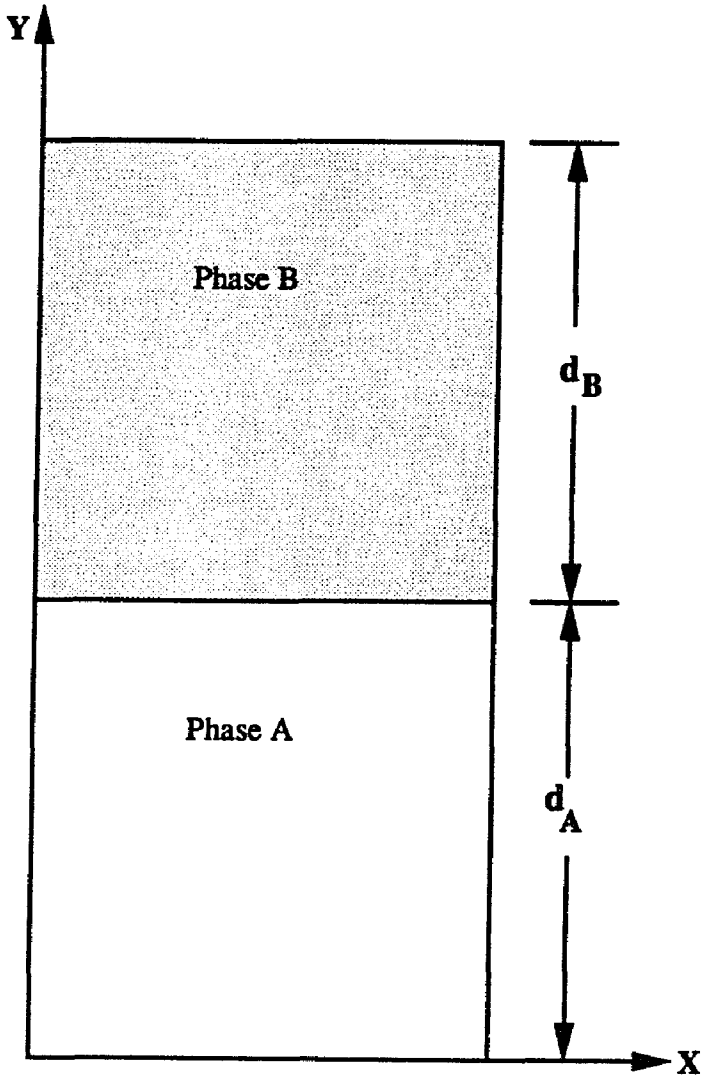

Figure 5.1

The geometry for the construction of a simple interface is shown. Phase A and B are in a parallel combination along the x-direction and a series combination along the y-direction. Periodic boundary conditions are applied making the width of the couple irrelevant. The width is set equal to one lattice constant.

an applied electric field changes direction too rapidly for the majority of charge carriers to move back and forth across the interface. In other words, the time scale is so short that the diffusion length is much smaller than d_A and d_B. Therefore, it is intuitively expected that at very high frequencies the effective diffusion coefficient for the series configuration should approach the results for the parallel case.

In general, it is expected that at sufficiently high frequencies the effective diffusion coefficient should go as

$$D(\omega) \rightarrow P_A D^A(\omega) + P_B D^B(\omega) \quad \text{at high frequencies} \tag{5.10}$$

where "high frequency" is such that the corresponding length scales being probed is much smaller than the typical cluster confinement lengths. If one is interested in the effective conductivity at these high frequencies, then the specific details in the carrier's mobility will become important.

The ratio of the conductivities of two materials as expressed in Eq. (5.2) conveniently summarizes the different ways the conductivities can differ from one another. Some properties of interest are the sensitivity of the results on the lattice constant and the accuracy compared to the predictions of Eq. (5.8) for geometries of macroscopic length scales. Furthermore, the dependence of the effective conductivity on the mean free path length, transport time and concentration of carriers is investigated.

In the following analysis of the couple configuration, the diffusion constant for phase B is fixed to be $D^B = 10^{14} nm^2/sec$ with a transport time of $\tau_{tr}^B = 10^{-12} sec$

which corresponds to a mean free path length of $l_B = \sqrt{2} \times 10^1 nm$. Various ratios in the conductivities for the two phases forming the couple are obtained by changing the properties of the A phase. As summarized in Table 5.1, the ratio of conductivities, carrier concentration and/or the d.c. diffusion coefficient will be varied and compared.

We used scattering rule # 1, as defined in Section 3 of Chapter 4, so that a particle scattering off an interface will reflect and reverse direction while satisfying an extended detailed balance. With this rule, the walker's motion *tangent* to an interface is not affected by that interface. Hence, the effective conductivity $\sigma_p(\omega)$ in the x-direction corresponding to the parallel case agrees with Eq. (5.10) at all frequencies. Therefore, only the effective conductivity $\sigma_s(\omega)$ in the y-direction corresponding to the two phases in series, will be discussed below.

We now address the question of coarse grain invariance. As explained in Chapter 4, there is a high frequency cut-off dependent on the coarse grain length scale. Below the cut-off frequency, the effective conductivity must be independent of the coarse grain length scale within reason. Without coarse grain invariance, it would be impossible to expect a coarse grain approach to be valid whatsoever.

As Fig. 5.2 demonstrates, the results for $\sigma_s(\omega)$ is invariant under three different coarse graining of the couple geometry as specified in Table 5.1 using cases A, B and C. Note that the couple geometry remains the same as the coarse grain length is varied. In particular, the interface is well defined provided that d_y/a = integer. The coarse graining is tantamount to dividing each region of phase in either smaller

Table 5.1

The frequency dependent diffusion coefficient for a couple geometry have been obtained for the cases tabulated here among others not listed. The physical properties of the B phase were set fixed with $D^B = 10^{14} nm^2/sec$ and $\tau_{tr} = 10^{-12} sec$ corresponding to a mean free path of about $14nm$. Note that the length $d_y = d_A = d_B$ refers to both regions of phase A and B along the y-direction.

case	$\frac{\sigma_A}{\sigma_B}$	$\frac{n^A}{n^B}$	$\frac{D^A}{D^B}$	$\frac{l_A}{l_B}$	$\frac{\tau^B}{\tau^A}$	$d_y\ (nm)$	$a\ (nm)$
A	10^{-2}	1	10^{-2}	10^{-1}	1	2000	100
B	10^{-2}	1	10^{-2}	10^{-1}	1	2000	10
C	10^{-2}	1	10^{-2}	10^{-1}	1	2000	1
D	10^{-2}	1	10^{-2}	10^{-1}	1	2×10^4	100
E	10^{-2}	1	10^{-2}	10^{-1}	1	200	1
F	10^{-2}	1	10^{-2}	10^{-1}	1	200	10
G	10^{-4}	10^{-2}	10^{-2}	10^{-1}	1	200	10
H	10^{-6}	10^{-4}	10^{-2}	10^{-1}	1	200	10
I	10^{-2}	1	10^{-2}	10^{-1}	1	20	0.05
J	10^{-2}	1	10^{-2}	1	10^{-2}	20	0.05
K	10^{-2}	10^{-2}	1	1	1	20	0.05

or larger grid sizes. This exercise illustrates the way in which the persistent random walk model has been parameterized to maintain coarse grain invariance.

In the calculation of $D(\omega)$, there is generally a finite window of frequencies that can be obtained for a given coarse grain length scale. The upper frequency limit is determined by the coarse grain length and the lower frequency limit will occur when the SACF does not converge sufficiently rapidly (a typical case). In this case, the best one may hope for is convergence in $D(\omega)$ such that $\omega\tau \approx 10^{-6}$ as explained in Section 3 of Chapter 3. The importance of coarse grain invariance is that calculations for $D(\omega)$ in different frequency ranges corresponding to different coarse grain length scales can be matched to obtain $D(\omega)$ over a much larger frequency range. In the case of a disordered system, however, the nature of coarse graining becomes a complicated issue because of the additional problem in correctly representing the ramification.

In Fig. 5.3 the conductivity $\sigma_s(\omega)$ for the cases B, D and E from Table 5.1 are compared to show the dependence of the *decoupling crossover frequency* on the system size. Just above the decoupling frequency, the system will respond in accordance to Eq. (5.10). The transition between the coupled and uncoupled response is not too sharp because there are always free carries *near* the interface that interact with it. The carriers near the interface consist of those particles that are a distance away less than the diffusion length. As a simple picture, assume that carriers farther from the boundaries than the diffusion length are decoupled. As the time scale decreases, the diffusion length decreases and this eventually leads

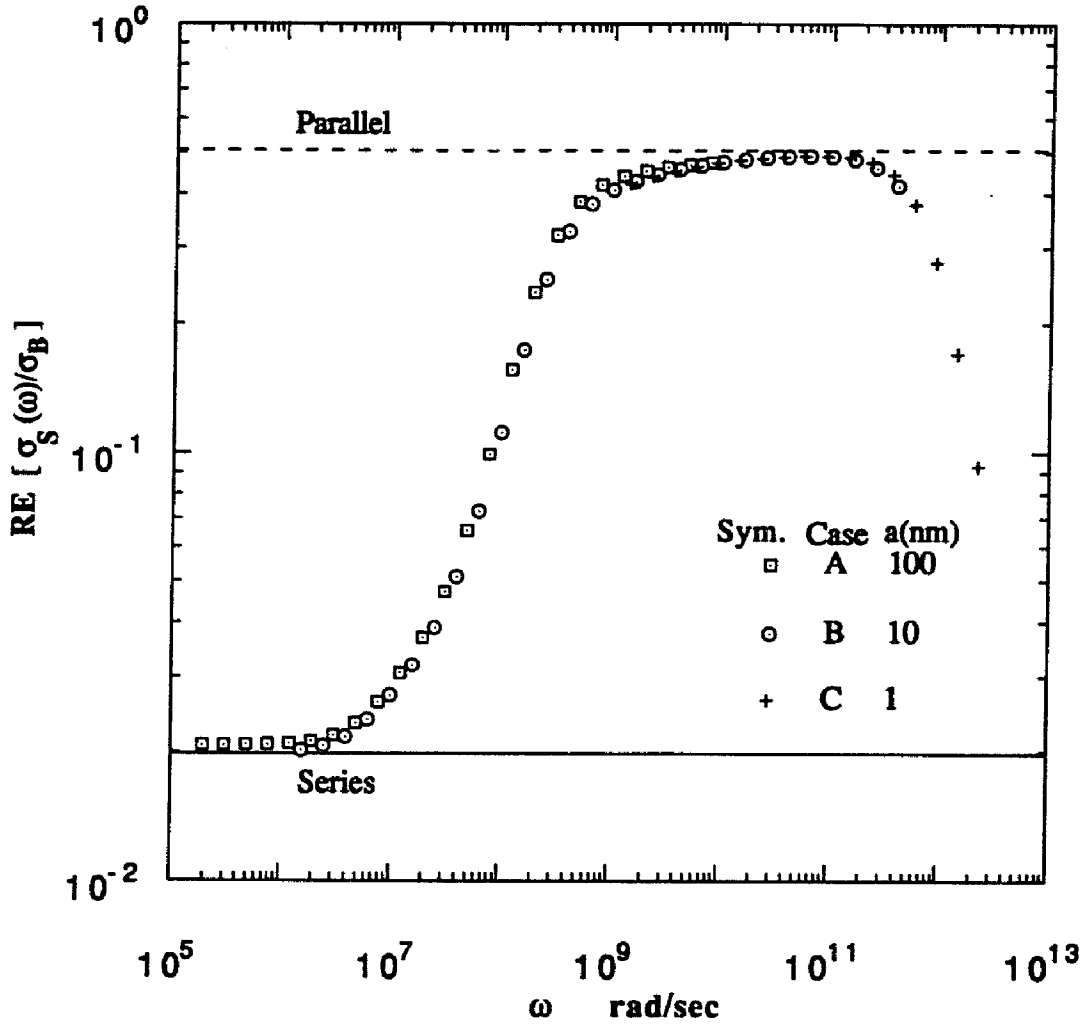

Figure 5.2

The real part of the effective conductivity for the two phase couple in the series direction is normalized with respect to the d.c. conductivity of phase B and is plotted verses frequency. Here $\sigma_A/\sigma_B = 10^{-2}$ and $\tau_{tr} = 10^{-12} sec$ for both phases. The symbols $\{\square, \bigcirc, +\}$ correspond to the cases $\{A, B, C\}$ in Table 5.1 respectively. The solid and dashed lines indicate the d.c. result for the series and parallel cases.

to a full decoupling between the two phases at high frequencies.

For the couple geometry, an estimate for the decoupling frequency can be made. We arbitrarily define the decoupling crossover frequency to occur when 80% of the free carriers are decoupled as suggested by the data used to obtain Fig. 5.3. Then the time scale t_c^X for phase X is estimated as:

$$fd_X = \sqrt{2D^X t_c^X} \tag{5.11}$$

where in this case $f = 0.1$ so that 20% of the carriers will still be within the diffusion length. Then it follows that

$$\omega_c^X = \frac{1}{t_c^X} = \frac{2D_B}{f^2 d_X^2} \tag{5.12}$$

is the frequency for which phase X of width d_X decouples. Although the fraction f is somewhat arbitrary, it is clear that the decoupling frequency is inversely proportional to the square of the linear size of the constant phase region. Since total decoupling only occurs when both phases are decoupled, the relative concentration of carriers in each phase is taken into account by a simple averaging to arrive at

$$\omega_c = P_A \omega_c^A + P_B \omega_c^B \quad . \tag{5.13}$$

Estimating the decoupling crossover frequency using Eq. (5.13) has been successful within an order of magnitude for many different cases in addition to those presented in Fig. 5.3. The length d_X cannot become arbitrarily large, however, because the entire length of the couple should be much less than the wave length of the applied

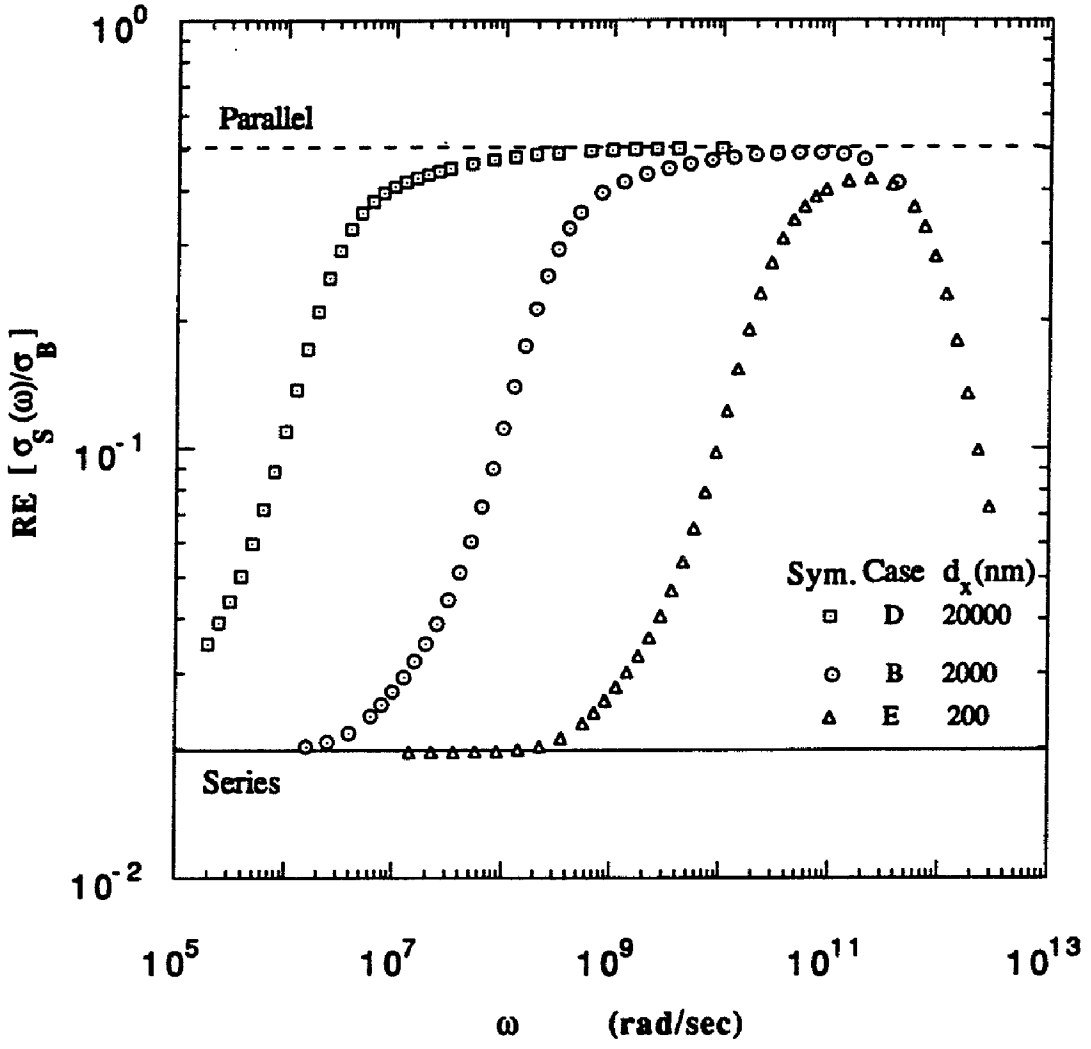

Figure 5.3

The same ratio $\sigma_s(\omega)/\sigma_B$ as plotted in Fig. 5.1 is plotted verses frequency for three different sizes of the couple. Again $\sigma_A/\sigma_B = 10^{-2}$ and $\tau_{tr} = 10^{-12} sec$ for both phases. The symbols $\{\square, \bigcirc, \triangle\}$ correspond to the cases $\{D, B, E\}$ in Table 5.1 respectively. The solid and dashed lines indicate the d.c. result for the series and parallel cases.

electric field in either medium. In this case, we are justified to consider an effective conductivity.

As shown in Fig. 5.4 for the cases F, G and H from Table 5.1, the conductivity $\sigma_s(\omega)$ obtained from the random walk is in very good agreement with the series and parallel predictions using Eq. (5.8) at low and high frequencies respectively. As the ratio of the d.c. conductivities σ_A/σ_B is decreased, it becomes clear that the transition from the d.c. series result to the d.c. parallel result has a frequency dependence of $\sim \omega^2$. As $\sigma_A \to 0$ the physical situation of having the carriers in phase B completely trapped is approached where $\langle R(t \to \infty)^2 \rangle \to R_{max}^2$, and it has been shown [68] that $D(\omega) \propto \omega^2$ at low frequencies with $D(\omega = 0) = 0$.

It is convenient to describe the real part of the conductivity in the series direction for the two phase couple as

$$\sigma_s(\omega) = \sigma_s^o + (\sigma_p^o - \sigma_s^o)F(\omega) \tag{5.14}$$

where the function $F(\omega)$ is *defined* through this equation. Solving for the function $F(\omega)$, it follows that

$$F(\omega) = \frac{\sigma_s(\omega) - \sigma_s^o}{\sigma_p^o - \sigma_s^o} = \frac{D(\omega) - D_s}{D_p - D_s} \tag{5.15}$$

where σ_s^o and σ_p^o are the predicted d.c. conductivities for the series and parallel case respectively from the equivalent resistance. Moreover, D_s and D_p are the d.c. effective diffusion coefficients for the couple in the series and parallel directions as given by Eq. (5.8) respectively. The function $F(\omega)$ is real at all frequencies. Using

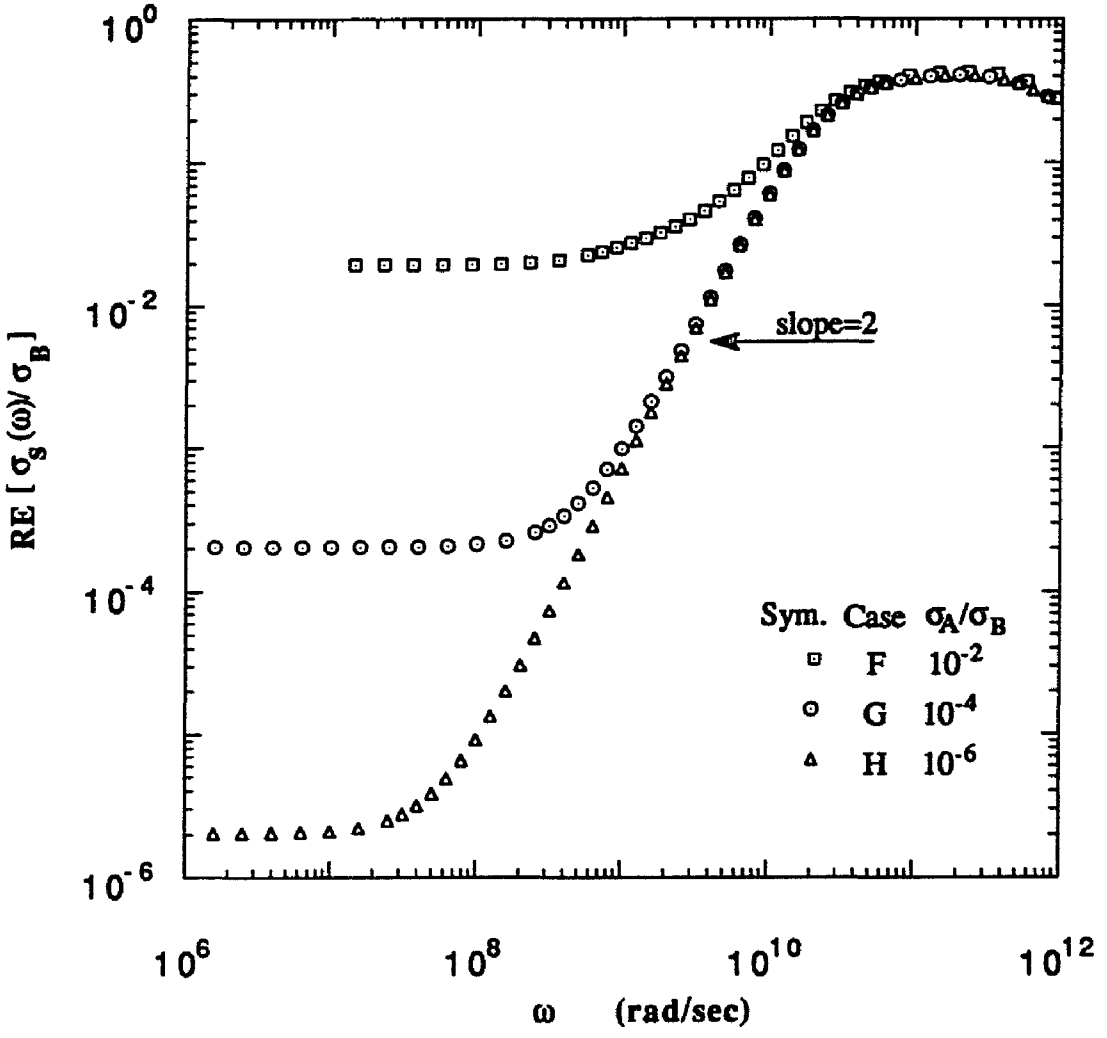

Figure 5.4

The same ratio $\sigma_s(\omega)/\sigma^B$ as plotted in Figs. 5.1-2 is plotted verses frequency for $\sigma_A/\sigma_B = \{10^{-2}, 10^{-4}, 10^{-6}\}$ as indicated by the symbols $\{\square, \bigcirc, \triangle\}$ corresponding to the cases $\{F, G, H\}$ in Table 5.1 respectively.

the random walk results for cases F, G and H from Table 5.1, and the predicted values for D_s and D_p from Eq. (5.8) we have found that

$$F(\omega) \approx \begin{cases} \frac{\omega^2}{\omega_c^2} & \text{if } \omega \leq \omega_c \\ 1 & \text{otherwise} \end{cases} \tag{5.16}$$

indicating that the approach to the series d.c. limit is the same as that of a trap for which $\sigma_s^o = 0$. By plotting the numerical data in the form defined by Eq. (5.15) on a Log-Log plot, not only was the functional form of $F(\omega)$ established, but the decoupling frequency could be accurately obtained from the y-intercept.

Other data sets have been analyzed to determine $F(\omega)$ including cases where $d_A \neq d_B$. In general, the same results as above were found with two exceptions. For the first exception, which in some way is a pathological case, occurred when $\sigma_A/\sigma_B = 10^{-4}$, $d_A = 2000nm$, $d_B = 200nm$, $n^A/n^B = 10^4$, $D^A/D^B = 10^{-8}$, $l_A/l_B = 10^{-4}$ and $\tau_{tr}^A = \tau_{tr}^B$. With these choices for the parameters, the characteristic frequency response for $\omega \leq \omega_c$ was given as $F(\omega) \approx A\sqrt{\omega} + B\omega$. Again the (low, high) frequency limit agreed with the effective conductivity for the (series, parallel) configuration. Further analysis on other cases where there is a strong opposition between the ratio in conductivities compared to the ratio in carrier concentration were not considered. It is believed that these cases are not very common because it is usually the concentration difference that predominately determines the difference in conductivities (not the mobilities). However, this case is interesting and should be pursued further. For the second exception, as described below, the lengths $d_A = d_B$ where allowed to become comparable to the mean free

path of the carriers. Therefore, this case must be treated separately because the assumption of having macroscopic length scales is invalid.

The conductivity $\sigma_s(\omega)$ is plotted in Fig. 5.5 for the cases I, J and K from table 5.1. Here the mean free path of at least one phase is of the same order but smaller than the dimension of the region of constant phase. A key result is that the effective d.c. conductivity is lower for all three cases than the d.c. series prediction. The reason for this *lower* conductivity is because the carriers scatter off the interface within a time scale for which normally their motion is positively correlated within homogeneous phase. Therefore, the effective mean free path decreases. Case I is not affected as much as cases J and K because only the carriers in phase B have a smaller effective mean free path. Since the mean free path of cases J and K are equal, in the d.c. limit their response is identical. However, in case K the transport time for the carriers in phase A is at $\tau_{tr}^A = 10^{-10} sec$ so that the dip near $\omega = 10^{10} rad/sec$ is a result of the Drude-like mobility of those carriers in phase A. As the frequency continues to increase above $1/\tau_{tr}^A$, the effective conductivity increases because of decoupling that is occurring in phase B.

The results for the effective electrical conductivity for the two phase couple geometry has by itself many interesting features. The results from the couple geometry give us more confidence in applying this model to randomly disordered media to estimate the effective conductivity. Our hope is to make use of the persistent random walk in disordered media where the linear dimensions of clusters are of the same order as the mean free path of the carriers.

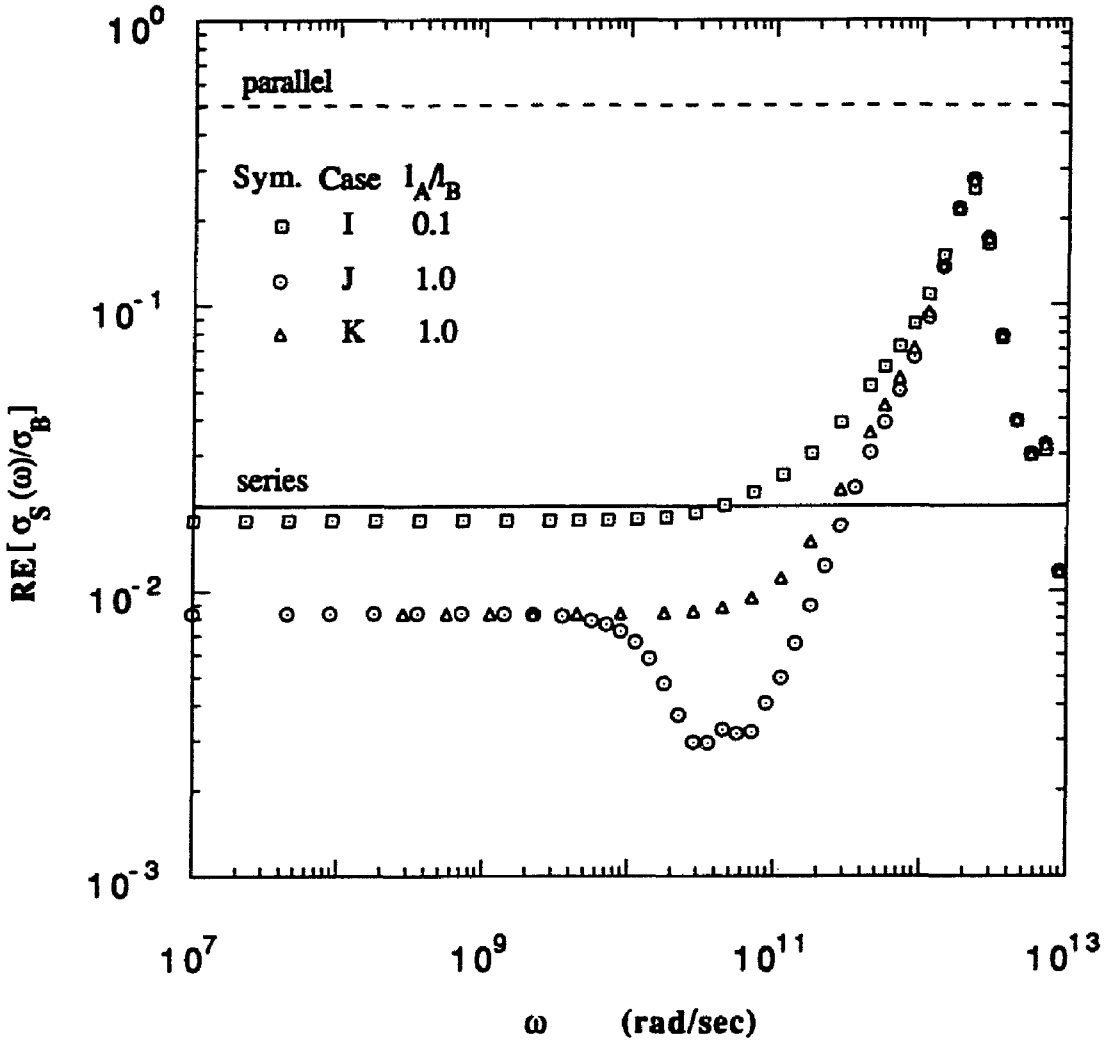

Figure 5.5

The same ratio $\sigma_s(\omega)/\sigma_B$ as plotted in Figs. 5.1-3 is plotted verses frequency. The symbols $\{\square, \bigcirc, \triangle\}$ correspond to the cases $\{I, J, K\}$ in Table 5.1 respectively. Note that for case J, $\tau_{tr}^A = 10^{-10} sec$. The solid and dashed lines indicate the d.c. result for the series and parallel cases.

5.3 Persistent Walks in Disordered Media

The characteristics of the persistent random walk in disordered media is now addressed. Although many interesting cases can be considered, we will look at the special case when the mobilities for two different phases are identical. In particular, we chose $D = D^A = D^B$, $\tau_{tr} = \tau_{tr}^A = \tau_{tr}^B$, with $n^A/n^B = 10^{-5}$ implying that the conductivity ratio is $\sigma_A/\sigma_B = 10^{-5}$. We will calculate the effective conductivity, normalized with respect to σ_B, as a function of frequency for various degrees of disorder and for various degrees of persistence. The d.c. diffusion coefficient D and transport time τ_{tr} will be left unspecified because the function $\sigma(\omega)/\sigma_B$ for a given disordered configuration will only depend on η.

We will study the real and imaginary parts of the normalized conductivity $\sigma(\omega)/\sigma_B$ verses $\omega\tau_{tr}$ because these curves do not change shape as D and τ_{tr} are varied provided the mean free path remains a constant (assuming the fixed carrier concentration ratio of $n_A/n_B = 10^{-5}$.) We proceeded to calculate $\sigma(\omega)/\sigma_B$ for the three cases $\eta = \{100, 1, 0.01\}$ for each disordered configuration generated. Experimentally, the mean free path of the carriers can be adjusted by changing the temperature.

At different volume fractions of the A phase, one disordered configuration is generated on a square mesh of side $L = 100$. A state in the site percolation model is ether of phase A (poor conductor) with probability p_A or phase B (good conductor.) Because both phases conduct, all 10000 cells in the 100×100 square mesh need to be included as part of the system. The system contains 40000 unique

states. See Appendix B for the FORTRAN code used in calculating the SACF.

The system under study now contains an ensemble over many B-phase and A-phase clusters. When the two phases have degenerate mobilities any difference in conductivity of the two phases is due entirely from the carrier concentration. The probability for the random walker to be reflected at the interface from the poor phase to the good phase is unity and from the good phase to the poor phase is $\approx n^A/n^B$. Therefore, the carriers are trapped within the good conducting clusters until time scales for which they have appreciable chance to exit. The frequency dependent conductivity will be influenced by the geometry of the good conducting phase for times less than the time scale of escape. At longer times, the carriers are not confined only to the good phase clusters, therefore, both phases participate in the diffusion process.

In Fig. 5.6 the real part of the normalized conductivity is plotted verses $\omega\tau_{tr}$ when $\eta = 100$ at four different volume fractions. Two volume fractions correspond to the limits for pure homogeneous phase A and B. The other two volume fractions are at $p_A = \{0.593, 0.407\}$ which are near the percolation threshold for the (poor, good) conducting phase respectively. Since the lattice constant is one hundred fold larger than the mean free path of the carrier, the persistent random walk is very similar to a blind ant. It is seen that at $p_A = 0.407$ the conductivity goes as $\sigma(\omega) \sim \omega^{0.35}$. The exponent of 0.35 is found instead of 0.30 because an ensemble over many cluster sizes is being considered and the appropriate walk exponent is d'_w. For frequencies $\omega\tau_{tr} \geq 10^{-4}$, the length scales that are being probed are of the

order of the coarse grain length scale. Therefore, the effective conductivity is that as if the two phases were in parallel as expected from the decoupling argument of the previous Section.

At the percolation threshold for the poor phase, nothing special happens because the good phase region has already been disconnected in isolated clusters. A characteristic increase in the effective conductivity as $\sim \omega^2$ is possibly occurring as in the case of the two phase couple. This behavior suggest that a second time scale exist as suggested by Bunde *et al*[15]

It is noted that at $P_A = 0.593$ and $P_A = 0.407$ for low frequencies $RE[\,\epsilon(\omega) - \epsilon_o\,]$ is greater than zero in contrast to the case of a homogeneous metal. We note that in general, the model of a harmonicaly bound charge with damping leads to $RE[\,\epsilon(\omega) - \epsilon_o\,]$ being positive, then negative, and finally goes to zero (but negative) as frequency increases from zero.[84] If $\epsilon(\omega)/\epsilon_o$ is negative (positive) the medium will (will not) be reflective. When the medium does not reflect, the larger the conductivity the greater the absorption. Therefore, the disordered composite will absorb at radio wave frequencies and lower although either constituent would totally reflect. The reason for the sign difference is from the fact that in homogeneous media, the SACF (VACF) is positive (exponential decay) whereas in the composite disordered medium the (SACF) (VACF) is negative. Furthermore the decay in the latter case is a slow power-law. The ramification in the medium is suppling an overall force on the particle to keep it bounded.

In Fig. (5.7) the real part of the normalized conductivity is plotted for the

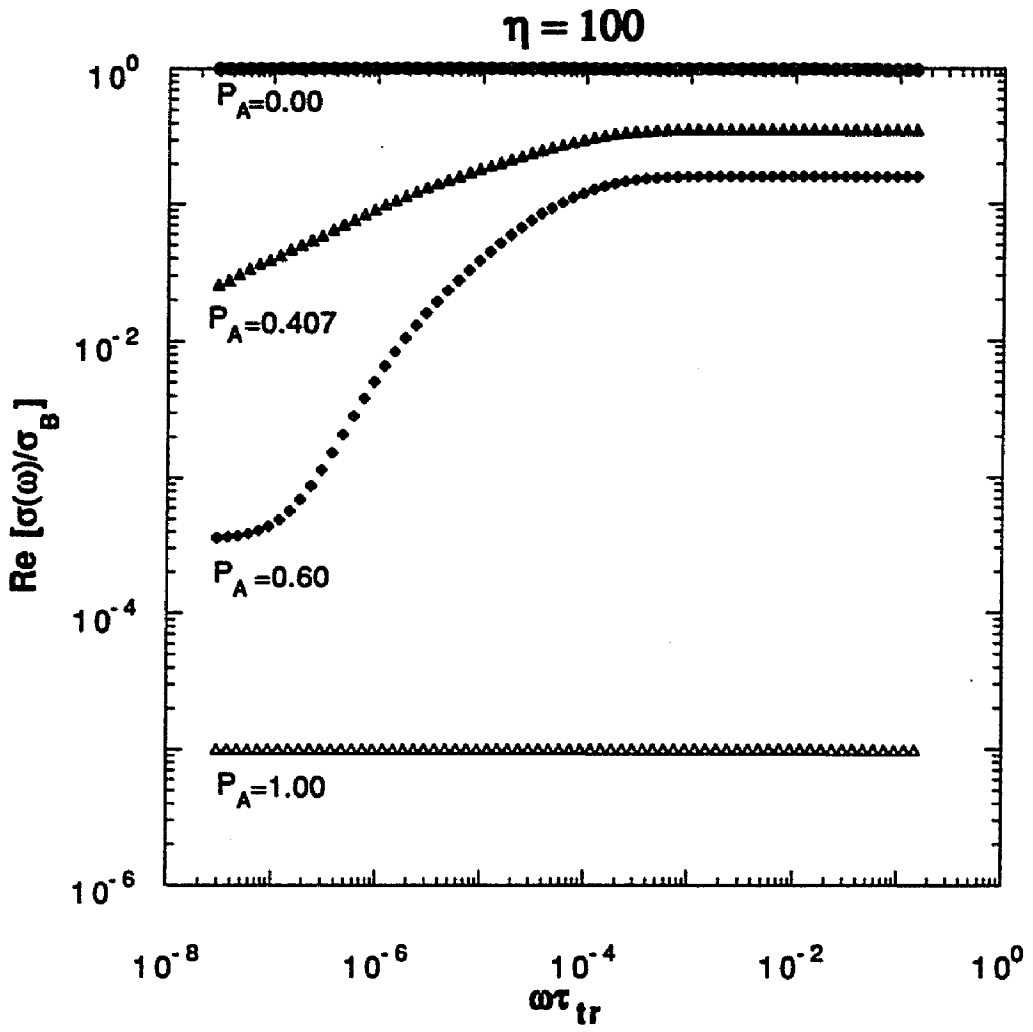

Figure 5.6

The real part of the normalized effective conductivity is plotted verses $\omega\tau_{tr}$. In this case the lattice constant is 100 times larger that the mean free path of the carrier.

case that $\eta = 1$. Two noticeable features has taken place. Firstly, the effective d.c. conductivity is lower than in the case for $\eta = 100$. Since the geometry and conductivities are identical to the case $\eta = 100$, one may have expected from a simple scaling argument that the effective conductivity should be identical as well. However, this is the crux of the problem. The d.c. limits for the effective conductivity are lower because there is much ramification on length scales of one mean free path. Therefore, the effective mean free path in the composite material is reduced by the scattering caused by the phase boundaries.

The second notable feature is that the effective conductivity remains nearly constant from the d.c. limit to higher frequencies than case $\eta = 100$. This implies that the long range correlations in the static geometry are playing less of a role for relatively more persistent walks. Other than these two features, similar characteristics are observed as in the $\eta = 100$ case.

The highest persistent case is plotted in Fig. (5.8). The same two trends, lower effective conductivity in the d.c. limit and the effective conductivity remaining a constant until higher frequencies is found. One reason for this is that since the cells are relatively smaller with respect to the mean free path, the decoupling frequency increases. In this case, the effective mean free path has been reduced enough to cause the d.c. effective conductivity to be lower than the d.c. conductivity of the poor conducting phase. This effect was already seen in the case of the two phase couple.

The fractal characteristics of the disordered configuration is not too apparent

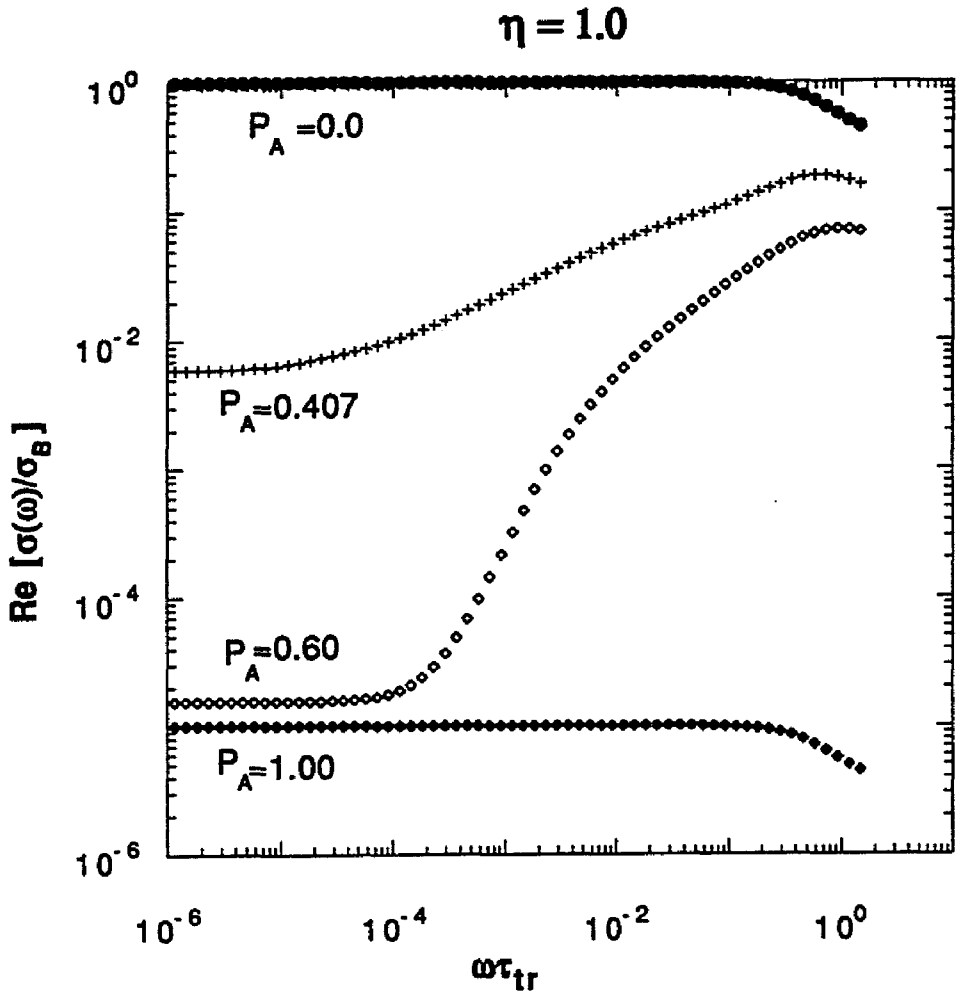

Figure 5.7

The real part of the normalized effective conductivity is plotted verses $\omega\tau_{tr}$. In this case the lattice constant equals the mean free path of the carrier.

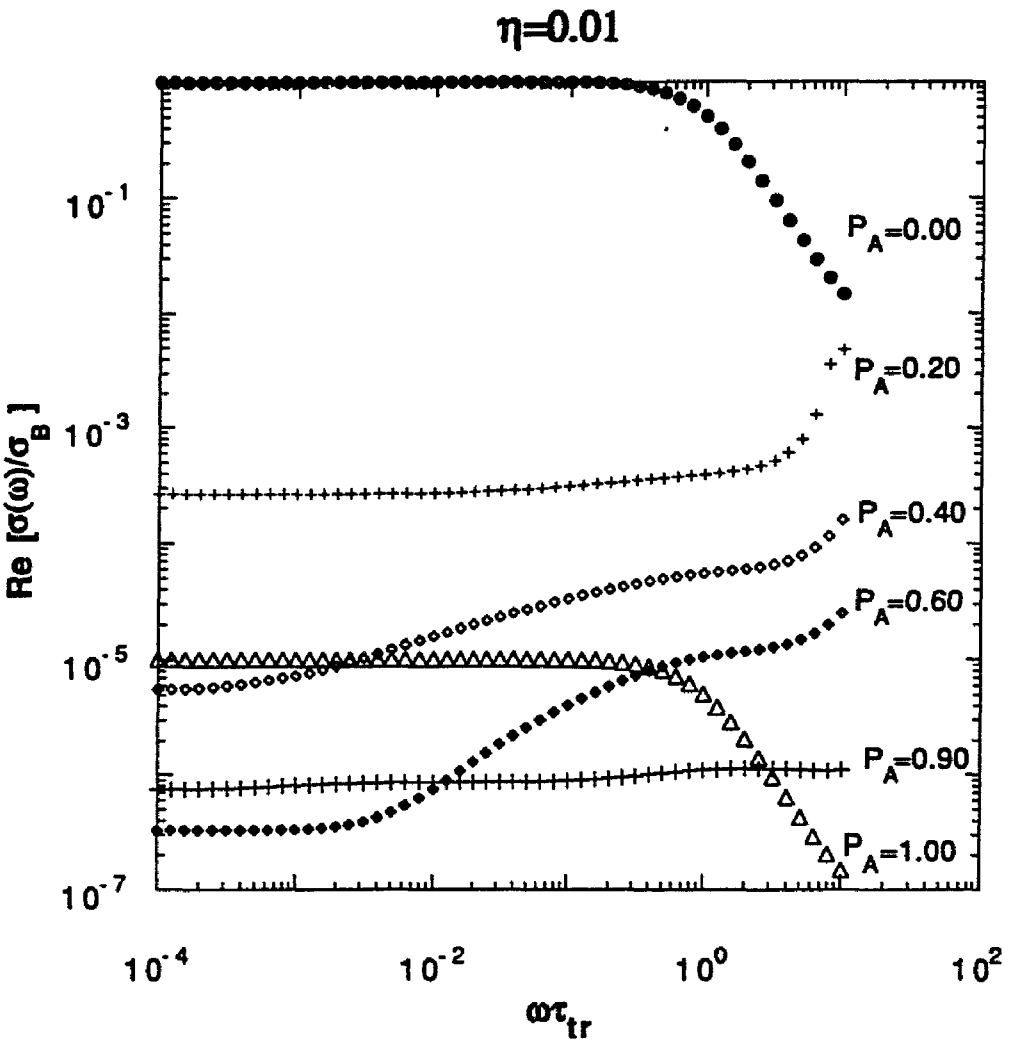

Figure 5.8

The real part of the normalized effective conductivity is plotted verses $\omega\tau_{tr}$. In this case the mean free path of the particle is 100 times that of the lattice constant.

for this case, although it is still present for frequencies $10^{-2} \leq \omega\tau_{t_r} \leq 10^{-1}$. The range in frequency for which the fractal characteristics of the cluster can be observe decrease as the persistency increases. The reason could be caused by the reflection scattering rule that was used. We suspect this because a very persistent walk will get trapped in small localized regions because of the small chance that the walker will take a step in a direction other than forward. A walker must be confined to a single cluster for a long enough time to explore the cluster. Until then, the fractal nature cannot be observed.

Each time the walker hits a phase boundary, there is a chance for the walker to escape. However, if the walker does not escape it will just keep bouncing in a localized area. There is a very small chance for the walker to turn and get out of a trap. Therefore, most of the time, the walker stays in one region so the average distance covered before successfully escaping a trap is too small for the walker to detect any self-similarity in the structure. Although the time scale for successfully escaping may be long, a trap allows the walker many chances to escape.

Another interesting point to be made is that at $P_A = 0.9$ the effective conductivity is still much lower than the conductivity of phase A. In other words, we see that a 10% volume fraction of a good conductor embedded into a poor conducting matrix has *lowered* the conductivity! The reason is because the effective mean free path is very low. The good phase is spread out into isolated regions which act as traps.

In addition to the real part of the normalized conductivity for the case $\eta = 0.01$,

in Fig. (5.9 we show a plot of the imaginary part verses $\omega\tau_{tr}$. The curves are not particularly insightful. However, the general characteristic of the imaginary part of the conductivity as shown here is similar to the other two cases. At low frequencies the imaginary part is approximately constant and then decreases. Sometimes the imaginary part will change from negative to positive around $\omega\tau_{tr} \approx 1$.

One application that was intended for the persistent random walk model was the determination of the frequency dependent effective conductivity of gold thin film experiment as described in Ref.[24] The experimental results disagree with the scaling theory predictions. It was thought that by introducing the persistent random walk the small dimensions of the clusters of gold could be handled properly. The results obtained for the disordered media as modeled by site percolation on a square lattice do not agree with the experimental results either. It was suggested [24] that inter-cluster hopping should be considered to explain the results. This could be incorporated into the general framework developed here.

Another point of interest is to continue to explore the persistent random walk model as set up here for the case that $\alpha \neq 0$ for a scattering rule. In this case even the extended detailed balance is destroyed. Preliminary results show that the stationary state deviates from a bi-level function tremendously. This opens the question of how important are the details in the scattering rules and what other physical constraints can be used in determining those rules.

In addition to changing the dynamical model, other models for the disorder could be considered.[90] Although the task seems quite difficult, a technique for

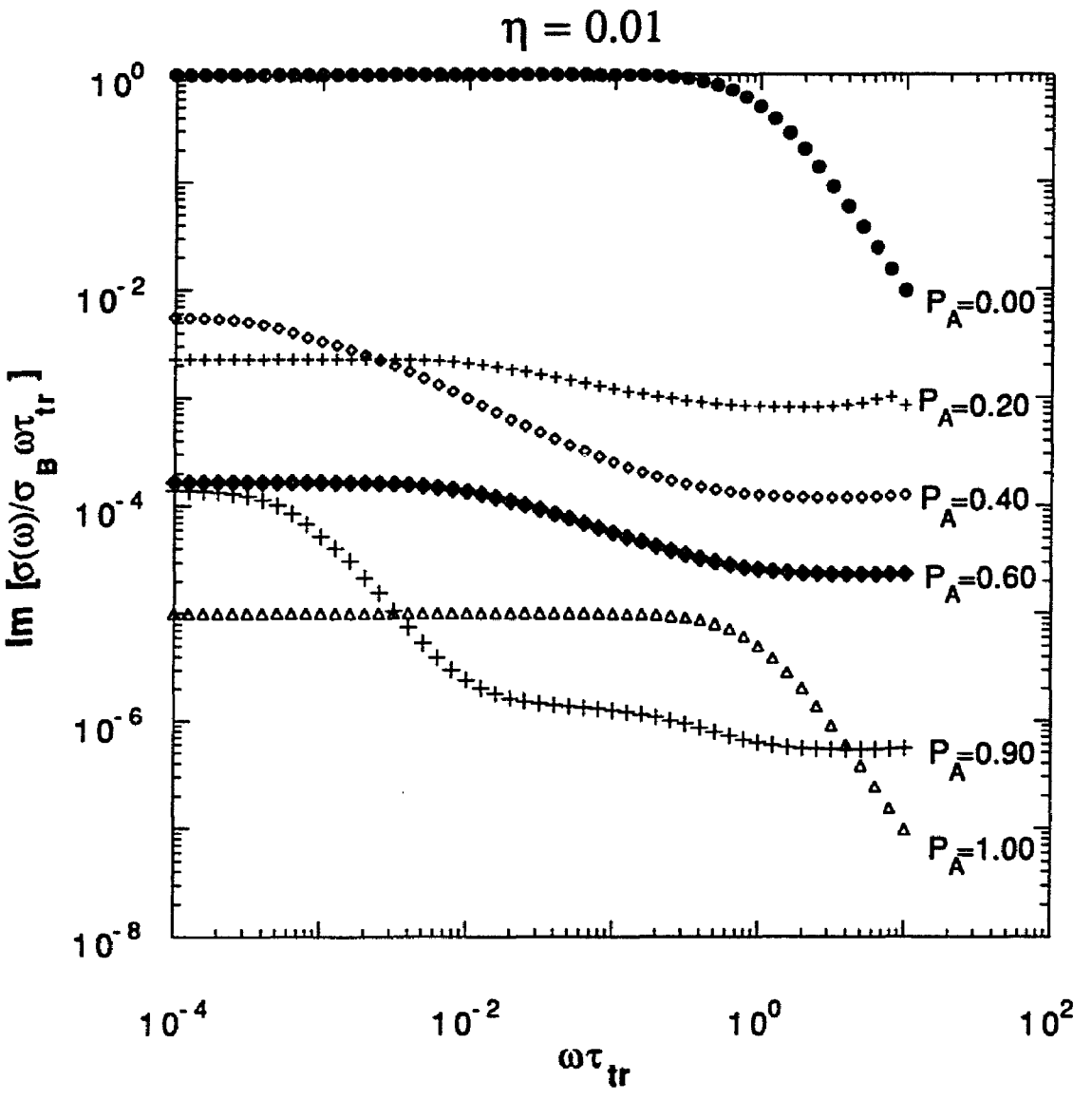

Figure 5.9

The imaginary part of the normalized effective conductivity is plotted verses $\omega\tau_{tr}$. In this case the mean free path of the particle is 100 times that of the lattice constant. The sign of the imaginary parts of the above curves is positive for $P_A = 0$ and $P_A = 1$, and are negative for all other volume fractions plotted.

matching the frequency domain solutions together as the coarse grain length scale is continuously increased could be considered.

6. CONCLUSIONS

The Brownian motion of a tagged particle in static disordered media has been studied extensively using discrete time random walks. The walk exponent d_w which characterizes the time dependence of the mean squared displacement of the random walker has been accurately estimated for the blind and myopic ant by exact enumeration over all Brownian paths from all starting points. Our estimate for d_w for the (blind, myopic) ant is given as $(2.84 \pm 0.03,\ 2.83 \pm 0.03)$ on $2-d$ percolation clusters, $(3.59 \pm 0.04,\ 3.57 \pm 0.04)$ on $3-d$ percolation clusters and $d_w = 2.63 \pm 0.04$ for the myopic ant on $2-d$ DLA clusters. Moreover, the estimates for d_w for the percolation clusters are in agreement with the universality of the blind and myopic ant models.

Only numerical data obtained from the ensemble of clusters generated from a seed site with free boundary conditions, for which saturation effects were taken into account, were used in the final estimates for d_w. We have noticed that the estimate for d_w on 2-d site percolation clusters is substantially lower when generated on a square mesh with periodic boundaries. One possible reason for the low estimate for d_w (closer to normal diffusion) is that our cluster ensemble did not include the percolating clusters that do not rap around the mesh. These clusters would have a saturation in the mean squared displacement, thereby, increase the estimate

for d_w. More importantly, a fitting form for the mean squared displacement that can account for the apparent homogeneity of the medium caused by the periodic boundary condition was not used.

In addition to the mean squared displacement, the entire position correlation matrix for the random walker on two dimensional site percolation clusters has been calculated. The usefulness of this correlation matrix is that the anisotropic properties of the diffusion process can be studied. We find[51] that the geometric anisotropic properties of the clusters directly influence the anisotropy of the diffusion process around a local region. A typical walk is anisotropic around any given origin, although any principal direction of the diffusion is equally probable. Thus, the self-averaging over many starting points makes the diffusion appear essentially isotropic. For this reason a scaler representation for the diffusion process is adequate to determine the frequency dependent diffusivity from correlation in the walker's step displacement. The physical picture is that a collection of many different skewed random motions are actually occurring.

Furthermore, we have derived a mean-field approximation for the position correlation matrix in terms of the moment of inertia as a function of the chemical distance from the origin. The anisotropy in the position correlation matrix reflects the changing anisotropy of successive shells within the cluster as the diffusing particle explores a greater chemical distance. Our Calculations show that the position correlation matrix can be approximated as the radius of gyration tensor of the cluster when the sites are weighted. The sites within a chemical distance l are

weighted by the average probability per site, $\overline{\tilde{p}(l,n)}$, that a random walker is located at a site in the lth shell at the nth time step. The quantity $\overline{\tilde{p}(l,n)}$ is a configurationally averaged probability and does not depend upon the details of a particular cluster. In addition to giving us a nice physical picture of the diffusion process, the mean-field approximation captures the essential physics quite accurately and therefore has potential to serve as a basis in further developments such as the derivation of an evolution equation for $p(x,y,n)$. Further analysis can be extended to three dimensions.

An alternate way to study the Brownian motion of a tagged particle is through the velocity auto-correlation function. In many cases the velocity auto-correlation function decays as a power-law. We have summarized the conditions for fast and slow anomalous diffusion depending on the decay exponent of the velocity auto-correlation function. We found that the presence of a long time tail is not sufficient to cause the diffusion process to be anomalous at all times, although it may cause the diffusion to be anomalous for short times. If the power-law decay is slower than $1/t^2$ the diffusion process will not have a correlation time. In the absence of a correlation time, a generalized Langevin equation can be used to describe the stochastic process. The memory kernel of the generalized Langevin equation can be obtained from the velocity auto-correlation function. In particular we have shown that a power-law friction kernel adequately describes the anomalous diffusion on site percolation clusters at the critical threshold.

A mapping between continuous time to discrete time was developed using a

master equation. The set of random rates in the master equation were normalized with respect to the maximum rate of the system. In this way the ratio of transition rates could be interpreted as hopping probabilities and each location in the disordered system would share the same exponential waiting time distribution governed by the maximum rate. Once this has been accomplished the problem of the Brownian motion could be cast into a discrete time random walk model.

The step auto-correlation function (SACF) of a random walker has been a key quantity of interest throughout the thesis. The SACF for the blind and myopic random walks were carefully analyzed and compared. Unlike the mean squared displacement, there is much non-universal behavior. The non-universal behavior is contained in the fine structure of the the mean squared displacement. The irrelevant small amplitude oscillating corrections in the mean squared displacement may become the leading order terms in the SACF. In some cases these oscillations are quite interesting. The SACF is the analog of the velocity auto-correlation function. The velocity auto-correlation function can be obtained from the SACF by using a Poisson waiting time distribution. At long times, the Poisson distribution tends to wash out the oscillations in continuous time.

In the case of the myopic ant on bipartite percolation clusters at the critical threshold, the SACF oscillates in sign at each time step. In general, the oscillation will persist indefinitely without decay. The residual oscillation amplitude has been shown to scale as $\sim 1/S$ where S is the size of the cluster. The oscillation envelope has been shown to decay as a power-law with the exponent given as half the spectral

dimension.

We have expressed the complex frequency dependent diffusion coefficient in terms of the SACF. It is found that the non-universal aspects of the oscillations in the SACF did not have any influence on $D(\omega)$. We suspect that oscillations of greater period than those of the blind or myopic ant may be important when calculating $D(\omega)$. This had lead us to look at non-detailed balance models that would lead to complex eigenvalues from the probability transition matrix. However, this route was not too successful. Although introduced for other reasons, the SACF for a highly persistent random walk in disordered media does have longer periods of oscillations than one time step. In this case as well, however, the oscillations in the SACF do not play that important of a role in the final result for $D(\omega)$.

The general method of calculating $D(\omega)$ from the SACF has the advantage that it goes beyond a mean-field description. Also the frequency dependence of the diffusion coefficient can be directly attributed to the spatial disorder of the medium. Furthermore, using the SACF instead of the mean squared displacement to calculate $D(\omega)$ is much easier because of convergence. Although this method works very well in the high frequency limit, the method does not work well at lower frequencies because of poor convergence. However, it is possible to monitor the rate of convergence and to decide when to truncate the sum over the SACF.

A random walk model with persistence is introduced for the analysis of the electrical conductivity of disordered composite materials. Within a region of constant phase the mobility of the material is modeled to be Drude-like. In this model, we

are able to independently choose the d.c. diffusion coefficient, transport times and carrier concentrations for each constituent phase. We found that the persistent random walk yields results that *depend* on the specific characteristics of conductivities of each phase. Only in the d.c. limit is the real part of the effective conductivity *independent* of the transport time and mean free path length provided that the typical geometrical length scales of regions of constant phase are much larger than the mean free path.

In disordered media, the fractal characteristics of the clusters may be washed out by highly persistent random walkers confined to the infinite percolating network. The general criteria for the fractal characteristics of the clusters to be present is that the root mean squared displacement of the random walker must not exceed the correlation length of the clusters. Moreover, the time scale must be less than the average time for the carriers to escape. Normal diffusion will take place once both phases participate in the diffusion process. The effective d.c. conductivity of a non-homogeneous medium will be less than the d.c. conductivity of either phase when the disorder length scale is smaller than the mean free path of either phase.

BIBLIOGRAPHY

BIBLIOGRAPHY

1. Studies in Statistical Mechanics, Volume VII, *Fluctuation phenomena*, (North Holland, Amsterdam, 1979. E.W. Montroll and J.L. Lebowitz, editors, See chapter 2, E.W. Montroll and B. J. West. *On the Enriched Collection of Stochastic Processes*, for short history of Brownian motion and general theory on random walks. See chapter 1, M. Kac and J. Logan. *Fluctuations*, for classical Langevin and Fokker-Planck approach to the Brownian movement.

2. R. Furth, editor. *Investigations on the theory of the Brownian Movement.* Dover Publications, Inc, New York, 1956. This Dover edition consist of an unaltered reproduction of the translation by A. D. Cowper originally published in 1926, of a collection of papers written by Albert Einstein.

3. Nelson Wax, editor. *Selected Papers on Noise and Stochastic Processes.* Dover Publications, Inc, New York, 1954.

4. E.L. Cussler. *Diffusion Mass Transfer in Fluid systems.* Cambridge University Press, 1989. Chapter 2 reviews the pioneering work of Fick and others.

5. L.E. Reichl. *A Modern Course in Statistical Physics.* University of Texas Press, Austin, 1987. In particular, simple random walk and central limit theorem can be found in chapter 5, elemetary transport theory in chapter 13, and the fluctuation-dissipation Theorem in chapter 15. Many other references can be consulted from therin.

6. William Jones and Norman H. March. *Theoretical Solid State Physics*, volume 2. Dover Publications, Inc, New York, 1973. see chapter 6.

7. H. J. Kreuzer. *Nonequilibrium Thermodynamics and its Statistical Foundations.* Clarendon Press, Oxford, 1981. see chapter 3.

8. M. Lax. *Reviews of Modern Physics*, 32(1):25–64, 1960.

9. J. W. Haus and K. W. Kehr. *Physics Reports*, 150:263–406, 1987.

10. M. F. Shlesinger and B. J. West, editors, *Random Walks and Their Applications in the Physical and Biological Sciences, (National Bureau of Standards, Washington D.C.)*, AIP Conf. Proc. No. 109, New York, 1984.

11. E. W. Montroll and G. H. Weiss. *Journal of Mathematical Physics*, 6(2):167–181, 1965. E. W. Montroll and H. Scher. *Journal of Statistical Physics*, 9(2):101–135, 1973. T. Morita and T. Horiguchi. *Journal Physics A*, 5:67–77, 1972. J. K. E. Tunaley. *Journal of Statistical Physics*, 12(1):1–10, 1975.

12. N. G. Van Kampen. *Stochastic Processes in Physics and Chemistry.* North Holland, Amsterdam, 1981. For discussion on the Fokker-Planck and Langevin equation see chapter 8.

13. R. K. Pathria, *Statistical Mechanics.* Pergamon, Oxford, 1977. or other typical text books on statistical mechanics. For original description see P. Langevin. *C.R. Acad. Sci.*, Paris, 146:530, 1908.

14. R. Kubo, K. Matsuo and K. Kitahara. *Journal of Statistical Physics*, 9(1):51–96, 1973.

15. A. Bunde, A. Coniglio, D.C. Hong, and H. E. Stanley. *Journal Physics A: Math. Gen.*, 18:L137–L144, 1985. D.C. Hong, H. E. Stanley, A. Coniglio and A. Bunde. *Pysical Review B*, 33(7):4564, 1986.

16. J. P. Straley. *Physical Review B*, 41(13):9340–9344, 1990.

17. W. T. Mo and J. Wei. *Chemical Engineering Science*, 41(4):703–710, 1986.

18. P. N. Sen. *Applied Physics Letters*, 39:667, 1981; *Geophysics*, 46:1417, 1981. W. C. Chew and P. N. Sen. *Journal of Chemical Physics*, 77:4683, 1982.

19. M. Koiwa and S. Ishioka. *Journal of Statistical Physics*, 30(2):477–485, 1983. S. A. Rice. *Physical Review*, 112(3):804–811, 1958. J. R. Manning. *Physical Review*, 139(1A):A126–A135, 1965.

20. R. J. Borg and G. J. Dienes. *Solid State Diffusion.* Academic Press, 1988.

21. P. Argyrakis and R. Kopelman. *Physical Review B*, 22(4):1830–1836, 1980.

22. H. Scher and M. Lax. *Physical Review B*, 7(10):4502–4519, 1973.

23. A. Kapitulnik and G. Deutscher. *Physical Review Letters*, 49(19):1444–1447, 1982. R. F. Voss, R. B. Laibowitz and E. I. Allessandrini. *Physical Review Letters*, 49(19):1441–1448, 1982.

24. R. B. Laibowitz and Y. Gefen. *Physical Review Letters*, 53(4):380–383, 1984.

25. W. Lamb, D. M. Wood and N. W. Ashcroft. *Physical Review B*, 21(6):2248–2246, 1980. D. M. Wood and N. W. Ashcroft. *Philosophical Magazine*, 35(2):269–280, 1977.

26. V. K. Shante and S. Kirkpatrick *Advances in Physics*, 20:325–357, 1971. D. Stauffer. *Physics Reports*, 54(1):2–74, 1979. J. W. Essam. *Reports on Progress in Physics*, 43:834, 1980. D. Stauffer. *Introduction to Percolation Theory.* Taylor and Francis, London. 1985.

27. P. L. Leath. *Physical Review B*, 14(11):5046–5055, 1976.

28. Z. Alexandrowicz. *Physics Letters*, 80A(4):284–286, 1980.

29. J.P. Straley. *Journal of Physics C*, 9:783–795, 1976.

30. P. G. de Gennes. *Recherche*, 7:919, 1976. J. P. Straley. *Journal of Physics C*, 13:2991–3002, 1980. C. D. Mitescu and J. Roussenq. *Ann. Israel Phys. Soc.*, 5:81, 1983 S. Wilke, Y. Gefen, V. Ilkovic, A. Aharony and D. Stauffer. *Journal of Physics A*, 17:647–656, 1984.

31. I. Majid, D. Ben-Avraham, S. Havlin and H. E. Stanley. *Physical Review B*, 30(3):1626–1628, 1984. The exact enumeration method had been earlier used in evaluation of discrete path intergrals, see for example D. Thirumalai, E. J. Bruskin and B. J. Berne. *Journal of Chemical Physics*, 79(10):5063–5069, 1983.

32. R. Muralidhar, D. Ramkrishna, H. Nakanishi and D. J. Jacobs *Physica A*, 167:539–559, 1990.

33. D. Bedeaux, K. Lakatos-Lindenberg and Kurt E. Shuler. *Journal of Mathematical Physics*, 12(10):2116–2123, 1971. J. Klafter and R. Silbey. *Physical Review Letters*, 44(2):55–58, 1980.

34. S. Alexander, J. Bernasconi, W. R. Schnider and R. Orbach. *Review of Modern Physics*, 53(2):175–198, 1981.

35. S. Havlin and D. Ben-Avraham. *Advances in Physics*, 36(6):695–798, 1987.

36. B. Mandelbrot. *Fractal Geometry of Nature* Freeman, San Francisco, 1982

37. A. L. Laskar, J. L. Bocquet, G. Brebec and C. Monty editors, *Diffusion in Materials*, 155-183 NATO ASI Series E: Applied Sciences Vol. 179, 1990. Kluwer Academic Publishers, Printed in the Netherlands.

38. R. B. Pandey, D. Stauffer, A. Margolina and J. G. Zabolitzky. *Journal of Statistical Physics*, 34(3):427–450, 1984.

39. H. Nakanishi. *Materials Science Forum*, 4:129-143, 1985. H. Nakanishi, Y. Meir, Y. Gefen, A. Aharony and P. Schofield. *Journal of Physics A*, 20:L153–L158, 1987.

40. J. Tobochnik, D. Laing and G. Wilson. *Physical Review A*, 41(6):3052–3058, 1990.

41. D. Jacobs and H. Nakanishi. *Physical Review A*, 41(2):706–719, 1990.

42. J. Bernasconi, S. Alexander and R. Orbach. *Journal De Physique*, 39(S8):C6.706–C6.707, 1978.

43. S. Alexander and R. Orbach. *Le Journal De Physique-Lettres*, 43(17):625–631, 1982. D. Ben-Avraham and S. Havlin. *Journal of Physics A: Math. Gen.*, 15:L691–L697, 1982. M. Daoud. *Le Journal De Physique-Lettres*, 44(23):L925–L928, 1983.

44. S. Ma. *Modern Theory of Critical Phenomena*, Benjamin, Reading, Mass., 1976.

45. Y. Gefen, A. Aharomy and S. Alexander. *Physical Review Letters*, 50(1):77–80, 1983.

46. S. Havlin, D. Ben-Avraham and H. Sompolinsky. *Physical Review A*, 27(3):1730–1733, 1983.

47. S. Havlin and R. Nossal. *Journal of Physics A*, 17:L427–L432, 1984.

48. F. Family, T. Vicsek and P. Meakin. *Physical Review Letters*, 55(7):641–644, 1985. S. Quandt and A. P. Young. *Journal of Physics A*, 20:L851–L56, 1987. J. P. Straley and M. J. Stephen. *Journal of physics A*, 20:6501–6504, 1987.

49. T. Vicsek. *Fractal Growth Phenomena.* World Scientific, 1989.

50. F. Family and T. Vicsek. *Journal of Physics A*, 18:L75–L81, 1985. P. Grassberger. *Mathematical Biosciences*, 63:157–172, 1983.

51. R. Muralidhar, D. Jacobs, D. Ramkrishna and H. Nakanishi. *Physical Review A*, 43(12):6503–6517, 1991.

52. F. Family, T. Vicsek and B. Taggett. *Journal of Physics A*, 19:L727–L732, 1986.

53. W. Feller. *An Introduction to Probability Theory and its Applications.* John Wiley and Sons, New York, 1968. C. W. Gardiner. *Handbook of Stochastic Methods for Physics, Chemistry and the Natural Sciences.* Springer-Verlag, New York, 1983. see books on stochastic and/or markov processes

54. Muhammad Sahimi, M McKarnin, T. Nordahal and M. Tirrell. *Physical Review A*, 32(1):590–595, 1985.

55. S. Havlin, D. Movshovitz, B. Trus and G. H Weiss. *Journal of Physics A*, 18:L719–L722, 1985.

56. S. Havlin and A. Bunde. *Physica D*, 38:184–191, 1989.

57. A. Bunde, S. Havlin and H. E. Roman. *Physical Review A*, 42(10):6274–6277, 1990.

58. J. R. Banavar and J. F. Willemsen. *Physical Review B*, 30(11):6778–6779, 1984. B. O'Shaughnessy and I. Procaccia. *Physical Review A*, 32(5):3073–3083, 1985. *Physical Review Letters*, 54(5):455–458, 1985.

59. L. F. Richardson. *Procedings from the Royal Society of London A*, 110:709, 1926.

60. B. J. Alder and T. E. Wainwright. *Physical Review A*, 1(1):18–21, 1970.

61. R. F. Fox. *Physica*, 118A:383–394, 1983. J. J. Erpenbeck and W. W. Wood. *Physical Review A*, 32(1):412–422, 1985.

62. B. J. Alder and T. E. Wainwright. *Physical Review Letters*, 18(23):988–990, 1967.

63. K. Ohbayashi, T. Kohno and H. Utiyama. *Physical Review A*, 27(5):2632–2641, 1983.

64. D. Frenkel. *Physics Letters A*, 121(8,9):385–389, 1987. M. H. Ernst, and A. Weyland. *Physics Letters*, 34A:39, 1971. Th. M. Nieuwenhuizen, P. F. J. van Velthoven and M. H. Ernst. *Physical Review Letters*, 57:2477, 1986. J. J. Brey, J. G. Ordonez and A. Santos. *ibid*, 127A:5, 1988.

65. C. Bruin. *Physical Review Letters*, 29(25):1670–1673, 1972. B. J. Alder and W. E. Alley. *Physica*, 121A:523–530, 1983.

66. B. J. Alder and W. E. Alley. *Journal of Statistical Physics*, 19(4):341–347, 1978. *Physica*, 121A:523, 1983. J. C. Lewis and J. A. Tjon. *Physics Letters* 66A:349, 1978.

67. H. van Beijeren. *Review of Modern Physics*, 54(1):195–234, 1982.

68. H. Scher and M. Lax. *Physical Review B*, 7(10):4491–4501, 1973.

69. S. D. Druger, M. A. Ratner and A. Nitzan. *Physical Review B*, 31(6):3939–3947, 1985.

70. H. Mori. *Progress of Theoretical Physics*, 33(3):423–455, 1965. *Progress of Theoretical Physics*, 34(3):399–416, 1965.

71. J. C. Dyre. *Journal of Applied Physics*, 64(5):2456–2468, 1988.

72. T. Odagaki, M. Lax and A. Puri. *Physical Review B*, 28(5):2755–2765, 1983.

73. J. C. Dyre. *Journal of Non-Crystalline Solids*, 88:271–280, 1986.

74. K. Kundu and P. Phillips. *Physical Review A*, 35(2):857–865, 1987.

75. P. J. H. Denteneer and M. H. Ernst. *Physical Review B*, 29(4):1755–1768, 1984.

76. J. W. Haus, K. W. Kehr. *Physics Review B*, 28(6):3573–3575, 1983. M. Lax and H. Scher. *Physical Review Letters*, 39(13):781–784, 1977. J. K. E. Tunaley. em Journal of Statistical Physics, 14(5):461–463,1976. em Journal of Statistical Physics, 11(5):397–408,1974. *Physical Review Letters*, 33(17):1037–1039, 1974.

77. E. W. Montroll. em The Annals of Mathematical Statistics, 18(1):1947.

78. N. H. Fuchs and H. Nakanishi. *Physical Review A*, 43(4):1721–1726, 1991.

79. S. Alexander. *Physical Review B*, 23(6):2951–2955, 1981.

80. P. Dorenbos. PhD thesis, Rijksuniversiteit Groningen, 1988.

81. J. C. Kimball and L. W. Adams, Jr. *Physical Review B*, 18(10):5851–5858, 1978.

82. J. W. Haus, K. W. Kehr and J. W. Lyklema. *Physical Review B*, 25(4):2905–2907, 1982.

83. T. Odagaki and M. Lax. *Physical Review B*, 24(9):5284–5294, 1981.

84. F. J. Milford, J. R. Reitz and R. W. Christy. *Foundations of Electromagnetic Theory.* Addison-Wesely Publishing Company, 3rd edition, 1980.

85. W. M. Saslow and G. Wilkinson. *American Journal Physics*, 39:1244–1248, 1971.

86. Ashcroft and Mermin. *Solid State Physics.* Holt, Rinehart and Winston, 1976.

87. L. Solymar and D. Walsh. *Lectures on the Electrical Properties of Materials.* Oxford Science Publications, 4th edition, 1988.

88. J. Tobochnik. *Computers in Physics*, pages 181–184, March/April 1990. J. Tobochnik, M. A. Dubson, M. L. Wilson, and M. F. Thorpe. *Physical Review A*, 40(9):5370–5376, 1989.

89. F. Lancon, L. Billard, W. Chambron and A. Chamberod. *Journal of Physics F*, 15:1485–1496, 1985.

90. D. D. Nolte. *Physical Review A*, 40(8):4817–4819, 1989.

91. P. L. Rossiter. *The Electrical Resistivity of Metals and Alloys.* Cambridge University Press, 1987.

92. N. E. Cusak. *The Physics of Structurally Disordered Matter.* Adam Hilger, 1987.

APPENDICES

Appendix A: The Method Used in Generating DLA Clusters

In this Appendix, we give a general description of the algorithm used in generating DLA clusters on the square lattice. The method incorporated here is partly standard[49] and partly new. The basic idea of generating a DLA cluster is to release a random walker from "infinity" and wait for it to randomly hit the aggregate. The practical problem in the computer simulation is to decide what is infinity. After a random particle sticks to the aggregate, a new particle from infinity is then released. In an operational sense, the particle should be released from a distance away from the center of mass that is much greater than the linear dimensions of the aggregate. As the aggregate grows in size the distance that the particle is released must grow in proportion. Therefore, without doing anything fancy, the total C.P.U. time will increase exponentially with cluster size. The algorithm presented here allows one to generate DLA clusters with the total C.P.U. time increasing *linear* with size. The entire method will be described, and then the subroutine in FORTRAN is included for future reference.

The first two "tricks" are described in Appendix A in ref.[49]. The first trick is to start the random walker on a shell that is reasonably larger than the aggregate. This radius is called *rstart*. The probability for the walker to start anywhere on this shell is uniform. It is important to make sure that the shell is centered around the aggregate, otherwise a bias in starting more walkers near the aggregate on a given side will occur.

The second "trick" is to kill the random walk if it drifts too far from the

aggregate. The logic behind this is that once a random walker gets so far from the aggregate, it may inter the field of influence of the aggregate again but as if it were another random particle. Therefore, instead of wasting time tracking the particle out to infinity and then back again, it is best to kill the walker and start a new random walker. This is accomplished when the random walker moves a distance form the origin $r > rkill$. It is good to set $rkill >> rstart$ in order not to introduce to much error.

When the particle is anywhere between $rstart < r < rkill$ the step length of the walker can be set to $dr = r - rstart$. This is the most efficient region as far as the particle's movement is concerned. However, when the particle is inside the smaller shell $r < rstart$ the process is slowed down because the particle has a possibility of sticking to the aggregate. In this region we use a third "trick" which is slightly different than that in ref.[49] but similar in spirit.

We incorporate the concept of coarse graining. The space is partioned off into very large cells. These cells are divided by a factor b. Then those cells are divided by a factor b and so on, until the last stage reaches the lattice structure. Each cell is referred to as a bin at its respective level such as $bin1(i,j)$, $bin2(i,j)$, etc. Then the $binX(i,j)$ for level X can be equal to 0 or 1. If a bin is equal to 0 that indicates there are no aggregate particles in that cell, otherwise there is. By checking nearest and next nearest neighboring bins at a given level, it can be determined whether a step size (of length equal to the cell) is appropriate or not. If there are aggregates in the neighboring bins, then the next level of bins must be checked. By proceeding

with this process, one can always maximize the step length in any given location. This method is believed to be faster than the one presented by Vicsek, because there is very little updating time. Since the step length is proportional to b^n at the nth level, one can reduce the exponential time dependence on size to a linear dependence.

```
      subroutine dlagn1(n,nb,link,mult,chain,x,y,stat,isd)
c This subroutine simulates the growth of a diffusion
c limited aggregate. The aggregate is generated on a
c underlying square lattice. The method of generation uses a
c variable jumping distance in order to speed the process.
c ---------------------------------------------------------------
c  input:  n= the number of particles contained in the aggregate
c          isd = the initial seed
c ---------------------------------------------------------------
c  output: link defines connectivity between particles (sites)
c          mult(s) defines number of connections for site s.
c          chain(s) = 1 or -1 which defines the parity of site s
c          x(s), y(s) yield the (x,y) coordinate of site s
c          stat(i) yields simulation statistics
c          n = -1  walker escaped
c          n = -2  too small of a grid error
c ---------------------------------------------------------------
c       Variable list (incomplete)
c s,k = site number
c imin,imax = (min, max) x coordinate that the aggregate spans
c jmin,jmax = (min, max) y coordinate that the aggregate spans
c xlatt,ylatt define lattice boundary given by
c       ie    xlatt = 0.5 * ( imax - imin )
c xc,yc the coordinates of the current center of the aggregate
c       ie    xc =  imin + xlatt
c xx,yy the current coordinates of random walker
c x(s),y(s) coordinates of site s of aggregate
c nbox2 = number of lattice constants of finest grained bin
c xbox2, xbox3, ... = length scale of bin 2, 3, ... respectively
c rstart = radius of starting shell w.r.t. origin
c rkill = radius the walker is killed if it moves more than this
c xkill = rkill/rstart
c mkill = maximum number of walkers that are allowed to be killed
c dr = a variable step distance for the random walker
c sloc(lp) = the latest site label that became a member of plane lp
c chain(s) yields a path between sites within the same plane
c lm = maximum number of site labels
c ii is used to mod the plane number
c iq( ) is used to define the normal to the planes
c lp = a general plane index for a site
c stat(i) = fraction of steps contained in ith length scale
c stat(i+10) = filled bin fraction for r < rstart of ith scale < 9
c stat(19) = total number of steps
c stat(20) = total number of walks killed
c ---------------------------------------------------------------
```

```
      integer n,s
      integer mult(n),chain(n),x(n),y(n)
      integer link(40000,4)
      integer sloc(40000)
      integer*2 bin2(-256:256,-256:256)
      integer*2 bin3(-128:128,-128:128)
      integer*2 bin4(-64:64,-64:64)
      integer*2 bin5(-32:32,-32:32)
      integer*2 bin6(-16:16,-16:16)
      integer*2 bin7(-8:8,-8:8)
      integer*2 bin8(-4:4,-4:4)
      integer iq(2),ii,idr(4,2),jc(4)
      dimension stat(20)
      data ii/9999/, iq/100,99/
      pi = 3.1415927
c ------------------------------------------------- set parameters
      nbox2 = 2
      xkill = 40
      mkill = 10000
      lm = 40000
      id = 2
      iz = 4
c ------------------------------------------------------ initialize
      idr(1,1) = 1
      idr(1,2) = 0
      idr(2,1) = 0
      idr(2,2) = 1
      idr(3,1) = -1
      idr(3,2) = 0
      idr(4,1) = 0
      idr(4,2) = -1
      jc(1) = 3
      jc(2) = 4
      jc(3) = 1
      jc(4) = 2
c
      nmax = min0(n,lm)
      n = nmax
      c1 = 2*pi
      nbox3 = 2*nbox2
      nbox4 = 2*nbox3
      nbox5 = 2*nbox4
      nbox6 = 2*nbox5
      nbox7 = 2*nbox6
      nbox8 = 2*nbox7
```

```
      xbox2 = float( nbox2 )
      xbox3 = float( nbox3 )
      xbox4 = float( nbox4 )
      xbox5 = float( nbox5 )
      xbox6 = float( nbox6 )
      xbox7 = float( nbox7 )
      xbox8 = float( nbox8 )
c
      do 50 i=1,n
   50 mult(i) = 0
      do 100 j=1,4
      do 100 i=1,n
  100 link(i,j) = 0
      do 150 i=1,lm
  150 chain(i) = 0
      do 200 i=1,20000
  200 sloc(i) = 0
      do 225 j=-256,256
      do 225 i=-256,256
  225 bin2(i,j) = 0
      do 250 j=-128,128
      do 250 i=-128,128
  250 bin3(i,j) = 0
      do 300 j=-64,64
      do 300 i=-64,64
  300 bin4(i,j) = 0
      do 350 j=-32,32
      do 350 i=-32,32
  350 bin5(i,j) = 0
      do 400 j=-16,16
      do 400 i=-16,16
  400 bin6(i,j) = 0
      do 450 j=-8,8
      do 450 i=-8,8
  450 bin7(i,j) = 0
      do 475 j=-4,4
      do 475 i=-4,4
  475 bin8(i,j) = 0
      do 500 j=-1,1
      do 500 i=-1,1
      bin2(i,j) = 1
      bin3(i,j) = 1
      bin4(i,j) = 1
      bin5(i,j) = 1
      bin6(i,j) = 1
```

```
        bin7(i,j) = 1
        bin8(i,j) = 1
  500   continue
c
        sloc(ii) = 1
        x(1) = 0
        y(1) = 0
        imin = 0
        imax = 0
        jmin = 0
        jmax = 0
        xc = 0
        yc = 0
        ikill = 0
        rstart = xbox3
        rkill = xkill * rstart
        istep1 = 0
        istep2 = 0
        istep3 = 0
        istep4 = 0
        istep5 = 0
        istep6 = 0
        istep7 = 0
        istep8 = 0
        istep9 = 0
c ---------------------------------- generate DLA containing n sites
        do 550 s=2,n
  405   continue
c ---------------------------------------- put new walker on shell
        temp = ranx(isd)
        phi = temp * c1
        xx = xc + rstart * cos( phi )
        yy = yc + rstart * sin( phi )
c ------------------------ check walker's distance away from center
  410   continue
        r2 = (xx - xc)**2 + (yy - yc)**2
        r = sqrt( r2 )
c ---------------------------------- check if walker is to be killed
        if( r .gt. rkill ) then
        ikill = ikill + 1
        if( ikill .lt. mkill ) goto 405
        n = -1
        return
        endif
c ------------------------------------------ determine step length
```

```
        if( r .gt. rstart) then
        dr = 0.9 * ( r - rstart ) + xbox2
        istep9 = istep9 + 1
        goto 420
        endif
c ---------------------------------- find walker's lattice position
        ixx = nint( xx )
        jyy = nint( yy )
c ------------------------------ determine the most coarsed bin size
        i8 = ixx/nbox8
        j8 = jyy/nbox8
        if( bin8(i8,j8) .eq. 0 ) then
        istep8 = istep8 + 1
        dr = xbox8
        goto 420
        endif
        i7 = ixx/nbox7
        j7 = jyy/nbox7
        if( bin7(i7,j7) .eq. 0 ) then
        istep7 = istep7 + 1
        dr = xbox7
        goto 420
        endif
        i6 = ixx/nbox6
        j6 = jyy/nbox6
        if( bin6(i6,j6) .eq. 0 ) then
        istep6 = istep6 + 1
        dr = xbox6
        goto 420
        endif
        i5 = ixx/nbox5
        j5 = jyy/nbox5
        if( bin5(i5,j5) .eq. 0 ) then
        istep5 = istep5 + 1
        dr = xbox5
        goto 420
        endif
        i4 = ixx/nbox4
        j4 = jyy/nbox4
        if( bin4(i4,j4) .eq. 0 ) then
        istep4 = istep4 + 1
        dr = xbox4
        goto 420
        endif
        i3 = ixx/nbox3
```

```
        j3 = jyy/nbox3
        if( bin3(i3,j3) .eq. 0 ) then
        istep3 = istep3 + 1
        dr = xbox3
            if( iabs( i3 ) .gt. 127 ) then
            n = -2
            return
            endif
            if( iabs( j3 ) .gt. 127 ) then
            n = -2
            return
            endif
        goto 420
        endif
  415   i2 = ixx/nbox2
        j2 = jyy/nbox2
        if( bin2(i2,j2) .eq. 0 ) then
        istep2 = istep2 + 1
        dr = xbox2
        goto 420
        endif
c ------------------------- check nearest neighbors for connections
        do 600 jz=1,iz
        in = ixx + idr(jz,1)
        jn = jyy + idr(jz,2)
        lp = iq(1)* in + iq(2)* jn
        lp = mod(lp,ii) + ii
        k = sloc(lp)
  70    if( k .eq. 0 ) goto 600
           if( in .ne. x(k) ) then
           k = chain(k)
           goto 70
           endif
           if( jn .ne. y(k) ) then
           k = chain(k)
           goto 70
           endif
c ------------------------------------------ connection established
c                                       note probability to stick = 1
       mult(k) = mult(k) + 1
       mult(s) = mult(s) + 1
       link(k,jc(jz)) = s
       link(s,jz) = k
  600  continue
       if( mult(s) .ne. 0 ) then
```

```
c ---------------------------------- update info when walker sticks
        x(s) = ixx
        y(s) = jyy
        lp = iq(1)* ixx + iq(2)* jyy
        lp = mod(lp,ii) + ii
        if( sloc(lp) .ne. 0 ) chain(s) = sloc(lp)
        sloc(lp) = s
        i8o = ixx/nbox8
        j8o = jyy/nbox8
        i7o = ixx/nbox7
        j7o = jyy/nbox7
        i6o = ixx/nbox6
        j6o = jyy/nbox6
        i5o = ixx/nbox5
        j5o = jyy/nbox5
        i4o = ixx/nbox4
        j4o = jyy/nbox4
        i3o = ixx/nbox3
        j3o = jyy/nbox3
        i2o = ixx/nbox2
        j2o = jyy/nbox2
        do 650 j=-1,1
        do 650 i=-1,1
        i8 = i8o + i
        j8 = j8o + j
        i7 = i7o + i
        j7 = j7o + j
        i6 = i6o + i
        j6 = j6o + j
        i5 = i5o + i
        j5 = j5o + j
        i4 = i4o + i
        j4 = j4o + j
        i3 = i3o + i
        j3 = j3o + j
        i2 = i2o + i
        j2 = j2o + j
        bin8(i8,j8) = 1
        bin7(i7,j7) = 1
        bin6(i6,j6) = 1
        bin5(i5,j5) = 1
        bin4(i4,j4) = 1
        bin3(i3,j3) = 1
        bin2(i2,j2) = 1
650     continue
```

```
c ------------------------------ recalculate:   rstart, rkill, etc
        if( ixx .gt. imax ) imax = ixx
        if( ixx .lt. imin ) imin = ixx
        if( jyy .gt. jmax ) jmax = jyy
        if( jyy .lt. jmin ) jmin = jyy
        xlatt = 0.5 * float( imax - imin )
        ylatt = 0.5 * float( jmax - jmin )
        xc = float(imin) + xlatt
        yc = float(jmin) + ylatt
        rstart = amax1( xlatt,ylatt)
        rstart = 1.42 * rstart + xbox3
        rkill = xkill * rstart
        goto 550
        endif
c ------------------------------------ walker moves on the lattice
        istep1 = istep1 + 1
        test = ranx(isd)
           if( test .le. 0.25 )  then
           ixx = ixx + 1
           elseif( test .le. 0.5 ) then
           jyy = jyy + 1
           elseif( test .le. 0.75 ) then
           ixx = ixx - 1
           else
           jyy = jyy - 1
           endif
        xx = float( ixx )
        yy = float( jyy )
        goto 415
c --------------------------------------- walker moves on continuum
  420   continue
        temp = ranx(isd)
        phi = temp * c1
        xxo = xx
        yyo = yy
        xx = xx + dr * cos( phi )
        yy = yy + dr * sin( phi )
        goto 410
  550   continue
c ------------------------------------------- construct output
        nb = 0
        do 700 s=1,n
        nb = nb + mult(s)
        itemp = x(s) + y(s)
        chain(s) = (-1)**itemp
```

```
700   continue
      nb = nb/2
      istep = istep1 + istep2 + istep3 + istep4 + istep5
     1      + istep6 + istep7 + istep8 + istep9
      step = float( istep )
      stat(1) = float(istep1)/step
      stat(2) = float(istep2)/step
      stat(3) = float(istep3)/step
      stat(4) = float(istep4)/step
      stat(5) = float(istep5)/step
      stat(6) = float(istep6)/step
      stat(7) = float(istep7)/step
      stat(8) = float(istep8)/step
      stat(9) = float(istep9)/step
      area = pi * rstart**2
      i2 = 0
      i3 = 0
      i4 = 0
      i5 = 0
      i6 = 0
      i7 = 0
      i8 = 0
      do 725 j=-256,256
      do 725 i=-256,256
725   i2 = i2 + bin2(i,j)
      do 750 j=-128,128
      do 750 i=-128,128
750   i3 = i3 + bin3(i,j)
      do 800 j=-64,64
      do 800 i=-64,64
800   i4 = i4 + bin4(i,j)
      do 850 j=-32,32
      do 850 i=-32,32
850   i5 = i5 + bin5(i,j)
      do 900 j=-16,16
      do 900 i=-16,16
900   i6 = i6 + bin6(i,j)
      do 950 j=-8,8
      do 950 i=-8,8
950   i7 = i7 + bin7(i,j)
      do 975 j=-4,4
      do 975 i=-4,4
975   i8 = i8 + bin8(i,j)
      stat(11) = float(s)/area
      stat(12) = float( i2 * nbox2**2 )/area
```

```
      stat(13) = float( i3 * nbox3**2 )/area
      stat(14) = float( i4 * nbox4**2 )/area
      stat(15) = float( i5 * nbox5**2 )/area
      stat(16) = float( i6 * nbox6**2 )/area
      stat(17) = float( i7 * nbox7**2 )/area
      stat(18) = float( i8 * nbox8**2 )/area
      do 1000 i=1,18
1000  stat(i) = stat(i) * 100
      stat(19) = step
      stat(20) = float(ikill)
      return
      end
      function ranx(i)
      i=i*1566083941 + 1
      ranx=float(i)*2.328306e-10+0.5
      return
      end
```

Appendix B: Recursion Relations for the Exact Enumeration Method

The recursion relations for calculating the step auto-correlation function (SACF) exactly are given below. The method described here calculates the SACF directly and then from this function the mean squared displacement can be is obtained from two summations over the SACF. Two major advantages of this method compared to exactly calculating the mean squared displacement directly are the following. In the first place, this method works for *periodic* boundary conditions as well as free boundary conditions. Secondly, the accuracy in calculating the SACF for very long times is *not* limited by the error induced in the loss of significant figures in subtracting huge numbers from one another to arrive at extremely small values for the SACF. The only disadvantage is that the mean squared displacement of the tracer particle starting from a non-stationary initial condition cannot be obtained directly from the SACF because time translation invariance is lost. Therefore, it is assumed here that the stationary state vector V_1 is used as the initial condition.

Using the same notion as introduced in Section 3 of Chapter 2, the recursion relations that were used for the blind and myopic ant models are given as:

$$p_j^0(s) = \sum_{s'} w(s,s') \left[x_j(s) - x_j(s') \right] V_1(s') \tag{B.1}$$

$$q_i(s) = \sum_{s'} w(s',s) \left[x_i(s') - x_i(s) \right] \tag{B.2}$$

$$p^{n+1}(s) = \sum_{s'} w(s,s')\, p_j^n(s') \tag{B.3}$$

$$\langle \rho_i(n) \rho_j(0) \rangle = \sum_{s} q_i(s) p_j^{n-1}(s) \quad \text{for } n \geq 1 \tag{B.4}$$

and

$$\langle \rho_i(0)\rho_j(0)\rangle = \sum_{s',s} [\, x_i(s') - x_i(s)\,]\, w(s',s)\, [\, x_j(s') - x_j(s)\,]\, V_1(s) \quad . \qquad \text{(B.5)}$$

Further complications arise with the persistent random walk, as defined in Chapter 4, because of the internal states associated with each cell. Since the basic recursion relations are the same, the part of the FORTRAN code in calculating the SACF for the persistent random walk is given below. In this way, the basic structure of the algorithm can be seen and the specific details of how the internal states for the persistent random walk model are handled is recorded here for future reference. The "input" portion of the program is also included here for future reference and to help define some variables. Note that the code given below is about 40% of the total program.

```
c                          Dynamic Rules
c The state space consist of site and internal state labels. Each site
c contains z (4 in this case) internal states. Each state is linked to
c 4 other states, 3 internal and one external.
c ------------------ Transmitted Scattering: (so,sf) nearest neighbors
c
c Gt(sf,jf,so,jo) = phop(so) * T[iph(sf),iph(so)]* gmax  +
c                   pstay(so)* (1- T[iph(so),iph(sf)])* gmax  if  jf=jo
c                 = 0                                         otherwise
c ------------------ Reflected Scattering:
c
c Gr(so,jf,so,jo)= dir(jf,jo,so)* Phop(so)* {1- T[iph(sf),iph(so)] }* gmax
c
c  dir(jf,jo,so | alpha ) = depending on  alpha  the reflected part of
c      the scattering rate  Gr  will be distributed among the internal
c      states according to this function.  Note: (0 .le. alpha .le. 1)
c            alpha = 0.0 => reverse internal direction change
c            alpha = 0.5 => uniform internal direction change
c            alpha = 1.0 => no internal direction change
c -----------------------------------<< variable list  (incomplete)
c   id defines the dimension
c   iz defines the coordination number
c   lngth1 = number of sites along first edge of rectangle
c   lngth2 = number of sites along second edge of rectangle
c   proba = probability for a square to have an A phase
c   phase(s) = iph = 1 or 2 for site s
c   (ns,nk) = number of (sites,states) in the configuration
c   nmax,kmax determines maximum size of matrices
c   so,sf,s defines a site label   (degenerate set of states)
c   jo,jf,j defines a set of internal states for site s
c   j       also defines a lattice vector
c   ko,kf,k defines a nondegenerate set of states describing the system
c   link(kf,jo) = ko  defines connectivity among states   (ko --> kf)
c   jj defines a component of a vector
c   v(j,jj) defines the displacement vector of the jth lattice vector
c   ds(j) are lattice translation vectors which define boundaries
c   jc(j) are the complementary lattice displacements relative to j
c   iii,jjj define the diffusion tensor x,y component respectively
c |-------------------------------------------------------<< dynamic
c   t = number of random events
c   error = how close the initial condition is to the stationary state
c   vxvy,vxvyo= <Vx(t)Vy(0)>,<Vx(0)Vy(0)> for iii,jjj => x,y respect.
c   phop(iph) = hopping probability for phase iph
c   pstay(iph) = internal backward & sideward probability for phase iph
c   rate(iph) = rates for phase iph
```

```
c   gmax = max( rate(1),rate(2) )
c   ea,eb = { Ga/gmax , Gb/gmax } respectively
c   tab,tba = transmission probabilities to go from {b->a,a->b} respect.
c   tp(iphf,ipho) transmission probabilities:  t(1,1)=t(2,2)=1
c                                              t(2,1)=tba  t(1,2)=tab
c   alph(iph) = scattering parameter for phase iph, (adjust internal scat.)
c   dir(i,j) (forward, sideward, backward) probabilities for i=(1,2,3)
c            respectively w.r.t. phase (a,b) for j=(1,2) respectively.
c   ca,cb = # of carriers per unit volume for phase (A,B) respectively
c   frac = ca/cb
c   pay(k),pby(k) are (after, before) state vectors and vice versa
c   qx(k) left vector for inner product with state vector
c   wd(k)  = diagonal transition probability to remain in state k
c   wc(kf,jo) = compressed form for the off diagonal elements of
c               the W matrix which represents w(kf,ko).
c ------------------------------------------------------
        integer t,s,so,sf,ds(4),jc(4)
        integer phase(40000),link(40000,4)
        double precision wd(40000),wc(40000,4)
        double precision eta1,eta2,ea,eb,tab,tba
        double precision dir(3,2),alpha(2),tp(2,2)
        double precision pay(40000),pby(40000),qx(40000)
        double precision v(4,2),rate(2),phop(2),pstay(2)
        double precision e,sumx,sumy,gmax,error,vxvyo,vxvy
        double precision zero,ao,ao2,doa,taua,dob,taub,ca,cb,cc,frac
        id = 2
        iz = 4
        kmax = 40000
        nmax = kmax/iz
        zero = 1d-25
c ---------------------------------- initialize displacement steps
        v(1,1) = 1
        v(1,2) = 0
        v(2,1) = 0
        v(2,2) = 1
        v(3,1) = -1
        v(3,2) = 0
        v(4,1) = 0
        v(4,2) = -1
c ----------------------------initialize complimentary directions
        jc(1) = 3
        jc(2) = 4
        jc(3) = 1
        jc(4) = 2
c ------------------------------------------------------<< input
```

```
    1   continue
        write(6,5045)
 5045   format(1x,' enter lattice constant:  ao')
        read(5,*) ao
        if( ao .lt. zero ) goto 1
        ao2 = ao**2
        write(6,5050)
 5050   format(1x,'      Phase A Characteristics ')
        write(6,*)
        write(6,5055)
        read(5,*) doa
        if( doa .lt. 0.0 ) goto 1
        write(6,5060)
        read(5,*) taua
        if( taua .lt. zero ) goto 1
              eta1 = ao/dsqrt(2*doa*taua)
              e = 0.25 * eta1
              phop(1) = 1/(1+0.75*eta1)
              pstay(1) = e * phop(1)
              cc = 4.0 * (1+2*e) * pstay(1)
              rate(1) = ( 1/taua )/cc
        write(6,*)
        write(6,5070)
 5070   format(1x,'      Phase B Characteristics ')
        write(6,*)
        write(6,5055)
        read(5,*) dob
        if( dob .lt. 0.0 ) goto 1
        write(6,5060)
        read(5,*) taub
        if( taub .lt. zero ) goto 1
              eta2 = ao/dsqrt(2*dob*taub)
              e = 0.25 * eta2
              phop(2) = 1/(1+0.75*eta2)
              pstay(2) = e * phop(2)
              cc = 4.0 * (1+2*e) * pstay(2)
              rate(2) = ( 1/taub )/cc
c ---------------------------------------<< determine the max rate
        gmax = dmax1( rate(1),rate(2) )
        gmax = gmax * 1.000001
        ea = rate(1)/gmax
        eb = rate(2)/gmax
        phop(1) = phop(1) * ea
        phop(2) = phop(2) * eb
        pstay(1) = pstay(1) * ea
```

```
        pstay(2) = pstay(2) * eb
c ---------------------------------------<< determine tab and tba
    2   write(6,5075)
 5075   format(1x,'      A-B Interface Characteristics ')
        write(6,5080)
 5080   format(1x,'enter the fraction: na/nb ')
        read(5,*) frac
        cc = 1/zero
        cb = 1.0
        ca = frac * cb
        if( frac .lt. zero ) goto 2
        if( frac .gt. cc ) goto 2
        write(6,5085)
 5085   format(1x,'enter the maximum transmission probability ')
        read(5,*) cc
        if( cc .lt. zero ) goto 2
        if( cc .gt. 1.0 ) goto 2
c ------------------------------------------------------------------
c   note:  PS = PB = pstay   and   PH = phop
c   detailed balance:
c [ PHa* tba + PBa * (1 - tab) ]*na = [ PHb * tab + PBb * (1 - tba) ]*nb
c ---------------
c        assume tab = max[ tab,tba ]   solve for tba given tab = cc
         e = pstay(1) * (cc-1) * frac  +  phop(2) * cc  +  pstay(2)
         tba = e/( phop(1) * frac  +  pstay(2) )
         tab = cc
c ---------------
            if( (tba .gt. 1) .or. (tba .le. 0) ) then
c           assume tba = max[ tab,tba ]      solve for tab given tba = cc
            e = pstay(2) * (cc-1)  +  ( phop(1) * cc  +  pstay(1) )* frac
            e = e/( phop(2)  +  pstay(1) * frac )
                 if( (e .gt. 1) .or. (e .le. 0) ) then
                 write(6,5090)
 5090            format(1x,'    tab      tba    no solution')
                 goto 2
                 endif
            tab = e
            tba = cc
            endif
c ---------------
        tp(1,1) = 1.0
        tp(2,1) = tba
        tp(1,2) = tab
        tp(2,2) = 1.0
c ----------------------------------<< input for scattering rules
```

```
    4   write(6,*)
        write(6,5100)
 5100   format(1x,'     Scattering Parameters: ')
        write(6,*)
        write(6,5105)
 5105   format(1x,'enter alpha for phase A')
        read(5,*) e
        if( e .lt. 0 ) goto 4
        if( e .gt. 1.0 ) goto 4
        alpha(1) = e
        write(6,5110)
 5110   format(1x,'enter alpha for phase B')
        read(5,*) e
        if( e .lt. 0 ) goto 4
        if( e .gt. 1.0 ) goto 4
        alpha(2) = e
c ---------------------------------- calculation of dir(iscat,iph)
c                                        iscat=1,2,3 => F,S,B scattering
        e = 1 + 4*alpha(1)*( 1-alpha(1) )
        dir(2,1) =  2*alpha(1)*( 1-alpha(1) )/e
        dir(1,1) =  alpha(1)/e
        dir(3,1) =  ( 1-alpha(1) )/e
c
        e = 1 + 4*alpha(2)*( 1-alpha(2) )
        dir(2,2) =  2*alpha(2)*( 1-alpha(2) )/e
        dir(1,2) =  alpha(2)/e
        dir(3,2) =  ( 1-alpha(2) )/e
c ----------------------------------------<< dimension specs.
    3   write(6,*)
           if( iopts .ne. 7 ) then
           write(6,5200)
 5200      format(1x,'enter the dimensions for the rectangle')
           write(6,5205) nmax
 5205      format(1x,'enter horizontal length L1 *ao  L1*L2 .le.',i7)
           read(5,*) lngth1
           if( lngth1 .eq. 0 ) goto 1
           endif
        write(6,5210)
 5210   format(1x,'enter the vertical length L2 *ao')
        read(5,*) lngth2
        if( lngth2 .le. 0 ) goto 1
             write(6,5211)
 5211        format(1x,'enter the A phase conc.  (proba)')
             read(5,*) proba
             if( proba .lt. 0.0 ) goto 1
```

```
            if( proba .gt. 1.0 ) goto 1
        ns = lngth1 * lngth2
        if( ns .gt. nmax) goto 3
        nk = iz * ns
             write(6,5255)
 5255        format(1x,'enter the seed isd')
             read(5,*) isd
c
        write(6,5260)
 5260   format(1x,'enter (i,j) for ViVj <=> Dij ')
        write(6,5261)
 5261   format(1x,'enter i: ')
        read(5,*) iii
        if( iii .lt. 1 ) goto 3
        if( iii .gt. id ) goto 3
        write(6,5262)
 5262   format(1x,'enter j: ')
        read(5,*) jjj
        if( jjj .lt. 1 ) goto 3
        if( jjj .gt. id ) goto 3
c ------------------ construct the link matrix for a rectangular box
        ds(1) = -1
        ds(2) = -1 * lngth1
        ds(3) = 1
        ds(4) = lngth1
c ---------------------- lattice labeling;        1st assume no boundary
c sj = so + ds(j)  :  (s,j) -> k  via  k = iz*(s-1) + j    for j=1,2,3,4
c ----------------- construct the external part of the link matrix
        do 100 jf=1,iz
        itemp = ds(jf) - 1
        do 100 s=1,ns
        kf = iz * (s-1) + jf
        ko = iz * (s+itemp) + jf
  100   link(kf,jf) = ko
c ------------------------------------------ left and right edges
        do 150 i= 1,lngth2
        klft = iz * ( lngth1 * (i-1) )
        krht = iz * ( lngth1 * i - 1 )
        kf1 = klft + 1
        kf3 = krht + 3
        link(kf1,1) = krht + 1
        link(kf3,3) = klft + 3
  150   continue
c ---------------------------------------- lower and upper edges
        itemp3 = iz * lngth1 * (lngth2 - 1)
```

```
        do 200 i= 1,lngth1
        klow = iz * ( i - 1 )
        kupr = itemp3 + klow
        kf2 = klow + 2
        kf4 = kupr + 4
        link(kf2,2) = kupr + 2
        link(kf4,4) = klow + 4
  200   continue
c ----------------- construct the internal part of the link matrix
        do 250 jf=1,iz
        do 250 jo=1,iz
        if( jo .eq. jf ) goto 250
        do 255 s=1,ns
        kf = iz*(s-1) + jf
        ko = iz*(s-1) + jo
        link(kf,jo) = ko
  255   continue
  250   continue
c ---------------------------------- generate random configuration
        do 410 ihor=1,lngth1
        do 410 iver=1,lngth2
        test = ranx(isd)
            if( test .gt. proba ) then
            itemp = 2
            else
            itemp = 1
            endif
        s = (iver - 1)*lngth1 + ihor
        phase(s) = itemp
  410   continue
c ---------------------------- calculate transmission probabilities
c           let qx(k) be temporarily used to contain {t1,t2,t3,t4}
        do 450 j=1,iz
        do 450 sf=1,ns
        km = iz*(sf-1) + j
        ko = link(km,j)
        so = (ko - j)/iz + 1
        ipho = phase(so)
        iphf = phase(sf)
        qx(ko) = tp(iphf,ipho)
  450   continue
c ------------------------------ construct the external part of wc
        do 500 jf=1,iz
        do 500 sf=1,ns
        kf = iz * (sf-1) + jf
```

```
        kt = link(kf,jf)
        kr = iz * (sf-1) + jc(jf)
        so = (kt-jf)/iz + 1
        iph = phase(so)
        wc(kf,jf) = phop(iph)* qx(kt)   +   pstay(iph)* ( 1-qx(kr) )
  500   continue
c ---------------------------- construct the internal part of wc
        do 550 jf=1,iz
        do 550 s=1,ns
        kf = iz*(s-1) + jf
        iph = phase(s)
        do 550 jo=1,iz
        kt = iz*(s-1) + jo
        itemp = jo + jf
c ---------------------------------------- sideward scattering
        if( 2*(itemp/2) .ne. itemp ) then
        e = dir(2,iph)
        wc(kf,jo) = pstay(iph)
c -------------------- external case done, forward scat --> wd(k)
        elseif( jo .eq. jf ) then
        goto 550
c ---------------------------------------- backward scattering
        else
        e = dir(3,iph)
        kr = link(kf,jf)
        wc(kf,jo) = pstay(iph) * qx(kr)
        endif
c ------------------------------------ reflected hopping scatter
        wc(kf,jo) = wc(kf,jo) + e * phop(iph) * ( 1 - qx(kt) )
  550   continue
c ------------------ construct diagonal part of transition matrix
        do 600 k=1,nk
  600   pay(k) = 0
        do 650 j=1,4
        do 650 k=1,nk
        pay(link(k,j)) = pay(link(k,j)) + wc(k,j)
  650   continue
        do 700 k=1,nk
  700   wd(k) = 1 - pay(k)
c ------------------------------------ get initial state vector
        sumx = 0
        do 750 s=1,ns
        k1 = iz*(s-1) + 1
        k2 = k1 + 1
        k3 = k2 + 1
```

```
        k4 = k3 + 1
        iph = phase(s)
            if( iph .eq. 1 ) then
            sumy = ca
            else
            sumy = cb
            endif
        pay(k1) = sumy
        pay(k2) = sumy
        pay(k3) = sumy
        pay(k4) = sumy
        sumx = sumx + sumy
  750   continue
        sumy = 0.25/sumx
        do 800 k=1,nk
  800   pay(k) = pay(k) * sumy
        iter = itermx
c note that the input for itermx has not been shown here.
c for alph(1) = alpha(2) = 0   itermx = 0
        call eqdstr2(nk,link,wd,wc,pay,pby,error,iter)
c ------------------------ calculate <V(0)> for the initial state
        sumx = 0
        sumy = 0
        do 850 jf=1,iz
c ----- do 850 jo=1,iz -- note v=0 for internal transitions  set jo=jf
        do 850 s=1,ns
        k = iz * (s-1) + jf
        sumx = sumx + wc(k,jf) * v(jf,1) * pay( link(k,jf) )
        sumy = sumy + wc(k,jf) * v(jf,2) * pay( link(k,jf) )
  850   continue
c ----------------------------- get left vector for inner product
c                          note only hopping transitions are summed
        do 1250 jf=1,iz
        do 1250 s=1,ns
        kf = iz * (s-1) + jf
        qx( link(kf,jf) ) = wc(kf,jf) * v(jf,iii) * ao2
 1250   continue
c ---------------------------------- calculation of <Vi(0)Vj(0)>
c                                  and get right vector for inner product
        vxvyo = 0
        do 1300 jf=1,iz
        do 1300 s=1,ns
        kf = iz * (s-1) + jf
        ko = link(kf,jf)
        sumy = wc(kf,jf) * pay(ko)
```

```
        vxvyo = vxvyo + v(jf,iii) * v(jf,jjj) * sumy
        pby(kf) = v(jf,jjj) * sumy
 1300   continue
        vxvyo = vxvyo * ao2
        vxvy = 0
        do 1350 k=1,nk
        vxvy = vxvy + qx(k) * pby(k)
 1350   continue
c <<<<<<<<<< some code using the results of vxvy and vxvyo >>>>>>
 1451   continue
        t = t + 1
        do 1450 k=1,nk
        sumy = wd(k) * pby(k)
        do 1500 j=1,iz
 1500   sumy = sumy + pby( link(k,j) ) * wc(k,j)
 1450   pay(k) = sumy
        vxvy = 0
        do 1550 k=1,nk
        vxvy = vxvy + qx(k) * pay(k)
 1550   continue
c <<<<<<<<<<<<< some code using the results of vxvy >>>>>>>>>>>
        t = t + 1
        do 1750 k=1,nk
        sumy = wd(k) * pay(k)
        do 1800 j=1,iz
 1800   sumy = sumy + pay( link(k,j) ) * wc(k,j)
 1750   pby(k) = sumy
        vxvy = 0
        do 1850 k=1,nk
        vxvy = vxvy + qx(k) * pby(k)
 1850   continue
c <<<<<<<<<<<<< some code using the results of vxvy >>>>>>>>>>>
        goto 1451
        end
        function ranx(i)
        i=i*1566083941 + 1
        ranx=float(i)*2.328306e-10+0.5
        return
        end
```

VITA

VITA

Donald John Jacobs, son of George F. Jacobs and Stella Jaracz, was born November 1963 in Amsterdam New York. He generally opposed his elementary school education because of the many assignments involving pure memorization. It was not until high school that he began to perform much better in school. At that time he earned his private pilot license at the age of 17 and was a member of the Experimental Aircraft Association. After entering Fulton-Montgomery Community College, majoring in Engineering science, did he enjoy school. It was at that time when he changed his major to physics.

After receiving his A.S. degree from Fulton-Montgomery in 1983, he transferred to Union College from where he earned his B.S. degree in Physics with honors. In 1985 he started his graduate studies in Physics at Purdue University. Being somewhat impractical, he postponed his Masters degree until 1991, although nearly finishing his Ph.D. that was obtained one year later at Purdue in 1992.